TECHNISCHE UNIVERSITÄT MÜNCHEN

Fachgebiet Biotechnologie der Naturstoffe

The lignification of strawberry fruit: molecular basis and effects on fruit quality

Su-Ying Yeh

Vollständiger Abdruck der von der Fakultät Wissenschaftszentrum Weihenstephan für Ernährung, Landnutzung und Umwelt der Technischen Universität München zur Erlangung des akademischen Grades eines

Doktors der Naturwissenschaften

genehmigten Dissertation.

Vorsitzender:	Univ.-Prof. Dr. K.-H. Engel
Prüfer der Dissertation:	1. Univ.-Prof. Dr. W. Schwab
	2. Univ.-Prof. Dr. A. Gierl

Die Dissertation wurde am 21.08.2012 bei der Technischen Universität München eingereicht und durch die Fakultät Wissenschaftszentrum Weihenstephan für Ernährung, Landnutzung und Umwelt am 23.11.2012 angenommen.

For my parents

Acknowledgements

I wish to express great appreciation and thanks to my doctor father, Prof. Dr. Wilfried Schwab, for giving me the opportunity to conduct research in his lab. Most special thanks go to him for his professional guidance, constructive suggestions and helpful discussions to broaden my knowledge base, as well as for providing a good research team and working place, scientific resources to expand my repertoire of experimental techniques throughout my study.

I would like to express sincere appreciation and thanks to Dr. Fong-Chin Huang for her advice and useful suggestions, as well as for providing practical laboratory experiences and professional skills throughout my study.

In addition, I would like to thank the following people and institutions:

- Dr. Thomas Hoffmann, thank you for your helpful discussions and assistance in RNAi experiments and statistical analysis. Special thanks go to him for his helpful comments on the manuscript.
- Dr. Stephanie Hücherig, thank you for your suggestions and assistance in conducting the FaPOD27 experiment.
- Dr. Yuh-Puu Han and Barbara Harris, thank you for your patience in proofreading the English grammar in my manuscript. Special thanks go to Hsiu-Jen Wang for generous help.
- Mechthild Mayershofer, thank you for your assistance in lignin composition analysis.
- Dr. Ruth Habegger, Katrin Franz, and Kilian Skowranek, thank each of you for your assistance in organizing the greenhouse space and strawberry availability. Many thanks go to Katrin Franz for generous help, especially in German translation.
- My colleagues (Heike Adamski, Dr. Quirin Sinz, Dr. Anja Preuß, Ludwig Ring, Christopher Fuchs, Doreen Schiller, Friedericke Bönisch, Hannelore Meckl, and Miriam González), thank all of you for your help.
- Department of Food Process Engineering and Dairy Technology, for providing the texture analyzer. Thanks go to Günther Unterbuchberger for your assistance in texture analysis.
- DFG, for providing financial support.

Finally, I thank to my beloved family, university teachers, and friends for their love and encouragement. Due to the valuable support from all of you, I can fulfill my dreams in Freising, Germany.

Table of contents

Abbreviations

4CL	4-coumaroyl-CoA ligase
ATP	adenosine-5'-triphosphate
bp	base pair
BSA	bovine serum albumin
BLAST	Basic Local Alignment Search Tool
C3H	*p*-coumaroyl shikimate 3´-hydroxylase
C4H	cinnamate 4-hydroxylase
C_T	cycle threshold
CAD	cinnamyl alcohol dehydrogenase
CCoAOMT	caffeoyl-CoA O-methyltransferase
CCR	cinnamoyl-CoA reductase
cDNA	complementary DNA
CHS	chalcone synthase
CoA	coenzyme A
COMT	caffeic acid O-methyltransferase
CTAB	cetyltrimethyl ammonium bromide
cv.	cultivar
d	days
DEPC	diethyl pyrocarbonate
DMSO	dimethyl sulfoxide
DNA	deoxyribonucleic acid
DNase	deoxyribonuclease
dATP	deoxyadenosine triphosphate
dNTP	deoxynucleoside triphosphate
dsRNA	double stranded RNA
DTT	dithiothreitol
E. coli	*Escherichia coli*
EDTA	ethylenediaminetetraacetic acid
F5H	ferulic acid 5-hydroxylase
FPLC	fast protein liquid chromatography
G-lignin	guaiacyl lignin
GC-MS	gas chromatography-mass spectrometry
GST	glutathione-S-transferase
h	hour
HCT	hydroxycinnamoyl transferase
H-lignin	*p*-hydroxyphenyl lignin
HPLC	high performance liquid chromatography
ihp RNA	intron-hairpin RNA
IPTG	isopropyl-β-D-thiogalactopyranoside
kb	kilo-base pair

k_{cat}	turnover number
kDa	kilodalton
K_m	Michaelis constant
LB	Luria-Bertani
LC-UV-ESI-MS^n	liquid chromatography ultraviolet electro spray ionization mass spectrometry
MES	morpholino ethanesulfonic acid
min	minute
MMLV-RT	moloney murine leukemia viruse-reverse transcriptase
MQ water	Milli Q water
mRNA	messenger ribonucleic acid
M.W.	molecular weight
MS	mass spectrometry
MS-Salt	Murashige and Skoog Basal Salt Mixture
m/z	mass-to-charge ratio
NaOAc	sodium acetate
NMR	nuclear magnetic resonance
nt	nucleotides
OD_X	optical density at X nm
ORF	open reading frame
p	para
PAGE	polyacrylamide gel electrophoresis
PAL	phenylalanine ammonia lyase
PCR	polymerase chain reaction
PMSF	phenylmethylsulfonyl fluoride
POD (or POD)	Peroxidase
PTGS	post-transcriptional gene silencing
PEG 6000	polyethylene glycol 6000
PVP	polyvinylpyrrolidone
qRT-PCR	quantitative real-time PCR
RdRP	RNA-dependent RNA polymerase
RISC	RNA-induced silencing complex
RNA	ribonucleic acid
RNAi	RNA interference
RNase	ribonuclease
rpm	revolutions per minute
RT	reverse transcription
T_m	melting temperature
SAD	sinapyl alcohol dehydrogenase
SDS	sodium dodecyl sulfate
sec	second
siRNA	small interfering RNA

S-lignin	syringyl lignin
TAE	Tris-acetate-EDTA
TE	Tris-EDTA
TLC	thin layer chromatography
Tris	tris(hydroxymethyl)aminomethane
U	unit
UV	ultraviolet
V	voltage
VIGS	virus induced gene silencing
V_{max}	maximum reaction rate
X-gal	5-bromo-4-chloro-3-indolyl-β-D-galactopyranoside

Table 1. Standard amino acid and abbreviations

Amino acid	3-Letter	1-Letter
Alanine	Ala	A
Arginine	Arg	R
Asparagine	Asn	N
Aspartic acid	Asp	D
Cysteine	Cys	C
Glutamine	Gln	Q
Glutamic acid	Glu	E
Glycine	Gly	G
Histidine	His	H
Isoleucine	Ile	I
Leucine	Leu	L
Lysine	Lys	K
Methionine	Met	M
Phenylalanine	Phe	F
Proline	Pro	P
Serine	Ser	S
Threonine	Thr	T
Tryptophan	Trp	W
Tyrosine	Tyr	Y
Valine	Val	V

Zusammenfassung

Die Erdbeere (*Fragaria* × *ananassa)* zählt zu den weltweit am häufigsten konsumierten Obstarten. Die Früchte sind jedoch sehr leicht verderblich und können nur kurze Zeit gelagert werden. Wenn die Frucht vollständig entwickelt und reif ist, tritt infolge der Verflüssigung und Depolymerisation der Zellwandkomponenten ein Verlust der Festigkeit ein. Lignin, ein phenolisches Polymer, ist mit Cellulose und Hemicellulose in der Zellwand assoziiert. Zimtsäure-CoA Reduktase (CCR), Zimtalkohol Dehydrogenase (CAD) und Peroxidase (POD) sind Enzyme des Monolignol-Biosyntheseweges und damit an der Lignin Bildung beteiligt. Der Ligningehalt und die Zusammensetzung der Zellwandpolymere können die Festigkeit der Frucht beeinflussen. Kenntnisse der Eigenschaften der korrespondierenden Gene könnten das Verständnis der Lignin Synthese in Früchten verbessern, zu einer verbesserten Erdbeerqualität führen und die Haltbarkeit von frischen Früchten auf dem Markt verlängern.

In der vorliegenden Arbeit wurden die vollständigen kodierenden Sequenzbereiche von *FaCCR*, *FaCAD*, *FaPOD* und *FaPOD27* aus der reifen Frucht kloniert. CCR (EC 1.2.1.44) ist das erste Enzym des Monolignol Biosyntheseweges. Durch die Reduktion von Kaffeesäure-, *p*-Cumarsäure- und Ferulasäure-CoA mittels CCR entstehen die korrespondierenden Hydroxyzimtaldehyde. Phylogenetische Analysen zeigten, dass FaCCR ein Mitglied der CCR-Familie ist. In der Proteinsequenz von FaCCR liegen das konservierte NWYCY Motiv und die NAD/NADP(H) Bindestelle vor. Der vollständige kodierende Sequenzbereich von *FaCCR* wurde heterolog in *Escherichia coli* exprimiert, um die biochemische Funktion zu untersuchen. Das rekombinante Fusionsprotein GST-FaCCR weist eine maximale Aktivität bei pH 6 in einem Natriumphosphat Puffer bei 25°C auf und setzt bevorzugt das Substrat Ferulasäure-CoA um. Die Umsetzung eines Substratgemisches (Kaffeesäure-, *p*-Cumarsäure- und Ferulasäure-CoA) durch GST-FaCCR zeigte, dass die Effizienz der Umsetzung von Ferulasäure-CoA (100%) deutlich höher ist als die der beiden anderen Substrate Kaffeesäure-CoA (3,27%) und *p*-Cumarsäure-CoA (3,17%). Die LC-UV-ESI-MS^n Analyse der GST-FaCCR-Ansätze zeigte große Mengen des Reaktionsproduktes Coniferylaldehyd und geringe Produktmengen an *p*-Cumaraldehyd und Kaffeealdehyd. Diese Ergebnisse spiegeln vermutlich die bevorzugte Bildung von G-Einheiten des Lignins in Früchten wider. CAD (EC 1.1.1.195) katalysiert die Umsetzung von Hydroxyzimtaldehyden zu deren korrespondierende Alkohole, welche die Endprodukte des Monolignol Biosyntheseweges darstellen. Ein phylogenetischer Baum der CADs belegt die

hohe Homologie von FaCAD zu Fxacad1 (*F. x ananassa* cv. Chandler) und PtSAD (*Populus tremuloides*). FaCAD verfügt sowohl über die konservierte NAD/NADP(H) Domäne als auch die Zn1 und Zn2 Bindungsstellen. Der vollständige kodierende Sequenzbereich von *FaCAD* wurde in Hefe (*Saccharomyces cerevisiae* INVSc.1) exprimiert. Die LC-UV-ESI-MS^n Analyse zeigte, dass die CAD Aktivität in Hefezellen geringfügig durch die Expression von FaCAD ansteigt und das Produkt Coniferylalkohol gebildet wird. Folglich könnte FaCAD an der Regulation der Lignin Biosynthese beteiligt sein und bei der Produktion von G-Einheiten in den Früchten mitwirken. Bei pflanzlichen Peroxidasen (EC 1.11.1.7) handelt es sich um Häm haltige Oxidoreduktasen. Lignin entsteht durch die von Peroxidasen vermittelte oxidative Polymerisation von Monolignolen unter Verbrauch von H_2O_2. „Prosite“ Analysen zeigten, dass FaPOD und FaPOD27 zu den pflanzlichen Häm-Peroxidasen gezählt werden, welche eine putative Ca^{2+} Bindedomäne aufweisen. Die beiden Enzyme weisen nur eine geringe Aminosäuren-Sequenz Übereinstimmung (31.9%) auf. Die vollständigen kodierenden Sequenzbereiche von *FaPOD* oder *FaPOD27* wurden heterolog in *Escherichia coli* exprimiert. Mittels des Guajakol Oxidase Assays konnte die enzymatische Aktivität von FaPOD27 bewiesen werden, wobei FaPOD jedoch inaktiv war. Die LC-UV-ESI-MS^n Analyse zeigte, dass das aktive FaPOD27 Enzym die Bildung von Dehydrodimeren von Ferulasäure und einem Decarboxylierungsprodukt des Dehydrodimer-Vorläufers katalysiert. Diese Ergebnisse deuten darauf hin, dass FaPOD27 eine wichtige Rolle bei der Polymerisation der Lignin Vorläufer spielt.

Durch quantitative PCR Analysen konnten unterschiedliche Expressionsmuster der *FaCCR, FaCAD, FaPOD* und *FaPOD27* Gene während der Erdbeerfruchtentwicklung nachgewiesen werden. Die höchste Expression von *FaCCR, FaCAD* und *FaPOD27* wurde in roten reifen Früchten gemessen. *FaPOD* wird in grünen unreifen Früchten exprimiert. Dieses entwicklungsabhängige Expressionsmuster kombiniert mit den Aktivitätsergebnissen der Enzyme weist daraufhin, dass die Expression von Genen der Lignin Biosynthese während der Fruchtreife der Erdbeere induziert wird, wobei *FaPOD* keine Rolle bei der Lignin Bildung in der Frucht spielt.

Zudem wurden unterschiedliche Expressionsmuster in verwundeten Früchten und Früchten nachgewiesen, welche mit *Agrobacterium tumefaciens* infiltriert wurden. Der Transkriptgehalt von Genen des Phenylpropanoid Biosyntheseweges (*FaPAL, FaCCR, FaCAD, FaPOD* und *FaPOD27*) zeigte keine Veränderung in verwundeten Früchten verglichen mit unbehandelten Früchten. Die Transkriptmenge von *FaPAL* wurde allerdings 24 Stunden nach der Agroinfiltration transient induziert. Auch der Transkriptgehalt von

FaPOD27 wurde stark und konstitutiv in Früchten nach der Infiltration mit *Agrobakterium tumefaciens* (von sechs Stunden bis zehn Tagen) induziert. Dies deutet daraufhin, dass beide Gene an der Abwehrreaktion der Pflanze beteiligt sind. Zudem konnte gezeigt werden, dass eine erhöhte Festigkeit der Frucht mit einer zunehmenden Lignin Produktion in agroinfiltrierten Früchten einhergeht. Agroinfiltrierte Früchte zeigen zudem eine erhöhte Festigkeit, wenn sie Konstrukte zur RNAi-vermittelten Gen-Stilllegung oder Überexpression von Genen der Monolignol Biosynthese exprimierten, die in Zusammenhang mit *FaCCR*, *FaCAD* und *FaPOD* stehen. Die erhöhte Festigkeit der Früchte geht jeweils einher mit einer zunehmenden Lignin Produktion in behandelten Früchten verglichen mit unbehandelten Wildtypfrüchten. Bei der pflanzlichen Lignifizierung werden Ligninpolymere in die Zellwand eingebaut. Mittels „Wiesner“ Färbung konnte nachgewiesen werden, dass die Lignin Ablagerung und Lignifizierung um die Leitbündel in Früchten, die mit *Agrobakterium tumefaciens* infiltriert worden waren erfolgt. Diese Ergebnisse weisen darauf hin, dass die Akkumulation von Lignin in Früchten, die mit verschiedenen Konstrukten infiltriert wurden, möglicherweise die Invasion von Agrobakterien einschränken soll. Lignin spielt somit eine wichtige Rolle in der strukturellen Verstärkung von Früchten, die mit *Agrobakterium* infiziert wurden.

Gene des Monolignol Biosyntheseweges wurden in Erdbeerfrüchten (*F. x ananassa* cv. Elsanta) hoch- und herabreguliert. Die Genexpression und Aktivität von *FaCCR* und *FaCAD* konnte durch RNAi in *FaCCRi* und *FaCADi* stillgelegten Erdbeeren effizient unterdrückt werden. Die Überexpression der pBI-*FaPOD* Konstrukte führte in Früchten zu signifikant erhöhten *FaPOD* Transkriptgehalten. Im Allgemeinen zeigte die vergleichende Analyse der Metabolite, dass der Gehalt an *p*-Cumarsäure-Glukose-Ester abnimmt, aber der an Kaffeesäure- und Ferulasäure-Glucose-Ester in behandelten Früchten zunimmt. Überraschenderweise bleibt die Hoch- und Herabregulation von Genen des Monolignol Biosyntheseweges in Früchten ohne Effekt auf die Fruchtentwicklung und den Ligningehalt, verglichen mit Früchten, die mit einem Kontrollkonstrukt infiltriert wurden. Dies lässt sich vermutlich auf ein erhöhtes *FaPOD27* Expressionsniveau in allen agroinfiltrierten Früchten zurückführen. Gleichzeitig dürfte eine größere Menge an Hydroxyzimtsäure-Derivaten in das Lignin Polymer durch *FaPOD27* eingebaut worden sein. Dies wiederum führt zu einem erhöhten Ligninanteil in agroinfiltrierten Früchten, die mit Überexpressions- oder Stilllegungskonstrukten der Gene des Monolignol Biosyntheseweges infiltriert wurden. Die Herabregulation von *FaCCR* und *FaCAD* in Früchten führt zu einem reduzierten Monolignolangebot. Demzufolge sind die G-Monomere in *FaCCR* stillgelegten Früchten

sowie die G- und S-Monomere in *FaCAD* stillgelegten Früchten signifikant erniedrigt. Zudem hat das Verhältnis von G- und S- Monomeren in *FaPOD* stillgelegten Früchten signifikant abgenommen.

Hoch- oder herabregulierende Konstrukte der Gene des Monolignol Biosyntheseweges wurden einzeln oder in verschiedenen Kombinationen mittels *Agrobakterium* in stabile transgene Antisense CHS^- *F. x ananassa* Calypso (CHS^-) infiltriert. Die Transkriptionsprofile zeigten, dass sowohl der *FaCCR* Transkriptgehalt in *FaCCR* stillgelegten Früchten als auch die *FaPAL* und *FaCAD* Transkriptmenge in *FaCAD* stillgelegten Früchten simultan abnahmen. Der FaPOD Transkriptgehalt nahm signifikant in pBI-FaPOD und pBI-O3 (pBI-FaPOD, -FaCAD, -CCR) Früchten zu. Ein erhöhter Ligningehalt und somit eine verbesserte Festigkeit der Frucht wurde bei CHS^- Früchten beobachtet, welche hoch- oder herabregulierende Konstrukte von *FaCCR, FaCAD* und *FaPOD* Genen als auch eine Kombination aller drei Gene exprimieren, verglichen mit CHS^- /pBI-Intron Kontrollfrüchten. Die behandelten Früchte, welche einen CHS defizienten Hintergrund aufwiesen, zeigten ein unterschiedliches Muster von Phenolsäurederivaten. Diese Ergebnisse deuten darauf hin, dass ein komplexes Netzwerk von transkriptioneller Regulation die Monolignol-Synthese in CHS^- Früchten bestimmt.

Somit liegen ein vielschichtiger Biosyntheseweg und regulatorische Mechanismen in Pflanzen vor, die die Lignin Ablagerung und Anordnung in der Zellwand kontrollieren. Unsere Vorgehensweise die Ligninbiosynthese zu untersuchen liefert weitere Einblicke in die genetische Kontrolle der Ligninsynthese in Erdbeeren. Die Forschungsergebnisse lassen vermuten, dass *FaPOD27* ein Schlüsselgen zur Verbesserung der Erdbeerfrucht-Festigkeit darstellt.

Summary

The strawberry (*Fragaria* × *ananassa*) is one of the most consumed fruits worldwide. Unfortunately, most fruits are highly perishable, with a short shelf life. The reduction in firmness that occurs as fruit mature and ripens is due to solubilization and depolymerization of cell wall components. Lignin is a phenolic polymer associated with cellulose and hemicellulose in plant cell walls. Cinnamoyl-CoA reductase (CCR), cinnamyl alcohol dehydrogenase (CAD), and peroxidase (POD) are involved in the formation of lignin in the monolignol biosynthetic pathway. Lignin content and composition of cell wall polymers could affect fruit firmness. Hence, the study of these three genes could increase understanding of lignin synthesis in fruits and lead to improved strawberry quality and prolong the shelf-life of fresh fruits in markets.

In this study, full-length coding region sequences of *FaCCR*, *FaCAD*, *FaPOD*, and *FaPOD*27 were cloned from ripe fruit. CCR (EC 1.2.1.44) is the first committed enzyme in the monolignol biosynthetic pathway and reduces caffeoyl-, *p*-coumaroyl-, and feruloyl-CoA to yield corresponding cinnamaldehydes. Phylogenetic analysis showed that FaCCR belonged to CCRs. The conserved NWYCY motif and NAD/NADP(H) binding site are present in FaCCR. The full-length coding region sequence of *FaCCR* was heterologously expressed in *Escherichia coli* to determine its biochemical function. The recombinant GST-FaCCR protein exhibited maximum activity at pH 6 in a sodium phosphate buffer at 25℃, and had the highest affinity for feruloyl-CoA. In addition, a GST-FaCCR reaction with mixed substrates (caffeoyl-, *p*-coumaroyl-, and feruloyl-CoA) indicated that the efficiency of feruloyl-CoA (100%) was more than that of both caffeoyl-CoA (3.27%) and *p*-coumaroyl-CoA (3.17%). At the same time, LC-UV-ESI-MS^n analysis showed that reaction products yield high amounts of coniferaldehyde, and low amounts of *p*-coumaraldehyde and caffeic aldehyde. These results probably reflected the preferential biosynthesis of G units in fruits. CAD (EC 1.1.1.195) catalyzes the conversion of cinnamaldehydes to their corresponding alcohols, which are end products of the monolignol biosynthetic pathway. A phylogenetic tree of CADs revealed that FaCAD is closely related to Fxacad1 (*F.* × *ananassa* cv. Chandler) and PtSAD (*Populus tremuloides*). The conserved NAD/NADP(H) domain, as well as the Zn1 and Zn2 binding site, were present in FaCAD. Moreover, the full-length coding region of *FaCAD* was expressed in yeast (*Saccharomyces cerevisae* INVSc.1). LC-UV-ESI-MS^n analysis indicated that FaCAD activity slightly increased in yeast cells and showed that coniferyl alcohol was generated. Thus, FaCAD may be involved in the

regulation of lignin biosynthesis and contribute to production of G units in fruits. Plant peroxidases (EC1.11.1.7) are heme-containing oxidoreductases. Lignin is derived from oxidative polymerization through peroxidases which utilize H_2O_2. Prosite analysis revealed that FaPOD and FaPOD27 belonged to a plant heme peroxidase containing a putative $Ca2^+$ binding domain. They had a low level (31.9 %) of identified amino acids. The full-length coding region sequence of *FaPOD* or *FaPOD27* was heterologously expressed in *Escherichia coli*. Using guaiacol oxidase activity assays, FaPOD27 was active whereas FaPOD activity was not detected. LC-UV-ESI-MS^n analysis showed that dehydrodimers of ferulic acid and a decarboxylation product of a dehydrodimer precursor were formed by FaPOD27. The results pointed out that FaPOD27 plays an important role in polymerization in the lignin biosynthesis.

Quantitative PCR analyses revealed different expression patterns of *FaCCR*, *FaCAD*, *FaPOD*, and *FaPOD27* genes during strawberry development. *FaCCR*, *FaCAD*, and *FaPOD27* were strongly expressed in the ripe red fruit, but *FaPOD* was expressed in the unripe green fruit. These developmental expression patterns along with the activity data demonstrated that expression of lignin biosynthesis genes is induced during strawberry ripening whereas *FaPOD* is not involved in lignin formation in the fruit.

Besides, different expression patterns were found in wounded and agroinfiltrated fruits. Transcript levels of phenylpropanoid biosynthesis genes (*FaPAL*, *FaCCR*, *FaCAD*, *FaPOD*, and *FaPOD27*) were unchanged in the wounded fruits when compared with untreated fruits. However, *FaPAL* transcripts were transiently induced at 24 h upon agroinfiltration. Also, *FaPOD*27 transcripts were strongly and constitutively induced (6 h to 10 days) in fruits exposed to infection by *Agrobacterium*, suggesting that these two genes participate in defense signaling. At the same time, enhanced firmness was associated with increased lignin production in agroinfiltrated fruits. Additionally, enhanced firmness in agroinfiltrated fruits, expressing RNAi-mediated gene silencing or overexpression constructs of monolignol genes that correspond to *FaCCR*, *FaCAD*, and *FaPOD*, was associated with increased lignin production in treated fruits, as compared to wild-type (untreated) fruits. Plant lignification generated lignin polymer within the cell wall. Wiesner staining confirmed that lignin deposition and lignification around the vascular bundles were observed in fruits exposed to *Agrobacterium.* These results suggested that the accumulation of lignin in fruits injected with different constructs might restrict *Agrobacterium* invasion. Thus, lignin plays an important role in structural reinforcement of fruits following infection by *Agrobacterium*.

Monolignol genes were down- or up-regulated in strawberry fruits (*F.* × *ananassa* cv. Elsanta). Gene expressions and activities of *FaCCR* and *FaCAD* could be efficiently suppressed through RNAi in *FaCCRi*- and *FaCADi*-silenced strawberries. Overexpressing pBI-*FaPOD* constructs in fruits significantly elevated *FaPOD* transcripts. In general, metabolic profiling indicated decreased levels of *p*-coumaroyl glucoside/glucose, but increased levels of caffeoyl glucose and feruloyl glucose in treated fruits. Surprisingly, down- and up-regulation of monolignol genes in fruits resulted in no effect on fruit development and lignin content, when compared with fruits agroinfiltrated with a control construct, presumably attributed to enhanced expression levels of *FaPOD27* in agroinjected fruits. At the same time, elevated amounts of hydroxycinnamate may have been incorporated into lignin polymers by *FaPOD27* and, thus, led to enhanced levels of lignin in agroinjected fruits carrying down- and up-regulation constructs of the monolignol genes. However, down-regulation of *FaCCR* or *FaCAD* in fruits led to a reduced monolignol supply. Therefore, levels of G-monomers were significantly reduced in *FaCCR*-silenced fruits, and those of G- and S-monomers were significantly reduced in *FaCAD*-silenced fruits. Moreover, the proportion of both G- and S-monomers significantly decreased in pBI-*FaPOD* fruits.

Individual or combined down- or up-regulation constructs of monolignol genes were infiltrated in stable transgenic antisense CHS *F. x ananassa* Calypso (CHS^-) by *Agrobacterium*. Transcriptional profiles showed that *FaCCR* transcripts decreased in *FaCCR*-silenced fruits as well as *FaPAL* and *FaCAD* transcripts simultaneously decreased in *FaCAD*-silenced fruits. *FaPOD* transcripts significantly increased in pBI-*FaPOD* and pBI-O3 (pBI-FaPOD, -FaCAD, -FaCCR) fruits. Moreover, enhanced firmness, accompanied with increased lignin levels, was revealed in CHS^- fruits expressing down-regulation or up-regulation constructs of individual *FaCCR*, *FaCAD*, and *FaPOD* genes as well as a combination of the three genes, when compared with CHS^-/pBI-intron control fruits. In the CHS-deficient backgrounds, these treated fruits showed different pattern of phenolic acid derivatives. The results suggested that a complex array of transcriptional regulation may be attributed to monolignol synthesis in the CHS^- fruits.

Therefore, a complex biosynthetic pathway and regulatory mechanisms exist in plants to control lignin deposition and assembly in the cell wall. These approaches to study the lignin biosynthesis provide further insights into the genetic control of lignin synthesis in strawberries. The research results suggest that *FaPOD27* is a key gene to improve the firmness of strawberries.

I. Introduction

1. Strawberry

1.1 Background

Strawberry (*Fragaria* × *ananassa*) is the most economically important crop plant belonging to the Rosaceae family (Potter et al., 2007). Many crop plants of this family (i.e., strawberries, apples, peaches, etc.) are polyploid species. Polyploidy is common in plants as 30% to 80% angiosperms harbor one or more polyploidization events in their evolutionary history (Bennett, 2004). The cultivated octoploid strawberry *F.* x *ananassa* originated from an accidental hybridization between the two New World species *F. virginiana* and *F. chiloensis* in European gardens (Darrow, 1966) and its genome is one of the most complex of any crop species. Despite the results of phylogenetic analyses, the relationship between the 11 diploid *Fragaria* species and the parental genomes of the polyploid species remains uncertain (Potter et al., 2000). Thus, knowledge of the germplasm base of strawberries is still limited.

Strawberries are an excellent crop to be used in genetic and physiological studies because they require only a small space to grow and have a short generation time, as compared with other Rosaceae families, such as apples or peaches. Recently, an international team of scientists, led by the University of North Texas and Florida, was the first to publish the complete DNA sequences (http://www.strawberrygenome.org/) of the woodland strawberry (*Fragaria vesca*). Most notably, the cultivated octoploid *F. x ananassa* ($2n=8x=56$) harbors eight sets of chromosomes, derived from four different diploid relatives (one of them is *Fragaria vesca*). The wild diploid *F. vesca* ($2n=2x=14$) has a very small genome that is estimated to be 240 Mb. From the genetic point of view, the *F. vesca* is similar to cultivated strawberry varieties. At the same time, the wild diploid *F. vesca* does provide substantial sequence identity with cultivated strawberry varieties and other important rosaceous crops. Also, the strawberry genomics database serves as a communication center providing genomics and genetics data and analytical tools. Thus, *F. vesca* has been developed as a genomic reference for the genus and has provided useful genomics information for cultivated strawberries (Shulaev et al., 2011).

Because many rosaceous plants have complex genomes, it is difficult to identify genes with valuable traits and useful allelic variants. However, reverse genetic strategies (i.e., RNAi techniques) have been applied to cultivated strawberries (*F.* x *ananassa*) to study gene functions (Hoffmann et al., 2006). Moreover, a pyrosequencing method has been applied to

cultivated strawberries to discriminate allele-specific gene expression. For example, *FaPGIP*1a and 1b exhibited fruit-specific expression based on results of pyrosequencing (Schaart et al., 2005). Based on results from these studies, the strawberry should be considered a model plant for the functional study of Rosaceae polyploids.

1.2 Fruit growth and firmness

Cultivated strawberries (*F.* × *ananassa*) are one of the most consumed fruits worldwide. These attractive and fleshy fruits are rich sources of vitamin C, dietary fibers (i.e., plant cell wall polysaccarides), antioxidant substances (i.e., anthocyanidins), and other phytonutrients (Hancock, 1999; Chapple and Carpita, 1998; Aaby et al., 2005), that make vital contributions to human health and diet (Santos-Buelga and Scalbert, 2000).

Fruit texture plays an important role as a quality marker for consumers and especially for many industrial processes, including food processing (Manning, 1998; Lefever et al., 2004). Botanically, the strawberry fruit is not an actual berry, but an aggregate accessory fruit, consisting of a number of small dry achenes embedded on the surface of a large fleshy receptacle (Hancock, 1999). For growth of the receptacle, cell division occurs in the first 10 d, and a combination of cell division and cell expansion occurs between 10 and 15 d after anthesis (Zhang et al., 2011). Also, accumulations of water and sugars, and the synthesis of cell walls were observed between 21 and 28 d (Knee et al., 1977). Subsequently, the receptacles are becoming red and soft 25 to 30 d after anthesis (Rosli et al., 2004; Zhang et al., 2011) when the chlorophylls are lost and anthocyanins begin to accumulate in the fruit. Anthocyanins such as pelargonidin 3-glucoside and cyaniding 3-glucoside, which are responsible for the red color of the receptacle, are found abundantly in strawberries (Hancock, 1999; Aaby et al., 2005). Between 30 to 40 d after anthesis the fruits are fully ripe, depending on the temperature and the genotype (Figure 1) (Zhang et al., 2011). The strawberry is considered to be a non-climacteric fruit because ethylene has little or no effect on the development of the receptacle. Besides, ripening of the fruit does not respond to ethylene (Perkins-Veazie, 1995).

The cell walls of fleshy fruits change structures and compositions during ripening (Lefever et al., 2004). These modifications are assumed to be related with fruit softening. The plant cell wall contains polysaccharides, phenolics, and structural proteins and is a major textural component of fruits (Chapple and Carpita, 1998). The reduction in firmness observed in mature fruit and during ripening is due to solubilization and depolymerization of cell wall components.

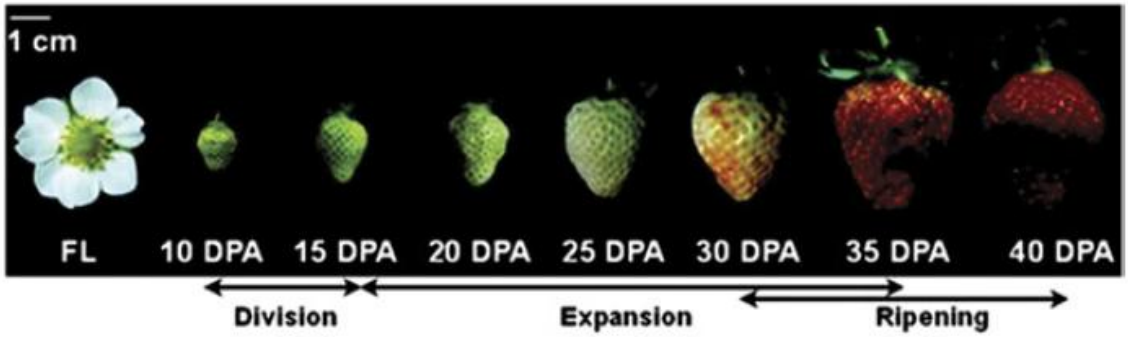

Figure 1. Fruit developmental stages of strawberry (Troyonoka) from FL (flower) to over-ripened fruit are shown. Fruits were grown in a glass greenhouse. Developing fruits are divided into three phases: cell division, cell expansion, and fruit ripening. DPA=Days after anthesis (Zhang et al., 2011).

In the early stages of maturity, fruits quickly soften between the large green ripening stage and the ripening stage with 25% red fruits (Table 2; Rosli et al., 2004). Eventually, the fully ripe fruit (100% red) is the softest of all of the mature fruit stages.

Table 2. Changes in fruit firmness during ripening of strawberry cultivars cv. Camarosa, Pajaro, and Toyonaka (Rosli et al., 2004)

Stage	Firmness (N)		
	Camarosa	Pajaro	Toyonaka
Large Green	20.34[a]	14.89[b]	13.39[c]
White	11.31[a]	3.79[b]	2.93[c]
25% red	3.62[a]	1.62[b]	1.16[c]
50% red	2.77[a]	1.42[b]	0.95[c]
75% red	2.00[a]	1.24[b]	0.89[c]
100% red	1.39[a]	0.87[b]	0.74[c]

Values with different superscript indicate significant differences when the cultivars are compared at the same stage ($P = 0.05$).

1.3 Application of genetic biotechnologies for improving fruit texture

Marketing of fresh fruit is usually limited by its short shelf life. Strawberry is a highly perishable fruit, with a short shelf life. Fruit softening leads to reduced fruit quality because a change in fruit softening causes a reduction in fruit firmness, facilitates pathogen infection, and increases fruit postharvest decay. In contrast, firm fruits display higher storage stability and reduce pathogen invasions. Thus, fruit firmness is an important target for genetic biotechnologies to improve the quality of strawberries and to prolong the shelf-life of fresh fruit in markets (Manning, 1998).

Many studies have been conducted to improve the texture of strawberries. In recent years, multiple genes encoding enzymes involved in the modification of the cell walls of strawberries have been studied. For example, particular enzymes, such as polygalacturonase (PG) and pectate lyase, have been found to affect on the pectin fraction of strawberry cell walls. The PG enzyme is considered to be the primary cell wall hydrolase involved in cell wall softening. However, this enzyme exhibits a low level of activity in strawberries (Nogata et al., 1993). Besides pectate lyase enzymes, which may be involved in cell wall softening, have a high expression level in strawberry (Medina-Escobar et al., 1997). Transgenic plants that harbor antisense pectate lyase genes showed reduced pectate lyase activity, as well as increased fruit firmness, as compared to control fruits (Jiménez-Bermúdez et al., 2002). Microarray analyses have demonstrated that strawberry cDNA samples isolated from fruits of different ripening stages display differential gene expression. Some of the differentially expressed genes are homologous to cell wall related genes. Among these candidate genes, cinnamoyl-CoA reductase (*CCR*) and cinnamyl alcohol dehydrogenase (*CAD*) are involved in the lignin biosynthesis pathway. Interestingly, these two genes displayed different expression levels among three varieties, producing fruits with firm (Holiday), intermediate firm (Elsanta), and soft (Gorella) structures. For instances, *CCR* showed higher expression levels in varieties that produce fruits with soft tissue, while *CAD* showed higher levels in the varieties with firm fruit tissue (Figure 2) (Salentijn et al., 2003). Thus, the impact of *CCR* and *CAD* on the degradation and/or rigidity of cell wall polymers should also be considered.

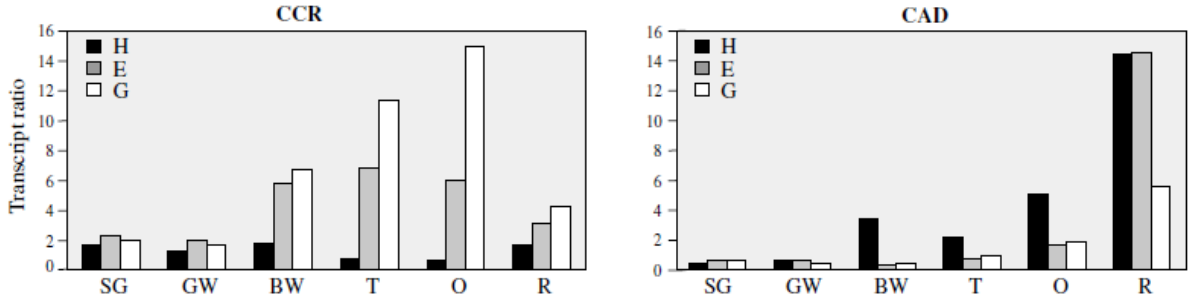

Figure 2. Gene expression levels of *CCR* and *CAD* in fruit developmental SG (small green), GW (green white), BW (white), T (turning), O (orange), and R (ripe) stages of strawberry cultivars cv. Holiday (H; firm), Elsanta (E; intermediate firm), and Gorella (G; soft) (Salentijn et al., 2003).

Lignification of plant cell walls is associated with the coordinated expression of lignin genes and enzymes. In the 'Luoyangqing' LYQ loquat fruit (*Eriobotrya japonica* Lindl.), lignification of plant tissue is associated with an increase in fruit firmness and with activities of CAD and peroxidase (POD) enzymes that are involved in lignin biosynthesis (Cai et al.,

2006; Boerjan et al., 2003). Moreover, in mangosteen fruit (*Garcinia mangostana* L.), impact damages were found to be related to enhanced lignin biosynthesis (Bunsiri et al., 2003). Until now, the basis for lignification of strawberry fruit has not been fully understood.

2. Biosynthesis pathways and core genes

2.1 Biosynthesis pathways

The phenylpropanoid branch pathways generate a wide range of phenolic compounds, including lignins, flavonoids (anthocyanins and chalcones), and hydroxycinnamates that are involved in the development of the plant and its interaction with the environment. For example, flavonoids serve as UV protection, and lignins make the wall rigid and cause plant tissue to be hydrophobic, as well as protect plants against pathogen infections (Pereira et al., 2009; Petersen et al., 1999).

Lignin biosynthesis involves three specific steps: the shikimate pathway, general phenylpropanoid pathway, and monolignol biosynthetic pathway (Vanholme et al., 2010). The shikimate pathway is the primary entry to the biosynthesis of phenylpropanoids (Vogt, 2010). In the general phenylpropanoid pathway, *p*-coumaroyl-CoA is situated at the branching point of the metabolic routes leading to either flavonoid or monolignol biosynthetic pathways (Besseau et al., 2007; Boerjan et al., 2003). Likewise, *p*-coumaroyl-CoA is the common substrate of the following three enzymes:

1) Chalcone synthase (CHS) catalyzes the reaction of one *p*-coumaroyl-CoA molecule with three malonyl-CoA molecules to produce naringenin chalcones (Figure 3). Naringenin chalcone is precursor for a large variety of flavonoids (i.e., flavonols and anthocyanins). Two major pigments found in strawberry, pelargonidin 3-glucoside and pelargonidin 3-glucoside-malonate, are derived from *p*-coumaroyl-CoA and malonyl-CoA (Hoffmann et al., 2006).

2) Hydroxycinnamoyl transferase (HCT) leads to the formation of guaiacyl (G)- and syringyl (S)-lignin building units (Figure 3). When the *HCT* gene was silenced in tobacco (*Nicotiana benthamiana*), the HCT-silenced plants had a higher level of H (*p*-hydroxyphenyl) -lignins, as well as a lower level of S-lignins in the lignin polymer, as compared to the control plants (Hoffmann et al., 2004). Besides, the flavonols and anthocyanins abounded in HCT-silenced *Arabidopsis* are accompanied with a high amount of H-lignins (Besseau et al., 2007).

3) Cinnamoyl-CoA reductase (CCR) leads to the biosynthesis of H-, G-, and S-lignin building units (Figure 3).

Lignin represents a carbon sink in the higher plants. When the carbon flow down the flavonoid pathway becomes limited, *p*-coumaroyl-CoA would flow toward the monolignol pathway (Besseau et al., 2007; Boerjan et al., 2003). Therefore, silencing of the *CHS* gene could make more *p*-coumaroyl-CoA available for the synthesis of H-, G-, and S-lignins.

The coordinated expression of several enzymes is involved in the synthesis of monolignol precursors *via* the general phenylpropanoid metabolism. Most of these enzymes required for the synthesis of lignin precursors have been extensively investigated and reviewed. In the following sections, their specific functions are briefly described (Chapple and Carpita, 1998; Boerjan et al., 2003; Whetten et al., 1998; Dixon and Reddy, 2003; Weng and Chapple, 2010).

(1) PAL (L-phenylalanine ammonia lyase)

PAL, the first enzyme of phenylpropanoid biosynthesis, catalyzes the deamination of L-phenylalanine to form *trans*-cinnamic acid at the entry point of the phenylpropanoid metabolism (Figure 4). The product, *trans*-cinnamic acid, is further channeled to lignins and related polyphenols. PAL is found in a variety of plants and plays an important role in primary and secondary metabolism. Moreover, *PAL* has been identified as one of the first plant defense genes and is involved in pathogen infections and stresses.

(2) C4H (cinnamate 4-hydroxylase)

C4H is the cytochrome P450-dependent monooxygenase (P450) enzyme involved in monolignol biosynthesis. C4H hydroxylates at the 4-position of the aromatic ring of cinnamic acid to yield *p*-coumaric acid (Figure 4). C4H is probably expressed in all tissues and upon exposure to wounding and fungal infection.

(3) 4CL (4-cinnamoyl-CoA ligase)

4CL catalyzes the conversion of hydroxycinnamic acids such as *p*-coumaric, caffeic, ferulic, and sinapic acid to their corresponding products *p*-coumaroyl-CoA, caffeoyl-CoA, feruloyl-CoA and sinapoyl-CoA (Figure 4). Phenylpropanoic acids are activated by 4CL through conjugation with coenzyme A (CoA) to form thioesters, which can be further channeled to the various branches of monolignol or flavonoid biosynthesis. Many 4CL isoenzymes present in different plant species utilize *p*-coumaric, caffeic, and ferulic acid as substrates. Recombinant His-tagged tobacco 4CL enzymes showed 70-100% activity with *p*-coumaric, caffeic, and ferulic acid, but exhibited 0% activity toward sinapic acid in *in vitro* analyses (Beuerle and Pichersky 2002). However, some isoenzymes of particular plants were able to convert sinapate into sinapoyl-CoA. *Arabidopsis At*4CL5 isoform has a high affinity for sinapic acid *in vitro* (Rautengarten et al., 2010).

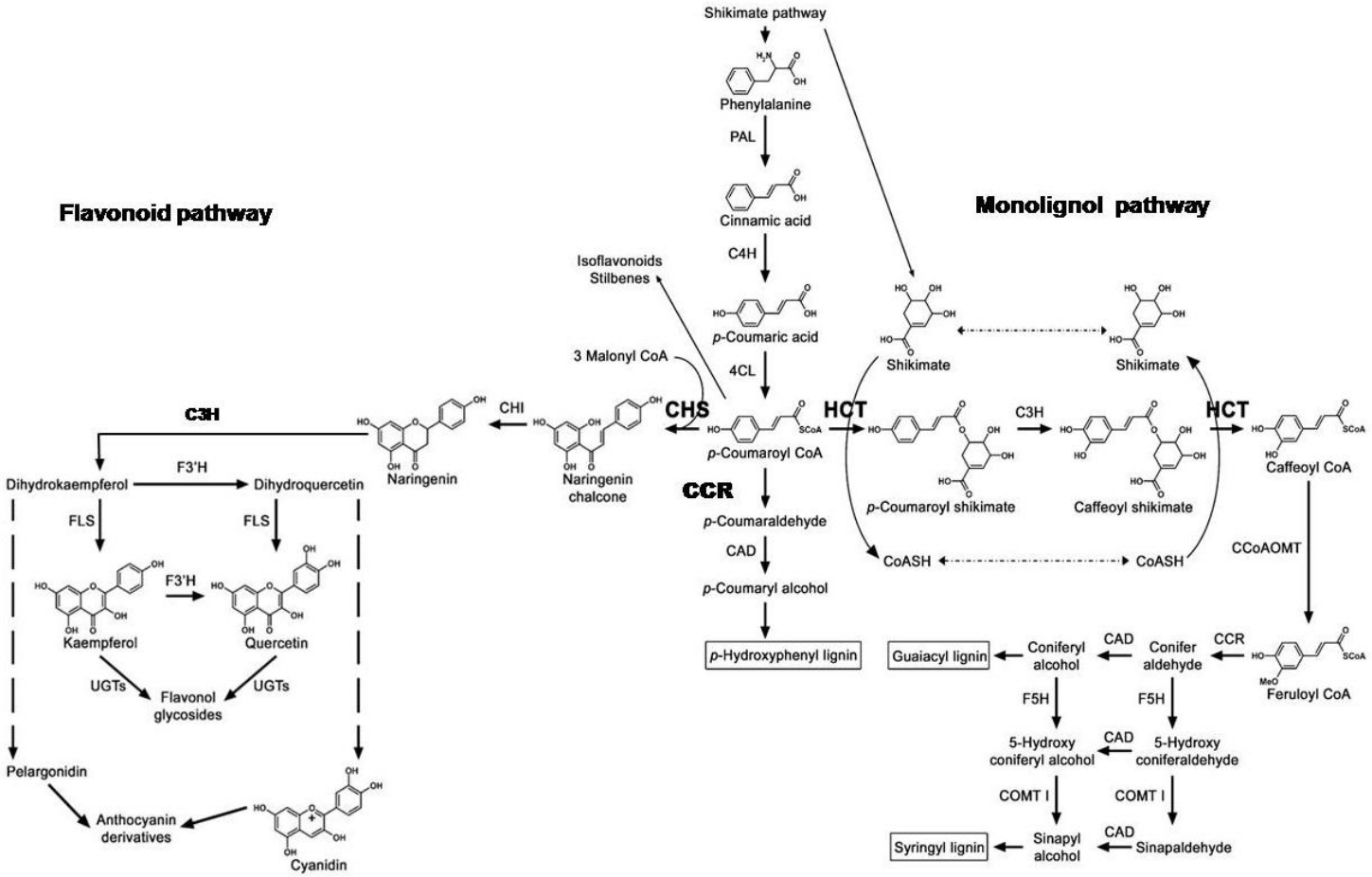

Figure 3. The phenylpropanoid pathway leading to the flavonoid and monolignol biosynthetic pathway.

Enzymes and their abbreviations are as follows: C3H, *p*-coumaroyl shikimate 3-hydroxylase; C4H, cinnamate 4-hydroxylase; F5H, ferulate 5-hydroxylase; HCT, hydroxycinnamoyl transferase; CAD, cinnamyl alcohol dehydrogenase; CCoAOMT, caffeoyl-CoA O-methyltransferase; CCR, cinnamoyl-CoA reductase; CHI, chalcone isomerase; 4CL, 4-coumaroyl-CoA ligase; COMT I, caffeic acid O-methyltransferase of class I; F3H, flavanone 3-hydroxylase; F3´H, flavonoid 3´-hydroxylase; FLS, flavonol synthase; PAL, phenylalanine ammonia lyase; UGTs, UDP sugar glycosyltransferases (Besseau et al., 2007).

(4) HCT (Hydroxycinnamoyl transferase)

HCT is an acyltransferase that catalyzes the conversion of *p*-coumaroyl-CoA and caffeoyl-CoA to their corresponding shikimate and quinate esters. These esters are intermediates in the phenylpropanoid pathway and they can be subsequently channeled to the biosynthesis of methoxylated phenylpropanoids.

(5) C3H (*p*-coumaroyl shikimate 3´-hydroxylase)

C3H is a cytochrome P450 that catalyzes aromatic hydroxylation reactions in the monolignol biosynthetic pathway. C3H hydroxylates, at the 3-position of the aromatic ring of *p*-coumaroyl shikimic (or quinic) acid, yields caffeoyl shikimic (or quinic) acid. C3H is associated with HCT, and is involved in the production of coniferyl and sinapyl alcohol (Figure 4).

(6) CCoAOMT (caffeoyl-CoA O-methyltransferase)

CCoAOMT is a bifunctional enzyme that catalyzes the methylation of caffeoyl-CoA to feruloyl-CoA as the first methyltransferase in the pathways leading to the biosynthesis of coniferyl alcohol. At the same time, it also catalyzes the methylation of 5-hydroxyferuloyl-CoA to sinapoyl-CoA as the second methyltransferase in the pathway leading to the biosynthesis of sinapyl alcohol. CCoAOMT is associated with COMT (Figure 4).

(7) COMT (caffeic acid O-methyltransferase)

COMT performs bifunctional methylation in the lignin-specific branch of the phenylpropanoid pathway leading to the formation of G and S lignin. COMT catalyzes both the methylation of caffeic acid to ferulic acid and 5-hydroxyferulic acid to sinapic acid (Figure 4).

(8) F5H (ferulic acid 5-hydroxylase)

F5H is a cytochrome P450-dependent monooxygenase that catalyzes the hydroxylation of ferulic acid, coniferaldehyde and coniferyl alcohol. The products of F5H are substrates for COMT in the pathway leading to the biosynthesis of S lignin (Figure 4).

(9) CCR (cinnamoyl-CoA reductase)

CCR, the first enzyme of the monolignol biosynthetic pathway, is situated at the branching point of the metabolic routes leading to the formation of H-, G-, and S-lignin. CCR reduces the CoA-thioesters of *p*-coumarate, ferulate, and sinapate to yield the corresponding aldehydes in the monolignol biosynthetic pathway (Figure 4). Detailed descriptions of CCR can be found in 2.2.

(10) CAD/ SAD (cinnamyl/sinapyl alcohol dehydrogenase)

CAD and/or SAD catalyze the reduction of hydroxycinnamyl aldehydes to their

corresponding alcohol, the last steps in the monolignol biosynthetic pathway (Figure 4). Detailed descriptions of CAD can be found in 2.2.

(11) Peroxidase/laccase

Peroxidases and laccases are heme-containing and copper-containing oxidoreductases, respectively. Both types of enzymes oxidize phenolic substrates *via* one-electron oxidations to create radicals (Figure 4). Detailed descriptions of POD can be found in 2.2.

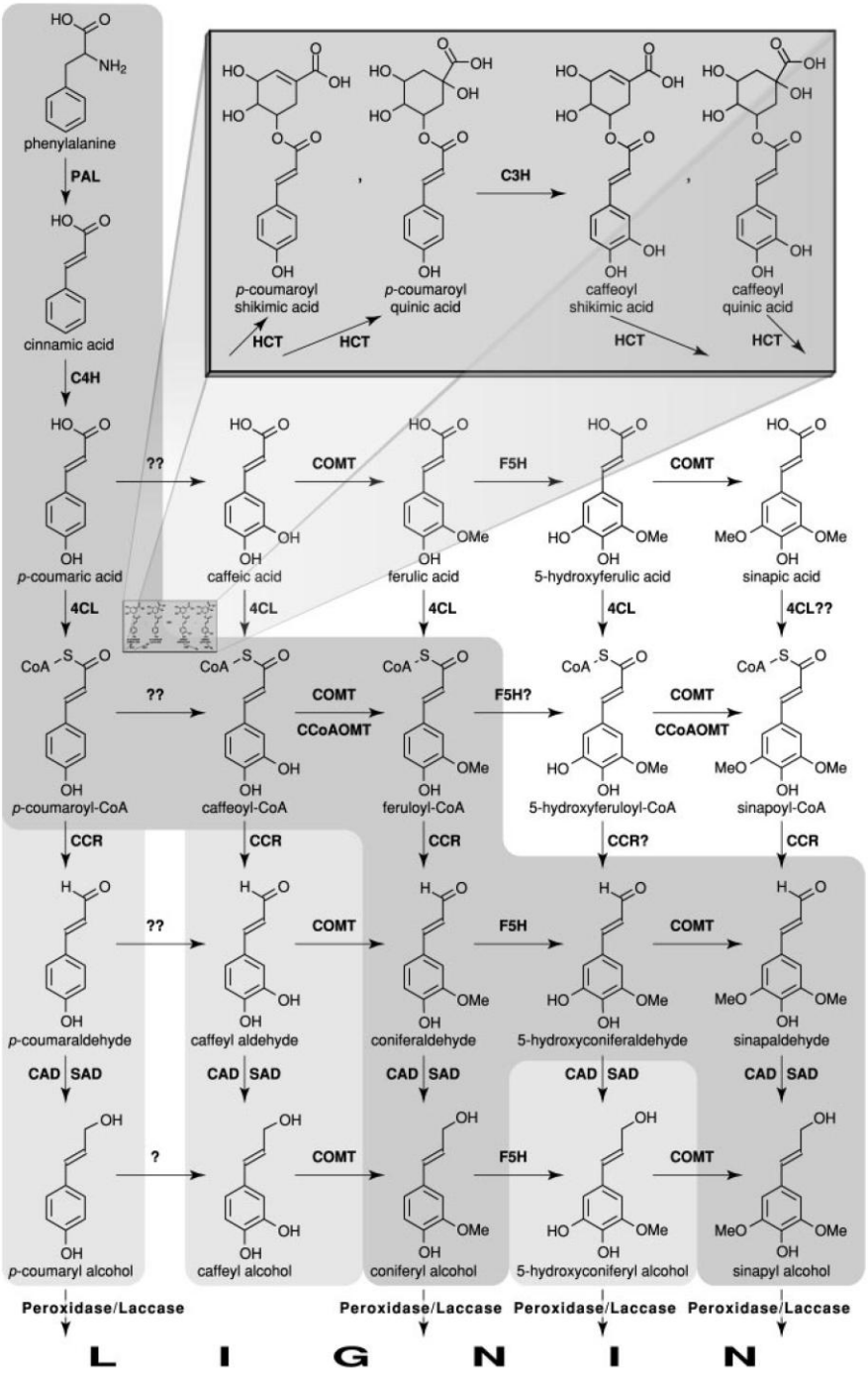

Figure 4. An outline of the general phenylpropanoid and monolignol biosynthetic pathways (Boerjan et al., 2003). The grey route is favored in angiosperms. ? = conversion has been demonstrated, but the enzyme needs to be identified further. Enzymes and their abbreviations are as described above (Figure 3).

2.2 Regulatory core genes for monolignol biosynthesis

CCR, CAD, and POD are considered to be the key enzymes that control the quantity and quality of lignins in the plants (Boerjan et al., 2003; Li and Chapple, 2010). These core genes have been extensively investigated in some plants. They have been cloned and characterized. This study mainly focused on a detailed analysis of these genes in strawberries.

(1) CCR (Cinnamoyl CoA reductase; EC 1.2.1.44)

CCR is the first committed enzyme of the lignin branch biosynthetic pathway, where CCR catalyzes the conversion of hydroxycinnamoyl-CoA thioesters to their corresponding aldehydes in the presence of NADPH as cofactor (Figure 5, Sarni et al., 1984). CCR has been shown to be a control point in regulating carbon flux to monolignol biosynthesis (Lacombe et al., 1997).

CCR enzymes with broad substrate specificities exist in various species such as tomatoes, wheat, *Arabidopsis*, and switchgrass. LeCCR2 from tomato (van der Rest et al., 2006) showed a high affinity only towards feruloyl-CoA, but PvCCR2 from switchgrass preferred caffeoyl and *p*-coumaroyl-CoA (Escamilla-Trevino et al., 2010). The predominant role of TaCCR1 from wheat (Ma and Tian, 2005) and LeCCR1 (van der Rest et al., 2006) was shown to be the formation of coniferaldehyde. In contrast, *p*-coumaroyl-CoA, caffeoyl-CoA, and sinapoyl-CoA were poor substrates for other CCRs. Most importantly, the substrate specificity of CCRs was the determining factor in the formation of H-, G-, and S-lignin in plants. CCRs that show a high affinity towards *p*-coumaroyl-CoA yielded higher levels of H-lignin in the plants.

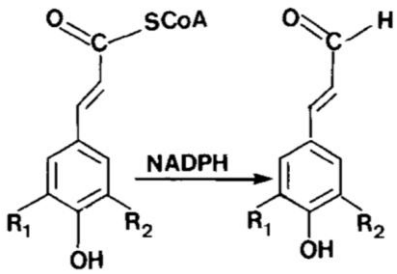

Figure 5. Enzymatic reaction catalyzed by hydroxycinamoyl CoA reductase (Sarni et al., 1984). R_1=R_2=H: *p*-coumaroyl-CoA→ *p*-coumaraldehyde, R_1=H, R_2=OH: caffeoyl-CoA → caffeyl aldehyde, R_1=H, R_2=OCH_3: feruloyl-CoA→coniferaldehyde, R_1=R_2=OCH_3: sinapoyl-CoA→sinapaldehyde

CCR genes have been cloned and characterized in several plant species. To date, cloning of a *CCR* gene from strawberry has not been reported. CCRs accumulate to high levels in tissues undergoing active lignifications. It has been shown that CCR enzymes have a diversity of functions depending on their distinct isoforms. *ZmCCR1* from maize was preferentially expressed in all lignifying tissues, and *ZmCCR2* was expressed in roots and induced by drought (Pichon et al., 1998). In *Arabidopsis thaliana*, *AtCCR1* and *AtCCR2* have been compared during development or infection with *Xanthomonas campestris*. *AtCCR1* was mainly expressed in growing tissues, whereas *AtCCR2* showed lower expression levels. However, *AtCCR2* was primarily involved in pathogen defense because mRNA was strongly induced following infection by *X. campestris* (Lauvergeat et al., 2001).

(2) CAD (Cinnamyl alcohol dehydrogenase; EC 1.1.1.195)

CAD catalyzes the NADPH-dependent conversion of hydroxycinnamyl aldehydes to their corresponding hydroxycinnamyl alcohols (Figure 6) that are lignin precursors for lignin polymerization in cell walls of gymnosperms and angiosperms (Sarni et al., 1984).

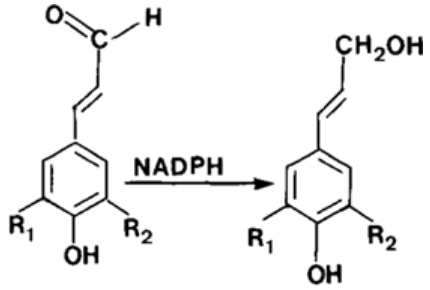

Figure 6. Enzymatic reaction catalyzed by cinnamyl alcohol dehydrogenase (Sarni et al., 1984). R_1=R_2=H: *p*-coumaraldehyde → *p*-coumaryl alcohol, R_1=H, R_2=OCH_3: coniferaldehyde→ coniferyl alcohol, R_1=R_2=OCH_3: sinapaldehyde→ sinapyl alcohol

Gymnosperm CAD is encoded by a single gene. Its activity is highly specific for the reduction of coniferyl aldehyde, and low for sinapyl aldehyde (O'Malley et al., 1992; Galliano et al., 1993). In contrast, angiosperm CAD is encoded by a multigene family that has affinity for both coniferyl and sinapyl aldehyde (Brill et al., 1999). Angiosperm aspen (*Populus tremuloides*) SAD preferentially reduces sinapaldehyde and aspen CAD reduces sinapaldehyde and coniferaldehyde to sinapyl and coniferyl alcohol, respectively. Remarkably, SAD may be responsible for the last step in the biosynthesis of syringyl lignin in angiosperms (Li et al., 2001). In addition, angiosperm CADs utilize diverse aromatic substrates, including benzylaldehydes. The recombinant FxaCAD1 (*F.* × *ananassa* cv.

Chandler) enzyme expressed in *Pichia pastoris* cells exhibited high activity with cinnamyl (100% activity = V_{max} of 0.62 umol $min^{-1}mg^{-1}$ protein), coniferyl (51.2%), and sinapyl (64.3%) aldehydes, and also low activity with other benzylaldehydes (less than 10%, (Blanco-Portales et al., 2002).

A number of *CAD* genes have been isolated and characterized in many plant species, including *Arabidopsis* (Kim et al., 2004), sorghum (Saballos et al., 2009), aspen (Li et al., 2001), and strawberry (Blanco-Portales et al., 2002). Of the nine identified CAD-homologues proteins in the *Arabidopsis* CAD family, AtCAD4 and AtCAD5 were identified as the main enzymes involved in lignification of the vascular tissue (Kim et al., 2004). Besides, Sorghum CAD2 is considered to be the predominant CAD involved in lignification (Saballos et al., 2009). Taken together, angiosperms are capable of forming guaiacyl-syringyl lignins in a plant body. However, it is not fully understood whether a single enzyme or several enzymes are responsible for the formation of the three hydroxycinnamyl alcohol intermediates. Also, individual CAD genes are not assigned a unique function because they undergo the complementation capacity of the CAD multienzyme network (Whetten et al., 1998).

In addition, CADs have been shown to be expressed in different stages of plant development or in response to elicitors, wounding, and plant defense reactions. Transgenic plants harboring CAD promoter-GUS constructs displayed high GUS activity in roots, stems, and leaves (Feuillet et al., 1995; Walter et al., 1994). Northern experiments showed a high *CAD* gene expression in the stems and tissues undergoing active lignifications (Grima-Pettenati et al., 1993). Moreover, high expression levels of *Fxacad* gene (*F.* × *ananassa* cv. Chandler) were observed in different fruit ripening stage (Blanco-Portales et al., 2002). In contrast, some of *CAD* genes are involved in defense responses or metabolic processes not related to the lignification of the vascular tissue (Brill et al., 1999). These data indicate that different members of the CAD gene family are differentially regulated or controlled in response to signals from either developmental growth or environmental stimuli.

(3) POD (plant peroxidases; EC 1.11.1.7)

Peroxidases (EC 1.11.1.X) belong to a superfamily that mainly falls into three different classes: (1) Class I intracellular peroxidases include cytochrome-*c* peroxidases, catalase-peroxidases, and ascorbate peroxidases (EC 1.11.1.5/.6/.11); (2) Class II peroxidases include manganese, lignin, and versatile peroxidases (Ruiz-Dueñas et al., 2001) (EC 1.11.1.13/.14/.16); and (3) Class III secretory peroxidases are from higher plants (EC

1.11.1.7) (Welinder, 1992). A variety of biological functions in plants are associated with these peroxidases. Class I ascorbate peroxidases show a very high affinity for ascorbate and are found in photosynthetic organisms (Teixeira et al., 2004). Class II peroxidases are capable of degrading lignin extensively (Martinez et al., 2005). Class III peroxidases catalyze the reduction of H_2O_2 by taking electrons from a number of electron donors, such as phenolic compounds, lignin precursors, or secondary metabolites. In particular, class III peroxidases are plant-specific oxidoreductase and are located in cell walls and vacuoles (Welinder, 1992; Cosio and Dunand, 2009). Hence, the role of class III peroxidases in the strawberry was analyzed in this study.

Class III peroxidases are haem-containing enzymes (also called plant peroxidase; hydrogen donor: hydrogen-peroxide oxidoreductase) that form large multigenic families (e.g., 73 genes in *Arabidopsis* and 138 genes in *Oryza sativa*) in all higher plants (Welinder, 1992; Welinder, 2002; Passardi et al., 2004a). Different abbreviations (POD, POX, POD, Px, and PER) are used for class III plant peroxidases in various research papers. Usually, PODs contain two structural Ca^{2+} ions, protohaemin IX (haem b) as the prosthetic group and they have a molecular mass in the 30-45 kDa range (Almagro et al., 2009). In higher plants, PODs exist as isoenzymes, whose expressions are differentially regulated. They occur in the plant life cycle, from the germination to senescence, and also exist in one organ or tissue within several isoforms that are expressed at the same time. PODs activity can be detected in most tissues of the plant (Passardi et al., 2005). Remarkably, PODs have the highest activity in the roots and the largest number of isoenzymes. Typically, plant species may contain 10 to 20 peroxidase isoenzymes. Some of these isoenzymes are from divergent genes, which show less than 50% identical amino acids in their peptide sequences (Welinder, 1992). Other isoenzymes may be from the same gene and they differ only in the carbohydrate moiety (Lagrimini et al., 1990).

Several studies have revealed that PODs are involved in a broad range of normal and stress-related physiological processes, such as regulation of cell elongation, phenol oxidation, production of lignins, lignification, cross-linking of cell wall components, and defense against pathogens (Figure 7A) (Almagro et al., 2009). However, the biological functions of most peroxidases remain elusive or have not been conclusively determined. Microarray data have shown that 44 out of 73 *Arabidopsis* class III peroxidases genes are putatively involved in specific mechanisms, such as monolignol polymerization and lignification of vascular bundles (Cosio and Dunand, 2009).

(A)

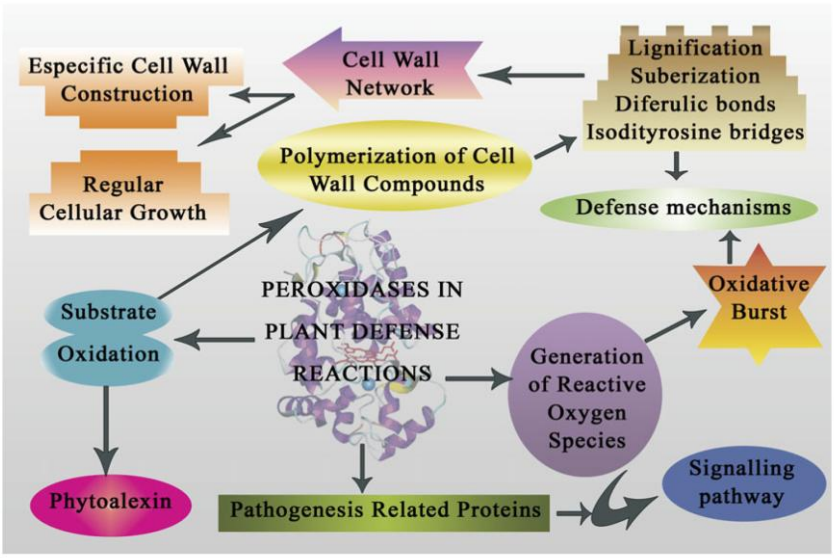

(B)

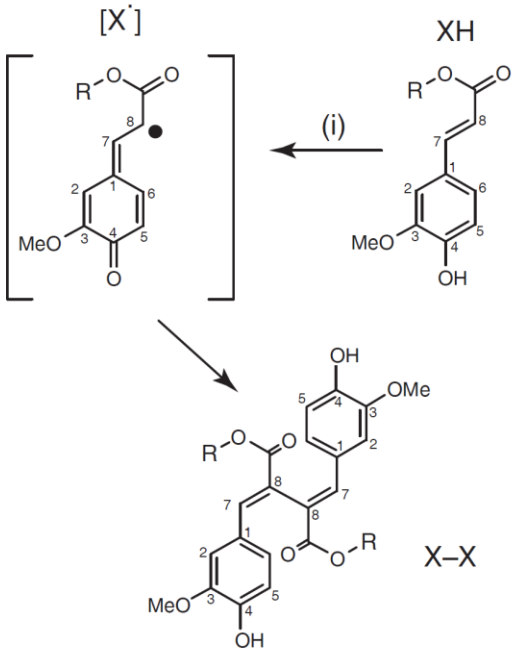

Figure 7. (A) Plant peroxidase plays specific roles in defense reactions (Almagro et al., 2009). (B) Peroxidases in the cell wall cross-linking mechanism (Passardi et al., 2004b). Coupling may occur at 5-5-, 8-5- (also called β-5)- or 8-O-4- (β-O-4)-coupled dehydroferulate ester positions. One example: (i), Peroxidase; R, bound polysaccharide; XH, ferulate ester; X´, ferulate ester radical intermediate; X-X, 8-8 (β-β)-coupled dehydroferulate ester.

Generally, PODs utilize H_2O_2 for cross-linking of cell wall components related to lignin formation and cross-linking of feruloylated polysaccharides. PODs oxidize various substrates such as monolignols, ferulic acids, and ferulate ester, which can be incorporated

in the branched lignin (Figure 7B; Passardi et al., 2004b). They produce phenoxy radicals leading to the formation of specific linkages (diphenolic) between cell wall polymers, causing cross-link formation and stiffening of the cell wall (Passardi et al., 2004a). However, different PODs have various abilities to oxidize a wide variety of substrates. Most of the PODs are able to oxidize coniferyl alcohol. Also, some of the PODs (i.e., tomato, poplar) can oxidize sinapyl alcohol *via* an unmediated way. However, sinapyl alcohol seems to be a poor substrate for some of PODs, suggesting that sinapyl alcohol dehydrogenation is mediated by other phenolic radicals during lignin synthesis (Marjamaa et al., 2009).

In addition, one of the most studied functions of PODs is their role in lignifications (Almagro et al., 2009). In particular, several POD isoforms have been found in lignifying secondary xylem. RT-PCR analysis has shown that *PabPOD02*, *PabPOD03*, *PabPOD08*, *PabPOD13*, and *PabPOD14* genes from Norway spruce (*Picea abies*) are expressed in all of the lignin forming materials, such as the lignifying tissue-culture line, and mature and young vertical xylems (Koutaniemi et al., 2007). Over-expression of the gene encoding POD has been found to cause ectopic lignification in transgenic tomato plants (*Lycopersicon esculentum*) (El Mansouri et al., 1999).

Besides, lignin production and lignification of plants have been accompanied by an increase in the activity of class III peroxidases when plants were responding to environmental stimuli, such as wounding and pathogen attacks (Passardi et al., 2006). The induction of POD genes in plant resistance against a bacterial pathogen has been demonstrated in interactions between rice and *Xanthomonas oryzae* pv. *oryzae* (Chittoor et al., 1997). Lignins have been proposed to act as barriers to obstruct the passage of the pathogen in plants (Passardi et al., 2005).

3. Lignin and lignification

3.1 Lignin

Lignin, the second most abundant natural compound after cellulose, is a phenolic polymer associated with cellulose and hemicellulose in plant cell walls. Lignin is a major component of some secondary walls where aromatic compounds (e.g., monolignols) are linked together (Boerjan et al., 2003).

Lignin is derived from oxidative polymerization of three different hydroxycinnamyl alcohols (monolignols: *p*-coumaryl alcohol, coniferyl alcohol, and sinapyl alcohol) referred to as *p*-hydroxyphenyl (H), guaiacyl (G), and syringyl (S) lignin, respectively. In general, monolignols are end products of the phenylpropanoid pathway. After monolignol

biosynthesis, these monolignols must be transported from the cytoplasm to the cell wall followed by free radical-mediated polymerization. However, the transport mechanisms of monolignols from the cytoplasm to the cell wall are still unclear (Marjamaa et al., 2009; Li and Chapple, 2010). The phenolic polymer lignin is polymerized by random phenol radical-radical coupling reactions of monomers in the cell wall. The precursors (monolignols) of lignin can couple radically and cross-couple at several sites with each other and with the growing lignin to produce a complex and cross-linked lignin polymer (Figure 8) (Weng and Chapple, 2010). Also, non-traditional phenolics (e.g., ferulic acid), hydroxycinnamyl aldehydes, acylated monolignols can be incorporated into growing lignins (Ralph et al., 2008; Hayashi, 2006).

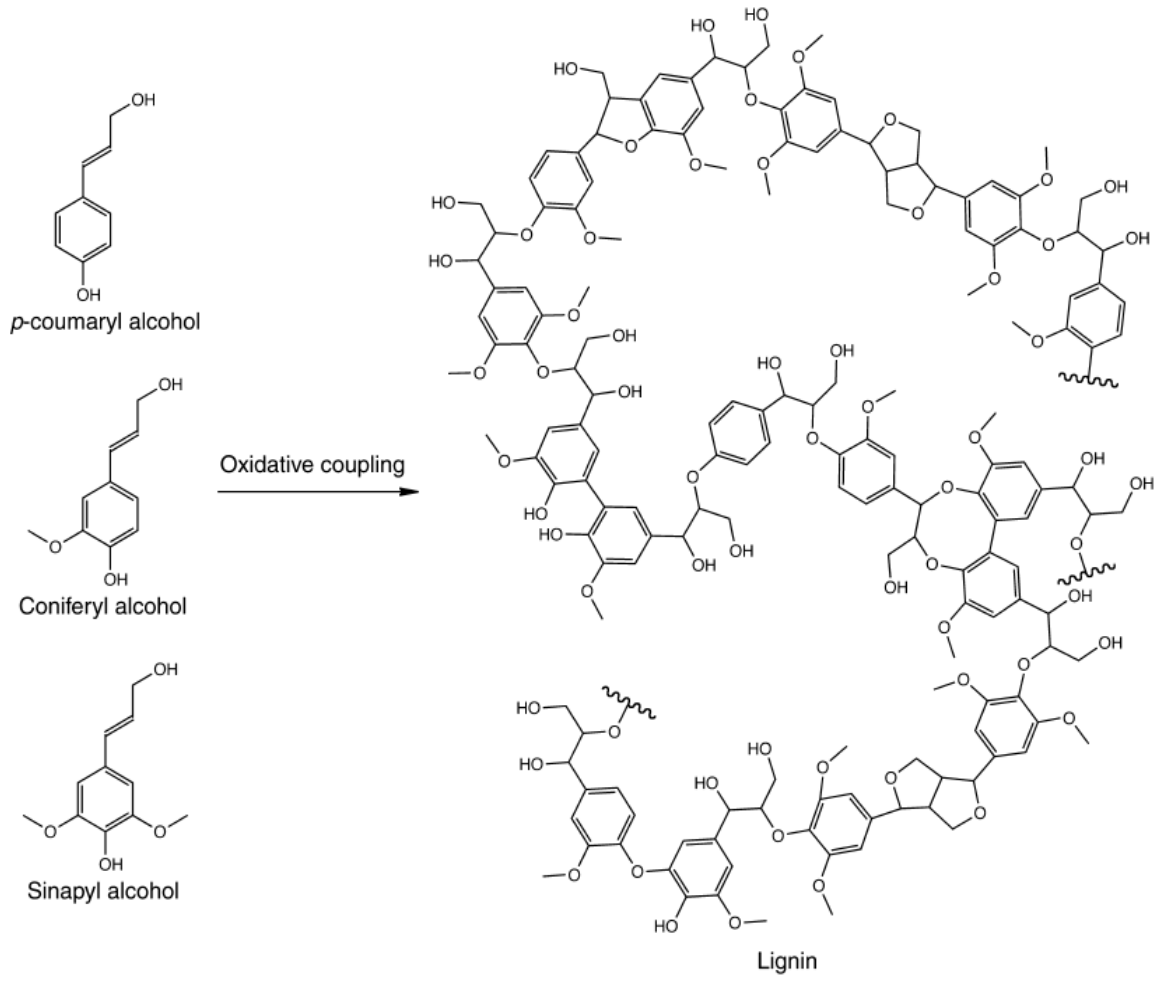

Figure 8. The phenolic polymer lignin is randomly polymerized from *p*-coumaryl alcohol, coniferyl alcohol, and sinapyl alcohol (Weng and Chapple, 2010).

Lignins are found in vascular plants such as gymnosperms and angiosperms (flowering plants). They are deposited in tracheary elements, sclerenchyma, phloem fibres, and periderm, especially in secondarily thickened walls of these cells (Dixon, 2001). Moreover,

lignin content and composition vary among different classes of plants. There are two major classes: (1) gymnosperm lignins primarily contain G-lignin (also called G units) derived from coniferyl alcohol and a low content of H-lignin (H units) derived from *p*-coumaryl alcohol; (2) angiosperm lignins contain both syringyl units (S units) derived from sinapyl alcohol and G units, and a low content of H units. Hardwood angiosperm produces primarily G- and S-lignin and a small proportion of H-lignin, whereas softwood gymnosperm lignin produces mostly G-lignin with low content of H-lignin (Boerjan et al., 2003; Whetten et al., 1998). Softwoods have higher lignin content than hardwoods. Remarkably, changes in lignin content and composition do exist in different cell types and stages of tissue development (Li and Chapple, 2010). The lignin in the tracheary elements of *Arabidopsis* vascular bundles mainly contains G units, whereas the adjacent highly lignified sclerenchyma contains large numbers of S units (Chapple et al., 1992). Such a difference in lignin composition is reflected in the substrate specificity of enzymes or the regulated differential carbon flow into the synthesis of various lignin precursors in lignin biosynthesis. This results in the incorporation of these subunits into lignins with variable proportions. Altogether, lignin is a complex three-dimensional polymer of hydroxylated and methoxylated phenylpropane units, and it functions as mechanical support for plant organs, in defense against pathogenic attacks, and in water transport in vascular plants (Boerjan et al., 2003; Dixon, 2001).

3.2 Lignification

Lignification is the process by which monomeric units are assembled *via* radical-radical coupling reactions (Boerjan et al., 2003). The monolignols are coupled at various sites, including β-O-4, and 1-carbon of coniferyl and sinapyl alcohol, and 5-carbon of coniferyl alcohol. They mainly couple their β-positions with phenolic ends on a growing polymer (Hayashi, 2006). The monomeric units in lignin are linked together through at least six different types of linkages, including β-O-4, β-5, β-β, 5-5, 4-O-5, and dibenzodioxocin (Figure 9; Weng and Chapple, 2010). The β-O-4 (β-aryl ether) group is the most frequent linkage, with lignin comprising more than 50% of this linkage group. In addition, lignification frequently produces various units, which may be from monolignol dimerization or bulk polymerization (Boerjan et al., 2003). Polymerization proceeds *via* free radical reactions, initiated by peroxidases, which utilize H_2O_2 as a substrate, or by laccases, which use O_2. Both types of enzymes are candidates for the oxidation of monolignols. Peroxidases build a dense extension network to make the cell wall rigid (Vanholme et al., 2010). Recently, a thioacidolysis method has been employed to determine the relative lignin

structures and proportions of monolignols. Thioacidolysis provides information on the ratio of syringyl to guaiacyl units (S/G ratio) and on the frequency of interunitary linkages in a lignin polymer (Ralph et al., 2008). However, peroxidases oxidize a wide range of substrates. For example, ferulic acid, caffeic acid, coniferyl alcohol, hydroxycinnamaldehydes, and dihydroconiferyl alcohol are precursors of the lignin formation (Whetten et al., 1998). Also, monolignols may form bonds to link other cell wall polymers such as cellulose. Thus, various linkages probably link lignin precursors together in the lignin polymer that leads to complexity in the three-dimensional network. Moreover, some types of bonds are hard to break in the lignin polymer network. The β-O-4 linkage is easily cleaved chemically, whereas the other linkages (β-5, β-β, 5-5, and 4-O-5) are more resistant to chemical degradation (Boerjan et al., 2003). Until now, the mechanisms that determine the relative proportion of the linkage types in the lignin polymer and the precise structure of the lignin polymer have generally remained unknown (Hayashi, 2006).

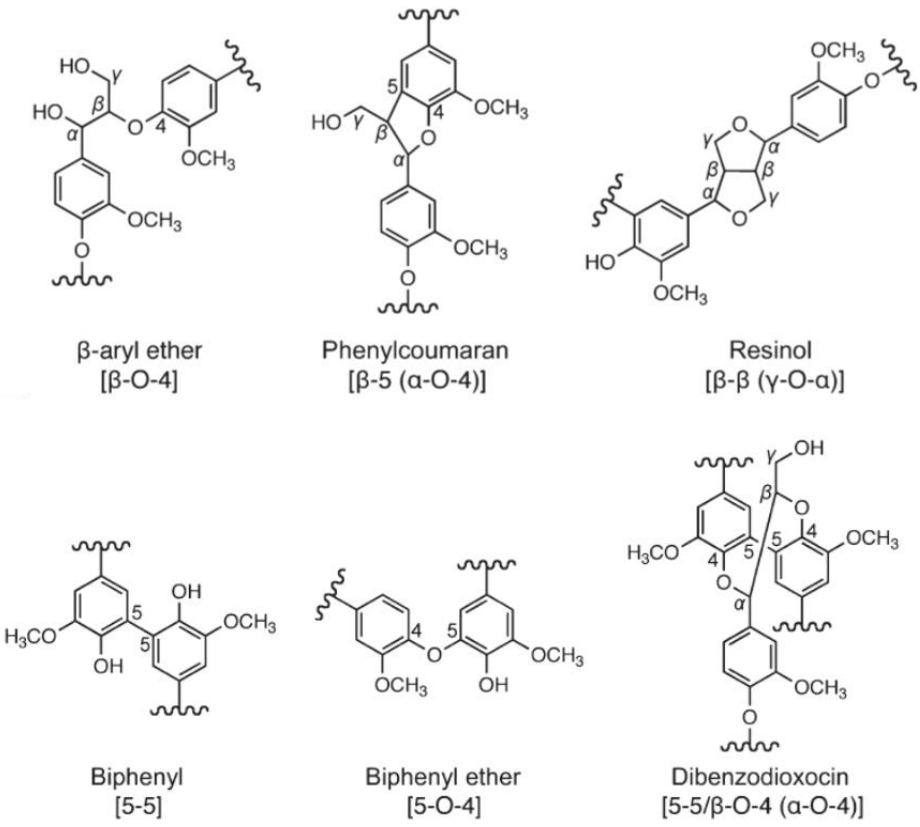

Figure 9. Major linkages present in the lignin polymer (Weng and Chapple, 2010).

Lignification changes the characteristics of a cell wall. Lignification usually occurs during plant growth, when cell growth is completed or cells undergo secondary growth (Passardi et al., 2004b). In addition, lignification is a well-known mechanism of disease resistance in

plants because it is a response to various environmental stresses such as pathogenic attacks (Dixon, 2001). Lignification of plant cells around the site of pathogen infections has been suggested as limiting the spread of pathogen. Besides, deposition of phenylpropanoid compounds is a part of cell wall reinforcement and is characteristic of infection (Nicholson and Hammerschmidt, 1992). During defense responses, lignin and lignin-like phenolic compound accumulation have been shown to occur in a number of plant-pathogenic bacterial or fungal interactions. Ferulic acid that accumulates in wheat exposed to *Agrobacterium* is a precursor of monolignol biosynthesis, suggesting that the existence of a defense response may reduce bacterial infection (Parrott et al., 2002).

4. Changes in the lignin content and composition

4.1. Stresses

Lignin biosynthesis is a complex genetic network, where several enzymes can be induced by various abiotic (plant injuries, mineral deficiency, drought, low temperatures, etc.) or biotic (fungi, bacterial infection, etc.) stresses (Moura et al., 2010). In order to resist various stresses, plants may modify lignin content and/or lignin composition in the plant body. In this study strawberry fruits were agroinfiltrated. Thus, they were exposed to wounding (i.e., perforation of the fruits by using a syringe) and infected with a pathogen (i.e., *Agrobacterium*). In this regard, the study focused on the plant injuries and pathogen infections that altered the quantity and composition of lignin in the plants. Further understanding of the expression of lignin-related genes will possibly allow researchers to elucidate genetic control of lignin synthesis and control lignin deposition in the cell wall.

(1). Plant injuries (wounding)

Plants have developed several strategies to avoid pathogen infections and water loss in response to injury or wounding, suggesting that these strategies include production of phytoalexins or physical barriers such as lignin accumulation and lignification (Moura et al., 2010). Microscopy and histochemical analyses showed the formation of a barrier zone in the wounded tissue (*Eucalyptus gunnii*), indicating that the cell walls were associated with intensification of lignin deposition (Hawkins and Boudet, 2003). *Chamaecyparis obtusa* exposed to injury led to the accumulation of lignin and ferulic acid in the phloem, and induction of lignification in the necrotic phloem after 7 d. The concentration of ferulic acid was higher 7 d after injury, suggesting that ferulic acid had accumulated in the cell before

formation of lignin (Kusumoto, 2005). Wound-induced deposition of polyphenolic acids is considered to play a role in resistance responses.

Based on this information, it is important to gain a better understanding of whether the spatial and temporal expression of lignin-related genes is responsible for promoting the formation of lignin to resist stress. Several studies have demonstrated that the induction of genes is related to lignin biosynthesis as a plant's response to wounding. In the case of wounding, peroxidase expression is probably triggered to repair the damaged tissue, as well as to provide a defense response against pathogen infections (El Mansouri et al., 1999). In another experiment, the expression of *At4CL* genes from *Arabidopsis thaliana* was induced in a wounded leaf. After wounding, *At4CL1* and *At4CL2* exhibited different induction times until they reached their maximum expression levels at 2.5 h and 48-72 h, respectively (Soltani et al., 2006). Also, gene expression of *4CL, CAD* and *CCR* increased in the injured leaves of *Arabidopsis* (Delessert et al., 2004).

The removal of the stem apex caused an increase in the activities of CAD and SAD, leading to G and S lignin assembly in *Eucalyptus gunnii* (Hawkins and Boudet, 2003). Also, the expression of *CaF5H1* from *Camptotheca acuminate* increased in detached leaf discs, resulting in promotion of the biosynthesis of S-lignin (Kim et al., 2006). These observations suggested that various expression levels of lignin-related genes caused various incorporation rates of coniferyl and sinapyl precursors into the lignin polymer.

(2). Pathogen infections

Plants have developed complicated defense strategies for responding to pathogen attacks, referred to as plant innate immunity. Plant innate immunity is coordinately regulated by a complex signaling network. Cell wall lignification, pathogen related (PR) gene induction and hypersensitive response (HR) also occur in plant immune systems (Cohn et al., 2001). For example, wheat exhibited a hypersensitive reaction following infection by *Puccinia graminis* (Moerschbacher et al., 1990). An increase in lignification was usually observed in response to pathogen infection, suggesting that a defense signal was generated.

The *CCR* gene is strongly induced by pathogens in *Arabidopsis* and rice, indicating that this gene may participate in the hypersensitive response to the pathogen (Lauvergeat et al., 2001; Kawasaki et al., 2006). Likewise, gene expressions of *PAL, CAOMT, F5H, CCoAMT,* and *CAD* are elevated in the epidermis of wheat (*Triticum monococcum*) infected with *Blumeria graminis* (Bhuiyan et al., 2009). Thus, plants trigger a series of defense responses accompanied by induction of particular lignin-related genes in the lignin biosynthesis pathway.

Lignin content increased in plants following pathogen infections (Bonello and Blodgett, 2003). Lignin induction occurs in the infected plants, in which a mechanical barrier may diminish the probability of pathogen invasion. *Sphaeropsis sapinea* exhibited an increase in the deposition of lignin after infection by *Pinus nigra* (Bonello and Blodgett, 2003) and Chinese cabbage increased H_2O_2 accumulation and peroxidase activity after exposure to *Erwinia carotovora* (Zhang et al., 2007). Induced H_2O_2 production may stimulate polymerization of monolignols in the infected regions (Almagro et al., 2009). Taken together, the production of lignin-building monolignol units are strongly activated in infected plants as the result of exposure to a pathogen or other elicitors.

4.2. Transgenic and mutagenic approaches

Most of the genes involved in monolignol synthesis have been cloned and characterized from plant model species such as *Arabidopsis*, tobacco, and poplar. Transgenic plants and mutants have provided first clues of the functions of lignin-related genes. Several studies have reported on the impact of *CCR, CAD,* and *POD* down-regulation and overexpression in transgenic plants and mutant lines on the reduction or increase of lignin content and modification of lignin composition (Whetten et al., 1998).

(1) CCR

CCR is the first enzyme in the lignin-specific branch of the monolignol biosynthetic pathway. Manipulation of *CCR* gene expression has been reported in dicots and monocots. Tobacco plants carrying an antisense *CCR* gene had a 75% decrease in lignin content and a 25% decrease in activity, as well as an increase in the S/G ratio (Table 3; Whetten et al., 1998). However, the lignin content in tobacco plants carrying a sense *CCR* gene construct was not affected. A slight change occurred in levels of CCR activity, as well as a decrease in the S/G ratio (Table 3; Whetten et al., 1998). In contrast, *Zmccr1*$^{-}$ (maize) mutants exhibited only a slight decrease in lignin content and significant changes in the lignin structure. An increase in the S/G ratio was revealed, as well as a decrease in H units, as compared to wild-type plants (Tamasloukht et al., 2011). Altogether, down-regulation of CCR in plants exhibited a decrease in total lignin content, along with a higher S/G ratio in the lignin polymer. The S/G ratio of lignin increased in down-regulated CCR transgenic plants or mutants probably due to a decrease in G units. The result could reflect the preferential reduction of feruloyl-CoA.

In addition, the xylem of *CCR*-down-regulated transgenic tobacco lines showed an orange-brown coloration, which may be caused by elevated levels of ester-linked ferulic

acid in the xylem cell walls (Piquemal et al., 1998). Many studies of CCR-deficient angiosperms (poplar, tobacco, and *Arabidopsis*) have shown increased incorporation of free ferulic acid into the lignin polymer by *bis*-β-O-4 cross-coupling. Evidence was provided by NMR and thioacidolysis analyses (Ralph et al., 2008; Vanholme et al., 2010).

(2) CAD

CAD is the last enzyme in the monolignol biosynthetic pathway. Transgenic plants with up- or down-regulated *CAD* gene showed a different lignin composition when compared to the wild type plants. The shift in the aldehyde-to-alcohol ratio was greater for S than G lignin in CAD deficient transgenic tobacco plants (Halpin et al., 1994). In addition, alteration in the synthesis of S lignin was observed in antisense-CAD tobacco, with higher levels of G lignin, leading to a reduction in the S/G ratio of lignins (Ralph et al., 1998). Thus, these compositional shifts may impact the structure of the polymer or alter cell wall properties (Vanholme et al., 2010).

However, transgenic plants with reduced levels of CAD activity accumulated the same content of lignin as the wild type plants (Table 3; Whetten et al., 1998). These transgenic plants increased the incorporation of hydroxycinnamyl aldehydes into the lignin polymer. One of the most prominent effects of CAD-down-regulation in plants is that it leads to lignin with increased hydroxycinnamaldehyde content. CAD-down-regulated poplars did not change the proportion of labile β-O-4 bonds or S units, but significantly increased amounts of syringaldehyde and vanillin (derived from coniferaldehyde) in the lignin (Lapierre et al., 1999). Some reports have shown an increased incorporation of certain hydroxycinnamaldehydes into the lignin polymer associated with a decrease in the corresponding alcohol-derived subunit (Whetten et al., 1998). These hydroxycinnamyl aldehydes are *β*-O-4-cross-coupled with a phenolic end of the polymer in CAD-deficient plants (Hayashi, 2006).

(3) CCR and CAD

Combined down-regulation of CCR and CAD in transgenic tobacco displayed normal xylem cell wall morphology. They exhibited a strong decrease in lignin content, as well as an increase in the S/G ratio (Chabannes et al., 2001). However, down-regulation of CCR in tobacco led to reduced growth with dramatic structural abnormalities in xylem vessel cell walls (Piquemal et al., 1998). Interestingly, CAD-down-regulated tobacco exhibited normal growth. (Ralph et al., 1998) Therefore, these unexpected results demonstrate the need for additional studies.

(4) POD

Peroxidases have been associated with the production of monolignol phenoxy radicals that form lignin polymers (Passardi et al., 2004b). Genetic studies in several plants showed that up- or down-regulation of certain class III peroxidases had an impact on either lignin content or composition. Up- and down-regulation of the *POD* gene in tobacco led to increased and reduced levels of POD activity in the transgenic plants. Transgenic tobacco with increased POD activity accumulated large amounts of lignin, but the lignin content in plants with reduced POD activity was not affected (Table 3; Whetten et al., 1998). Down-regulation of *NtPOD60* (TP60) gene in tobacco with an antisense *POD* gene (Nicotiana spp.) resulted in a 50% reduction in the amount of lignin and vascular tissue modification (Blee et al., 2003). However, up-regulation of the *NtPOD60* gene in tobacco showed no impact on the lignin content of roots, leaves, and stems (Lagrimini et al., 1997). Transgenic aspen plants with down-regulated *PkPOD03* (PODA3a) gene (antisense suppression) had up to a 20% reduction in lignin content and a decreased proportion of G units, as well as an increased proportion of S units (Li et al., 2003). These transgenic plants have contributed to our understanding of the *in vivo* role of various peroxidase isoenzymes.

Table 3. Modification of lignin in transgenic plants (Whetten et al., 1998)

Transgenic method	Species	Enzyme effect[1]	Lignin content[2]	Lignin composition[3]
Antisense *ccr*	Tobacco	CCR 25%	Decreased to 75%	Increased S:G
Sense suppression *ccr*	Tobacco	CCR 2%	n.d.	Decreased S:G
Antisense *cad*	Tobacco	CAD 7%	No effect	Increased aldehyde
Antisense *cad*	Tobacco	CAD 50%	No effect	Increased aldehyde
Antisense *cad*	Poplar	CAD 30–50%	No effect	Increased aldehyde
Antisense *pod*	Tobacco	POD decreased	No effect	
Overexpression *pod*	Tobacco	POD increased	Increased to ~130%	n.d. slower growth

[1]Enzyme effect: level of enzyme activity relative to wild type (%)
[2]Effect on lignin content, % of wild type content, n.d., not determined
[3]Effect on lignin composition relative to wild type

Other peroxidases, such as ZPOD01 (Sato et al., 2006) and ZPOD15 (Gabaldón et al., 2005) from *Zinnia*, have also been shown to be involved in the lignification process. A peroxidase gene was overexpressed with its own promoter in a transgenic plant. Its transcript levels increased in the epidermis, trichomes, and parenchymal tissues associated with vasculature, but not in vascular tissue (Lagrimini et al., 1997). Altogether, the precise roles of individual class III peroxidase isoforms are still largely unclear due to functional redundancy of these peroxidases in plants. Individual gene family members have been more difficult to tackle due to the high number of genes and diversity in their structure. In addition, substrate specificity is difficult to obtain because peroxidases also exhibit low substrate specificity *in vitro* (Chittoor et al., 1997; Pedreira et al., 2011). Thus, understanding of the precise functions and specific roles of plant peroxidases are still a challenge.

5. RNA silencing in plants

RNA silencing has been achieved in transgenic plants with homologous sense and antisense RNAs, double-stranded RNA and virus induced gene silencing (VIGS) (Figure 10; Vance and Vaucheret, 2001; Vaucheret et al., 2001). The underlying mechanism of these techniques is called RNA interferenece (RNAi). RNAi was discovered accidentally in transgenic petunias in the early 1990s. Plant biologists attempted to enhance color in pigmented petunia petals. A petunia sense *CHS* gene was introduced into plants to enhance pigmentation in the flowers but, instead, the plants produced pure white or patterned flowers. This co-suppression phenomenon of homologous genes has been linked with post-transcriptional inhibition of gene expression and leads to homologous mRNA degradation in plants (Napoli et al., 1990).

RNAi-mediated silencing occurs in animals, fungi, *Drosophila*, and plants (Hannon, 2002; Ronald, 2002; Schwab et al., 2011). All of these organisms utilize the mechanism that recognizes dsRNA as a signal to suppress the expression of homologous genes (Figure 10; Waterhouse et al., 2001b). Long dsRNAs are cleaved by the endonuclease Dicer into 19-23 nt fragments with 5’ phosphorylated ends and 2-nt unpaired and unphosphorylated 3’ ends (Bernstein et al., 2001). The fragments are called mall interfering RNAs (siRNAs). A RNA-induced silencing complex (RISC), associated with siRNAs, acts as the guide strand to recognize complementary mRNA and to trigger sequence-specific degradation of the target mRNA. In plants, siRNAs are not only guides to target the homology-dependent degradation of RNA, but also the mobile silencing signal for systemic spread of post transcriptional gene silencing (PTGS; Waterhouse et al., 2001a).

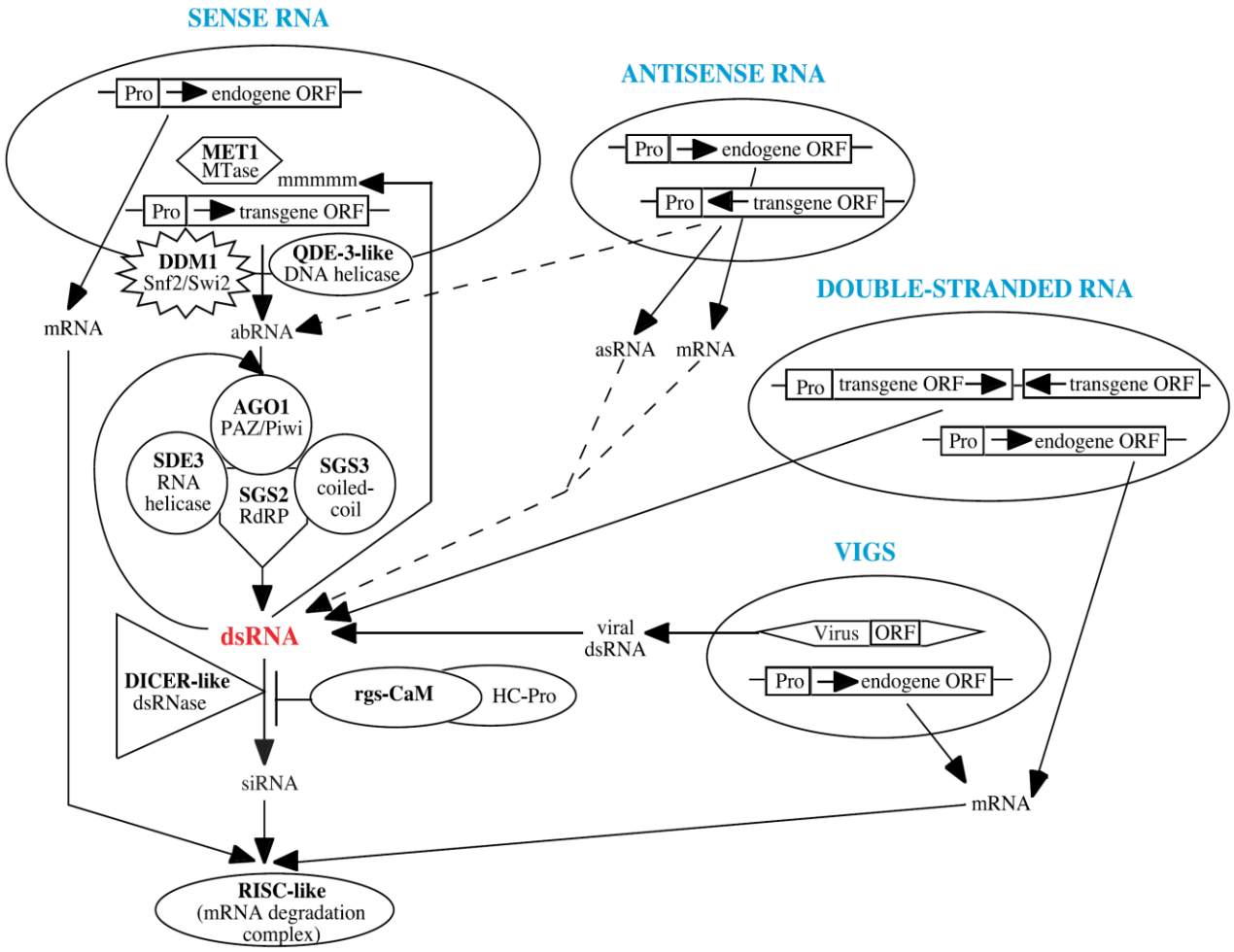

Figure 10. Different types of RNA silencing in plants.
The initial RNA silencing is linking dsRNA derived from sense RNA, antisense RNA, double-stranded RNA, and VIGS. Transgenes expressing sense RNA produces aberrant (ab)RNAs and transgenes expressing antisense RNA could produce either asRNA or abRNA. These abRNAs could be used as templates by an RdRP (SGS2) associated with SGS3 (coiled-coil), AGO1 (PAZ/Piwi) and RNA helicase (SDE3) to synthesize dsRNAs. The siRNAs derived from dsRNA combine with a RISC-like silencing complex to mediate sequence-specific mRNA degradation. PTGS needs SGS3 and MET1 (which encodes a DNA-methyltransferase) in plants (Vance and Vaucheret, 2001; Vaucheret et al., 2001).

RNA silencing, as a powerful tool for gene function studies, has been applied to many plant species. Several recent studies have shown that transgenic plants with double-stranded or self-complementary hairpin RNAs (ihpRNA) induced PTGS to suppress target gene expression (Abbott et al., 2000; Smith et al., 2000; Wesley et al., 2001). The expression of homologous genes in strawberry fruits were inhibited using RNAi technology to target *FaCHS*, *FaOMT*, *FaGT1*, *FaDFR*, *FaANS*, and *Fra* genes (Schwab et al., 2011). Agroinfiltrated fruits containing *FaCHS*-ihpRNA constructs that encode double stranded (ds)

or self-complementary hairpin (hp) RNA caused the loss of pigmentation in the fruits, resulting in the silencing of the homologous *CHS* gene (Hoffmann et al., 2006). RNAi-mediated silencing has become an important method for analyzing gene functions *in vivo*.

6. Intention of the study

Lignin is the second most abundant polymer found in nature after cellulose. Among the many roles lignin plays in plant growth and development are those providing structural support for land plants. Until recently, only carbohydrate polymers such as pectin and cellulose and to a lesser extent proteins such as the expansins have been regarded as structure forming and stabilizing components in fruits. Microarray analyses, however, have recently provided evidence that the expression of specific genes involved in lignin formation affect strawberry fruit firmness (Salentijn et al., 2003). As a consequence, it is the intention of the study to clone *CCR*, *CAD*, and *POD* genes from *Fragaria x ananassa*, to functionally characterize the corresponding enzymes and to determine their gene expression levels in different tissues. It is also proposed to transiently down-regulate and up-regulate *CCR*, *CAD*, and *POD* genes in fruits and to quantify the effects on fruit firmness, lignin content, and composition.

Functional studies of *CCR*, *CAD*, and *POD* have been carried out by evaluating stable transgenic plants (Table 3; Whetten et al., 1998). Down- and up-regulation of *FaCCR*, *FaCAD*, and *FaPOD* gene expression in strawberry fruit by RNAi and overexpression strategies, respectively, have not been reported, yet. In this study, it is proposed to infiltrate fruits with *Agrobacterium* harboring intron-hairpin or overexpression constructs corresponding to *FaCCR*, *FaCAD*, and *FaPOD*. Eventually, the ultimate goal is to manipulate useful genes to alter cell wall structures and properties in order to improve the firmness of strawberries. The results can be used to develop strawberry varieties with improved firmness, storage stability and thus fruit quality.

II. Materials and Methods

1. Materials

1.1 Plant materials

The octaploid strawberry plants (*Fragaria* × *ananassa* cv. Elsanta) were obtained from a producer (Kraege Beerenpflanzen, Telgte, Germany), and transgenic strawberry lines carrying the antisense *CHS* gene (*Fragaria* × *ananassa* cv. Calypso) were provided by the research group. Plants of both strawberry genotypes cv. Elsanta and cv. Calypso were grown under greenhouse conditions (16 h /8 h, light/dark period).

1.2 Chemicals

All chemicals, solvents, and reference compounds were purchased from Sigma-Aldrich (Munich, Germany), Fluka (Munich, Germany), Merck (Darmstadt, Germany), Roth (Karlsruhe, Germany), Sigma (Steinheim, Germany), or J. T. Baker (Austin, TX, USA). The following chemicals were used in different studies.

A. Chemicals and reference compounds for assaying enzyme activity were obtained from the following suppliers:

Sigma-Aldrich: *p*-coumaric acid, caffeic acid, trans-cinnamaldehyde, coniferyl aldehyde, syringaldehyde, cinnamyl alcohol, coniferyl alcohol, and sinapyl alcohol

Fluka: ferulic acid

Roth: ATP, NADPH, guaiacol, and H_2O_2

B. Chemicals and solvents for lignin composition analysis were obtained from the following suppliers:

Roth: 1,4-dioxane, diethyl ether, and sodium sulfate anhydrous

Aldrich: boron trifluoride diethyl etherate and ethanethiol methylene chloride

J.T. Baker: dichloromethane

Fluka: docosane and sodium bicarbonate

SupeLco (USA): *N*,*O*-bis(trimethylsilyl) trifluoroacetamide (BSTFA) kit

Sigma-Aldrich: pyridine

C. Solvents for LC-UV-ESI-MS^n and GC-MS were obtained from the following suppliers:

J. T. Baker: methanol and water

Roth: formic acid

1.3 Bacterial and yeast strains

- *E. coli* JM 109 (Promega, Mannheim, Germany)
- *E. coli* TOP10 (Invitrogen, Darmstadt, Germany)
- *E. coli* BL21 (DE3) pLysS (Novagen, Darmstadt, Germany)
- *E. coli* Rosetta (DE3) pLysS (Novagen)
- *Agrobacterium tumefaciens* AGL0 (Lazo et al., 1991)
- *Saccharomyces cerevisiae* INVSc-1(Invitrogen)

1.4 Enzymes, markers, and other

DNA polymerase:

- *Taq* DNA Polymerase (5U/µl, New England Biolabs, Frankfurt, Germany)
- *Pfu* DNA Polymerase (3U/µl, Promega)
- Phusion™ (2U/µl, Finnzymes, Espoo, Finland)

Reverse transcriptase: M-MLV RNase H Minus Point Mutant (Promega)

Restriction enzymes: -*Bam*HI, *Ecl*136II, *Eco*RI, *Nhe*I, *Not*I, *Sma*I, *Spe*I, *Xba*I, and *Xho*I (Fermentas, St. Leon-Rot, Germany)

Other enzymes:-DNase I and RNase-free (Fermentas)
-RNaseA (New England Biolabs)
-T4 DNA Ligase (Fermentas)
-RNaseOUT™ Recombinant Ribonuclease Inhibitor (40U/µl, Invitrogen)

DNA markers: -GeneRuler™ 1kb DNA Ladder (Fermentas)
-GeneRuler™ DNA Ladder Mix (Fermentas)

Protein markers: Protein Marker Broad Range (14-66 kDa) (Sigma-Aldrich Chemie GmbH, Taufkirchen, Germany)

Other: -dNTPs (10 mM, Fermentas)
- dATP (100 mM, Fermentas)

1.5 Vectors

- **pSKAscI35SIntTER** (Hoffmann, 2001)

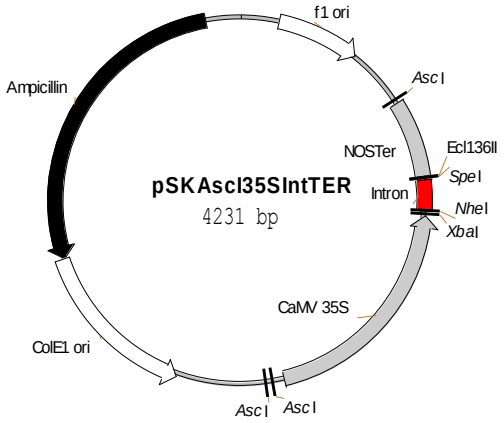

- **pBIAscI** (Hoffmann, 2001)

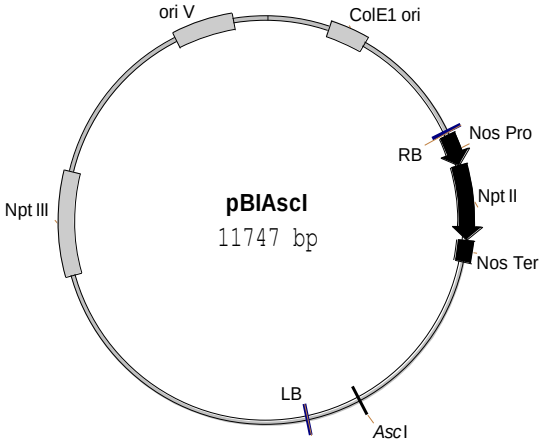

- **pBI-intron** (Hoffmann et al., 2006)

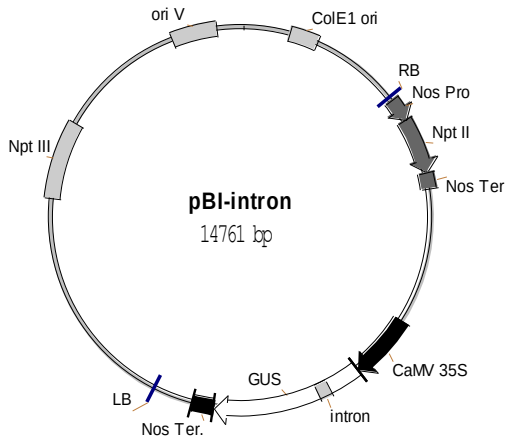

- **pBI-*CHSi*** (Hoffmann et al., 2006)

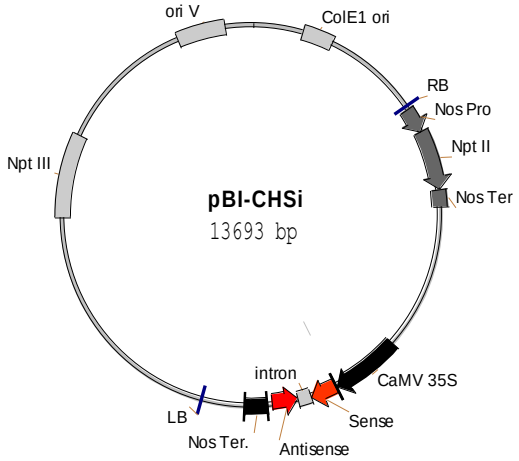

- **pYES2 (Invitrogen)**

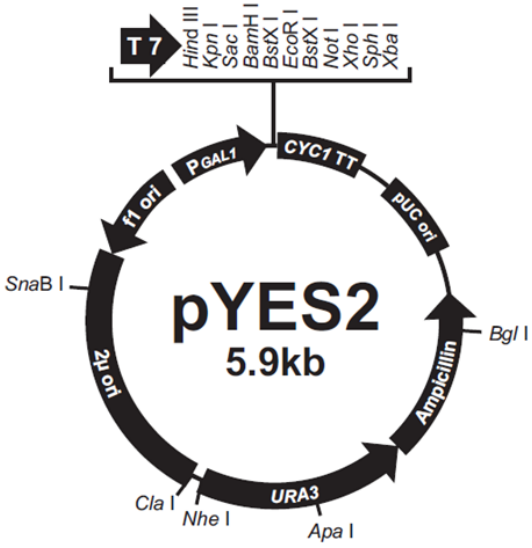

1.6 Vectors containing antibiotics for bacterial selection and primers for sequencing (Table 4)

Table 4. Vectors with appropriate antibiotics and sequencing primers

Primer name	Antibiotics	Sequencing primers
pGEM-T (Promega)	Ampicillin	T7, SP6
pET-29a(+) (Novagen)	Kanamycin	T7, T7_Term
pGEX-4T-1(GE Healthcare)	Ampicillin	pGEX-F, pGEX-R
pSKAscI (Hoffmann, 2001)	Ampicillin	T3, T7
pBIAscI (Hoffmann, 2001)	Kanamycin	Specific primers
pYES2 (Invitrogen)	Ampicillin	pYES2F, pYES2R

1.7 Antibiotics (Table 5)

Table 5. Stock solution and solubility of antibiotics

Antibiotics	Stock solution	Solubility	*Final concentration
Ampicillin (Sigma)	100 mg/ml	MQ water	100 µg/ml
Chloramphenicol (Sigma)	34 mg/ml	Ethanol	34 µg/ml
Carbenicillin (Roth)	50 mg/ml	MQ water	50 µg/ml
Kanamycin (Sigma)	25 mg/ml	MQ water	25 µg/ml
Rifampicin (Fluka)	25 mg/ml	Methanol	25 µg/ml

(*Final concentration used for selection and propagation of bacteria cells)

1.8 Primers

All oligonucleotide primers were synthesized by the Microsynth Company (Balgach, Switzerland) and used as the following:

A. The oligonucleotide primers were used for sequencing (Table 6)

Table 6. Primers of sequencing

Primer name	Sequence (5' to 3')
T3	AATTAACCCTCACTAAAGGG
SP6	CATTTAGGTGACACTATAG
T7	AATACGACTCACTATAGGG
T7_Term	CTAGTTATTGCTCAGCGGT
pGEX-F	ATAGCATGGCCTTTGCAGG
pGEX-R	GAGCTGCATGTGTCAGAGG
pYES2 F	TACCTCTATACTTTAACGTC
pYES2 R	TCTAACTCCTTCCTTTTCGG

B. cDNA synthese primers: Random-Hexamer (50 µmol/µl): 5´-NNNNNN-3´

C. The primers were used for cloning of cDNAs and genomic DNA(gDNA) (Table 7)

Table 7. Primers of *FaCCR*, *FaCAD*, and *FaPOD*

Primer name	Sequence (5' to 3')	Tm	Target gene
CCR-FD	ATGCCTGYYGATVHYWSMTC	50℃	*FaCCR*
CCR-RD	TTATTGRATYTTSAHRGASTC		
CAD-FD	ATGKCTATCGAGCAAGAACAC	50℃	*FaCAD*
CAD-RD	TTAAGASCTARCCTTCAGTGT		
gPOD F	ATGGGTTCCAGAGCTCTCTTC	50℃	*FaPOD*
gPOD R	CTAGTGGAGCTTGTTGGCCAC		

(FD: degenerate forward primer; RD: degenerate reverse primer; an underline indicates H= A/T/C; K= G/T; M=A/C; R= G/A; S=G/C; V=G/A/C; W= A/T; Y=T/C; F: forward primer; R: reverse primer)

D. The primers were used for construction in intron-hairpin vectors (Table 8)

Table 8. Primers of *FaCCR*, *FaCAD*, and *FaPOD*

Primer name	Sequence (5' to 3')	Tm	Target gene
CCR-NheI F	CTAGCTAGCGTCGTCTTCACGTCTTC	55℃	*FaCCR*
CCR-SpeI R	GCGACTAGTAGAATTGGCATAAGTCTT		
CAD-NheI F	CGCGCTAGCTTCTACAGAAGGGAAAC	55℃	*FaCAD*
CAD-SpeI R	GCAACTAGTGTAGTACTTGGCACCGTA		
POD-NheI F	CATGCTAGCCTCTACAAGCGCCACAAG	55℃	*FaPOD*
POD-SpeI R	GCGACTAGTATCTCTCCTTCCAGTT		

(F: forward primer; R: reverse primer; engineered restriction sites are underlined)

E. The primers were used for construction in overexpression vectors (Table 9)

Table 9. Primers of *FaCCR*, *FaCAD*, and *FaPOD*

Primer name	Sequence (5' to 3')	Tm	Target gene
CCR F_BamHI	CAGGGATCCATGCCTGTTGATAACTG	55℃	*FaCCR*
CCR R_SmaI	CTGCCCGGGTTATTGGATTTTGAAG		
CAD F_BamHI	CGTGGATCCATGTCTATCGAGCAAG	55℃	*FaCAD*
CAD R_SmaI	TATCCCGGGTTAAGAGCTAGCCTTC		
POD F_BamHI	TCTGGATCCATGGGTTCCAGAGCTC	55℃	*FaPOD*
POD R_SmaI	TATCCCGGGCTAGTGGAGCTTGTTG		

(F: forward primer; R: reverse primer; engineered restriction sites are underlined

F. The primers were used in qRT-PCR (Table 10)

Table 10. Primers of *FaCCR*, *FaCAD*, *FaPOD*, *FaPOD27*, *FaPAL*, *FaCHS*, and *IS*

Primer name	Sequence (5' to 3')	Reference
Gene-specific primers:		
CCR-F	GAGAGGCTATAATGTGAGAGGAACCGTCAG	this study (refer to appendix B.1)
CCR-R	GCGATGCAGTGTGGAAAACGCCATCACAGC	
CAD-F	CATGGTCAAGAATGAATGGGGCTTCTCTAC	this study (refer to appendix B.2)
CAD-R	GCACCGTAAGTGAGTATCTGTTTGGGGCAG	
POD-F	GCTGAGATCCTTGAGGAGTACCTTCCTGAC	this study (refer to appendix B.3)
POD-R	TGTGAGGGACATGGTCTGGGTTCAGAGCTG	
POD27 F	ATTTCCATGATTGCTTTGTCA	this study (refer to appendix B.4)
POD27 R	CAACGGCTAAGATGTCAGAAC	
PAL F	TTGAAGCTCATGTCTTCCAC	Almeida et al., 2007
PAL R	CAAGTTCTCCTCCAAATG	
CHS F	GCTGTCAAGGCCATTAAGGA	Almeida et al., 2007
CHS R	GAGCAAACAACGAGAACACG	
Interspacer primers:		
IS F	ACCGTTGATTCGCACAATTGGTCATCG	16S-23S interspacer region
IS R	TACTGCGGGTCGGCAATCGGACG	

(F: forward primer; R: reverse primer)

G. The primers were used for construction of protein expressing vectors (Table 11)

Table 11. Primers of *FaCCR*, *FaCAD*, and *FaPOD*

Primer name	Sequence (5' to 3')	Expressing vector
CCR F_BamHI	CAGGGATCCATGCCTGTTGATAACTG	pGEX-4T-1
CCR R_SmaI	CTGCCCGGGTTATTGGATTTTGAAG	
CAD F_BamHI	CGTGGATCCATGTCTATCGAGCAAG	pGEX-4T-1
CAD R_SmaI	TATCCCGGGTTAAGAGCTAGCCTTC	
POD F_BamHI	TCTGGATCCATGGGTTCCAGAGCTC	pGEX-4T-1
POD R_SmaI	TATCCCGGGCTAGTGGAGCTTGTTG	
CAD R_XhoI	GGACTCGAGAGAGCTAGCCTTCAG	pET-29a(+)
CAD_YF	GCTGGATCCAACACAATGTCTATCGAGCAAG	pYES2
XbaI _YR	GCATCTAGAGTTAGCAGCCGGATCTCA	

For pET-29a(+), CAD R_XhoI and CAD F_BamHI were used as a pair of primers in a PCR reaction. (Tm = 55°; F/R: forward/reverse primer; engineered restriction sites are underlined)

1.9 Media, buffers, and solutions

A. media

LB medium/plates

10 g/l Tryptone
5 g/l Yeast Extract
10 g/l NaCl
15 g/l Agar 1.5% (for plates)
Adjust pH to 7.0 with NaOH

LB plates / Ampicillin /IPTG/X-gal

500 mL LB medium containing 1.5% agar
0.5 mL Ampicillin (100 mg/ml)
0.4 mL X-Gal (50 mg/mL stock in N-N'-dimethyl formamide)
2.5 mL IPTG (0.1mM stock in MQ water)

MMA medium

4.3 g/l MS-salt (Sigma)
1.952 g/l MES (10 mM)
20 g/l Sucrose
Adjust pH to 5.6 with KOH

SOC medium

20 g/l Tryptone
5 g/l Yeast Extract
0.584 g/l NaCl
0.186 g/l KCl
2.03 g/l $MgCl_2 \cdot 6H_2O$
1.204 g/l $MgSO_4$
3.603 g/l Glucose
Adjust pH to 7 with NaOH

SC-U medium/plates (synthetic minimal defined medium for yeast)

0.67% yeast nitrogen base (without amino acids)
2% carbon source (glucose or galactose)
amino acids:
0.01% (adenine, arginine, cysteine, leucine, lysine, threonine, tryptophan)
0.005% (aspartic acid, histidine, isoleucine, methionine, phenylalanine, proline, serine, tyrosine, valine)
2% agar (for plates)
Up to 900 ml distilled water
Add 100 ml of filter-sterilized 20% glucose or galactose after autoclaving

20% glucose or galactose
100 g of glucose or galactose in 400 ml distilled water
Add distilled water to 500 ml and sterilize through a 0.22 μm filter after dissolving

B. DNA buffer and solution

DNA Extraction buffer
2.0% CTAB (w/v)
1.4 M NaCl
20 mM EDTA (pH 8.0)
100 mM Tris-HCl (pH 8.0)
Add 0.2 % ß-mercaptoethanol to the buffer before use and then heat to 60℃ for pre-warmed buffer

TE buffer
1 mM EDTA (pH 8.0)
10 mM Tris-HCl (pH 8.0)

C. RNA buffer and solution

RNA extraction buffer
3% CTAB (w/v)
3% PVP, K30 (Roth)
25 mM EDTA (pH 8.0)
2 M NaCl
100 mM Tris-HCl (pH 8.0)
Add 40 μl/ml ß-mercaptoethanol to the buffer before use and then heat to 65℃ for pre-warmed buffer

D. Protein buffer and solution

His-tag wash/bind buffer
20 mM Sodium phosphate (pH 7.4)
0.5 M NaCl
20 mM Imidazole

His-tag elution buffer
20 mM Sodium phosphate (pH 7.4)
0.5 M NaCl
400 mM Imidazole

GST wash/bind buffer (pH 7.3)
4.3 mM Na_2HPO_4
1.47 mM KH_2PO_4
0.137 M NaCl
2.7 mM KCl

GST elution buffer (prepare fresh buffer)
10 mM L-Glutathione reduced (Roth)
50 mM Tris-HCl (pH 8.0)

Peroxidase extraction buffer
100 mM Potassium phosphate (pH 6.6)
2 mM EDTA
0.5 % Triton X-100
Add 20 mM PMSF to 1 ml buffer before use

Bradford solution
100 mg/l Coomassie Brilliant Blue G250 (Roth)
50 ml/l Ethanol (96%)
100 ml/l Phosphoric acid (85 %)

SDS-PAGE
12% Tris-glycine SDS-PAGE gel (Anamed, Groß-Bieberau, Germany)
4× Roti® Protein Loading buffer (Roth)

1× Electrode (Running) buffer
25 mM Tris
192 mM Glycine
0.1% SDS

Staining solution
0.33g Coomassie Brilliant Blue G250
120 ml Methanol
24 ml Acetic acid
120 ml H_2O

Destaining solution
20% Ethanol
10% Acetic acid

E. Other buffer and solution

10× DNA loading dye
0.21% Orange G
0.1 M EDTA (pH 8.0)
50% Glycerol

50× TAE buffer
242 g/l Tris
57.1 ml/l Acetic acid
100 ml/l 0.5M EDTA (pH 8.0)

Glycerol for cell stocks
65 % Glycerol (v/v)
0.1 M $MgSO_4$
25 mM Tris
pH 8.0 with HCl

Chemically competent cells
Trituration buffer (prepared fresh and filter-sterilized buffer):
100 mM $CaCl_2 \cdot 2H_2O$
70 mM $MgCl_2 \cdot 6H_2O$
40 mM NaOAc
Adjust pH to 5.5 with HCl

1.10 Commercial kits

-Purification of DNA fragments from gel:

QIAEX II Gel Extraction Kit (QIAGEN, Hilden, Germany)

NucleoSpin® Extract II (Macherey-Negel, Düren, Germany)

- Purified plasmid DNA for sequencing or other molecular biologic experiments:

Wizard® Plus SV Minipreps DNA Purification System (Promega)

- *S. c.* EasyComp. Transformation Kit (Invitrogen)

- Fast SYBR® Green Master Mix (Applied Biosystems, Foster City, CA, USA)

- SensiMix™SYBR Kit (Bioline GmbH)

2. Apparatus

2.1 FPLC (Fast protein liquid chromatography)

ÄKTApurifier System (GE Healthcare, Biosciences AB, Uppsala, Sweden) with the following equipment:

Pump	P-900 (with four pump heads in two pump modules)
Monitor	UPC-900 (including the combined measurement of UV absorption, pH and conductivity)
Monitor	UV-900 (with variable wavelength in the range 190-700 nm)
Valve	INV-907 (with rotary 7-port valve)
Mixer	M-925 (single chamber mixer)
Fraction collector	Frac-950
Software	UNICORN (version 5.20)

Program for purification of His-tag protein

Column	5 ml HisTrap FF Column (GE Healthcare)

Solution	B1: Elution buffer (II.1.9.D); B2: MQ water A1: Wash/bind buffer (II.1.9.D); A2: 20% ethanol
Column equilibration	
Flow rate	2.00 ml /min
Gradient	100 %
Running solution	5 column volumes of MQ water (B2) 5 column volumes of binding buffer (A1)
Monitor at 280 nm	Baseline should be stable after washing.
Column loading	
Flow rate	0.5 ml /min
Gradient	100 %
Loading protein	10 ml protein extracts
Running solution	Along with MQ water (B2)
Column washing	
Flow rate	2.00 ml /min
Gradient	100 %
Running solution	5-10 column volumes of binding buffer (A1) until A_{280} is stable (to reach the baseline).
Protein elution	
Flow rate	1.00 ml /min
Gradient	100 %
Running solution	10 column volumes of elution buffer (B1)
Collected fractions	Collect fractions (3-6) for SDS-PAGE and enzymes analysis
Column washing	
Flow rate	5.00 ml /min
Gradient	100 %
Running solution	5 column volumes of MQ water (B2) 5 column volumes of 20% ethanol (A2)
Storage	Store the HisTrap column at 4 ℃ after washing with 20% ethanol

2.2 Liquid chromatography ultraviolet electro-spray ionization mass spectrometry (LC-UV-ESI-MS^n)

System I

HPLC	Agilent 1100 Series (Agilent Technologies Inc., Santa Clara, California, USA)
Pump	Agilent 1100 Quaternary Pump
Autosampler	Agilent Autosampler

Injection volume	5 µL
Separation column	Luna 3 µm C18 (2) 100 Å 150 x 2.0 mm (Phenomenex® Aschaffenburg, Germany) (Part Number: 00F-4251-B0)
Precolumn	Security Guard Cartridges C18 4 x 2 mm (Penomenex®)
Column temperature	25 ℃
Solvents	A: Water plus 0.1 % formic acid B: Methanol plus 0.1 % formic acid
Flow Rate	0.2 ml/min
Gradient	0-30 min: 0-50 % B, 30-35 min: 50-100% B, 35-50 min: 100% B, 50-55 min: 100-0% B, 55-65 min: 0% B
UV-Detector	Agilent 1100 variable wavelength detector
Wavelength	According to different analyses, the wavelength should be changed as follows:

Analysis	**Wavelength (nm)**
Metabolites	280
CCR enzyme	340
POD enzyme	320 (DAD detector)

Mass Spectrometer Bruker Daltonics esquire 3000^{plus} (Bruker, Bremen, Germany)

Spray gas	Nitrogen (30.0 psi)
Dry gas	Nitrogen (330 ℃, 9 l/min)
Scan range	*m/z* 100 to 800
Polarity	positive/negative
ICC target	20, 000 or 200 ms
Target mass (SPS)	*m/z* 400
Capillary voltage	- 4000 V
End pate offset	- 500 V
MS/MS	Auto-tandem MS^2
Collision gas	Helium 5.0 (3.56×10^{-6} mbar)
Collision voltage	1.0 V
Data analysis	Bruker Daltonics Esquire 5.1 with Data Analysis 3.1 and Quant Analysis 1.5 package (Bruker Daltonics, Bremen, Germany) Agilent 6300 series ion trap LC/MS system software (version 6.2) with Data Analysis and Quant Analysis

System II

HPLC	Agilent 1100 Series
	(Agilent Technologies Inc., Santa Clara, California, USA)
Pump	Agilent 1100 Capillary Pump
Autosampler	Agilent 1100 Micro Wellplate Autosampler
Injection volume	5 µL
Separation column	Luna 3 µm C18 (2) 100 Å 150 x 2.0 mm (Phenomenex®
	Aschaffenburg, Germany) (Part Number: 00F-4251-B0)
Precolumn	Security Guard Cartridges C18 4 x 2 mm (Penomenex®)
Column temperature	28 °C
Solvents	A: Water plus 0.1 % formic acid
	B: Methanol plus 0.1 % formic acid
Flow Rate	0.1 ml/min
Gradient	60% A, 40% B (isocratic)
UV-Detector	Agilent 1100 series DAD
Wavelength	260 nm for products; 340 nm for substrates (CAD enzyme)
Mass Spectrometer Agilent Technologies 6340 ion Trap LC/MS	
Spray gas:	Nitrogen (30.0 psi)
Dry gas:	Nitrogen (330 °C, 9 l/min)
Scan range:	*m/z* 100 to 800
Polarity:	positive
ICC target:	500,000 or 200 ms
Target mass (SPS):	*m/z* 200
Capillary voltage:	- 4000 V
End pate offset:	- 500 V
MS/MS:	Auto-tandem MS^2
Collision gas:	Helium 5.0 (3.56×10^{-6} mbar)
Collision voltage:	1.0 V
Data analysis:	Agilent 6300 series ion trap LC/MS system software (version 6.2) with Data Analysis and Quant Analysis

2.3 Gas chromatography-mass spectrophotometer (GC-MS)

GC	Thermo Finnigan Trace GC 2000 Ultra (Thermo Finnigan, Egelsbach, Germany)
Autosampler	Thermo Finnigan AI 3000 (Thermo Finnigan)
Injector	Split injector (1:10)
Separation column	Rtx® 5ms (15 m x 0.25 mm, df=0.25 µm) (RESTEK, USA)
Mass spectrometer	Thermo Finnigan Trace DSQ (Thermo Finnigan)
Ionization	Electron impact ionization (EI), 70 eV, (Positive ions)
Temperature	ion source: 250°C, transfer line: 280°C
Photomultiplier	1340 V
Scan rate	500 amu/s
Injection	Temperature: 220°C, Split injection: 2 µl
Carrier gas	Helium with flow rate at 1.1 ml min^{-1}
Mass range	*m/z* 40 to 600
Temperature program	Initial step: 90°C; hold time: 3 min Ramp step: from 90°C to 260°C; 5°C min^{-1} (ramp rate) Static step: 260°C; hold time: 15 min Total run time: 52 min
Data analysis	Xcalibur software (version 1.4) in Windows XP (Thermo Electron, San Jose, USA)

2.4 Other equipment

Agarose gel electrophoresis bio-imaging system G:BoX	Syngene, Cambridge, UK
Autoclave (Systec V95)	Systec, Wettenberg, Germany
Centrifuge	Sigma 4K15C (Sigma, Osterode, Germany) Eppendorf 5415R (Eppendorf, Hamburg, Germany)
Electrophoresis	Roth, Karlsruhe, Germany
Freeze Dryer	Thermo Scientific, Munich, Germany
Mixer Mill MM 400	Retsch®, Haan, Germany
NanoDrop ND-1000	peQLab Biotechnologie GmbH, Erlangen, Germany
pH meter	CG 820 (Ingold, Hofheim)
Power supply	Consort E 835 (Consort, Turnhout, Belgien)

Scales	Scaltec SPB61 (Scaltec Instruments GmbH, Göttingen)
	Sartorius X634 Sartorius AG, Göttingen, Germany
Shaking incubator	GFL, Burgwedel, Germany
StepOnePlus™ Real-time PCR system	Applied Biosystems, Californien, USA
Spectrophotometer	Nicolet evolution 100 (Thermo, Cambridge, England)
Speed-Vac	Christ RVC 2-18 (Christ, Osterode)
Texture Analyzer	TA-XT2i (Stable Micro Systems, Godalming, Surrey, UK)
Thermocycler	Primus 96 advanced (Peqlab Biotechnologie, Erlangen, Germany)
Thermomixer	Eppendorf, Hamburg, Germany
Ultra Turrax	T18 basic (IKA® Works Inc. Wilmington, NC, USA)
Ultrasonic bath	RK103H (Bandelin Electronic, Berlin, Germany)
Ultrasonic Homogenizer	Bandelin Sonopuls UW2200 (Bandelin Electronic)
Vortexer	VWR, Darmstadt, Germany
Water bath	Julabo, Seelbach, Germany
-80℃ freezer	Skadi Europe, WREDE, Netherlands
-20℃ freezer	Quelle, Fürth, Germany
4℃ refrigerator	SEG, Rehlingen-Siersburg, Germany

2.5 Software and internet sources

- ACD/ChemSketch Version 12.0
  (Advanced Chemistry Development, Toronto, Canada)
- BioEdit
- BLAST
  http://www.ncbi.nlm.nih.gov/BLAST/Vector NTI (Invitrogen, Carlsbad, USA)
- GeneDoc
- MegAlign Version 4.0 (DNA STAR)
- SigmaPlot 10.0 (Systat Software)
- The R project for statistical computing:
  http://www.r-project.org/
- Vector NTI

3. Methods

3.1 Molecular biologic experiments

3.1.1 Extraction of genomic DNA

Genomic DNA was isolated from young leaves according to the method described by Lodhi et al. (1994) and modified by Ma et al. (2008). One gram of fresh or frozen leaves was ground into a fine powder in liquid nitrogen, using a mortar and pestle, and then 10 ml of pre-warmed DNA extraction buffer (II.1.9.B) was added. Afterwards, the mixture was transferred into a 50 ml polypropylene centrifuge tube with 100 mg PVP (100 mg PVP/g tissue) and placed at 60℃ for 25 min. Subsequently, the mixture was supplemented by 10 ml of chloroform/isoamyl alcohol (24:1, v/v) and mixed gently by inverting the tube 20 to 25 times. Following centrifugation at 6,000 rpm for 15 min at room temperature, the top aqueous phase was transferred to a new 50 ml tube. A second chloroform/isoamyl alcohol extraction was performed in the same manner as described above. The collected supernatants from two extractions were mixed with 0.5 volume of 5M NaCl, and two volumes of cold (-20℃) 95% ethanol and then the tubes were placed at 4℃ for one hour or overnight. After centrifugation at 5,000 rpm for 5 min at 4℃, the supernatant was discarded. The pellet was washed with cold (4℃) 76% ethanol and air-dried. Finally, the pellet was dissolved in 300 µL of TE (II.1.9.B) with 3 µl of RNase A (10 mg/ml) and incubated at 37℃ for 30 min to remove RNA. The concentration and quality of DNA were determined using a spectrophotometer. DNA was kept at -20℃ until used.

3.1.2 Extraction of total RNA

Total RNA was prepared as described by Liao et al. (2004). 1-2 g of frozen plant materials was ground or milled to a fine powder in liquid nitrogen, using either a mortar and pestle or a mixer mill. Then, the fine powder was added to 20 ml of pre-warmed RNA extraction buffer (II.1.9.C) and incubated at 65℃ for 10 min. The tube with the mixture was inverted manually every 3 min during the incubation. Afterwards, the mixture was supplemented by an equal volume of chloroform/isoamyl alcohol (CI; 24:1, v/v), and mixed manually for 10 min. CI extractions were performed twice before precipitating the RNA. Following centrifugation at 12,000 rpm for 10 min at 10℃, the supernatant was transferred to a new falcon tube. The collected supernatants from two extractions were mixed with 1/3 volume of 8 M LiCl (Roth) by vortexing and placed at 4℃ overnight for precipitating RNA. Subsequently, the RNA pellet was collected by centrifugation at 12,000 rpm for 30 min at 4℃. After removal of the supernatant, the pellet was mixed with 500 µl of 0.5 % SDS and

an equal volume of CI (24:1) by vortexing for 30 s. The mixture was centrifuged at 12,000 rpm for 10 min at 4℃, and the supernatant was transferred to a new Eppendorf tube containing a 2-fold volume of 100% ethanol. The tube was placed at -20℃ for 2 h. Then, the RNA pellet was collected by centrifugation at 13,200 rpm for 30 min at 4℃. After removal of the supernatant, the RNA pellet was successively washed with 70% ethanol and 100% ethanol followed by centrifugation at maximum speed for 5 min at 4℃. Afterwards, the supernatant was discarded and the RNA pellet was air-dried for 5 min at room temperature and then dissolved in 20-50 μl of DEPC-treated water. The concentration of total RNA was determined using either the NanoDrop or spectrophotometer. 3-5 μg of total RNA was checked for integrity by 1% agarose gel electrophoresis. The total RNA was stored at -80℃ until used.

3.1.3 PCR reaction

Based on different objectives (colony PCR screen, amplification, and isolation of coding region sequences and genes), 20-30 μl PCR reaction containing appropriate DNA polymerase, reaction reagents, and primers were used with PCR conditions (Table 12) and the following programs.

Table12. PCR conditions

Colony PCR Screen	Amplification	Isolation
Taq	Phusion™	*Pfu*
2 μl 10× ThermoPol buffer	6 μl 5× HF buffer	3 μl 10× Rxn buffer
1 μl of 2.5 mM dNTPs	1.5 μl of 2.5 mM dNTPs	1.5 μl of 2.5 mM dNTPs
1 μl of 10 μM_F primer	1.5 μl of 10 μM_F primer	1.5 μl of 10 μM_F primer
1 μl of 10 μM_R primer	1.5 μl of 10 μM_R primer	1.5 μl of 10 μM_R primer
Bacterial cells as template	1.5 μl template (50 ng/μl)	1.5 μl template (100 ng/μl)
0.3 μl DNA polymerase	0.5 μl DNA polymerase	0.5 μl DNA polymerase
Up to 20 μl H_2O	Up to 30 μl H_2O	Up to 30 μl H_2O

(F: forward primer; R: reverse primer)

PCR programs:

Initial denaturation	94℃	for 2 min		
cycling	94℃	for 30 sec	(Denaturation)	35-45 cycles
	(Tm) 50-60℃	for 30 sec	(Annealing)	
	72℃	for 1 min	(Extension) for 1 kb/min	
Final extension	72℃	for 10 min		
		hold at 4°C		

3.1.4 Agarose gel electrophoresis

Appropriate weight of agarose (1-2 % gel, w/v) and 80 ml of 1× TAE buffer (II.1.9.E) were placed in a 250 mL flask and then swirled to mix. The flask with the mixture was put into a microwave oven for about 2-3 min to dissolve the agarose and then cooled in a water bath for 1-2 min (about 60℃). The cooling agarose was poured into a gel tray and 4 µl of ethidium bromide (10 mg/ml) was added to the tray, and then swirled to mix. After 20-30 min, the gel was transferred to a gel tank and 1× TAE buffer was poured inside. Subsequently, 10-20 µl of the sample or the DNA marker was mixed with 1-2 µl of 10× DNA loading dye (II.1.9.E) and these mixtures were loaded into each well. Then, the power supply was set at 100-120 V, and electrophoresis was performed for about 30 min. After electrophoresis, DNA or RNA fragments were separated and visualized by a UV box (bio-imaging system G: BoX).

3.1.5 Purification of DNA fragments from agarose gels

The DNA fragments were excised from the gel and purified using either QIAEX II Gel Extraction Kit or NucleoSpin® Extract II. Finally, the DNA was eluted with an appropriate amount of water and stored at -20℃ until used.

3.1.6 Restriction endonuclease reaction

For complete digestion, the following proper amounts of plasmid DNA, reaction buffer, and enzyme, were added to 20-50 µl reaction volume (Table 13) and incubated at an appropriate temperature for 1 hour, or overnight.

Table 13. Restriction endonuclease reaction mixture

Component	Amount
Plasmid DNA (1-5 µg)	X µl
10× Reaction buffer	2-5 µl
Restriction enzyme (20 U/µl)	0.5-2 µl*
Reaction volume	20-50 µl

*One unit of restriction enzyme completely digests 1 µg of plasmid DNA in 1 hour. Usually, 1 µg of plasmid DNA is added to 5-10 units of restriction enzyme for digestion.

3.1.7 Ligation reaction

A. Method I

Insert DNA fragments (plasmid DNA or PCR products cut with appropriate restriction enzymes) and vector DNA cut with the same restriction enzyme were mixed together with the following reagents in a total volume of 10 µl (Table 14). This ligation reaction mixture was incubated at 4℃, overnight.

Table14. Ligation reaction mixture of method I

Component	Amount
T4 DNA ligase 10× buffer	1 µl
T4 DNA ligase (1 weiss, 1U/µl)	1 µl
Cut vector (20 ng /µl)	2 µl
Cut insert DNA fragments (50 ng /µl)	6 µl

B. Method II

PCR products were added with A-tailing at the 5'-ends by treatment with *Taq* DNA polymerase and dATP, according to the manufacturer's instructions for the pGEM-T Easy vector system (Promega). Afterwards, PCR fragments with A-tailing and a liner pGEM-T Easy vector containing 3´-terminal deoxythymidine were mixed with the following reagents in a total volume of 10 µl (Table 15). This ligation reaction mixture was incubated at 4℃, overnight.

Table 15. Ligation reaction mixture of method II

Component	Amount
T4 DNA ligase 10× buffer	1 µl
T4 DNA ligase (3U/µl))	1 µl
pGEM-T Easy vector (50 ng /µl)	2 µl
Insert fragments with A-tailing (50 ng /µl)	6 µl

3.1.8 Preparation of chemically competent cells

A single colony of *E. coli* strain was inoculated in 5-10 ml of LB containing appropriate antibiotics at 37 ℃, with shaking at 150 rpm overnight. 1 ml of overnight culture was diluted in 100 ml of fresh LB medium, plus appropriate antibiotics, and incubated additionally at 37 ℃, with shaking at 150 rpm for 2-3 h. When the OD_{600} of growing cells reached 0.5-0.6, the bacterial culture was submerged in an ice-water bath for 30 min. Cells were harvested by centrifugation at 5,000 rpm for 10 min at 4℃. After removal of the supernatant, the pellet was washed with 90 ml of ice-cold trituration buffer (II.1.9.E) and placed on ice for 10 min. Following another centrifugation at 5000 rpm for 10 min at 4℃, the pellet was resuspended in 10 ml of ice-cold trituration buffer. Then, 200 µl aliquots were used directly for transformation or competent cells with 7% DMSO (v/v) were frozen in liquid nitrogen and stored at -80℃.

3.1.9 Transformation

Owing to competent cells from various types of cells (*E. coli*, or *A. tumefaciens*) and their strains, different conditions of transformation were used that are listed in Table 16.

Table 16. Competent cells and conditions of transformation

Competent cells with different strains	*E. coli* (JM109 or TOP 10)	*E. coli* *[BL21 (DE3) pLysS or Rosetta(DE3) pLysS]	*A. tumefaciens* (AGL0)
A. Heat shock	42℃ for 45 sec	37℃ for 3 min	37℃ for 5 min
B. Incubation	37℃ for 1 h	37℃ for 1 h	28℃ for 2 h
C. Incubated plates	37℃ for 12-16 h	37℃ for 12-16 h	28℃ for 2 d

*For BL21 (DE3) pLysS and Rosetta (DE3) pLysS, 3.4 µl of 0.18% ß-mercaptoethanol is added to 200 µl competent cells and then incubated on ice for 10 min.

A brief description of the standard procedure for transformation is: 200 µl of competent cells was mixed with the appropriate ligation DNA or 0.5-1 µg of plasmid DNA. The mixture was incubated successively on ice for 30 min, heat shocked (referred to A in Table 16), and then put on ice for 3-5 min. (for *A. tumefaciens*, the mixture was incubated on ice for 20 min, placed in liquid nitrogen for 5 min, and then heat shocked at 37℃ for 5 min.) Afterwards, the mixture was added to 1 ml of LB or SOC medium (II.1.9.A) and incubated (referred to B in Table 16) with shaking at 150 rpm. Then, the transformed bacterial cells were plated on the LB plate containing appropriate antibiotics and incubated plates at an appropriate temperature (referred to C in Table 16).

3.1.10 Isolation of plasmid DNA and glycerol stocks

Different colonies were picked from the selective LB medium and inoculated with 5-10 mL LB plus appropriate antibiotics (II.1.7) at 37 ℃ or 28 ℃, with shaking at 150 rpm overnight. Bacterial cells were collected for 1 min by centrifugation at 13,200 rpm. The isolation of plasmid DNA was conducted using the Wizard® Plus SV Minipreps kit. After restriction analysis (II.3.1.6), bacterial culture of the positive clone was kept as follows: 0.7 ml of bacterial liquid culture was mixed with 0.7 ml of sterile glycerol solution (II.1.9.E) (1:1, v/v) by vortexing, and then immediately frozen in liquid nitrogen.

3.1.11 Removal of genomic DNA from total RNA

Reaction mixture was as follows:

30-50 µg of total RNA
10 µl of 10× Reaction buffer with $MgCl_2$
5 µl of DNase I, RNase-free (1U/µl)
Up to 50 µl of DEPC-treated water

After incubation at 37℃ for 30 min, the mixture was added to an equal volume of phenol/chloroform to terminate the reaction. Subsequently, the mixture was vortexed for 30

sec and then centrifuged at top speed at 4℃ for 3 min. The top supernatant was transferred to a new tube, and then added with 10 μl of 3 M sodium acetate (pH5.2) (1/10 volume) and 275 μl of ethanol (2.5 volumes). The mixture was kept at -20℃ overnight. After ethanol precipitation, the solution was centrifuged at 13,200 rpm for 20 min at 4℃. The pellet, after being washed with 70% ethanol and then 100% ethanol, was centrifuged at 13,200 rpm for 5 min at 4℃. After removal of the supernatant, the RNA pellet was air-dried for 5 min and then resuspended in 10-20 μl of DEPC-treated water. The concentration and quality of total RNA were determined using a NanoDrop.

3.1.12 First-strand synthesis of cDNAs

First-strand cDNA was synthesized from 1 μg of DNase I-treated total RNA using the M-MLV RT H(-) (Promega), according to the manufacturer's instructions as follows:

1 μg DNase I-treated total RNA
1 μl Random Hexamers (50 μM)
1 μl dNTPs (10 mM)
up to 12 μl H_2O

12 μl of the reaction mixture was incubated at 65℃ for 5 min and then cooled on ice for 2 min, and the following reagents were added:

4 μl 5× M-MLV RT reaction buffer
2 μl 0.1M DTT
1μl RNaseOUT^{TM} Recombinant Ribonuclease Inhibitor (40U/μl)

19 μl of the reaction mixture was incubated at 37℃ for 2 min. Then, the mixture was added to 1 μl of M-MLV RT H (-) and incubated in three successive stages: 25℃ for 10 min, 55℃ for 50 min, and 70℃ for 15 min. Afterwards, the first-strand cDNA was used as a template for quantitative real-time PCR analysis.

3.1.13 Quantitative real-time PCR (qRT-PCR) analysis

For qRT-PCR analysis, total RNA was extracted from plant materials, according to the CTAB method (II.3.1.2), and first-strand cDNA was synthesized as described in methods (II.3.1.12). To achieve more precise results, a SYBR Green qPCR Kit with ROX dye Passive Reference was used in this work. ROX is an inert dye whose fluorescence does not change during a PCR reaction, allowing normalization of fluorescent fluctuations (e.g., well-

to-well variations). These variations may occur from pipetting errors or instrument limitations.

Real-time polymerase chain reactions were performed in a 96-well reaction plate (ABI), with a StepOnePlus™ real-time PCR system (Applied Biosystems), using SYBR Green to monitor dscDNA synthesis. Gene-specific primers were used for amplification of the target gene and interspacer (IS) primers were used for amplification of the interspacer gene. All primers for the target and interspacer genes are listed in Table 10. The reaction was performed as shown in Table 17.

Table 17. qRT-PCR condition

Component	Target gene	Interspacer gene
2 x Power SYBR Green Mix	10 µl	10 µl
Primer (F)	0.6 µl of 10 µM stock	0.6 µl of 10 µM stock
Primer (R)	0.6 µl of 10 µM stock	0.6 µl of 10 µM stock
cDNA	2 µl of a 50-fold dilution	2 µl of a 4000-fold dilution
Mini$Q H_2O$	6.8 µl	6.8 µl
Total volume	20 µl	20 µl

PCR reactions were performed in three technical replicates of each sample under the following standard thermal conditions:

Holding stage	95°C	for 10min	
Cycling stage	95°C	for 15 sec	40 cycles
	60°C	for 1 min	
Melt curve stage	95°C	for 15 sec	
	60°C	for 1 min	
	95°C	for 15 sec	
		A standard ramp speed was selected (about 2 h to complete a run)	

(Use of the cycling stage in the SensiMix™SYBR kit required changes at 95℃ for 15 sec, 60℃ for 15 sec, and 72℃ for 15 sec.)

Data were analyzed using the StepOne™ Software V. 2.0.1. The qRT-PCR, C_T (threshold cycle) value is the number of cycles required to reach a defined fluorescence intensity threshold. In this study, the C_T values of both target and internal control genes were calculated using StepOne™ Software. For data analysis of all samples, relative gene expression was quantified using the $2^{-\Delta\Delta C_T}$ method (Livak and Schmittgen, 2001) to indicate fold changes of each sample related to the selected reference sample. In addition, the

interspacer gene was used as an internal control for normalized expression values. The following formulas were used for calculating the $2^{-\Delta\Delta C_T}$.

$$\Delta C_T = C_T \text{ (target)} - C_T \text{ (internal control gene)} \quad (1)$$
$$\Delta\Delta C_T = \Delta C_T \text{ (target)} - \Delta C_T \text{ (reference)} \quad (2)$$
$$\text{Relative gene expression} = 2^{-\Delta\Delta C_T} \quad (3)$$

The ΔC_T value is the difference between the C_T value of the target gene and the interspacer gene (internal control gene; Equation 1). From the difference between the ΔC_T target and another sample, such as untreated control (set as ΔC_T reference), the $\Delta\Delta C_T$ value is calculated using Equation 2. Then, the relative gene expression is determined using Equation 3. The numerical values obtained from $2^{-\Delta\Delta C_T}$ were transformed into graphics by using either the R software or SigmaPlot software.

3.1.14 Bradford assay

Protein concentration was determined according to the Bradford (1976) method and each sample was measured as follows. 10-50 µl of protein extract was mixed with an appropriate amount of water (a total volume of 100 µl), and 100 µl of water was used as a blank. 1 ml of Bradford solution (II.1.9.D) was added separately to each sample and the blank. After 5 min, the protein content was determined spectrophotometrically at 595 nm against the blank. The amount of protein was calculated from a linear calibration curve (range: 0-20 µg) with a standard BSA, as seen in Equation (1), and concentration was calculated using Equation (2).

$$\text{Protein [µg]} = (A_{595} + 0.0091) / 0.0338 \quad (1)$$
$$\text{Protein [µg/µl]} = \text{Protein [µg]} / \text{measured sample (µl)} \quad (2)$$

3.1.15 SDS-PAGE

The 12% Tris-glycine SDS-PAGE gel was set in a gel tank and 1x running buffer (II.1.9.D) was poured in. Subsequently, 20 µl of each sample, with 5 µl of 4x protein loading dye, was heated at 95 °C for 5 min. After heating, the protein mixture (or protein marker) was loaded into each well. Then, the power supply was set at 100-120 V, and electrophoresis was performed until the protein dye reached the bottom of the gel (about 1.5-2 h). After migration, the proteins were stained with a staining solution (II.1.9.D) at room temperature, with shaking at 20 rpm for 30 min. The staining solution was discarded, and the gel was destained twice with a destaining solution (II.1.9.D) at room temperature with shaking at 20 rpm for 15-30 min.

3.2 Primer design, cloning, and sequence analysis

In order to amplify alleles of the *FaCCR* or *FaCAD*, degenerated primers were designed based on deduced amino acid sequences of the *CCR* or *CAD* in the GenBank database (www.ncbi.nlm.nih.gov) (Appendix A). Besides, a partial sequence of *POD* (*Fragaria* × *ananassa* peroxidase) was obtained from the GenBank (accession number AY679597). To search further, a full-length coding sequence of POD (*Fragaria vesca*, contig64026), based on a partial *POD* sequence (accession number AY679597), was obtained from the *Fragaria Vesca* Genome Browser database (https://strawberry.plantandfood.co.nz/index.html). Since a diversity of N- or C-terminal ends of deduced amino acid sequences is present in PODs from different species (Welinder, 1992; Welinder, 2002; Passardi et al., 2004a), specific primers (II.1.8.C) of *FaPOD* were designed based on the full-length coding sequence of POD (*Fragaria vesca*).

The isolation of full-length coding region sequences of *FaCCR*, *FaCAD*, and *FaPOD* was performed by PCR (II.3.1.3) using a high-fidelity *Pfu* DNA polymerase and degenerated primers or specific primers (II.1.8.C). The expected amplification products were added with A-tailing by treatment with *Taq* DNA polymerase (II.3.1.7). Subsequently, the amplification products plus A-tailing were ligated into a pGEM T-Easy vector and then transformed into *E.coli* JM109. After transformation, the cells were plated on a LB/Ampicillin/IPTG/X-gal plate (II.1.9.A) and subjected to ß-galactosidase blue/white screening. Several white colonies were picked for cell propagation in 5 ml of LB with 100 µg ml^{-1} ampicillin (II.3.1.10). After restriction analysis (II.3.1.6), plasmid DNA of positive clones was sequenced. Sequence analysis was performed using software Vector NTI and MegAlign.

Additionally, the *FaPOD*27 sequence was obtained from the FraGenomics project, and gene cloning was done by Dr. S. Hücherig (BiNa, TUM 2011). A full-length coding sequence of *FaPOD*27 was cloned into a pGEX-4-1 vector to produce FaPOD27 in the *E. coli*.

3.3 Construction of ihpRNA and overexpression of individual *FaCCR*, *FaCAD*, and *FaPOD*

3.3.1 ihpRNA constructs

The following procedure was performed to assemble individual *FaCCR*-, *FaCAD*-, and *FaPOD*-ihpRNA constructs that comprised partial fragments (300 bp coding sequence) of target genes in sense and antisense orientations, flanked by an intron to produce a double-stranded (ds) RNA hairpin.

A pSKAscI35SIntTER vector (II.1.5) was used as a base vector that contained the second intron of the *F.* × *ananassa* quinone oxidoreductase gene (AY158836, nucleotides 4886-4993), a CaMV (cauliflower mosaic virus) 35S promoter, and a NOS terminator. To insert fragments, PCR products of *FaCCR*, *FaCAD*, or *FaPOD* were amplified by PCR (II.3.1.3) using its primers (II.1.8.D) based on a 300-bp coding sequence (Appendix C), and a high-fidelity Phusion DNA polymerase to introduce *Nhe*I and *Spe*I sites with blunt-end RCR fragments. Then, PCR fragments were digested with *Spe*I and cloned into the compatible site of a *Spe*I-*Ecl*136II pSKAscI35SIntTER vector to produce an intermediate pSKAscIA.

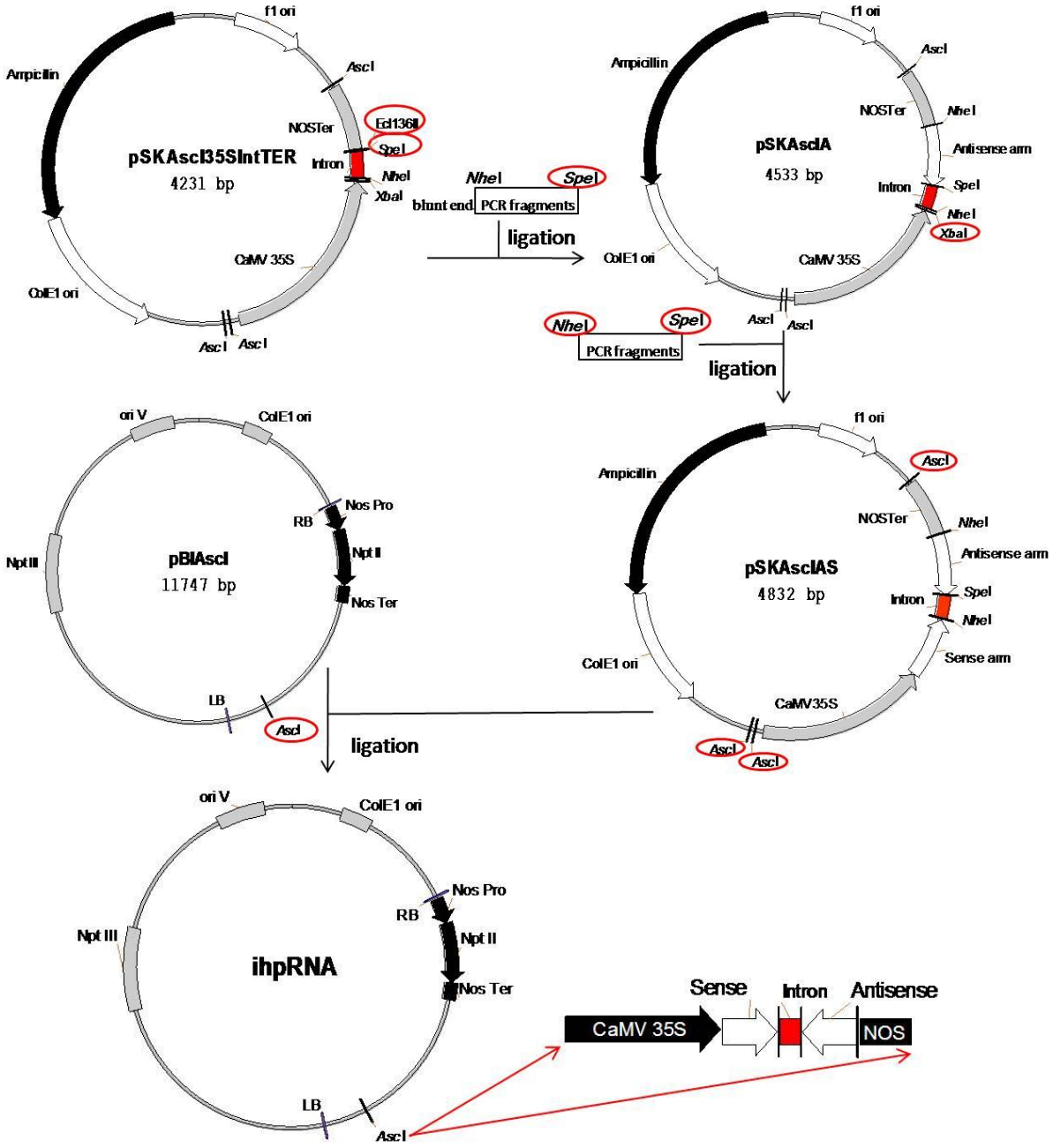

Figure 11. The construction of the plasmids pBI-*FaCCRi*, pBI-*FaCADi*, and pBI-*FaPODi*. The modification and restriction sites are circled.

Afterwards, the same PCR products were additionally digested with *Nhe*I and *Spe*I and cloned into a compatible *Xba*I site of the pSKAscIA vector to produce a pSKAscIAS vector. The orientation of sense- and antisense-mediated fragments in the vector was confirmed by using restriction enzyme analysis. Finally, the sense- and antisense-mediated fragments were cut *Asc*I from the pSKAscIAS vector and then cloned into the same sites of a binary pBIAscI vector (II.1.5) to produce the resulting plasmid individual *FaCCR*-, *FaCAD*-, *FaPOD*-, or *FaPOD*27-ihpRNA. The names are pBI-*FaCCRi*, pBI-*FaCADi*, and pBI-*FaPODi* (Figure 11), respectively.

3.3.2 Overexpression constructs

A full-length coding sequence of individual *FaCCR*, *FaCAD*, or *FaPOD* was amplified by PCR (II.3.1.3) using the Phusion DNA polymerase and its primers (II.1.8.E) based on the sequencing results (Appendix B.1-3). PCR fragments cut by *Bam*HI and *Sma*I were cloned into the same sites of the binary vector pBI121 containing a CaMV 35S promoter and NOS terminator to produce the resulting plasmid pBI-*FaCCR*, pBI-*FaCAD*, and pBI-*FaPOD* (Figure 12).

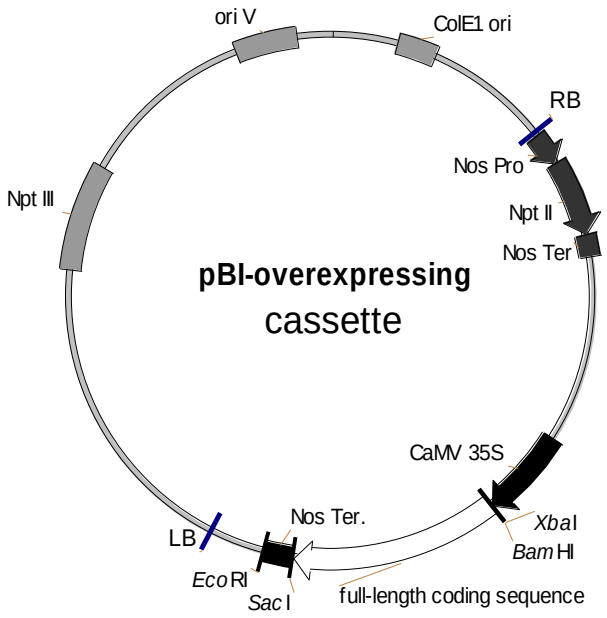

Figure 12. Plasmid pBI-*FaCCR*, pBI-*FaCAD*, and pBI-*FaPOD*. The full-length coding sequence is from *FaCCR*, *FaCAD*, and *FaPOD*.

3.4 Recombinant protein expression and purification

3.4.1 Construction of expression plasmid

In order to heterologously express FaCCR, FaCAD, and FaPOD protein in *E. coli*, the full-length coding region was subcloned into an expressing vector of pGEX-4T-1 or pET-29a(+). To subclone target genes into the pGEX-4T-1 vector, primers (II.1.8.G) based on the full-length coding region (Appendix B.1-3) were designed with the restriction sites of *Bam*HI and *Sma*I. After PCR reactions (II.3.1.3), PCR fragments of *FaCCR*, *FaCAD*, and *FaPOD* cut with *Bam*HI and *Sma*I were subcloned into a *Bam*HI-*Sma*I cut pGEX-4T-1 vector, in frame with the coding region of an N-terminal GST (glutathione S-transferase) tag (Figure 13A). To subclone target genes into the pET-29a(+) vector, primers (II.1.8.G) were designed to remove the native stop codon and add restriction sites of *Bam*HI and *Xho*I. After PCR reaction (II.3.1.3), PCR fragments of *FaCAD* cut with *Bam*HI and *Xho*I were subcloned into a *Bam*HI-*Xho*I cut pET-29a (+) vector, in frame with the coding region of the C-terminal 6X histidine region (Figure 13B).

(A)

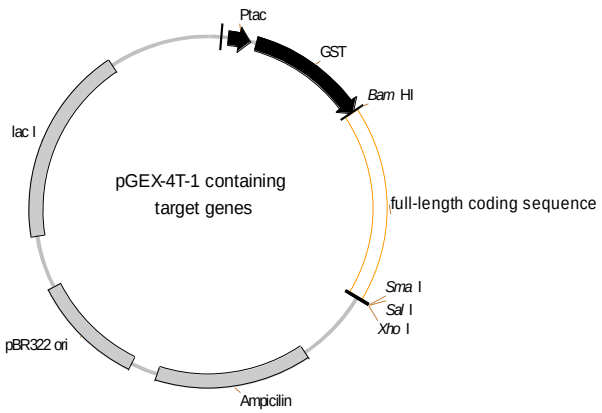

(B)

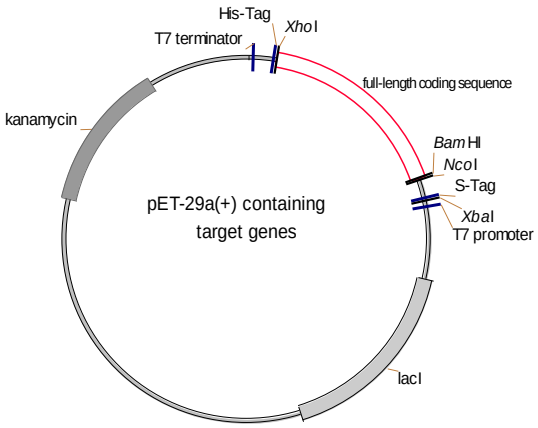

Figure 13. Expression plasmid GST-FaCCR, GST-FaCAD, GST-FaPOD (A), and His-FaCAD (B). The full-length coding region is from *FaCCR*, *FaCAD*, and *FaPOD*.

After sequencing, the plasmid DNA with different target genes (*FaCCR*, *FaCAD*, and *FaPOD*) in the pGEX-4T-1 and pET-29a (+) vector was transformed into *E. coli* BL21 (DE3) pLysS (II.3.1.9). The resulting expression plasmid was GST-FaCCR, GST-FaCAD, GST-FaPOD, and His-FaCAD (Figure 13), respectively.

3.4.2 Expression and purification of GST-fused proteins in *E. coli* BL21 (DE3) pLysS

A. GST-FaCCR and GST-FaCAD fusion proteins were purified as follows:

A single colony was inoculated into 20 ml of LB plus 100 µg ml^{-1} ampicillin and 34 µg ml^{-1} chloramphenicol at 37°C, and grown with shaking at 150 rpm overnight. The overnight bacterial cells were diluted 1:50 in LB plus 100 µg ml^{-1} ampicillin and 34 µg ml^{-1} chloramphenicol and grown at 37°C, with shaking at 150 rpm (GST-FaCAD was added with

an additional 1 mM of $ZnCl_2$ in the medium as well). When OD_{600} reached 0.5-0.6, IPTG was added to a final concentration of 0.2 mM in a bacterial culture to induce the expression of the GST-tag fusion protein at 16℃, with shaking at 150 rpm for 16-18 h. Cells were harvested by centrifugation at 5,000 rpm for 20 min at 4℃. After removal of the supernatant, the pellet was suspended in 10 ml of wash/bind buffer (II.1.9.D). Following another centrifugation at 5,000 rpm for 10 min at 4℃, the pellet was frozen at -80℃ until used.

To disrupt cells, a pellet with 10 ml of wash/bind buffer was sonicated three times. Each time, it was sonicated for 30 sec, followed by 1 min on ice. Subsequently, 10 µl of resin Glutathione-Sepharose 4B beads (Amersham Pharmacia Biotech) was added to the mixture and then it was incubated at 4℃, with shaking at 20 rpm for 30 min. After incubation, the mixture was centrifuged at 12,000 rpm for 20 min at 4℃. The supernatant was removed and beads containing GST-tagged fusion proteins were washed twice with 5 ml of wash/bind buffer. Following centrifugation at 5,000 rpm for 5 min at 4℃, the supernatant was discarded. Finally, the beads were added with 200-500 µl of elution buffer (II.1.9.D). After 5 min incubation at room temperature, the mixture was centrifuged at 5,000 rpm for 5 min at 4℃. The GST-tagged fusion proteins were transferred into a new tube. The purity of protein was monitored by SDS-PAGE. Afterwards, the proteins were prepared for measurement of enzyme activities.

B. Peroxidase was expressed in *E. coli* Rosetta (DE3) pLysS and extracted as follows:

The overnight bacterial cells were diluted 1:100 in LB with 50 µg ml^{-1} carbenicillin and 34 µg ml^{-1} chloramphenicol and grown at 30℃ with shaking at 150 rpm. When OD_{600} reached 0.3-0.4, IPTG was added to a final concentration of 0.5 mM in a bacterial culture and incubated at 16℃ with shaking at 150 rpm for 16-18 h. Cells were harvested by centrifugation at 5,000 rpm for 20 min at 4℃. After removal of the supernatant, the pellet was frozen at -80℃ until used.

To disrupt cells, the pellet, with 10 ml of peroxidase extraction buffer (II.1.9 D), was sonicated three times. Each time, it was sonicated for 30 sec, followed by 1 min on ice. Subsequently, the mixture was passed through a sterile 10 ml syringe with a 27G needle. Then, the mixture was centrifuged at 5,000 rpm for 20 min at 4℃ and the supernatant was prepared for measurement of enzyme activities.

3.4.3 Expression and purification of His-fused proteins in *E. coli* BL21 (DE3) pLysS

His-FaCAD and His-4CL fusion proteins were purified as follows:

For His-FaCAD, the overnight bacterial cells were diluted 1:50 in LB containing 25 µg ml^{-1} kanamycin and 34 µg ml^{-1} chloramphenicol and grown at 37℃, with shaking at 150 rpm. His-FaCAD protein was induced by 0.2-1 mM of IPTG in a bacterial culture (OD_{600}= 0.5-0.6) at 16℃, with shaking at 150 rpm for 16-18 h. For His-4CL, LB contained 100 µg ml^{-1} ampicilline and 34 µg ml^{-1} chloramphenicol, protein was induced by 0.8 mM of IPTG in the bacterial culture at room temperature with shaking at 150 rpm for 20-24 h. Cells were harvested by centrifugation at 5,000 rpm for 20 min at 4℃. The pellet was frozen at -80℃ until used.

To disrupt cells, the pellet with 10 ml of wash/bind buffer (II.1.9.D) was sonicated three times. Each time, it was sonicated for 30 sec, followed by 1 min on ice. Following centrifugation at 12,000 rpm for 20 min at 4℃, FPLC was performed on the supernatant with a His-trap column (II.2.1). Briefly, the column was successively washed with MQ water and binding buffer first, then crude proteins were loaded onto it. After loading, the column was successively washed with wash/bind buffer and elution buffer (II.1.9.D). Fractions (Fraction 3-6) were collected in the tube and protein was quantified using the Bradford method (II.3.1.14). The purity of protein was monitored by SDS-PAGE. Afterwards, the proteins were prepared for measurement of enzyme activities.

3.4.4 Construction and expression of the recombinant protein in yeast (*Saccharomyces cerevisae* INVSc.1)

Plasmid DNAs of pET-*FaCAD* containing his-tag were used for PCR template DNAs. Primers with restriction enzyme sites (II.1.8.G) were used to amplify a full-length coding sequence by the PCR method (II.3.1.3). The amplified PCR product of *FaCAD* cut *Bam*HI and *Xba*I were subcloned into a *Bam*HI-*Xba*I pYES2 vector containing a galactose-inducible promoter (II.1.5). The resulting plasmid pYES2-*FaCAD* contained 6X His-tag at a C-terminal end of the full-length coding region.

After sequencing of pYES2-*FaCAD*, yeast cells of the *S. cerevisae* INVSc.1 strain were transformed using the *S. c.* EasyComp. Transformation Kit (Invitrogen) and they were grown in a SC-U selective medium (II.1.9.A), plus 2% glucose, for 2-3 days at 30℃. Positive clones were confirmed by PCR screen (II.3.1.3), and inoculated in a SC-U selective medium, plus 2% galactose, to express pYES2-FaCAD in the yeast cells. Cells were harvested at different times. The culture cells were centrifuged at 1500 × g for 5 min at 4℃ and the pellet was frozen at -80℃ until used.

To disrupt cells, the pellet, with an appropriate volume of breaking buffer (50 mM of sodium phosphate, pH 7.4, 1 mM of EDTA, 5% glycerol, 1 mM of PMSF) and an equal

volume of glass beads (Roth), was disrupted by vortexing, which was performed ten times. Each time, cells were also sonicated for 45 sec, followed by 45 sec on ice. Afterwards, the mixture was centrifuged at 13,200 rpm for 10 min at 4℃. The supernatant was used for enzymatic assays.

3.5 FaCCR activity assay

3.5.1 Preparation of hydroxycinnamoyl-CoA as FaCCR substrates

Enzymatic synthesis of hydroxycinnamoyl-CoA (cinnamoyl-CoA, *p*-coumaroyl-CoA, caffeoyl-CoA, and feruloyl-CoA) was carried out with purified 4CL, according to the method of Beuerle and Pichersky (2002). In this study, the His-tag 4CL was kindly provided by Dr. Till Beuerle, Technical University Braunschweig. His-tag 4CL recombinant protein was expressed in *E.coli*, as described in methods (II.3.4.3), and purified using FPLC (II.2.1).

To obtain sufficient amounts of hydroxycinnamoyl-CoA products, 20 ml of reaction mixture was prepared as shown in Table 18 and incubated at room temperature. After 6 h incubation, an additional 13.8 mg of ATP, 4 mg of coenzyme A, and 0.5 mg of purified 4CL were added to the reaction mixture. It was then incubated for 12-16 h.

Table 18. Hydroxycinnamoyl-CoA reaction mixture

Component	**Amount**
Substrates (cinnamic acid, *p*-coumaric acid, caffeic acid, and ferulic acid)	6.6 mg
Coenzyme A	4 mg
ATP	13.8 mg
Tris-HCl (pH7.5)	50 mM
$MgCl_2$	2.5 mM
Purified 4CL	0.5 mg
Total volume	20 mL

To purify hydroxycinnamoyl-CoA, 0.8 g of ammonium acetate was added to the reaction mixture. Before the reaction mixture was loaded onto a 50 ml ISOLUTE C8(EC) SPE column (Biotage, UK), the column was washed successively with 50 ml of methanol, distilled water, and 4% ammonium acetate solution. Then, the reaction mixture was loaded onto the SPE column. After loading, the column was washed with 4% ammonium acetate solution until free CoA was detectable, which was determined spectrophotometrically when absorbance was measured at 259 nm. The CoA esters were obtained by elution with MQ water. Fractions (5 ml, 2-6) were collected and lyophilized. After freeze-drying, reaction products were dissolved in MQ water and purity was checked by thin layer chromatography

(TLC, Polygram SIL G/UV_{254}, Macherey-Negel) with 1-butanol/water/acetic acid (60:35:25).

Concentration of the reaction products was determined spectrophotometrically by measuring the absorbance at the absorption maxima of the reaction products (caffeoyl-CoA at 346 nm, *p*-coumaroyl-CoA at 333 nm and feruloyl-CoA at 346 nm). Concentration was calculated by using the reported extinction coefficients of hydroxycinnamoyl-CoAs, (wavelength-dependent absorptivity coefficient): caffeoyl-CoA ε_{346}=18 $mM^{-1}cm^{-1}$, *p*-coumaroyl-CoA ε_{333}=21 $mM^{-1}cm^{-1}$ and feruloyl-CoA ε_{346}=19 $mM^{-1}cm^{-1}$ (Lüderitz et al., 1982; Stöckigt and Zenk, 1975).

$$c = \frac{A \times V_t}{\varepsilon \times \ell \times V_s}$$

A = Absorbance of the sample
ε = wavelength-dependent absorptivity coefficient (mM^{-1} cm^{-1})
ℓ = light path (cm)
c = concentration of the sample
V_t = total volume (µl)
V_s = sample volume (µl)

3.5.2 Determination of pH and temperature optima

GST-FaCCR recombinant protein was expressed in *E.coli* and purified using the resin, as described in methods (II.3.4.2). The purified GST-FaCCR was used for the following experiments: II.3.5.2, II.3.5.3, and II.3.5.5.

FaCCR activity was determined spectrophotometrically by measuring the decrease in absorbance at 366 nm due to transformation of feruloyl-CoA to coniferaldehyde and oxidation of NADPH (Wengenmayer et al., 1976). In order to determine the pH optimum, reaction mixtures were prepared containing the following buffers: 100 mM of different buffers with pH at varied ranges (sodium phosphate, pH 6-7; citrate, pH 4-6; Tris-HCl, pH 8-9), 0.1 mM of NADPH, 70 µM of feruloyl-CoA, and 2 µg of purified GST-FaCCR in a total volume of 150 µl. The reaction was started by the addition of GST-FaCCR at room temperature in a spectrophotometer. Each treatment was performed in triplicate. Based on the linear decrease in A_{366}, FaCCR activity was calculated by the formula shown in II.3.5.4.

To determine temperature optimum, the FaCCR activity was incubated at various temperatures (15-45°C). The reaction mixture was composed of 100 mM of sodium phosphate (pH 6), 0.1 mM of NADPH, 70 µM of feruloyl-CoA, and 0.5 µg of purified GST-FaCCR in a total volume of 100 µl. Each treatment was performed in triplicate, and incubated at different temperatures (15-45°C) for 10 min. This was stopped by the addition

of 25 µl of acetic acid. After centrifugation at top speed for 10 min, the clear supernatant was analyzed by LC-UV-ESI-MS^n. The amount of coniferaldehyde was calculated from a linear calibration curve (0-100 µM) of the standard coniferaldehyde. The specific activity value was calculated taking into account the protein level, and was expressed as µM mg^{-1} min^{-1}.

3.5.3 Determination of kinetics

Kinetic parameters of the purified recombinant GST-FaCCR were determined spectrophotometrically (Wengenmayer et al., 1976). Reaction mixtures (150 µl), containing different concentrations of substrates within a range of 0-140 µM of substrate (*p*-coumaroyl-CoA, feruloyl- CoA, and caffeoyl-CoA), 100 µM of NADPH, 100 mM of sodium phosphate (pH 6), and 0.5-2 µg of GST-FaCCR, were monitored by following the absorbance decrease at 366 nm at room temperature. Each treatment was performed in triplicate. Activity was calculated based on the linear decrease at A_{366} due to the conversion of hydroxycinnamoyl-CoA to its corresponding aldehydes and to the oxidation of NADPH. Equation shown in II.3.5.4 was used. Both K_m and V_{max} values were calculated for each substrate using Microsoft® Excel® with the Solver form. The turnover number (K_{cat}) was calculated on the basis of the GST-FaCCR molecular mass (37.3 KDa).

3.5.4 FaCCR activity calculation

FaCCR activity and specific activity were calculated using the following equations:

$$\text{Enzyme activity (Unit)} = \frac{(\Delta A\,/\text{minute} \times V_t)/\text{Factor}}{\varepsilon_{NADPH} \times \ell}$$

$$\text{Specific activity (U/mg)} = \frac{\text{Unit}}{\text{mg protein}}$$

Abs= Absorbance
ΔA= Abs $_{\text{starting}}$ – Abs $_{\text{ending}}$
V_t= total volume (µl)
Factor= $\varepsilon_{(\text{substrate+NADPH-product})}/\varepsilon_{NADPH}$
ε = extinction coefficient (mM^{-1} cm^{-1})
ℓ = light path (cm)

Extinction coefficients (ε_{366}):
NADPH=3 m $M^{-1}cm^{-1}$
p-Coumaroyl-CoA=7.5 m $M^{-1}cm^{-1}$, *p*-coumaraldehyde=3.5 m $M^{-1}cm^{-1}$
Feruloyl-CoA=13 m $M^{-1}cm^{-1}$, coniferaldehyde=10 m $M^{-1}cm^{-1}$
Caffeoyl-CoA=13 m $M^{-1}cm^{-1}$, caffeic aldehyde =10 m $M^{-1}cm^{-1}$

3.5.5 Identification of reaction products by LC-UV-ESI-MS^n

To verify the identity of the reaction products, 100 µl of a reaction mixture consisting of 100

mM of sodium phosphate (pH 6), 0.1 mM of NADPH, 70 µM of hydroxycinnamoyl-CoA (cinnamoyl-CoA, *p*-coumaroyl-CoA, caffeoyl-CoA, and feruloyl-CoA), and 2 µg of purified GST-FaCCR was incubated at 25 ℃ for 20 min. The reaction was stopped by the addition of 25 µl of acetic acid, and then centrifuged at top speed for 10 min. The clear supernatant was analyzed by LC-UV-ESI-MS^n under the conditions described in methods (II.2.2_system I).

All data were acquired and analyzed using DataAnalysis 3.1 software (Bruker Daltonics). Because of lack of authentic *p*-coumaraldehyde and caffeic aldehyde (3,4-dihydroxy cinnamaldehyde) references chromatographic properties and mass fragmentation patterns of GST-CCR products formed from *p*-coumaroyl-CoA and caffeoyl-CoA could not unambiguously assigned to the expected products but $[M-H]^-$ ions were in accordance to the anticipated data. Retention time, mass spectrum, and product ion spectrum of coniferaldehyde formed by GST-CCR were confirmed by comparison with those of authentic coniferaldehyde reference. The MS and MS^2 spectral data of the products and authentic chemicals were acquired in negative ion mode targeting the $[M-H]^-$ ions. Retention times and mass fragmentation patterns of GST-CCR reaction products are listed in Table 19.

Table 19. Retention times and dominant ion masses in ESI(-)-MS spectra of hydroxycinnamoyl aldehyde products formed by GST-FaCCR

	R_t (min)	**$[M-H]^-$** (*m/z*)	**$-MS^2$** (*m/z*)
Products			
p-Coumaraldehyde	31.4	147	147, 119
Coniferaldehyde	32	177	177, 175, 162, 147
Caffeic aldehyde	27.5	163	163, 161, 143,135

3.6 FaCAD activity assays and analysis of standard chemicals *via* LC-UV-ESI-MS^n

GST-tag FaCAD or His-tag FaCAD recombinant protein was expressed in *E. coli* and purified as described in methods (II.3.4.2 or II.3.4.3). The pYES2-FaCAD plasmid was expressed in yeast (II.3.4.4). Purified GST-FaCAD, His-FaCAD, and crude protein of pYES2-FaCAD were used for the following experiments.

FaCAD activity was determined spectrophotometrically by measuring the decrease in absorbance at 340 nm due to the production of hydroxycinnamyl alcohols. The reaction mixture was prepared as shown in Table 20.

Table 20. FaCAD reaction mixture for spectrophotometer and LC-UV-ESI-MS^n

	Spectrophotometer	LC-UV-ESI-MS^n	Final concentration
Protein	5-20	10-100	(μg)
Sodium phosphate (pH 6.5)	100	100	(mM)
NADPH	200	200	(μM)
Aldehyde substrates	34	100	(μM)
Total volume	100	100-500	(μl)

The reaction was started by the addition of purified protein or crude protein. FaCAD activity was calculated using the extinction coefficients of the substrates (NADPH:ε_{340} = 6.3 $mM^{-1}cm^{-1}$; coniferaldehyde:ε_{340} = 18.5 $mM^{-1}cm^{-1}$; sinapaldehyde:ε_{340} = 15.8 $mM^{-1}cm^{-1}$, Somssich et al., 1996).

In addition, reaction products were identified by LC-UV-ESI-MS^n. Enzyme reactions were prepared using the parameters described in Table 20 at 30°C for 30 min. Then, the reaction mixtures were extracted twice with an equal volume of ethyl acetate by vortexing for 30 sec. After centrifugation at top speed for 1 min, the supernatant was dried by *Speed-Vac*. The pellet was added with 30 μl of 50% methanol (v/v) and then analyzed by LC-UV-ESI-MS^n under the conditions described in methods (II.2.2 system II).

All data were acquired and analyzed using the Agilent 6300 series ion trap LC/MS system software. Retention times, mass spectra, and ion spectra of the FaCAD reaction products (coniferyl alcohol and sinapyl alcohol) were confirmed by comparison with the chromatographic properties and mass fragmentation patterns of authentic chemicals. Authentic coniferaldehyde, sinapaldehyde, coniferyl alcohol, and sinapyl alcohol were subjected to LC-UV-ESI-MS^n. The MS and MS^2 spectral data of these authentic chemicals were acquired in positive ion mode targeting the $[M+Na]^+$ ions. Retention times and mass fragmentation patterns of these authentic chemicals are listed in Table 21.

Table 21. Retention times and dominant ion masses in ESI(+)-MS spectra of substrates and products formed by using authentic chemicals

	R_t (min)	$[M+Na]^+$ (*m/z*)	$+MS^2$ (*m/z*)
Substrates			
Coniferaldehyde	14.6	201	201, 198, 186, 179
Sinapaldehyde	13.8	231	231, 228
Products			
Coniferyl alcohol	10	203	203, 201, 199, 187, 185, 171
Sinapyl alcohol	9.6	233	233, 231, 214, 201, 193

3.7 FaPOD activity assays

FaPOD and FaPOD27 were expressed in *E. coli*. Crude protein was extracted, as described in methods (II.3.4.2.B). Afterwards, protein extracts of FaPOD and FaPOD27 were used for guaiacol oxidase activity assays. This method is widely used for quantifying activity of various peroxidases. FaPOD activity was determined spectrophotometrically by measuring the increase in absorbance at 470 nm due to the formation of oxidation products of guaiacol. The 300 µl of reaction mixture contained 230 µl of 0.1 M potassium phosphate buffer (pH 7.0), 25 µl of 18 mM guaiacol, 25 µl of 9.8 mM H_2O_2 (30% solution, Roth) and 20 µl of crude protein. The reaction was started by the addition of crude protein at room temperature. Each treatment was performed in triplicate. Enzymatic activity was calculated using the extinction coefficient of 26.6 $mM^{-1}cm^{-1}$ at 470 nm (Vitali et al., 1998).

To verify the identity of the reaction products, 300 µl of the reaction mixture, that included 50 mM of sodium tartrate buffer (pH 3.5) and 50 µl of crude protein (1.9 mg), was incubated at room temperature. 135 µM of H_2O_2 (a 30% solution) was added to the mixture at 1-min intervals, one at a time for a total of 4 mM of H_2O_2 (Ward et al., 2001). After 30 min, the reaction mixture was extracted with an equal volume of ethyl acetate by vortexing for 30 sec. Supernatant was transferred into a new tube after centrifugation at top speed for 1 min. The extraction process was repeated as described above. Finally, ethyl acetate extracts were dried by *Speed-Vac*. After drying, the pellet was added to 30 µl of 50% methanol (v/v) and used directly for LC-UV-ESI-MS^n analysis under the conditions described in methods (II.2.2_system I).

3.8 Strawberry fruit

3.8.1 Gene expression studies

The differential expression of lignin biosynthetic genes (*FaCCR*, *FaCAD*, and *FaPOD*) in the flower, fruit, and vegetative tissue of the strawberry cv. Elsanta was investigated. Developed fruits at small green (SG), green white (GW), white (W), turning (T), red (R) stages, and vegetative tissues (leaves, roots, stems, and runners), as well as flowers, were collected from strawberry plants. All samples were immediately frozen in liquid nitrogen and stored at -80℃ until used.

3.8.2 Wounding treatment

To simulate wounding (i.e., fruits perforated by a syringe), the fruit of *F. x ananassa* cv. Elsanta, at the turning stage, was infiltrated throughout the entire fruit with MMA medium

(II.1.9.A) by using a sterile 1 ml hypodermic syringe. After infiltration, wounded fruits remained attached to the plant until harvested. Non-infiltrated fruit was used as control fruit. Wounded and control fruits were harvested at different times (0, 0.2, 6, 12, 24, and 48 h) and immediately frozen in liquid nitrogen before being stored at -80°C.

3.8.3 Pathogen treatment

To simulate pathogen infection in a fruit, *F. x ananassa* cv. Elsanta fruit in the turning ripening stage was infiltrated throughout the entire fruit with a suspension of *Agrobacterium tumefaciens* AGL0, or half of the fruit with *Agrobacterium* suspension containing a pBI-*CHSi* construct (II.1.5) by using a sterile 1 ml hypodermic syringe. The preparation of the *Agrobacterium* suspension for the fruit infiltration is described in II.3.8.4.1.

All pathogen-infected fruits treated with *Agrobacterium* remained attached to the plant until harvest. For entire-fruit infiltration, samples were collected at different times (1 h-10 d). For half-fruit infiltration, samples were harvested at 14 days. In addition, non-infiltrated fruits were used as controls. All samples were immediately frozen in liquid nitrogen and stored at -80°C until RNA extraction.

3.8.4 Down-regulation and up-regulation of lignin biosynthetic genes (*FaCCR*, *FaCAD*, and *FaPOD*) in fruit

To assess the effects of independent down-regulation and up-regulation of lignin biosynthetic genes on *F. x ananassa* cv. Elsanta and cv. Calypso (CHS^-), fruits of the white developmental stage were injected with *Agrobacterium* suspensions. *Agrobacterium* carrying a pBI-*FaCCRi*, pBI-*FaCADi*, and pBI-*FaPODi* construct (II.3.3.1) were used to down-regulate lignin genes whereas *Agrobacterium* suspensions carrying a pBI-*FaCCR*, pBI-*FaCAD*, and pBI-*FaPOD* construct (II.3.3.2) were applied to up-regulate lignin genes.

In addition to down-regulation and up-regulation of individual lignin biosynthetic genes in *F. x ananassa* cv. Calypso (CHS^-), a mixture of *Agrobacterium* suspensions with three different constructs, was used and injected into fruits. Preparation of the *Agrobacterium* suspension and infiltration of the fruit are described in methods (II.3.8.4.1). Fruit of the white developmental stage was injected with an *Agrobacterium* mixture containing pBI-*FaCCRi*, pBI-*FaCADi*, and pBI-*FaPODi* constructs to co-down-regulate lignin genes (named pBI-Si3) and with *Agrobacterium* containing pBI-*FaCCR*, pBI-*FaCAD*, and pBI-*FaPOD* constructs to co-up-regulate lignin genes (named pBI-O3).

3.8.4.1 Preparation of the *Agrobacterium* suspension and infiltration of fruits

Infiltration of strawberry fruit was carried out according to the method of Hoffmann et al. (2006). A single colony of AGLO strain carrying the vector with the target gene was inoculated in 20 ml of LB with appropriate antibiotics at 28 ℃, with shaking at 150 rpm overnight. Then, 2 ml of culture was diluted in 200 ml of fresh LB medium plus appropriate antibiotics and incubated at 28 ℃, with shaking at 150 rpm overnight. When an OD_{600} of growing cells reached 0.8-1, the cells were harvested at 4℃ by centrifugation at 5,000 rpm for 10 min. After removal of the supernatant, the pellet was washed with 200 ml of the cold MMA medium (II.1.9.A). Following another centrifugation at 5,000 rpm for 10 min at 4℃, the pellet was resuspended in 20 ml of cold MMA medium to a final OD_{600} of 2.2-2.4. A suspension containing *Agrobacterium* carrying different constructs was injected throughout the entire fruit by using a sterile 1-ml hypodermic syringe. Injected fruits remained attached to the plant until harvest (14 days). Harvested fruits were analyzed for texture, gene expression levels, enzymatic activities, metabolite analysis, lignin content, and lignin composition.

3.8.4.2 Fruit firmness

Fruit firmness was determined by a TA-XT2i texture analyzer (Bourne, 2002; Singh and Reddy, 2006). The measuring force was made with a probe of 0.5 mm in diameter to penetrate the surface of the fruit. Each fruit was penetrated at a speed rate of 1 to 10 mm/s. Based on the bio-yield point, the maximum of force developed during the measurement was recorded and expressed in Newtons (N). Each fruit was measured twice on the two opposite sides of the fruit. The penetrated fruit was frozen in liquid nitrogen immediately, and stored at -80℃ until used.

3.8.4.3 Gene expression level assay

Achenes were manually removed from the frozen fruits. Afterwards, total RNA was prepared as described in II.3.1.2. Then, 1 µg of the total RNA was used for synthesizing cDNA, as described in II.3.1.12 after removal of the genomic DNA from the total RNA (II.3.1.11). The cDNA was ready for a gene expression level assay by using real-time PCR, as described in II.3.1.13.

3.8.4.4 Enzyme extraction and assays

Enzyme extraction was performed according to Chabannes et al. (2001). Briefly, 200 mg of

frozen powder from the deachened fruit was added with 1 ml of extraction buffer consisting of 0.1 M of Tris-HCl (pH 7.5), 2% PEG 6000 (w/v), 5 mM of DTT, and 2% PVP K30 (w/v). Crude protein was extracted by vortexing for 30 sec and incubated on ice for 5 min. After centrifugation at 13,200 rpm for 10 min at 4℃, the supernatant was used for the measurement of enzyme activity. Protein concentration was determined using the Bradford method (II.3.1.14). For FaCCR or FaCAD assays, the reaction mixture was prepared as shown in Table 22.

Table 22. FaCCR and FaCAD reaction mixture for enzyme assays

	FaCCR	FaCAD
Crude protein	30 μg	30 μg
Sodium phosphate	100 mM (pH 6)	100 mM (pH 6.5)
NADPH	100 μM	200 μM
Substrates	70 μM feruloyl-CoA	100 μM coniferaldehyde
Total volume	500 μl	500 μl
Incubated time and temperature	25℃ for 30 min	30℃ for 30 min

After 30 min of incubation, the reaction mixture was extracted with an equal volume of ethyl acetate by vortexing for 30 sec. Top supernatant was transferred into a new tube after centrifugation at top speed for 1 min. An equal volume of ethyl acetate was added to the original tube for extracting, as described above. The supernatants from both extractions were collected in the tube. Finally, ethyl acetate extracts were dried by *Speed-Vac*. After drying, the pellet was added to 30 μl of 50% methanol (v/v) and used directly for LC-UV-ESI-MS^n analysis under the conditions mentioned previously (II.2.2 system I for FaCCR and II.2.2 system II for FaCAD). FaCCR activity was determined by LC-UV-ESI-MS^n based on the formation of the product coniferaldehyde. Similarly, FaCAD activity was determined by the formation of the product coniferyl alcohol. Both products were quantified using DataAnalysis 3.1 (Bruker Daltonics). The amounts of coniferaldehyde and coniferyl alcohol were calculated from linear calibration curves 0-150 μM and 0-1000 μM, respectively. The specific enzymatic activities of FaCCR and FaCAD were calculated and expressed as μM mg^{-1} min^{-1}.

3.8.4.5 Extraction and metabolite analysis *via* LC-UV-ESI-MS^n

250 mg of frozen powder from the deachened fruit was dissolved in 500 μl of methanol containing 50 mg of biochanin A as an internal standard. The mixture was extracted by vortexing for 1 min, sonicating for 5 min, and centrifuging at 13,200 rpm for 10 min. The

supernatant was transferred to a fresh tube and 500 µl of methanol was added to the original tube to extract the residue. The supernatants from both extractions were collected in the tube and placed in *Speed-Vac* to evaporate the methanol. The extracts were added with 35 µl of water (LC-MS quality), followed by vortexing for 1 min and sonicating for 3 min. After centrifugation at 13,200 rpm for 10 min, the supernatant was used for metabolite analysis.

Metabolite analysis was performed by LC-UV-ESI-MS^n under the conditions described in methods (II.2.2 system I). All mass spectra were acquired in the negative and positive ion mode. Auto-tandem mass spectrometry was used to break down the most abundant ($[M+H]^+$, $[M-H]^-$, or $[M]^+$) ions of the different compounds in the extracts. Identity of metabolites was confirmed by comparing the retention times, mass spectra, and ion spectra of the different compounds in the extracts with those of the reference compounds (Table 23). Reference compounds were isolated, synthesized, and from Roth. Enzymatic synthesis of phenylpropanoyl glucose esters was carried out with the FaGT2 (Lunkenbein et al., 2006a). Pelargonidin 3-glucoside, quercetin glucoside, kaempferol glucoside, catechin, epicatechin, and biochanin A were obtained from Roth. Proanthocyanidins and pelargonidin 3-glucoside-malonate were isolated from strawberry and identified as described by Fossen et al. (2004) and Gu et al. (2003).

In addition to qualitative identification based on fragmentation patterns and retention times each compound was quantified by using QuantAnalysis 1.5. All results were normalized against the internal standard and expressed as mg-equ. kg^{-1}.

3.8.4.6 Lignin histochemical staining

Lignified tissues were visualized using Wiesner staining (Clifford, 1974), according to the method of Blanco-Portales et al. (2002). Slices of fruits were immersed in 1% (w/v) phloroglucinol solution in 70% ethanol until tissues were cleared (1-2 days). After removal of the phloroglucinol solution, a few drops of 37% concentrated HCl were added the slices. Subsequently, lignified tissues appeared pink-red and then the color faded within 30 min of staining. Therefore, all photographs were taken immediately.

Table 23. LC-UV-ESI-MS^n retention times and fragmentation patterns of *F. x ananassa* metabolites

Compounds	Rt [min]	MS [*m/z*]	MS^2 [*m/z*]
Phenolic acid derivatives			
Cinnamoyl glucose	31.7	333 $[M+H]^+$	185
p-Coumaroyl glucoside	23.3	325 $[M-H]^-$	163[aglycon]$^-$, 119, 325
Caffeoyl glucose	20.2	341 $[M-H]^-$	179[aglycon]$^-$, 161, 203
Feruloyl glucose	24.6	355 $[M-H]^-$	193[aglycon]$^-$, 217, 175
p-Hydroxybenzoyl glucose	17.3	299 $[M-H]^-$	137[aglycon]$^-$, 179, 239
Flavonols			
Kaempferol glucoside	35.4	447$[M-H]^-$	285[aglycon]$^-$, 255, 447, 327
Quercetin glucoside	30.6	465$[M+H]^+$	303[aglycon]$^+$
Catechin	22.1	289$[M-H]^-$	245
Anthocyanins			
Pelargonidin 3-glucoside	24.6	433$[M]^+$	271[aglycon]$^+$
Pelargonidin 3-glucoside-malonate	30.4	519 $[M]^+$	271[aglycon]$^+$, 475, 433
Pelargonidin rutinoside	20	579 $[M]^+$	271[aglycon]$^+$, 433
Proanthocyanidins			
(Epi)catechin-(epi)catechin (isomer 1)	19.4	577$[M-H]^-$	289, 425, 451, 560
(Epi)catechin-(epi)catechin (isomer 2)	19.8	577$[M-H]^-$	289, 425, 451, 560
(Epi)afzelechin-(epi)catechin (isomer 1)	22.3	561$[M-H]^-$	289
(Epi)afzelechin-(epi)catechin (isomer 2)	22.6	561$[M-H]^-$	289
Internal standard			
Biochanin A	40.8	283$[M-H]^-$	283$[M-H]^-$, 268

3.8.4.7 Lignin content

3.8.4.7.1 Cell wall preparation

The cell wall was prepared according to the method of Meyer et al. (1998). 250 mg of frozen strawberry powder was extracted with 1.5 ml of 0.1 M phosphate buffer (pH 7.2), followed by sonication for 3 min and incubation for 30 min at 40℃. After centrifugation at 13,200 rpm for 10 min, the pellet was resuspended in 1.5 ml of 80% ethanol, then sonicated for 3 min and incubated at 80℃ for 10 min. The mixture was centrifuged at 13,200 rpm for 10 min. After removal of the supernatant, the pellet was resuspended in 1.5 ml of 80% ethanol,

as described above. Finally, the pellet was added to 1.5 ml of acetone and then sonicated for 3 min. Following centrifugation at 13,200 rpm for 10 min, the pellet was subjected to hydrolysis treatment.

3.8.4.7.2 Hydrolysis

Hydrolysis was prepared according to the method of Franke et al. (2002). The pellet was dissolved in 950 µl of 1 M NaOH and placed at room temperature for about 16 h. Subsequently, 950 µl of 1 M HCl was added to the tube and mixed well. The mixture was centrifuged at 13,200 rpm for 10 min. After removal of the supernatant, the pellet was washed twice with 1 ml of distilled water then sonicated for 3 min. Following centrifugation at 13,200 rpm for 5 min, the pellet was collected for thioglycolic-acid assay.

3.8.4.7.3 Thioglycolic-acid assay

The thioglycolic-acid assay was performed by the method of Campbell and Ellis (1992). The pellet obtained after hydrolysis was mixed with 750 µl of distilled water, 250 µl of 37% HCl, and 100 µl of thioglycolic acid (Aldrich) and incubated at 80°C for 3 h. After centrifugation at 13,200 rpm for 10 min, the pellet was washed with 1 ml of distilled water, followed by sonication for 3 min and centrifugation at 13,200 rpm for 5 min. After removal of the supernatant, the pellet was resuspended in 1 ml of 1 M NaOH and placed at room temperature with gentle shaking for about 16 h. Subsequently, the mixture was centrifuged at 13,200 rpm for 5 min, and the supernatant was transferred to a fresh tube. Then 200 µl of concentrated HCl (37%) was added to each tube, followed by vortexing for 5 sec, and incubation at 4°C for 4 h. After lignin precipitation, the mixture was centrifuged at 13,200 rpm for 10 min at 4°C. The supernatant was discarded and the insoluble lignin was dissolved in 1 ml of 1 M NaOH. The absorbance of the lignin sample was determined spectrophotometrically by measuring at 280 nm. The amount of lignin was calculated from a linear calibration curve (0-20 µg) with hydrolytic lignin (Sigma).

3.8.4.8. Lignin composition

3.8.4.8.1 Preparation of plant material

120±20 g of deachened strawberry fruit was cut into small pieces and homogenized using an Ultra Turrax (power set at 10,000/min). After homogenizing, 45 ml of distilled water was added into each Falcon™ tube and centrifuged at 5,100 rpm for 15 min. After removal of the supernatant, 45 ml of distilled water was added to each Falcon™, followed by vortexing for

3 min and centrifuging at 5,100 rpm for 15 min. The pellets were washed until the supernatant was determined to be neutral using pH indicator paper. Finally, 10 ml of ethanol (99%) was added to each Falcon™. After centrifugation at 5,100 rpm for 15 min, the pellets were placed at 37℃ for drying, overnight.

3.8.4.8.2 Isolation of lignin

Isolation of lignin was performed by the method of Evtuguin et al. (2001). Dried pellets were transferred in a three-necked flask with 22.5 ml of distilled dioxan and 2.5 ml of 0.2M HCL (9:1, v/v). The reaction mixture in the three-necked flask, connected with a reflux condenser and nitrogen bubbler, was heated at 90-95℃ under nitrogen for 40 min. After extraction # 1, the liquid was transferred to a round-bottom flask where the liquid was allowed to cool down to about 50℃. For extraction # 2, 18 ml of distilled dioxan and 2 ml of 0.2M HCL were added to the same three-necked flask, as described above, and heated at 90-95℃ for 30 min. This process was repeated for extraction # 3. For extraction # 4, 18 ml of distilled dioxan and 2 ml water were added to the three-necked flask, as described above and heated at 90-95℃ for 30 min. Liquid collected from the processes was concentrated to 16 ml, and lignin was precipitated by adding 160 ml of ice-cold water. Lignin was filtered on the glass fiber paper (Schleicher and Schuell GF6 Glasfaser Rundfilter Ø 55mm) and 10 ml of diethyl ether and water were added successively to the glass fiber paper. Then, the isolated lignin on the glass fiber paper was dried at room temperature, overnight. Subsequently, distilled dioxan was added to the glass fiber paper to extract the lignin mixture. The lignin mixture was transferred to a glass Wheaton vial, followed by heating at 40 ℃ under nitrogen. After evaporation of distilled dioxan, the lignin sample was subjected to thioacidolysis assays.

3.8.4.8.3 Thioacidolysis

Thioacidolysis was performed by the method of Robinson and Mansfield (2009). Briefly, to each vial containing a lignin sample, 1 ml of freshly-made reaction mixture consisting of 2.5% boron trifluoride diethyl etherate and 10% ethanethiol in distilled dioxan (v/v) was added. The vials were sealed with Teflon-lined screw-caps and were kept at 100 ℃ for 4 h and manually agitated each hour. The reaction was stopped by placing the vials at -20 ℃ for 5 min or overnight. Subsequently, 0.3-0.6 ml of 0.4 M sodium bicarbonate was added to each vial to bring the solution to pH 3-4. Additionally, 0.2 ml of 1 mg ml^{-1} internal standard docosane, 2 ml of distilled water, and 1 ml of methylene chloride were added to each vial.

The mixture was vortexed and the phases were allowed to separate.

Before loading the mixture into a prepared Pasteur pipette (150 mm, Roth) with small glass wool (Roth) plus 50 mg of anhydrous sodium sulfate, 1 ml of methylene chloride was added to this Pasteur pipette for washing. Subsequently, 1.5 ml of liquid mixture was taken from the lower phases, containing organic and lignin breakdown products, to the prepared Pasteur pipette. After the solution passed through the Pasteur pipette, the products were collected into a new 2-ml tube and evaporated by *Speed-Vac* at 45 ℃ for 1.5-2 h. Then, 0.1 ml of methylene chloride was added to the dried lignin products and sonicated for 2 min. Afterwards 20 µl of resuspended lignin products was transferred into a new vial and mixed with 20 µl of pyridine and 100 µl of BSTFA by vortexing. Following incubation at room temperature for at least 2 h, 2 µl of the reaction products was used directly for GC-MS analysis under the conditions described in methods (II.2.3).

Lignin breakdown units of each lignin sample were quantified using Xcalibur software (version 1.4). Based on fragmentation patterns and retention times of different lignin units, the following formula was used for the quantification of each lignin sample.

$$\frac{C\,(IS)}{A\,(IS)} = \frac{C\,(sample)}{A\,(sample)} \rightarrow C\,(sample) = \frac{0.2\ mg \times A\,(sample)}{A\,(IS)}$$

$$C_{ref}\,(sample) = X\ \mu mol$$

$$C_{ref}\,(sample)\,\% = \frac{X\ \mu mol}{W\ mg} \times 100$$

C (IS)= concentration of the internal standard (0.2 mg)
A (IS)= peak area of the internal standard
C (sample)= concentration of the sample (unknown)
A (sample)= peak area of the sample
W= lignin content (mg)

3.8.4.9 Box plots and statistical analysis

The numerical values from different treatments were transformed into box-whisker plot graphics using the software package R (www.r-project.org). In box-whisker plots, the horizontal line in the middle of the box indicated the median, which is also the 50th percentile. The lower and upper boundary of the box represented the 25th and 75th percentiles, respectively. Open dots were used to visualize the maximum or minimum values in the box-whisker plot.

Wilcoxon-Mann-Whitney *U*-test was used for statistical analysis (Hart, 2001; Hoffmann et al., 2006) due to biological variation of each group. The statistical value (*P*-value), based on data of two groups, was calculated by performing the Wilcoxon-Mann-Whitney *U*-test with a non-parametric statistical analysis using the software package R. *P*-value was used to determine whether or not significant differences existed between treatments.

III. Results

1. Sequence analysis

1.1 Cloning and characterization of *FaCCR*, *FaCAD*, and *FaPOD*

Total RNAs were isolated from ripe fruit and transcribed to cDNAs. Genomic DNAs were isolated from young leaves. To amplify the full-length coding regions of *FaCCR*, *FaCAD*, and *FaPOD* genes, cDNAs were used as PCR templates. In addition, to amplify the genomic sequence of these three genes, genomic DNAs were used as PCR templates. The PCR products that corresponded to *FaCCR*, *FaCAD*, and *FaPOD* were amplified using templates (cDNAs or genomic DNAs), with degenerate primers of *CCR* and *CAD*, as well as specific primers of *POD* (II.3.2). After a PCR reaction, the expected PCR bands that corresponded to *FaCCR*, *FaCAD*, and *FaPOD* were cloned in a pGEM-T vector (II.3.2). In order to identify allelic variations in these three genes, 20 random clones of each gene were selected for sequencing.

After sequence analysis, full-length coding region sequences of *CCR*, *CAD*, and *POD*, that corresponded to the expected sizes of 1020, 1080, and 993 bp in length were named *FaCCR*, *FaCAD*, and *FaPOD*, respectively. The results showed that 18, 12, and 16 clones of *FaCCR*, *FaCAD*, and *FaPOD* were unique. A multiple comparison of coding regions among the unique *FaCCR*, *FaCAD*, and *FaPOD* sequences revealed 95.5%, 94.9%, and 97.8% identity at the nucleotide level, respectively (Table 24).

Sequence analysis of the three genes (without 3’ and 5’ non-translated sequences) revealed that the *CCR* gene was 1361 bp in length and its structure contained three exons and two introns (intron 1 = 220 bp; intron 2 = 121 bp). The *CAD* gene ranged from 1449 to 1497 bp in length and its structure contained five exons and fours introns (intron 1 = 142 bp or 98 bp; intron 2 = 87 bp; intron 3 = 95 bp; intron 4 = 106 or 90 bp). The *POD* gene was 1370 bp in length and its structure contained four exons and three introns (intron 1 = 95 bp; intron 2 = 112 bp; intron 3 = 169 bp). Exon-intron junctions of these three genes conformed to the GT-AG rule. Furthermore, the intron lengths varied among the unique clones. All *CCR*, *CAD*, and *POD* genes were named *gCCR*, *gCAD*, and *gPOD*, respectively (Table 24).

Additionally, partial sequences were analyzed using 20 clones of each gene. The results revealed that 9, 16, and 14 clones of *gCCR*, *gCAD*, and *gPOD* were unique, respectively. A multiple comparison of partial sequences among the unique *gCCR* (480 bp), *gCAD* (600 bp), and *gPOD* (500 bp) revealed that identity at the nucleotide level was 94.9%, 90.7 %, and 96.2 %, respectively (Table 24).

Table 24. Profiles of nucleotide sequences of the coding regions of *FaCCR*, *FaCAD*, and *FaPOD* and their genes (*gCCR*, *gCAD*, and *gPOD*) from *F.* × *ananassa* cv. Elsanta

Name	***FaCCR***	***gCCR***	***FaCAD***	***gCAD***	***FaPOD***	***gPOD***
Sequences (bp)	1020	1361	1080	1449-1497	993	1370
Introns and exons	-----	2 and 3	-----	4 and 5	-----	3 and 4
% identity, (amounts of unique clones)	95.5 (18)	94.9 (9)	94.9 (12)	90.7 (16)	97.8 (16)	96.2 (14)

1.2 A possible *CCR*, *CAD*, and *POD* gene family from *Fragaria vesca*

In order to build a possible *CCR*, *CAD*, and *POD* relationship between octoploid *F.* × *ananassa* cv. Elsanta and diploid *F. vesca* (http://www.strawberrygenome.org/), a phylogenetic analysis was performed. The analysis showed that *FaCCR* is most similar to gene15845 of *F. vesca* (probable dihydroflavonol-4-reductase, DFR), and gene32333 (DFR, probable bifunctional dihydroflavonol 4-reductase/flavanone 4-reductase) with 98.2% and 37.3% identity, respectively (Figure 14). It has already been shown that *CCR*s and *DFR*s share sequence identities (Lacombe et al., 1997). *FaCAD* is most similar to gene20700 (probable mannitol dehydrogenase), gene09243 (probable mannitol dehydrogenase), and gene24970 (probable mannitol dehydrogenase) with 98.3%, 96.7%, and 83.8% identity, respectively (Figure 15). Whereas *FaPOD* and gene09649 (similar to POD 21, precursor) show only 44.3% identity, *FaPOD27* and gene19544 (similar to POD 27, precursor) display 97.9% identity (Figure 16).

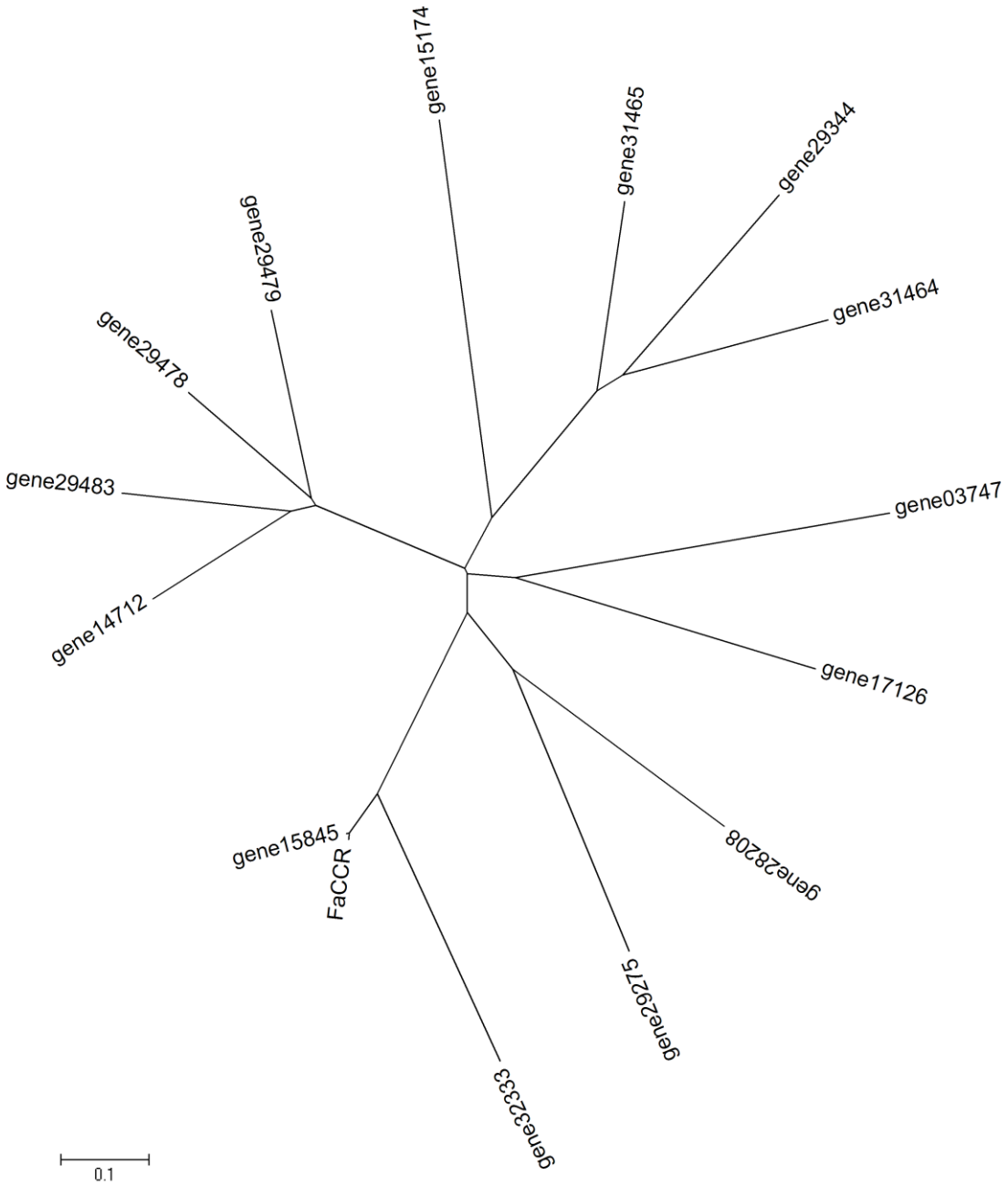

Figure 14. A possible *CCR* gene family from *Fragaria vesca*.

The tree was constructed using the MEGA4 package with 500 bootstrap replications, Poisson correction, and a complete deletion option, with the Neighbor-Joining method. All branches are drawn to scale and the scale bar indicates the number of substitutions per site. *FaCCR* was obtained in this study (*F.* × *ananassa* cv. Elsanta). Gene sequences have been retrieved from the *Fragaria Vesca* Genome Browser database and their accession numbers with probable functions are as follows. Gene03747, gene15845, gene29275, gene29479, gene29483, gene31465 (DFR, probable dihydroflavonol-4-reductase); gene14712, gene15174, gene17126, gene29344, gene29478, gene28208, gene31464, and gene32333 (DFR, probable bifunctional dihydroflavonol 4-reductase/ flavanone 4-reductase).

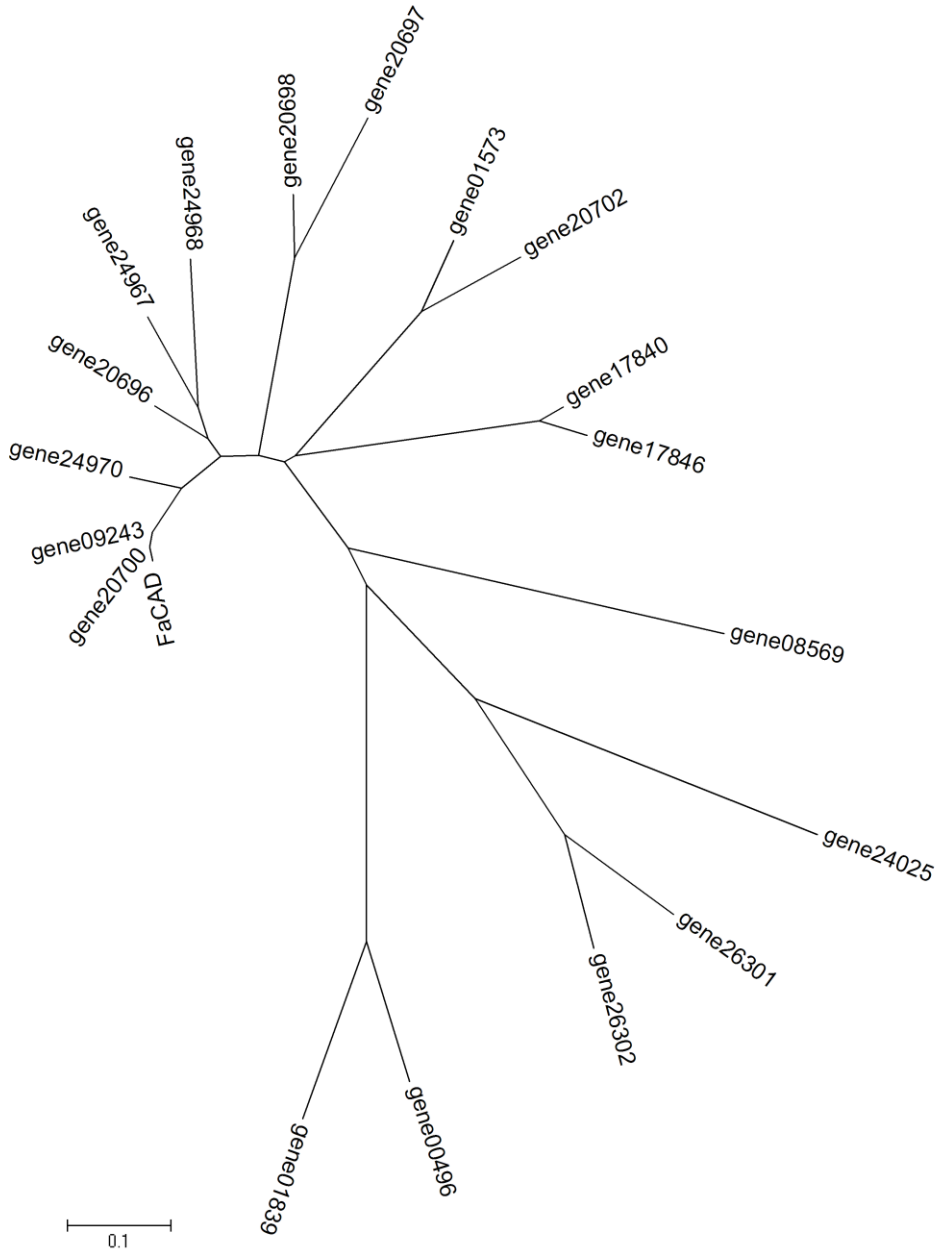

Figure 15. A possible *CAD* gene family from *Fragaria vesca*.

The tree was constructed using the MEGA4 package with 500 bootstrap replications, Poisson correction, and a complete deletion option, with the Neighbor-Joining method. All branches are drawn to scale and the scale bar indicates the number of substitutions per site. *FaCAD* was obtained in this study (*F.* × *ananassa* cv. Elsanta). Gene sequences have been retrieved from the *Fragaria Vesca* Genome Browser database and their accession numbers with probable functions are as follows. Gene01573, gene09243, gene20696, gene20697, gene20698, gene20700, gene20702, gene24967, gene24968, gene24970 (probable mannitol dehydrogenase); gene00496, gene01839, gene08569, gene17840, gene17846, gene24025, gene26301, and gene26302 (probable cinnamyl alcohol dehydrogenase).

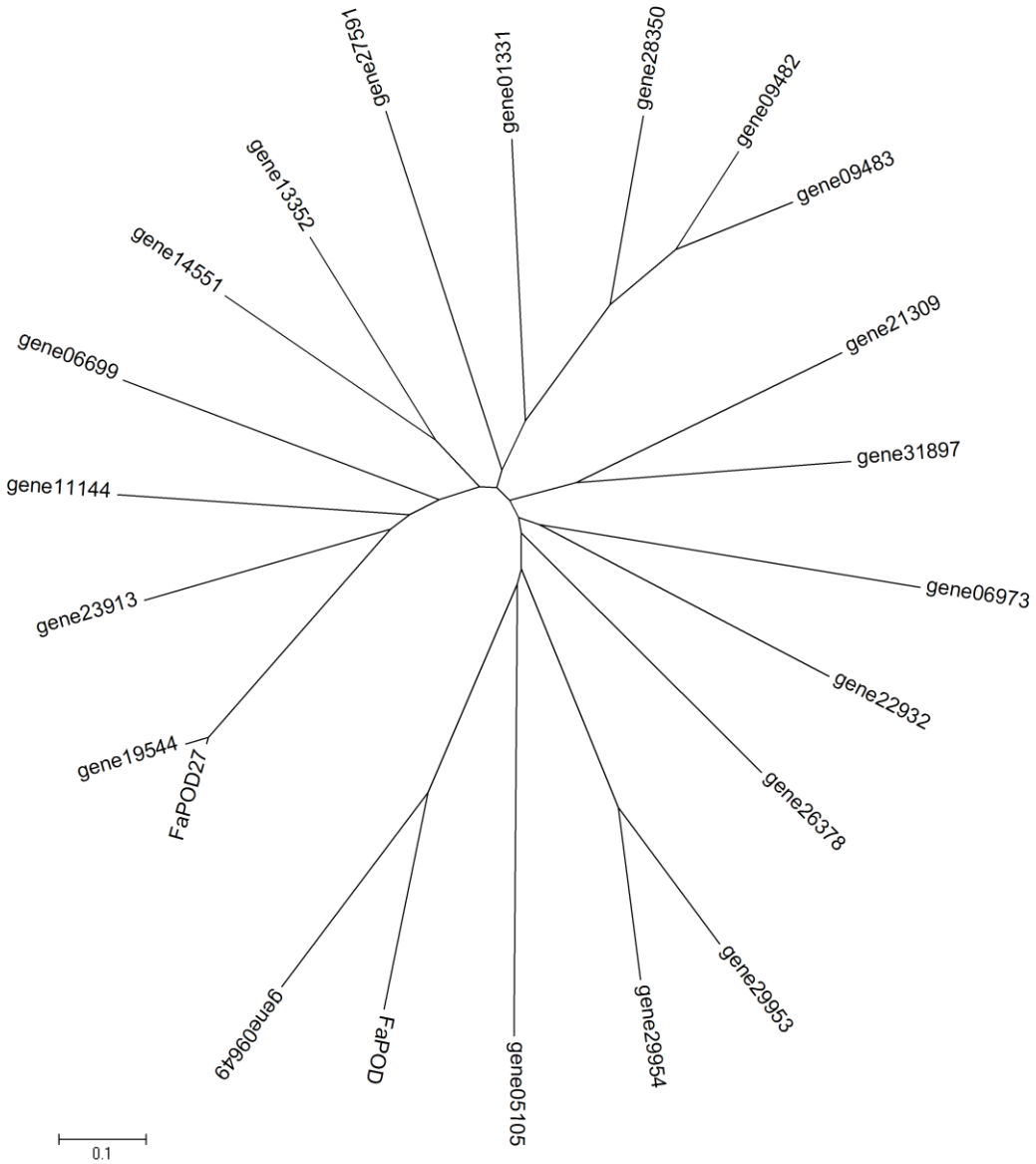

Figure 16. A possible *POD* gene family from *Fragaria vesca*.

The tree was constructed using the MEGA4 package with 500 bootstrap replications, Poisson correction, and a complete deletion option, with the Neighbor-Joining method. All branches are drawn to scale and the scale bar indicates the number of substitutions per site. *FaPOD* and *FaPOD27* were obtained in this study (*F.* × *ananassa* cv. Elsanta). Gene sequences have been retrieved from the *Fragaria Vesca* Genome Browser database and their accession numbers with probable functions are as follows. Gene01331 (putative POD55, precursor), gene05105 (probable POD29, precursor), gene06699 (similar to POD24, precursor), gene06973 (probable POD5), gene09482 (putative POD41, precursor), gene09483 (similar to POD41, precursor), gene09649 (similar to POD21, precursor), gene11144 (similar to POD3, precursor), gene13352 (putative POD66, precursor), gene14551 (putative POD64, precursor), gene19544 (similar to POD27, precursor), gene21309 (putative POD4, precursor), gene22932 (similar to POD5), gene23913 (putative POD3, precursor), gene26378 (putative POD44, precursor), gene27591 (similar to POD12, precursor), gene28350 (putative POD63, precursor), gene29953 (putative POD48, precursor), gene29954 (putative POD48, precursor), and gene31897 (putative POD10, precursor).

1.3 Phylogenetic tree of partial genome and gene sequences

In order to build a possible genomic relationship between octoploid *F.* × *ananassa* cv. Elsanta and diploid *F.* × *vesca*, a phylogenetic analysis of the genes was performed with partial genome sequences containing one intron (480 bp *gCCR* with intron 2; 600 bp *gCAD* with intron 2; 500 bp *gPOD* with intron 1).

The analysis showed that *gCCR*, *gCAD*, and *gPOD* were classified into two major groups (A and B), with subgroups (Figure 17-19). The two major groups of *gCCR*, *gCAD*, and *gPOD* with subgroups were designated as follows: *gCCR* (Figure 17); group A (gCCR1, 8, 21, *vesca* gCCR, and gene15845) and group B (gCCR 2, 5, 11, 13, 15, 17, and FaCCR); *gCAD* (Figure 18); group A (gCAD 1, 2, 11, 12, 13, 14, 16, 20, and *vesca* gCAD) and group B (gCAD 3, 4, 8, 18, and *Fxa* cad2); *gPOD* (Figure 19); group A (gPOD 3, 5, 7, 12, 17, 21, *vesca* gPOD, and FaPOD), and group B (gPOD 1, 2, 4, and 13). The results suggest that gene15845 and gene19544 represent the *F. vesca* orthologous genes of *FaCCR* alleles and *FaPOD27*, respectively (Figure 17 and 19). The identification of the orthologues of *FaCAD* and *FaPOD* in the *F. vesca* genome is less obvious. Gene09243 and gene20700 are probable candidates for *FaCAD* (Figure 18) whereas gene05105 and gene09649 are assumed orthologues of *FaPOD* (Figure 19).

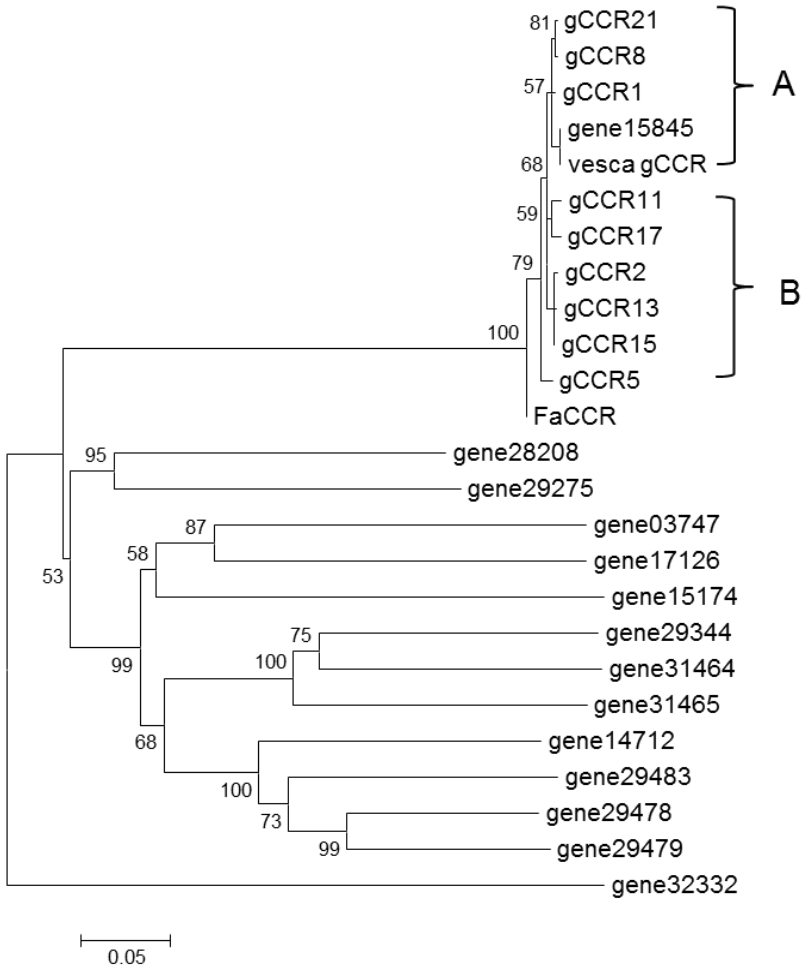

Figure 17. Phylogenetic tree of partial genomic sequences of *F. x ananassa gCCR* and of *F.* × *vesca*. The tree was generated using the MEGA4 package with 1000 bootstrap replications, pairwise deletion, and a *p*-distance option, with the Neighbor-Joining method. All branches are drawn to scale and the scale bar indicates the number of substitutions per site. Sequences of *gCCR* (*F.* × *ananassa* cv. Elsanta) with identification clone numbers (e.g., gCCR1) and *FaCCR* (*F.* × *ananassa* cv. Elsanta) were obtained in this study. Sequences of *F.* × *vesca* [*vesca gCCR* (contig002402), gene03747, gene15845, gene29275, gene29479, gene29483, gene31465, gene14712, gene15174, gene17126, gene29344, gene29478, gene28208, gene31464, and gene32333] were obtained from the *Fragaria Vesca* Genome Browser database.

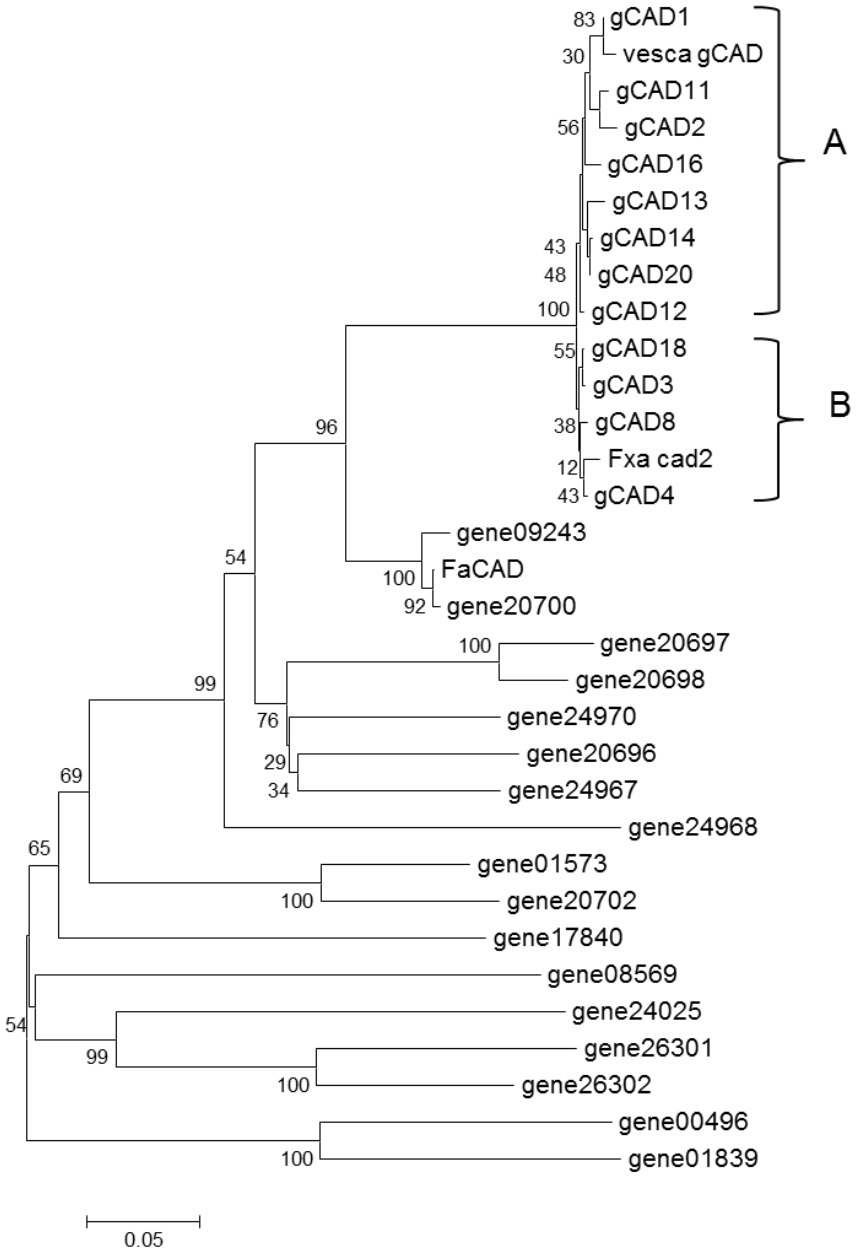

Figure 18. Phylogenetic tree of partial genomic sequences of *F. x ananassa gCAD* and of *F.* × *vesca*.

The tree was generated using the MEGA4 package with 1000 bootstrap replications, pairwise deletion, and a *p*-distance option, with the Neighbor-Joining method. All branches are drawn to scale and the scale bar indicates the number of substitutions per site. Sequences of *gCAD* (*F.* × *ananassa* cv. Elsanta) with identification clone numbers (e.g., gCAD1) and *FaCAD* (*F.* × *ananassa* cv. Elsanta) were obtained in this study. Sequences of *F.* × *vesca* [*vesca gCAD* (contig108115), gene01573, gene09243, gene20696, gene20697, gene20698, gene20700, gene20702, gene24967, gene24968, gene24970, gene00496, gene01839, gene08569, gene17840, gene24025, gene26301, and gene26302] were obtained from the *Fragaria Vesca* Genome Browser database and *F.* × *ananassa* cv. Chandler (*Fxacad2*, AF320110) from the GenBank database.

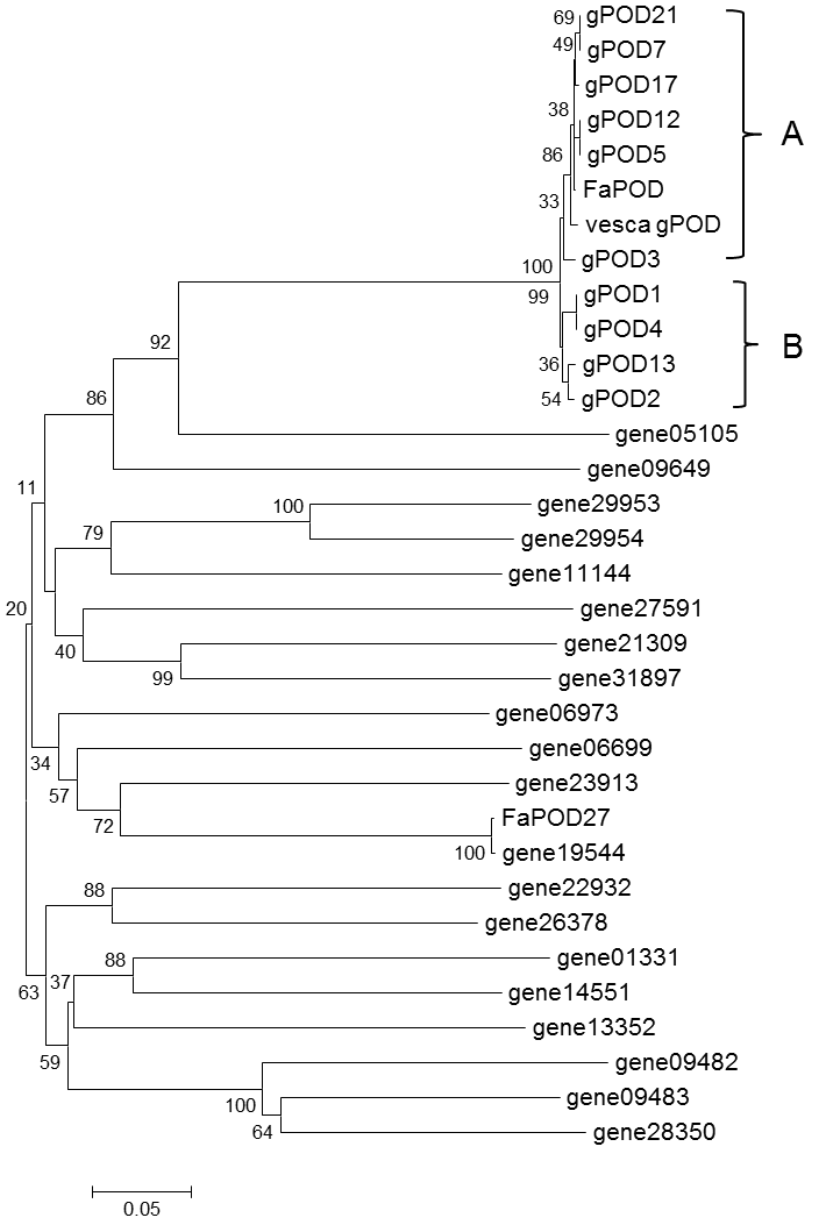

Figure 19. Phylogenetic tree of partial genomic sequences of *F. x ananassa gPOD* and of *F.* × *vesca*.

The tree was generated using the MEGA4 package with 1000 bootstrap replications, pairwise deletion, and a *p*-distance option, with the Neighbor-Joining method. All branches are drawn to scale and the scale bar indicates the number of substitutions per site. Sequences of *gPOD* (*F.* × *ananassa* cv. Elsanta) with identification clone numbers (e.g., gPOD1), *FaPOD*, and *FaPOD27* (*F.* × *ananassa* cv. Elsanta) were obtained in this study. Sequences of *F.* × *vesca* [*vesca gPOD* (contig64026), gene01331, gene05105, gene06699, gene06973, gene09482, gene09483, gene09649, gene11144, gene13352, gene14551, gene19544, gene21309, gene22932, gene23913, gene26378, gene27591, gene28350, gene29953, gene29954, and gene31897] were obtained from the *Fragaria Vesca* Genome Browser database.

1.4 Phylogenetic analysis of proteins

To understand possible functional roles and functional divergence of FaCCR, FaCAD, and FaPOD, a phylogenetic analysis was performed using deduced amino acid sequences. In this study, one sequence of FaCCR, FaCAD, and FaPOD was randomly selected from their unique clones (Table 24) and the FaPOD27 sequence was obtained from another project (strawberry functional genomics) (Appendix B).

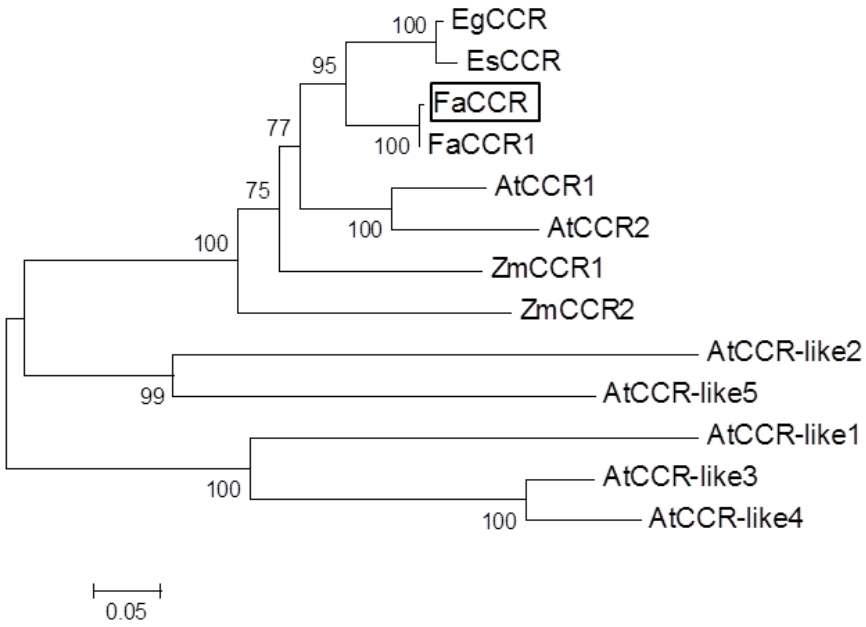

Figure 20. Phylogenetic tree of CCR proteins from various plants.
The tree was constructed using the MEGA4 package with 500 bootstrap replications, Poisson correction, and a complete deletion option, with the Neighbor-Joining method. The bootstrap values greater than 50% are shown in each branch. All branches are drawn to scale and the scale bar indicates the number of substitutions per site. FaCCR in this study (*Fragaria* × *ananassa* cv. Elsanta) has been boxed. Protein sequences from other plants have been retrieved from the GenBank database and their accession numbers are as follows. AtCCR1 (*Arabidopsis thaliana*; AF320624), AtCCR2 (AF320623), AtCCR-like1-5 (AAF16654, AAC78522, AAN15374, AAM13142, and AAO22571), EgCCR (*Eucalyptus gunnii*; X79566), EsCCR (*Eucalyptus saligna*; AF297877), FaCCR1 (*Fragaria* × *ananassa* cv. Elsanta, CCR-1 allele; AY285922), ZmCCR1 (*Zea mays*; X98083), ZmCCR2 (Y15069).

CCR (EC 1.2.1.44) enzymes catalyzed the conversion of different cinnamoyl-CoA esters to their corresponding cinnamaldehydes in the monolignol pathway. In this study, the open reading frame (ORF) of FaCCR was 1017 bp, encoding 339 amino acids with a calculated molecular mass of 37.3 kDa and an isoelectric point (pI) value of 6.12. *CCR* genes have

been cloned and partially characterized in some plants. Thus, a phylogenetic tree of CCRs was built from deduced amino acid sequences from selected species. Phylogenetic analysis showed that FaCCR is most closely related to FaCCR1 (98.2% identity), EgCCR (84.1% identity), and EsCCR (82.9% identity) proteins (Figure 20). FaCCR1 (AY285922) has also been isolated from *F. x ananassa* cv. Elsanta and shows some amino acid exchanges. *EgCCR* was shown to be highly expressed in the differentiating xylem zone (Lacombe et al., 1997). In addition, *ZmCCR1* was mainly expressed in all lignifying tissues, and *ZmCCR2* was expressed in roots and induced by drought (Pichon et al., 1998). AtCCR1 and AtCCR2 showed a high affinity towards feruloyl-CoA, but a low affinity towards caffeoyl-CoA and sinapoyl-CoA (Lauvergeat et al., 2001).

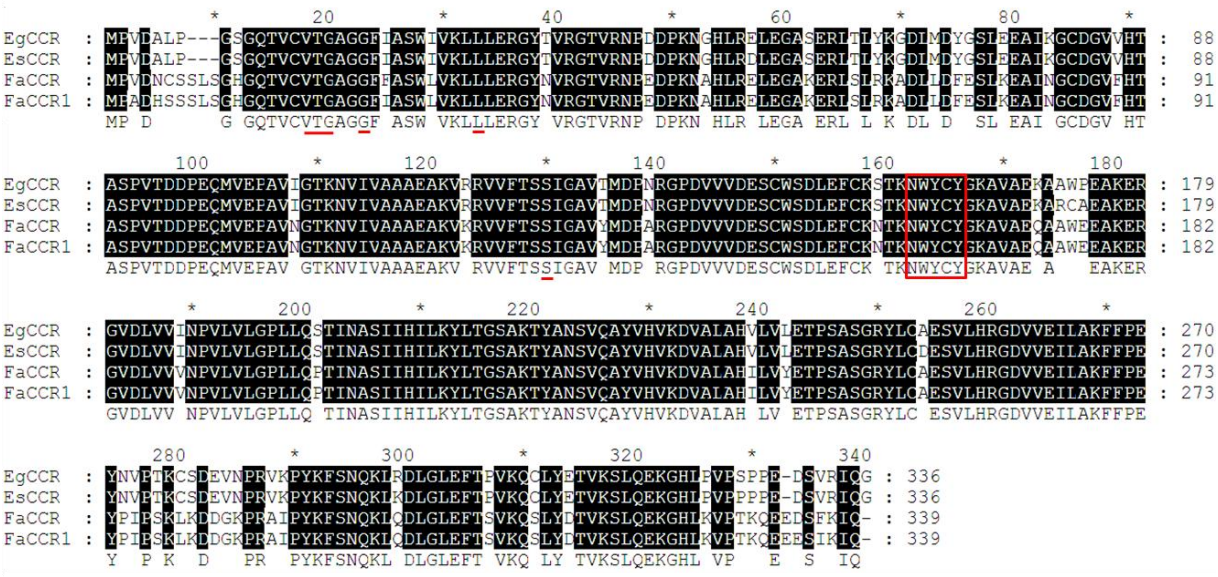

Figure 21. Alignment of amino acid sequences of CCR proteins from selected plants.
All sequences were aligned using the AlignX program of Vector NTI and GeneDoc software. A consensus sequence, found in a majority of the sequences, is shown below the sequence. Identical amino acids in the sequences are shaded in black. Underlines indicate putative amino acids involved in cofactor binding. Protein sequences from other plants have been retrieved in the GenBank database and their accession numbers are as follows. The putative signature of all CCRs is boxed. EgCCR (*Eucalyptus gunnii*; X79566), EsCCR (*Eucalyptus saligna*; AF297877), FaCCR in this study (*Fragaria* × *ananassa* cv. Elsanta), FaCCR1 (*Fragaria* × *ananassa* cv. Elsanta, CCR-1 allele, accession AY285922).

Moreover, conserved motifs of other plant CCRs are present in FaCCR protein. A conserved motif, NWYCY, is present in all sequences and is putatively involved in the catalytic site of CCRs (Pichon et al., 1998). The NWYCY motif of FaCCR protein was

identified in amino acid residues 162-166 (Figure 21). A second conserved motif is the NAD/NADP(H) binding site in the N-terminal portion of CCRs (Lacombe et al., 1997). The NAD/NADP(H) binding site of FaCCR protein is represented by amino acid residues VTG (18-20), G (23), L (33), and S (130) (Figure 21).

CAD (EC 1.1.1.195) enzyme catalyzes the reduction of cinnamyl aldehydes to their corresponding alcohols. CADs have been partially characterized in several angiosperms. FaCAD has a 1077-bp open reading frame encoding a protein of 359 amino acid residues with a relative molecular mass of 39 kDa and a pI value of 5.96.

CAD amino acid sequences of different species were obtained from the NCBI database and a phylogenetic tree was built. The tree revealed two groups of CADs (Figure 22). FaCAD belongs to group II and is close to Fxacad1 (98.1% identity). Members of group II show diverse substrate preferences (Li et al., 2001; Blanco-Portales et al., 2002; Raes et al., 2003). A sinapyl alcohol dehydrogenase (SAD) was suggested to be involved in the reduction of sinapaldehyde to corresponding sinapyl alcohol in *Populus tremuloides*. PtSAD has been characterized and shown to use sinapaldehyde as the most preferred substrate (Li et al., 2001). In addition, *Arabidopsis* AtCAD2, 3, 6, 7, 8, and 9 belong to group II (Figure 22). AtCAD7 and AtCAD8 are expressed in lignifying tissues (Kim et al., 2007) and are pathogen-inducible defense genes (Somssich et al., 1996). AtCAD2 and 6 are considered the predominant candidates for the monolignol pathway in *Arabidopsis* (Raes et al., 2003) whereas group I CADs have been considered as the predominant CADs in lignin biosynthesis and lignifications in wheat (TaCAD1) and sorghum (SbCAD2; Ma, 2010; Saballos et al., 2009). Besides, TaCAD1 (Ma, 2010) and PtCAD (Li et al., 2001) have shown a strong preference for coniferaldehyde. Kinetic analysis of putative *Arabidopsis* CAD proteins has shown that activity against phenylpropanoid aldehydes in group I (AtCAD4 and AtCAD5) is higher than in group II (Saballos et al., 2009; Kim et al., 2004). AtCAD7 displayed a wide substrate affinity for aromatic aldehydes (Somssich et al., 1996).

Conserved domains are present in the FaCAD protein (Li et al., 2001; Blanco-Portales et al., 2002). Amino acid residues 189-194 GLGG(L)G were identified as cofactor NAD/NADP(H) binding site. The FaCAD contains also the conserved Zn1 and Zn2 binding motif represented by amino acid residues 69-83 and 89-115. On the basis of these motifs, FaCAD proteins appear to be a zinc-dependent alcohol dehydrogenase (Figure 23).

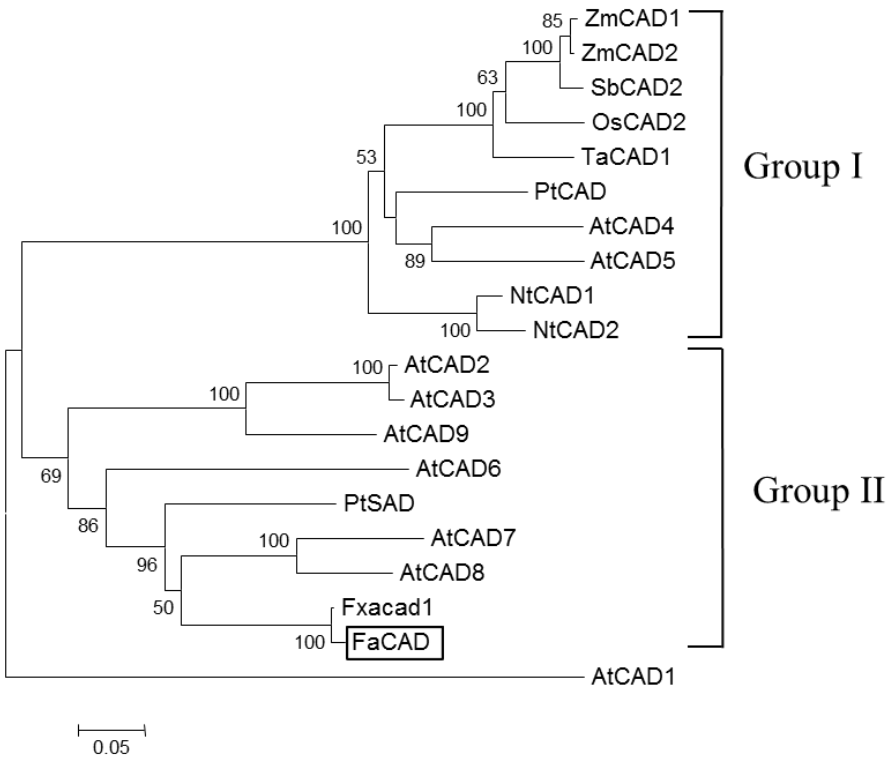

Figure 22. Phylogenetic tree of CAD proteins from various plants.
The tree was constructed using the MEGA4 package with 500 bootstrap replications, Poisson correction, and a complete deletion option, with the Neighbor-Joining method. The bootstrap values greater than 50% are shown in each branch. All branches are drawn to scale and the scale bar indicates the number of substitutions per site. FaCAD in this study (*Fragaria* × *ananassa* cv. Elsanta) has been boxed. Protein sequences from other plants have been retrieved from the GenBank database and their accession numbers are as as follows. AtCAD1 (*Arabidopsis thaliana*; AY288079), AtCAD2 (AY302077), AtCAD3 (AY302078), AtCAD4 (AY302081), AtCAD5 (AY302082), AtCAD6 (AY302075), AtCAD7 (AY302079), AtCAD8 (AY302080), AtCAD9 (AY302076), Fxacad1 (*Fragaria* × *ananassa* cv. Chandler, U63534), NtCAD1 (*Nicotiana tabacum*; X62343), NtCAD2 (X62344), OsCAD2 (*Oryza sativa*; DQ234272), PtCAD (*Populus tremuloides*; AF217957), PtSAD (AF273256), SbCAD2 (*Sorghum bicolor*; ACL80889), TaCAD1 (*Triticum aestivum*; GU563724), ZmCAD1 (*Zea mays*; AJ005702), ZmCAD2 (Y13733).

Plant peroxidases (EC1.11.1.7) are a large superfamily in a variety of species, such as the *Arabidopsis* peroxidase family which has 73 isoenzymes involved in diverse functions (Welinder, 2002; Cosio and Dunand, 2009). FaPOD and FaPOD27 that were obtained from strawberry fruit belong to the class III peroxidase family. Prosite analysis (http://prosite.expasy.org/) revealed that both of them are plant heme peroxidases containing a putative Ca^{2+} binding domain. The open reading frames of FaPOD and FaPOD27 of 990

and 987 nucleotides encode proteins of 330 or 329 amino acids with molecular masses of 37.6 and 35.1 kDa and pI values of 7.7 and 8.65, respectively.

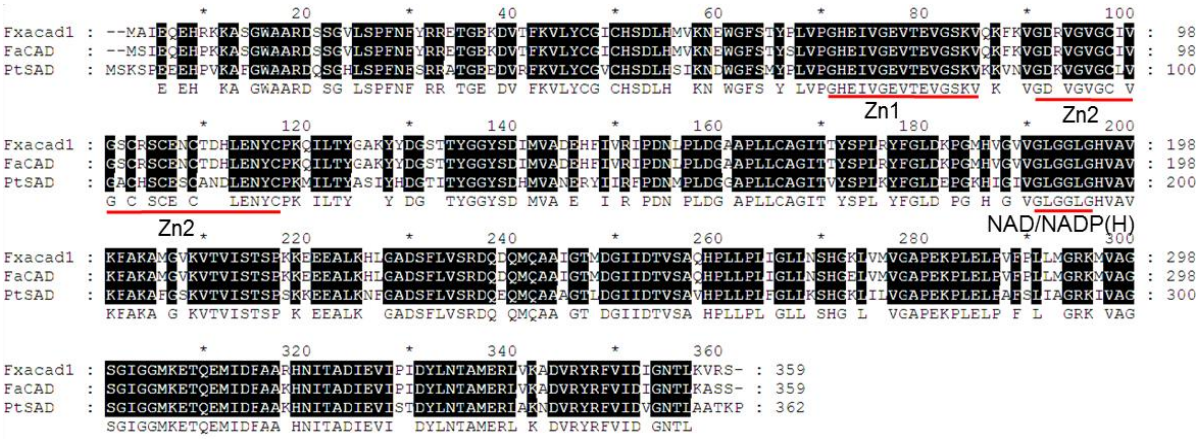

Figure 23. Alignment of amino acid sequences of SAD and CAD proteins from selected plants.

All sequences were aligned using the AlignX program of Vector NTI and GeneDoc software. A consensus sequence, found in a majority of the sequences, is shown below the sequence. Identical amino acids in the sequences are shaded in black. The underline indicates putative amino acid involved in Zn1, Zn2, and NADP binding motifs. Protein sequences from other plants have been retrieved from the GenBank database and their accession numbers are as follows: Fxacad1 (*Fragaria* × *ananassa* cv. Chandler, U63534), FaCAD in this study (*Fragaria* × *ananassa* cv. Elsanta), PtSAD (*Populus tremuloides*; AF273256).

To understand the relationship of the two strawberry peroxidases FaPOD and FaPOD27 and selected plant peroxidases a phylogenetic tree was constructed (Figure 24). Phylogenetic analysis revealed that FaPOD and FaPOD27 had a low level of identity (31.9 %) in primary structure. The two isoforms do not belong to the same cluster. FaPOD was found to be closely related to FvPOD02 (100% identity), NtPOD60 (82.7% identity), and AtPOD42 79.1% identity). Downregulation of *NtPOD60* in tobacco led to a 50% reduction in total lignin (Blee et al., 2003). AtPOD42 has been identified by microarray analysis and was found to be involved in xylem secondary cell wall formation (Yokoyama and Nishitani, 2006). FaPOD27 was shown to be most closely related to AtPOD30 (50.6% identity), which is associated with monolignol polymerization (Ehlting et al., 2005). AtPOD71 (43.2% identity) is involved in xylem secondary cell wall formation (Yokoyama and Nishitani, 2006) and also responds to environmental stress (Cosio and Dunand, 2009). In addition, PtPOD3 (Li et al., 2003), ZePOD01 (Sato et al., 2006), AtPOD66 and AtPOD664 (Tokunaga et al., 2009) have been associated with lignifications. IbPOD4 (Kim et al., 2008) has been associated with hydrogen peroxide production.

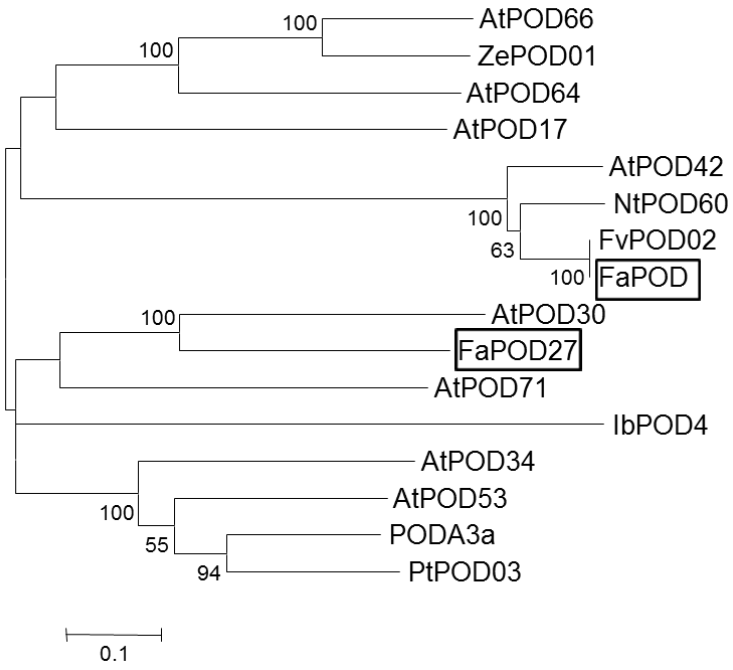

Figure 24. Phylogenetic tree of POD proteins from various plants.

The tree was constructed using the MEGA4 package with 500 bootstrap replications, Poisson correction, and a complete deletion option, with the Neighbor-Joining method. The bootstrap values that were greater than 50% are shown in each branch. All branches are drawn to scale and the scale bar indicates the number of substitutions per site. FaPOD and FaPOD27 in this study (*Fragaria* × *ananassa* cv. Elsanta) have been boxed. Protein sequences from other plants have been retrieved from the GenBank database and their accession numbers are as follows. AtPOD17 (*Arabidopsis thaliana*; NM_127806), AtPOD30 (NM_113072), AtPOD34 (NM_114771), AtPOD42 (NM_118317), AtPOD53 (NM_120755), AtPOD64 (NM_123583), AtPOD66 (NM_124568), AtPOD71 (NM_125808), IbPOD4 (*Ipomoea batatas*; AY206409), NtPOD60 (*Nicotiana tabacum*; AF149251), PODA3a (*Populus sieboldii* × *Populus grandidentata*; D38050), PtPOD03 (*Populus trichocarpa*; X97350), ZePOD01 (*Zinnia violacea*; AB023959). FvPOD02 (*Fragaria* × *vesca*; 3306) has been retrieved from the PeroxiBase database with its ID number.

2. Biochemical characteristics of the recombinant FaCCR

2.1 Heterologous expression of *FaCCR* in *E. coli*

In order to characterize the enzymatic activity of FaCCR, the full-length coding sequence of *FaCCR* was subcloned into a pGEX4-T1 vector containing the nucleotide sequence of glutathione *S*-transferase (GST). GST-FaCCR was not present in uninduced cells (lane 1), but successfully expressed in *E. coli* BL21(DE3) pLysS after induction of protein with 0.2 mM IPTG at 16℃ (lane 2; Figure 25). SDS-PAGE showed a band at 63.3 kDa after

purification (lane 3) confirming the relative mass of GST-FaCCR which consists of the molecular mass of 37.3 kD (FaCCR) and 26 kD (GST). One mg of purified GST-FaCCR was obtained from 300 mL of cultured cells. The enzyme was stored in a buffer with 10% glycerol at -80℃ and remained stable for one year.

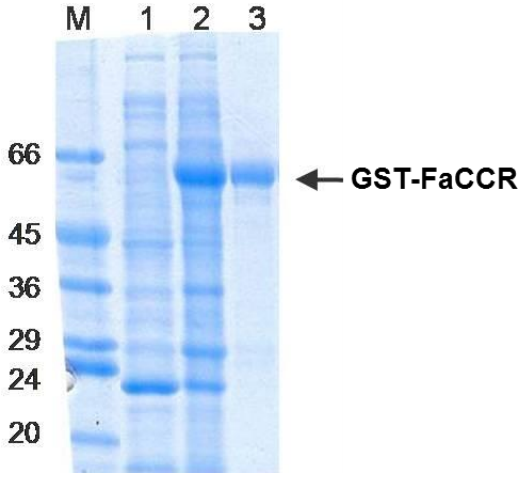

Figure 25. Expression of FaCCR protein in *E. coli* strain BL21(DE3)pLysS.
Lane (M) molecular mass markers; total protein extract of *E. coli* harboring *FaCCR* without IPTG (20 μg protein, lane 1) and after induction with IPTG (20 μg protein, lane 2); purified recombinant GST-FaCCR (5 μg protein, lane 3).

2.2 Determination of optimal pH and temperature for GST-FaCCR activity

To examine the effect of either pH or temperature on the activity of purified GST-FaCCR, GST-FaCCR was incubated in different buffers (100 mM citric acid, sodium phosphate, and Tris-HCL buffer) at various pH values and temperatures (Figure 26). GST-FaCCR exhibited optimal activity at pH 6 and was active at pH values, ranging from 5.5 to 8.5. Besides, GST-FaCCR activity was two times higher in sodium phosphate buffer than in the citric acid buffer at pH 6 (Figure 26A). Moreover, FaCCR activity gradually increased from 15 ℃ to 25℃, and then decreased (Figure 26B). Thus, this enzyme showed a pH optimum at 6 in sodium phosphate buffer and a temperature optimum at 25℃.

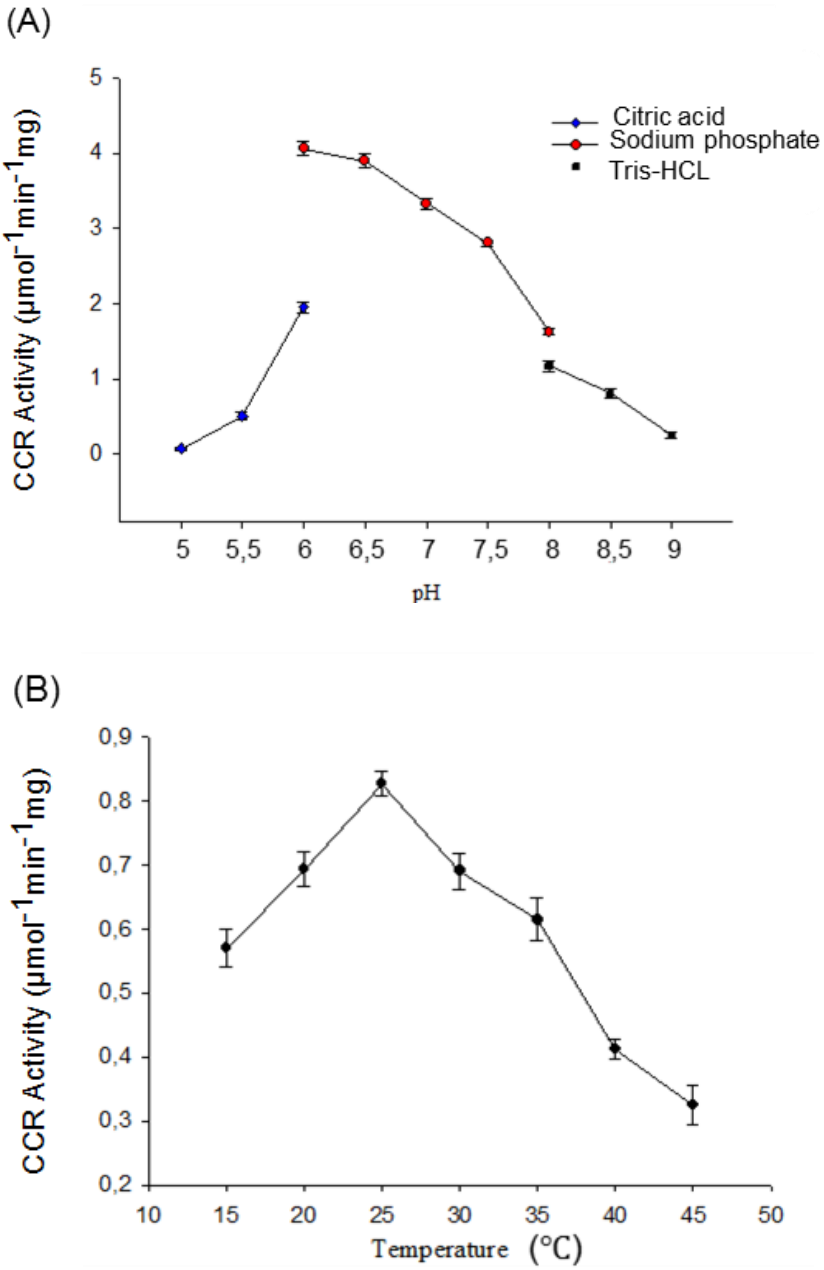

Figure 26. Effects of pH (A) and temperature (B) on recombinant GST-FaCCR activity.
The reaction mixture was prepared as described in methods (II.3.5.2). (A) FaCCR activity at various pH values and buffers was measured spectrophotometrically at 366 nm. (B) All reaction mixtures were incubated at different temperatures for 10 min and activity was determined by LC-UV-ESI-MS^n. Each value is the mean of three independent samples and vertical bars represent standard errors.

2.3 Substrate specificity of GST-FaCCR

Purified recombinant FaCCR protein was used to determine K_m values. The reaction mixture was prepared as described in methods (II.3.5.3). GST-CCR proteins exhibited Michaelis-Menten kinetics with apparent K_m values for different substrates. K_m values of 16.11, 25.48, and 24.75 µM were obtained for feruloyl-CoA, caffeoyl-CoA, and *p*-coumaroyl-CoA, respectively (Table 25). The K_{cat}/K_m ratios revealed that GST-FaCCR had a high affinity for feruloyl-CoA, but a lower affinity for both caffeoyl-CoA and *p*-coumaroyl-CoA as the catalytic efficiency (K_{cat}/K_m) of feruloyl-CoA was 100 times higher than that of both caffeoyl-CoA and *p*-coumaroyl-CoA. In addition to LC-UV-ESI-MS^n analysis of individual enzymatic assays, a GST-FaCCR reaction with a mixture of equal molar amounts of three substrates (caffeoyl-, *p*-coumaroyl-, and feruloyl-CoA), yielded three major peaks that were identified as caffeic aldehyde (3,4-dihydroxycinnamaldehyde), *p*-coumaraldehyde, and coniferaldehyde, respectively (Figure 27, 1-3). The retention time for each of the three metabolites was identical to that of the single products formed by GST-FaCCR reaction of the individual substrates (Table 19). At the same time, the activity of GST-FaCCR towards the different CoA esters was calculated from the peak areas and indicated that feruloyl-CoA (100%) was the preferred substrate compared with both caffeoyl-CoA (3%) and *p*-coumaroyl-CoA (3%; Figure 27).

Table 25. Kinetic properties of the recombinant GST-FaCCR protein

Substrate	K_m (µM)	V_{max} (nkat mg^{-1} protein)	K_{cat} (S^{-1})	K_{cat}/K_m (S^{-1} μM^{-1})
Feruloyl-CoA	16.11±1.39	272.45±15.88	$2.34\times10^{-3}\pm1.43\times10^{-4}$	1.45×10^{-4}
Caffeoyl-CoA	25.48±0.82	3.75±0.24	$2.93\times10^{-5}\pm2.06\times10^{-6}$	1.15×10^{-6}
p-Coumaroyl-CoA	24.75±1.23	3.12±0.03	$2.65\times10^{-5}\pm7.51\times10^{-7}$	1.07×10^{-6}

Values are the mean ±SE for three independent assays.

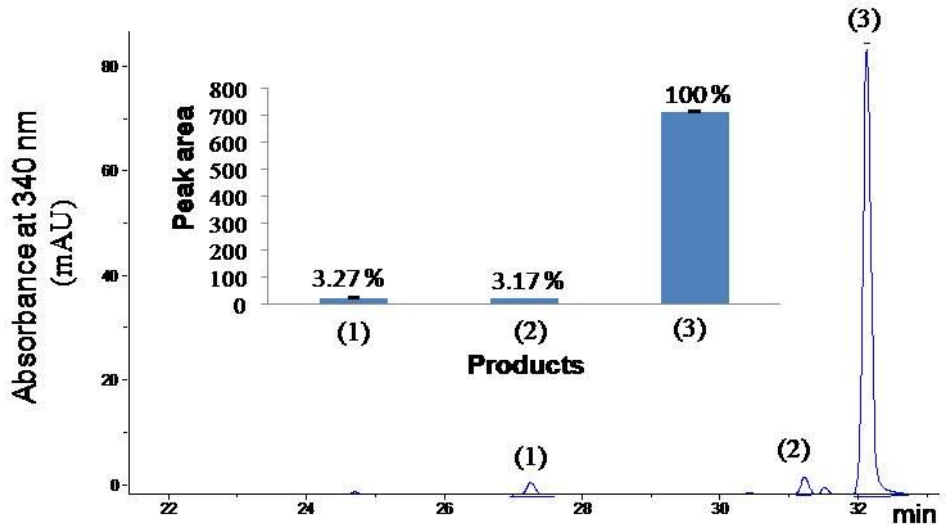

Figure 27. LC-UV-ESI-MS^n analysis of the GST-FaCCR reaction containing a mixture of equal molar concentration of the substrates caffeoyl-CoA, *p*-coumaroyl-CoA, and feruloyl-CoA. Three products were monitored at 340 nm and were identified as (1) caffeic aldehyde, (2) *p*-coumaraldehyde, and (3) coniferaldehyde, respectively. Since molar extinction coefficients (ε340) of the products are almost identical (18.5 x 10^3 M^{-1} cm^{-1} and 23.5 x 10^3 M^{-1} cm^{-1} for coniferaldehyde and *p*-coumaraldehyde, respectively) they were not taken into account for the calculation of the relative enzyme activities (Somssich et al., 1996)

2.4 Identification of the GST-FaCCR reaction products

Products formed by GST-FaCCR from hydroxycinnamoyl-CoAs were identified by LC-UV-ESI-MS^n. When *p*-coumaroyl-CoA, caffeoyl-CoA, and feruloyl-CoA was added to GST-FaCCR, a single metabolite was detected by LC-UV-ESI-MS^n. The products corresponded to *p*-coumaraldehyde (Figure 28A), caffeic aldehyde (Figure 28B), and coniferaldehyde (Figure 28C). In contrast, when GST was incubated with these substrates, no peaks were found (Figures 28 A-C).

The molecular weights of the three products were 148, 164, and 178 corresponding to *p*-coumaraldehyde (Figure 28A), caffeic aldehyde (Figure 28B), and coniferaldehyde (Figure 28C), respectively. MS spectral data for the three products were acquired in negative ion mode. The $[M-H]^-$ ions were targeted, which were observed at *m/z* 147 (Figure 28A), 163 (Figure 28B), and 177 (Figure 28C), respectively. At the same time, negative-ion MS^2 spectra of *p*-coumaraldehyde (Figure 28A_bottom), caffeic aldehyde (Figure 28B_bottom), and coniferaldehyde (Figure 28C_bottom) were recorded. Furthermore, retention time and mass fragmentation pattern of coniferaldehyde formed by GST-FaCCR (Figure 28C) were identical to those of the authentic coniferaldehyde reference (Figure 28D).

3. Heterologous expression of *FaCAD* in *E. coli* and yeast cells

In order to characterize the enzymatic activity of FaCAD, the full-length coding sequence of *FaCAD* was subcloned into the pGEX4-T1 vector. GST-FaCAD (or GST-FaCAD with 1 mM $ZnCl_2$) was expressed in the *E. coli* Rosetta (DE3) pLysS, as described in methods II.3.4.2. The enzymatic activity of purified GST-FaCAD was determined in sodium phosphate buffer (pH 6.5) with NADPH and coniferaldehyde. The decrease in absorbance at 340 nm resulting from the oxidation of NADPH of either GST-FaCAD or GST-FaCAD with $ZnCl_2$ was more rapid than that of GST (Figure 29A). The specific activity of GST, GST-FaCAD, and GST-FaCAD with $ZnCl_2$ was 0.0007, 0.04, and 0.11 U/mg, respectively. The reaction mixture was analyzed by LC-UV-ESI-MS^n. Although the substrate (coniferaldehyde) concentration in GST-FaCAD reactions decreased in comparison with GST reactions, no product (coniferyl alcohol) was detected (Figure 29B). There was a fivefold decrease in the level of coniferaldehyde in GST-FaCAD, as compared with GST (Figure 29C).

To detect the assumed product, the full-length coding sequence of *FaCAD* was alternatively subcloned into a pYES2 vector (pYES2-FaCAD) and was expressed in yeast cells. The activity of pYES2-FaCAD was measured by LC-UV-ESI-MS^n (Figure 30A). CAD activity increased in pYES2-FaCAD after 8 h with the highest activity occurring at 48 h (Figure 30B). The activity was two times higher in pYES2-FaCAD than in pYES2 (control) at 24-48 h.

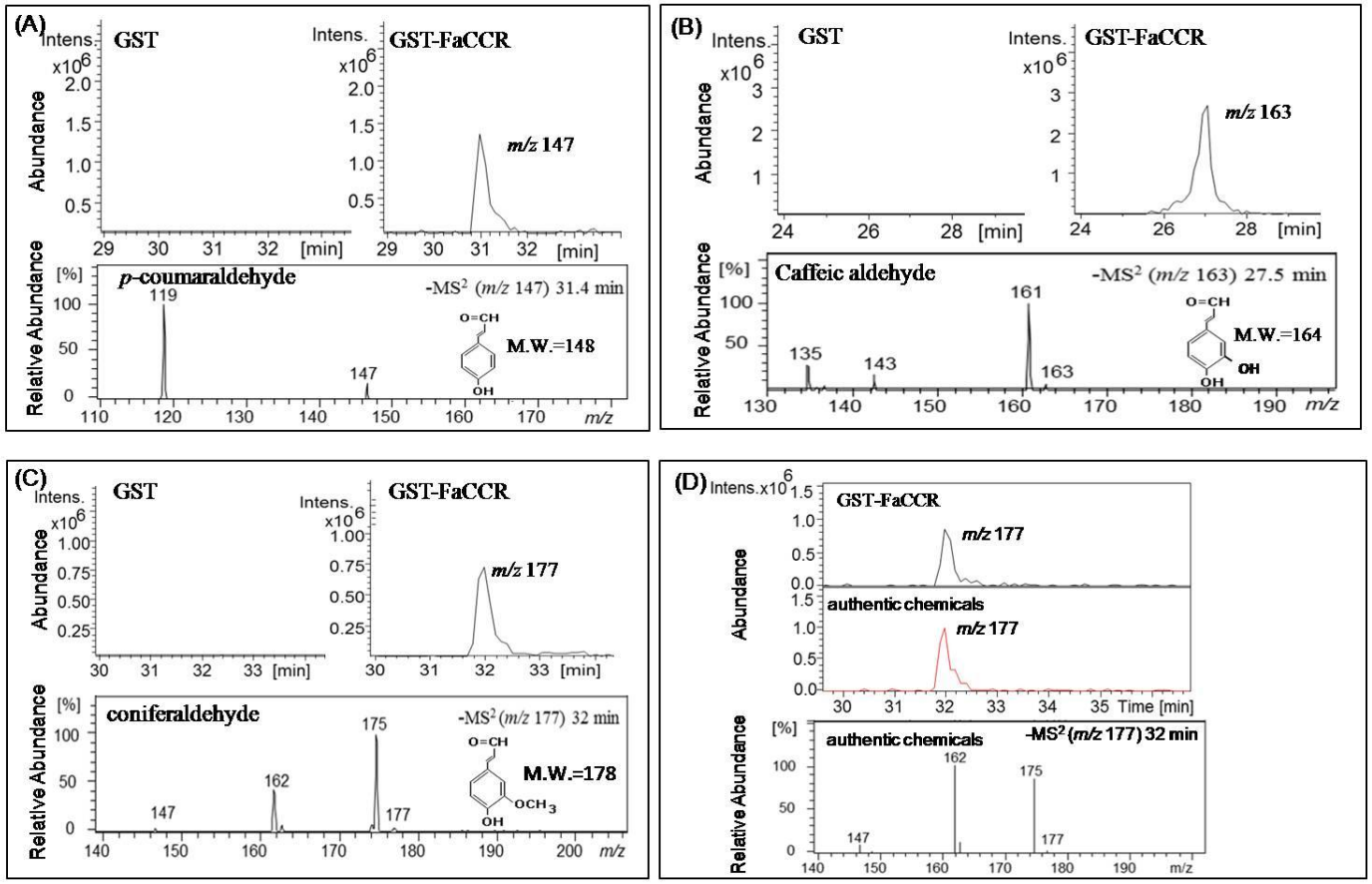

Figure 28. Identification of products formed by recombinant GST-FaCCR.

The reaction mixture of either purified GST or recombinant GST-FaCCR was prepared as described in methods (II.3.5.5). Reaction products and authentic coniferaldehyde (reference) were analyzed by LC-UV-ESI-MS^n and recorded at 340 nm (A-D_top). The MS^2(-) spectra are showed (A-C_bottom). M.W. = molecular weight; *m/z* = mass-to-charge ratio.

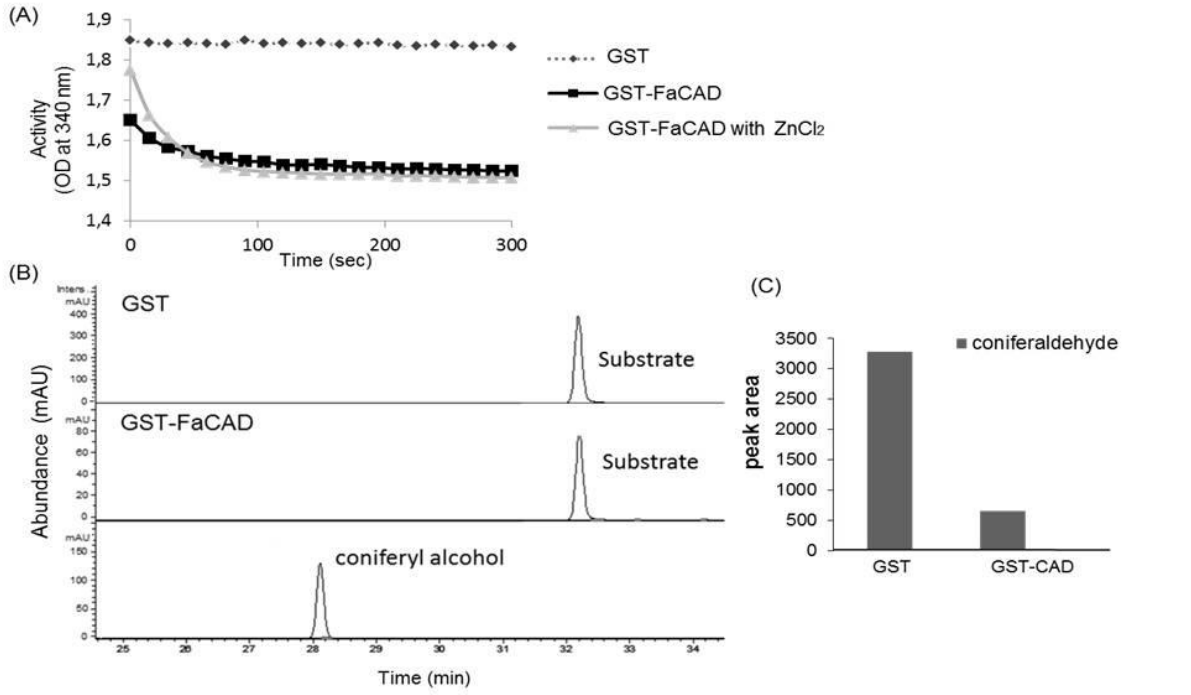

Figure 29. FaCAD activity expressed in *E. coli*.

The reaction mixture of either purified GST or recombinant GST-FaCAD was prepared as described in methods (II.3.6). (A) Activity was measured at 340 nm by spectrophotometer. (B) Reaction products were identified by LC-UV-ESI-MS^n and recorded at 260 nm. (C) Coniferaldehyde (substrate) of the reaction was quantified based on the peak areas shown in (B) (substrate=coniferaldehyde, product=coniferyl alcohol).

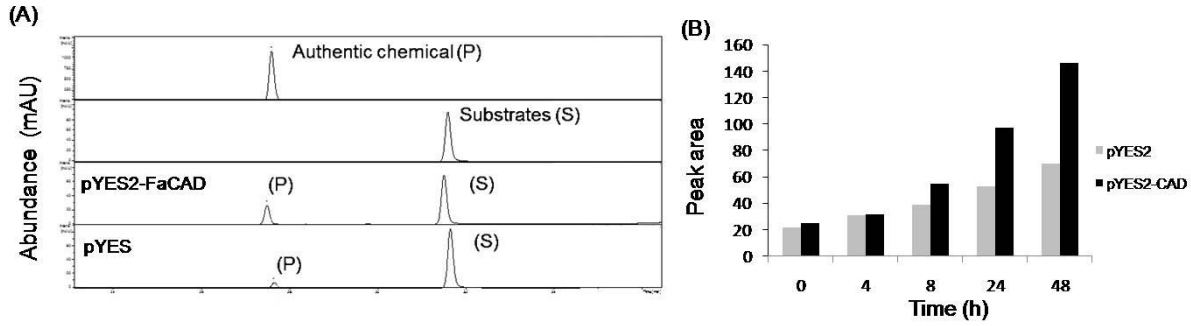

Figure 30. FaCAD activity expressed in *S. cerevisiae*.

Crude protein of pYES2 and pYES2-FaCAD was used for enzyme activity assays. All reaction mixtures were prepared as described in methods (II.3.6). (A) Reaction products were identified by LC-UV-ESI-MS^n (S=coniferaldehyde, P=coniferyl alcohol). UV detection was done at 260 nm. (B) Coniferyl alcohol (product) formed in the pYES2 and pYES2-FaCAD reactions was quantified based on the peak areas of the UV traces.

4. Heterologous expression of *FaPOD* and *FaPOD27*: two peroxidase isoforms

To characterize the activities of two *F. x ananassa* peroxidases, the full-length coding sequence of *FaPOD* and *FaPOD27* was subcloned into the pGEX4-T1 vector. pGEX-FaPOD and pGEX-FaPOD27 was expressed in *E. coli* Rosetta (DE3) pLysS after induction of the protein with 0.5 mM IPTG. The pGEX4-T1 vector, without an inserted DNA sequence, served as a control.

In general, peroxidases utilize H_2O_2 in the oxidation of various substrates such as monolignols, and ferulic acids (Passardi et al., 2004b). To test strawberry peroxidase activity, crude proteins of pGEX4-T1, FaPOD, and FaPOD27 were added to guaiacol (model substrate) in the presence of H_2O_2. The reaction mixture with FaPOD27 quickly changed color to purple, but the solutions containing FaPOD and control (pGEX4-T1) remained colorless (Figure 31A). The activity of FaPOD27 (166×10^{-4} µmol min^{-1} mg^{-1} total protein) was elevated to 48-fold and that of FaPOD (7.2×10^{-4} µmol min^{-1} mg^{-1} total protein) to 1.8-fold as compared with the control pGEX4-T1 vector (4.2×10^{-4} µmol min^{-1} mg^{-1} total protein; Figure 31B).

The products formed by FaPOD27 from ferulic acid (M.W. = 193 g/mol) were analysed by LC-UV-ESI-MS^n (Figure 32A, Ward et al., 2001). LC-UV-ESI-MS^n analysis indicated dimeric products (dehydrodimer of ferulic acid; M.W. = 386 g/mol; Figure 32B1), products formed by decarboxylation of a dehydrodimer precursor (M.W. = 342 g/mol; Figure 32B2), and unknown products (Figure 32B3) that were formed by FaPOD27. Unlike FaPOD27, these compounds were not produced in the mixture reaction of FaPOD or control GST (Figure 32A). The results indicate that FaPOD27 is presumably associated with polymerization of ferulic acid in lignin biosynthesis.

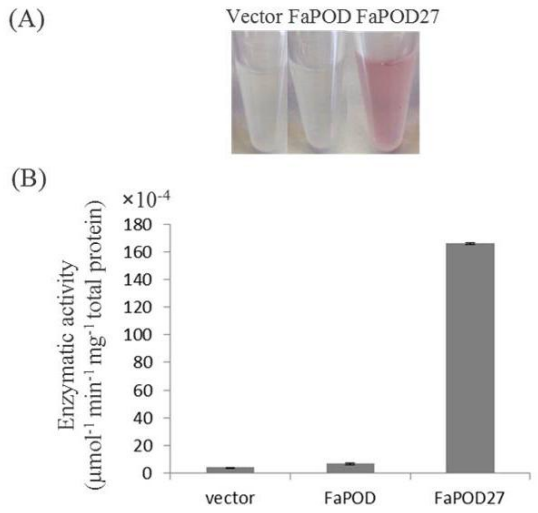

Figure 31. Expression of FaPOD and FaPOD27 protein in *E. coli* strain Rosetta (DE3) pLysS.

The reaction mixtures were prepared as described in methods (II.3.7). (A and B) The reaction mixture contained total protein extract from cells harboring the control vector (pGEX-4X-1), FaPOD, and FaPOD27 after induction with IPTG. Values are mean ± SE of triplicate.

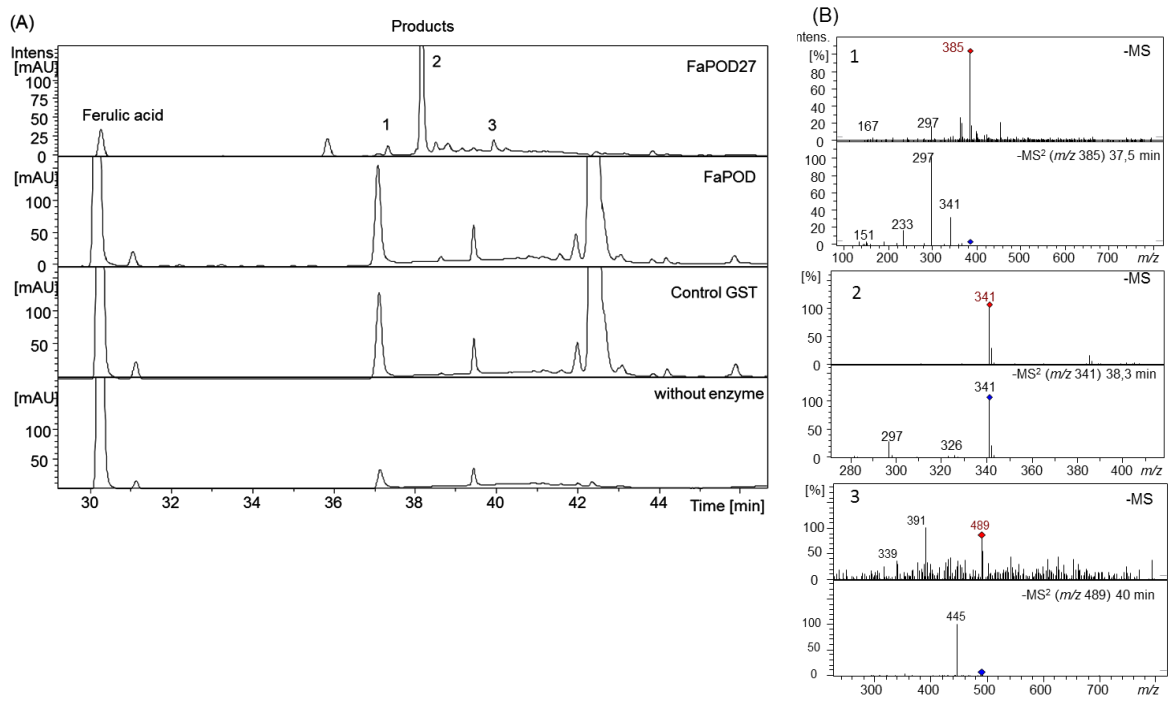

Figure 32. LC-UV-ESI-MS^n analysis of strawberry peroxidase reaction products.

(A) The reaction mixture contained the substrate ferulic acid and H_2O_2 with crude protein FaPOD27, FaPOD, control GST (pGEX-4X-1 vectors), or without enzymes. Substrate and products were monitored at 320 nm. The three products (A1-3) formed by FaPOD27 corresponded to the dehydrodimer of ferulic acid (B1), a decarboxylation product of the dehydrodimer precursor (B2), and unknown products (B3), respectively (Ward et al., 2001).

5. Lignin biosynthetic genes in strawberry fruit

5.1 Expression of lignin biosynthetic genes in vegetative tissues, flowers, and fruit developmental stages

To study the expression profiles of *FaCCR*, *FaCAD*, *FaPOD*, and *FaPOD27* in *F. x ananassa* cv. Elsanta, expression levels of the four genes in vegetative tissues (leaves, stems, runners, and roots), flowers, and fruits at different developmental stages (small green, green white, white, turning, and red; Figure 33A) were determined by qRT-PCR. Total RNA was isolated from the samples and transcribed to cDNAs. Primers of *FaCCR*, *FaCAD*, and *FaPOD* were designed based on conserved regions from coding sequences of alleles (Table 24) to allow the detection of multiple gene copies or allele transcripts of each gene. Primers of *FaPOD27* were obtained from a strawberry functional genomics projects (FraGenomics; II.1.8 F).

Low expression levels of both *FaCCR* and *FaCAD* were determined in unripe fruit from the SG (small green) to W (white) stages, but high expression levels of both genes were detected in the mature fruit (T and R; Figure 33B). Moreover, varied expression levels of both *FaCCR* and *FaCAD* were detected in vegetative tissues and flowers. *FaCAD* was highly expressed in the roots as well. Interestingly, the highest expression level of *FaPOD* was detected in the SG stage and expression levels decreased after the SG stage. *FaPOD* was undetectable at red stages (R), but varied expression levels were detected in vegetative tissues and flowers. In addition, *FaPOD27* transcripts were clearly detected in the ripe fruit (R) and roots, but lower expression levels were found in other fruit stages (SG, GW, W, and T), vegetative tissues and flowers. The expression level of *FaPOD27* showed a 20-fold increase in the ripe stage (R) as compared with other developmental stages of fruit (SG, GW, W, and T), and there was a 15-fold increase in the root as compared with other vegetative tissues and flowers. Therefore, *FaCCR*, *FaCAD*, and *FaPOD27* genes were strongly expressed in the ripe red fruit, except for *FaPOD*, which was expressed in the SG fruit.

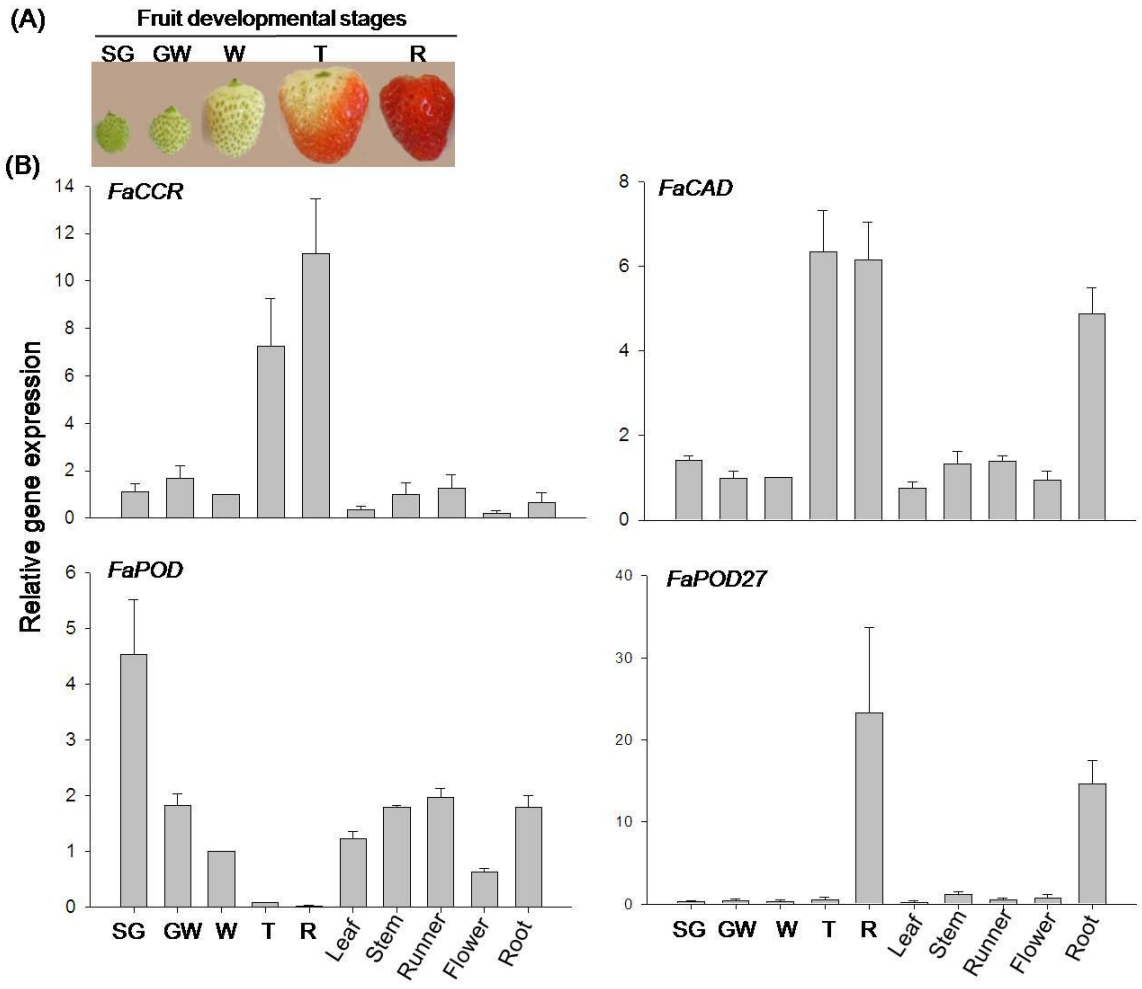

Figure 33. Relative expression profiles of monolignol biosynthesis genes in vegetative tissues, flowers, and fruit developmental stages of *F. x ananassa* cv. Elsanta.
Total RNA was isolated from (A) fruit developmental stages at small green (SG), green white (GW), white (W), turning (T), and red (R) after pollination. (B) Expression levels of vegetative tissues (leaves, stems, runners, and roots), flowers, and fruit developmental stages (SG, GW, W, T, and R) were monitored by qRT-PCR using specific primers for target genes (*FaCCR*, *FaCAD*, *FaPOD*, and *FaPOD27*) and the interspacer gene. The latter was used as an internal control for normalization. The white fruit was used as the reference with one for each graph. Values are mean ± SE of 5-6 replicates from two sets of cDNAs and are shown as relative changes.

5.2 Strawberry fruit in response to stress tolerance

5.2.1 Effect of wounding and pathogen on gene expression levels in fruit

Lignin biosynthesis is a complex genetic network, where several genes and enzymes can be induced by various abiotic (plant injuries) or biotic (bacterial infection) stresses (Moura et al., 2010). Agroinfiltrated fruits are exposed to wounding (perforation of the fruit epidermis

by a syringe) and pathogen infections (*Agrobacterium tumefaciens*). To investigate the effect of wounding and *Agrobacterium* infection on the expression of phenylpropanoid biosynthesis genes (*FaPAL*, *FaCHS*, *FaCCR*, *FaCAD*, *FaPOD*, or *FaPOD*27) in the fruit, total RNAs were isolated from single fruits exposed to wounding (fruits injected with MMA medium) and *Agrobacterium*-infection (fruits injected with *Agrobacterium* suspensions) at different time points and transcribed to cDNAs. Expression levels of the genes in the untreated and treated fruits were monitored by qRT-PCR.

No significant induction of *FaPAL*, *FaCCR*, *FaCAD*, *FaPOD*, and *FaPOD*27 genes were detected in the wounded fruits, as compared to control (untreated) fruits during 2 days (Figure 34). In addition, no significant induction of *FaCHS*, *FaCCR*, *FaCAD*, and *FaPOD* genes were detected in the fruits injected with *Agrobacterium* as compared to control fruits during 4 days (Figure 35). However, the expression level of *FaPAL* was two times higher in fruits injected with *Agrobacterium* than that in the control fruits at 24 h. *FaPOD*27 transcript level in the fruits injected with *Agrobacterium* gradually started to increase at 6 h and the highest level was reached at 96 h after agroinfiltration (Figure 35). Besides, expression level of *FaPOD*27 in the fruits injected with *Agrobacterium* was induced within 1 to 10 days, with the highest level being detected 10 days after injection. The expression level of *FaPOD27* in the fruits injected with *Agrobacterium* was 30 times higher than that in the control fruits at 10 days (Figure 36). These results clearly demonstrated that the expression of *FaPOD*27 is strongly induced by *Agrobacterium*. Other genes (*FaPAL*, *FaCHS*, *FaCCR*, *FaCAD*, *FaPOD*, and *FaPOD*27) were not affected by wounding or *Agrobacterium*. *FaPOD*27 transcripts are up-regulated in fruits as a response to infection with *Agrobacterium*, suggesting that this gene plays an important role in pathogen defense.

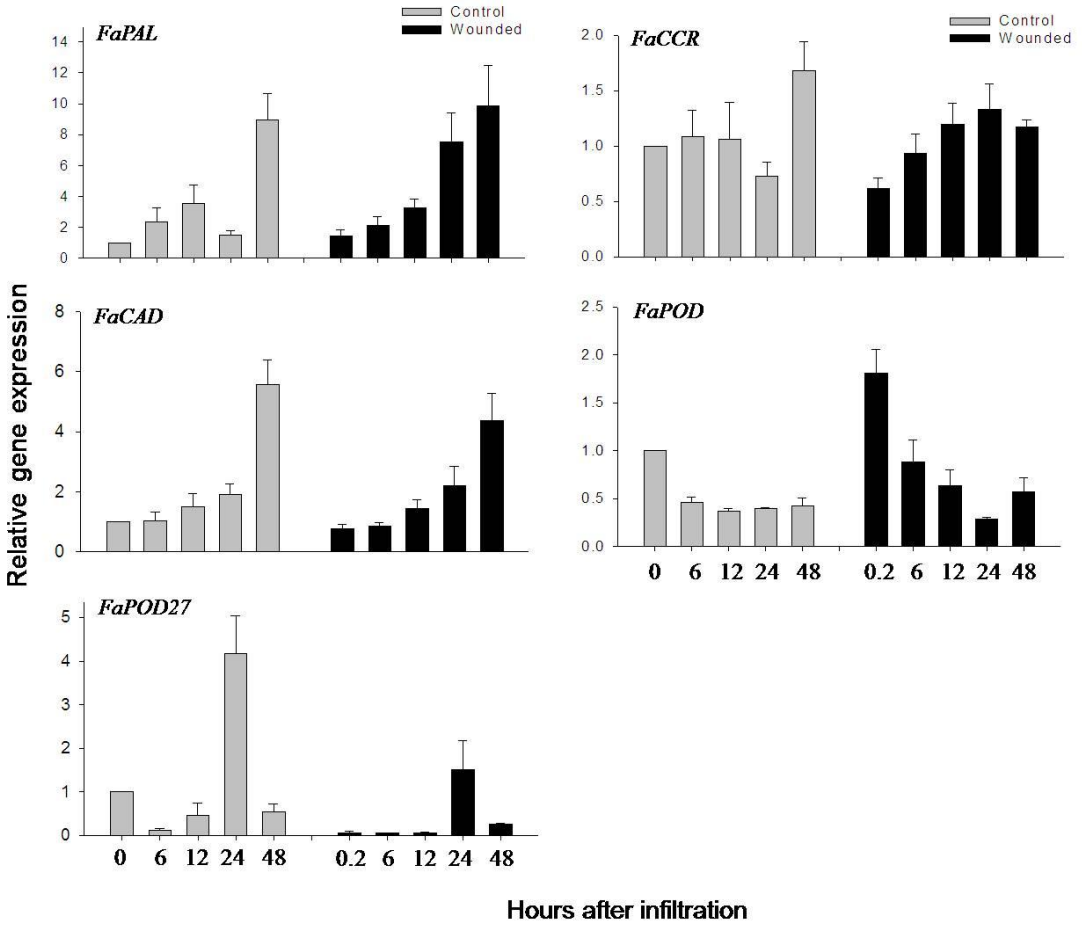

Figure 34. Relative expression profiles of monolignol biosynthesis genes of *F. x ananassa* cv. Elsanta in response to wounding.

The turning fruit was infiltrated with MMA medium for all treatments. After infiltration, fruits were harvested at 0.2 (12 min), 6, 12, 24, and 48 h. Wild-type (untreated) fruits were used as controls and harvested at the same time points. Expression levels in the control (grey column) and wounded fruit (black column) were monitored by qRT-PCR using specific primers for the target genes (*FaPAL*, *FaCCR*, *FaCAD*, *FaPOD*, and *FaPOD*27) and the interspacer gene. The latter was used as an internal control for normalization. The control fruit (0 h) was used as reference with one for each graph. For *FaCCR*, *FaCAD*, and *FaPOD*, values are mean ± SE of 9 triplicates from three independent fruits. For *FaPAL* and *FaPOD27*, values are mean ± SE of 4-6 replicates from two independent fruits. All values are shown as relative changes.

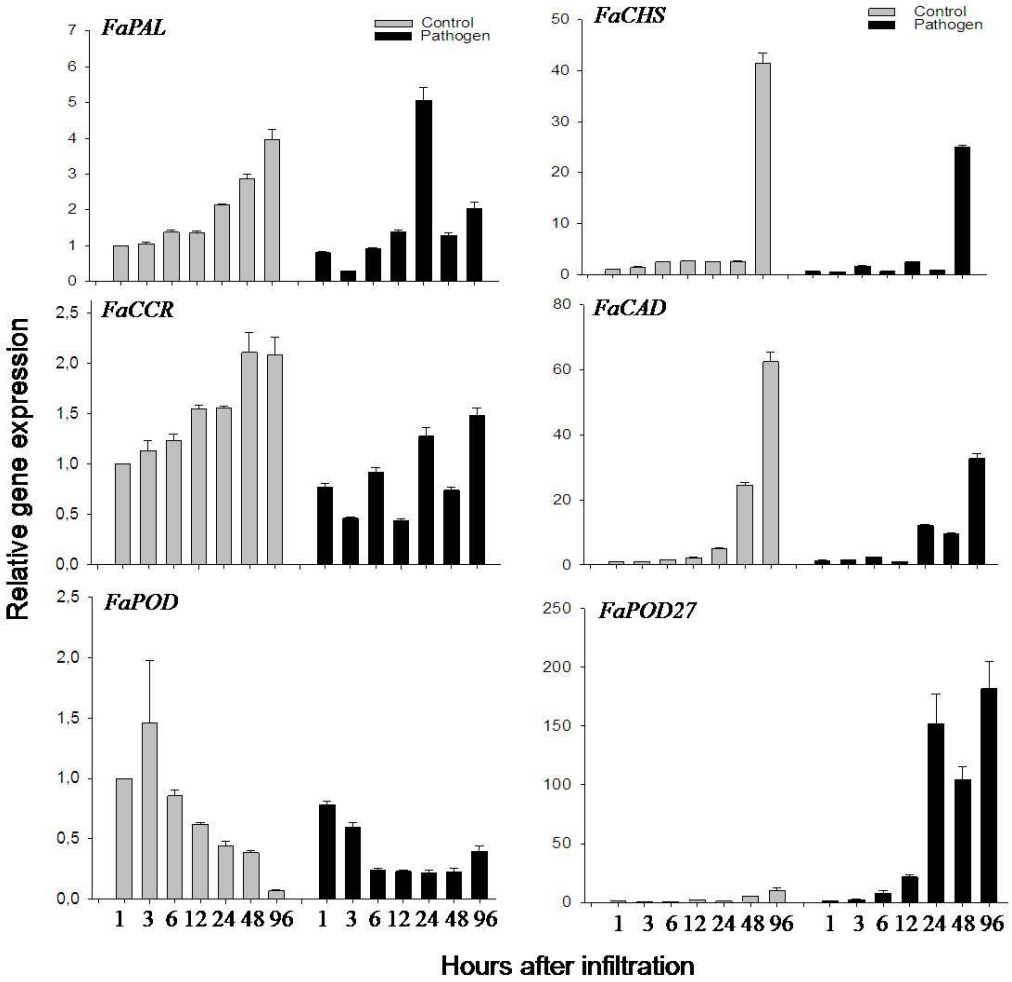

Figure 35. Relative expression profiles of phenylpropanoid biosynthesis genes of *F. x ananassa* cv. Elsanta in response to *Agrobacterium*.

The turning fruit was infiltrated with *Agrobacterium* cells for all treatments. After infiltration, fruits were harvested at different time points (1, 3, 6, 12, 24, 48, and 96 h). Wild-type (untreated) fruits were used as controls and harvested at the same time points. Expression levels in control (grey column) and agroinfiltrated fruit (black column) were monitored by qRT-PCR using specific primers for target genes (*FaPAL*, *FaCHS*, *FaCCR*, *FaCAD*, *FaPOD*, and *FaPOD27*) and the interspacer gene. The latter was used as an internal control for normalization. The control fruit (1 h) was used as the reference with one for each graph. Values are mean ± SE of 2-3 replicates from one fruit and are shown as relative changes.

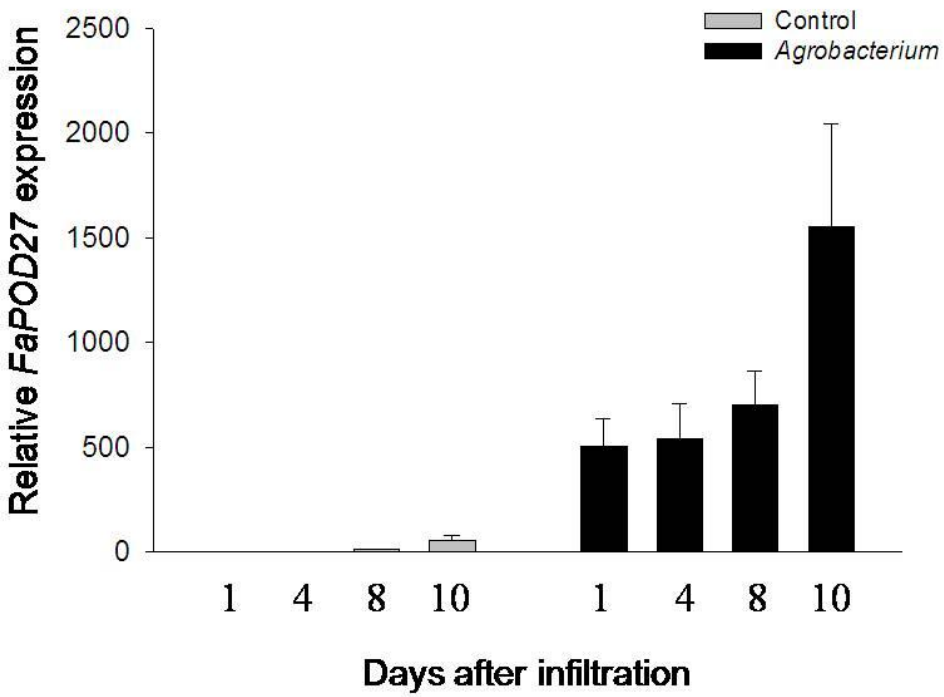

Figure 36. Relative expression of *FaPOD27* in response to *Agrobacterium*.
The turning fruit was infiltrated with *Agrobacterium* cells for all treatments. After infiltration, fruits were harvested at 1, 4, 8, and 10 d. Wild-type (untreated) fruits were used as controls and harvested at the same time points. Expression levels in control (grey column) and agroinfiltrated fruit (black column) were monitored by qRT-PCR using specific primers for *FaPOD*27 and the interspacer gene. The latter was used as an internal control for normalization. The control fruit (1 d) was used as the reference (set to one). Values are mean ± SE of 6 replicates from two independent fruits and are shown as relative changes.

5.2.2 Effect of wounding and pathogen infection on fruit firmness

To test whether a fruit respond to stress with increased firmness, the fruits were infiltrated with MMA medium as a wounding treatment, and fruits were infiltrated with *Agrobacterium* as a pathogen-infection treatment. Fruit firmness was measured at 14 days after infiltration. Its firmness, based on bioyield point, was determined by using a TA-XT2i texture analyzer.

The Wilcoxon-Mann-Whitney *U*-test was used for non-parametric comparison of WT (untreated) and either wounded or pathogen-infected fruits (Figures 37A-B). A *P*-value <1.00E-02 was considered as significantly different. Fruit firmness was significantly increased (*P*=4.33E-05) in fruits infiltrated with *Agrobacterium*, but not in wounded fruits (*P*=9.72E-01) as compared to WT fruits. Both wounded and wild-type fruits were soft, whereas fruits infiltrated with *Agrobacterium* tended to be hard. The result suggests that fruit firmness significantly increased following infiltration with *Agrobacterium*.

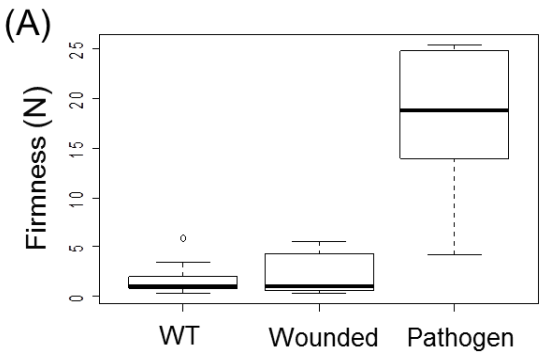

(B)

Two groups	*P*-value
WT vs. Wounded	9.72E-01
WT vs. Pathogen	4.33E-05

Figure 37. Effect of wounding and pathogen infection on fruit firmness of *F. x ananassa* cv. Elsanta.

Fruit firmness was measured 14 days after infiltration. (A) The Box plot shows data from three groups. WT (Wild type; *n*=10); fruits infiltrated with MMA medium (wounded; *n*=12) and *Agrobacterium tumefaciens* AGLO (pathogen; *n*=10). (B) The Wilcoxon-Mann-Whitney *U*-test was used for a non-parametric comparison of two groups from WT and wounded or pathogen-infected fruits. Values showing statistically significant increased levels (*P* <1.00E-02) are marked by a yellow background.

5.2.3 Effect of *Agrobacterium*-infection on fruit firmness and lignin content

To test whether fruit firmness is affected in response to *Agrobacterium*, a half side of a fruit was injected with *Agrobacterium* carrying the ihpRNA-*FaCHS* constructs (II.1.5) whereas the other side was not injected. The wild-type (untreated) fruit was used as a control.

Fruits were analyzed at 14 days after infiltration. The side of the fruit that did not receive an injection (Figure 38A, a) exhibited a red color that was similar to wild-type fruits (Figure 38A, c). The other half of the fruit exhibited the white color of a *FaCHS*-silenced fruit due to silencing of the *CHS* gene (Figure 38A, b; Hoffmann et al., 2006). Interestingly, firmness also significantly increased (*P*<1.00E-02) in the white area which was injected with *Agrobacterium* carrying ihpRNA-*FaCHS* constructs, but did not increase in the red part (Figures 38B-C). Thus, the ihpRNA-*FaCHS* construct function as an indicator since impaired color formation correlates with fruit firmness due to *Agrobacterium*-infection.

To investigate further, whether fruit firmness correlates with lignin content, lignin from the treated fruits was assayed. Lignin content significantly increased (*P* <1.00E-02) in the white colored region injected with *Agrobacterium*, but did not increase in the red part without injection of *Agrobacterium* (Figures 38 B-C). The color, firmness, and lignin content in the red area were the same as those in wild-type fruits. Interestingly, increased firmness

and lignin content in the white part injected with *Agrobacterium* did not affect either firmness or lignin content in the other area without *Agrobacterium* (Figure 38). The increase in firmness was clearly associated with an increased formation of lignin in the fruits due to *Agrobacterium* infection. The injection of *Agrobacterium* cells in one half one the fruit cannot cause a response in the entire fruit.

These data, taken together, indicate that high expression levels of *FaPOD27* are associated with enhanced firmness, as well as increased production of lignin in fruits exposed to *Agrobacterium*.

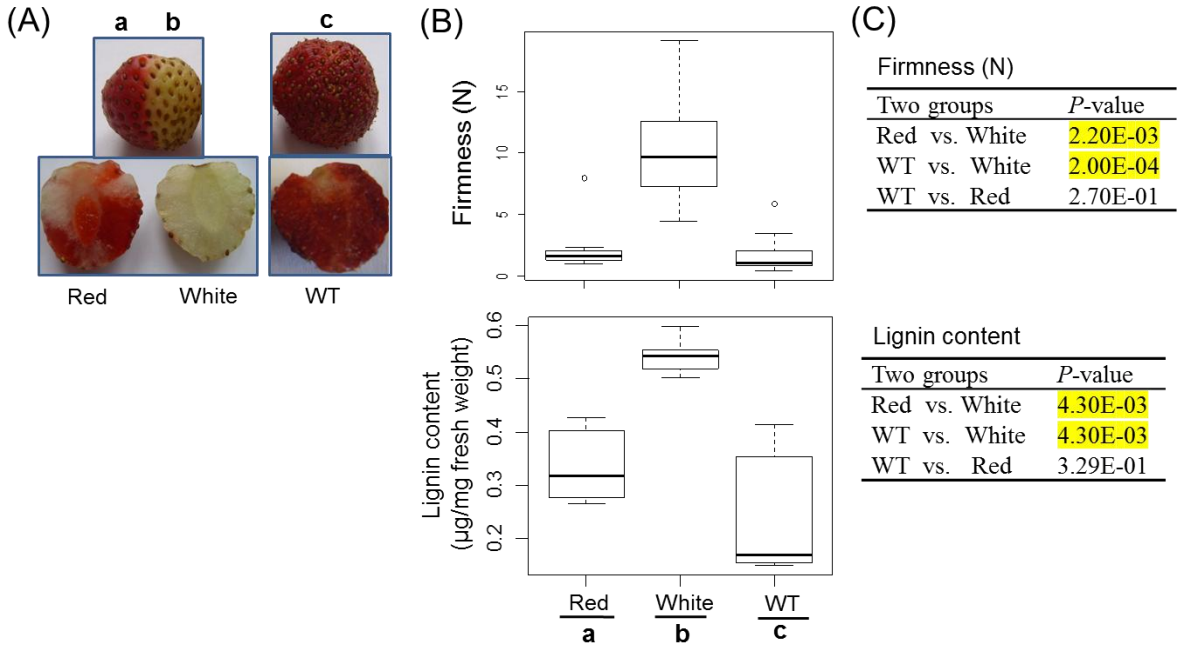

Figure 38. Effect of pathogen infection on fruit firmness and lignin content of *F. x ananassa* cv. Elsanta.

Fruit firmness and lignin content were measured 14 days after infiltration. (A) Phenotypes of a fruit whose left side was not infiltrated with *A. tumefaciens* (a; red part), whereas the right side was injected with *A. tumefaciens* containing *FaCHS*-ihpRNA constructs (b; white part) and of a wild type fruit (WT; c) are compared. (B) The Box plots show data from different groups with the following biological replicates: firmness of red (n=8), white (n=8), and WT (n=10) and lignin content of each group (n=6). (C) The Wilcoxon-Mann-Whitney U-test was used for a non-parametric comparison of two groups as described in the table above. Values showing statistically significant increased levels (P <1.00E-02) are marked by a yellow background.

5.3 Down- and up-regulation of lignin biosynthetic genes in *F. x ananassa* cv. Elsanta fruit

5.3.1 ihpRNA and overexpression constructs used for silencing and overexpression of lignin biosynthetic genes in fruit

In order to manipulate quantity and quality of lignin in strawberry fruit, we utilized an ihpRNA- or overexpression-cassette with individual *FaCCR*, *FaCAD*, and *FaPOD* to silence or overexpress *FaCCR*, *FaCAD*, and *FaPOD* in the fruit.

The control construct (pBI-intron) contained a *GUS* gene interrupted by an intron under the control of a CaMV 35S promoter (Figure 39A). To silence the monolignol biosynthesis genes in the fruit, the ihpRNA-cassette construct contained an intron flanked by partial coding sequences (300 bp) of target genes (*FaCCR*, *FaCAD*, or *FaPOD*) in sense and antisense orientations under the control of the CaMV 35S promoter (II.3.3.1) (resulting plasmid pBI-*FaCCRi*, pBI-*FaCADi*, and pBI-*FaPODi*) (Figure 39B). In addition to overexpress monolignol biosynthesis genes in the fruit, the construct comprised the full-length coding sequence of target genes (*FaCCR*, *FaCAD*, or *FaPOD*) under the control of the CaMV 35S promoter (II.3.3.2) (resulting plasmid pBI-*FaCCR*, pBI-*FaCAD*, and pBI-*FaPOD*) (Figure 39C). All constructs were used for agroinfiltration of fruits.

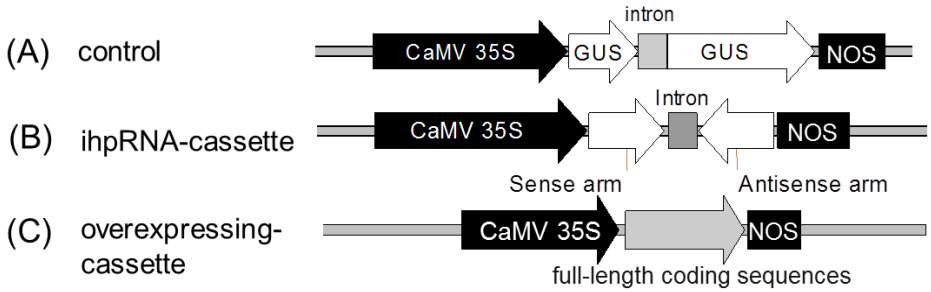

Figure 39. Schematic diagram of constructs used in this study.
All constructs (A-C) are in the binary vector pBI121. CaMV 35S, the 35S promoter of *cauliflower mosaic virus*; intron, the second intron of strawberry *FaQR* gene (Raab et al., 2006); NOS, terminator of the nopaline synthase gene; a partial coding sequence of target genes (*FaCCR*, *FaCAD*, or *FaPOD*) in the sense and antisense arm; full-length coding sequences of target genes (*FaCCR*, *FaCAD*, or *FaPOD*).

5.3.2 Phenotype and lignin staining

An agroinfiltration method has already been successfully applied for gene functional studies of strawberry fruit (Hoffmann et al., 2006). In order to control the quantity and quality of lignin in *F. x ananassa* fruit, individual pBI-intron, pBI-*FaCCRi*, pBI-*FaCADi*, pBI-*FaPODi*, pBI-*FaCCR*, pBI-*FaCAD*, and pBI-*FaPOD* (Figures 39A-C) constructs were infiltrated into fruits for gene transfer by *Agrobacterium*. Comparison of the WT phenotype

(untreated fruit) (Figures 40A, a and c) with fruits injected with different constructs (pBI-intron, pBI-*FaCCRi*, pBI-*FaCADi*, pBI-*FaPODi*, pBI-*FaCCR*, pBI-*FaCAD*, or pBI-*FaPOD* fruits) (Figures 40A b and d) showed that the injected fruits retained their red color and were similar in appearance to the WT fruit after 14 days (Figure 40A). In contrast, the texture of the fruits injected with different constructs was more solid than that of the untreated fruits (WT). The texture of the untreated fruits was soft (Figure 40A, c) whereas the texture of all the injected fruits was firm (Figure 40A, d).

Additionally, WT (Figures 40B, a and c) and fruits injected with different constructs (Figures 40B, b and d) were compared before and after Wiesner staining. All treated fruits (pBI-intron, *FaCCR*-, *FaCAD*-, *FaPOD*-silenced, *FaCCR*-, *FaCAD*-, or *FaPOD*-overexpression fruits) showed the formation of pink-red colors around vascular bundles within 1 min (Figure 40B, d), and then disappeared within 30 min after staining. In contrast, slight pink-red colors were observed in the control fruit within 30 min after staining (Figure 40B, c). This result suggests that lignification around vascular bundles is induced by *Agrobacterium* infiltration. The accumulation of lignin in fruits infiltrated with different constructs might enable these fruits to resist *Agrobacterium* invasion.

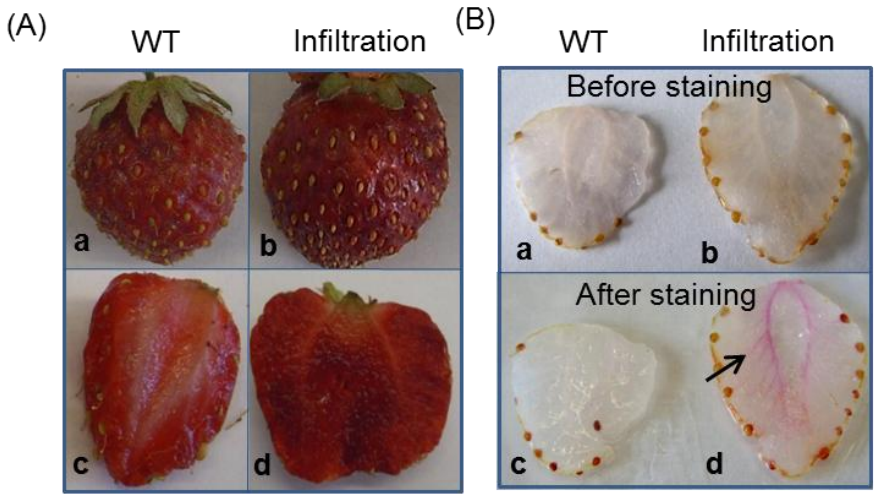

Figure 40. Phenotype and lignin staining of wild-type and infiltrated fruits.
All photographs were taken 14 days after infiltration. WT (Wild type; a, c) was used as a non-infiltrated fruit. Infiltrated fruits (b, d) are those injected with *Agrobacterium* suspensions harboring independent pBI-intron, *FaCCR*-, *FaCAD*-, *FaPOD*-ihpRNA, *FaCCR*-, *FaCAD*-, and *FaPOD*-overexpression constructs. (A) Phenotypes of WT (a, c) and infiltrated fruits (b, d). (B) Cross-sections of WT (a, c; n=2) and infiltrated fruits (b, d; n=2) before and after Wiesner staining. The arrow indicates lignified vascular bundles with pink-red colors after staining with phloroglucinol. Lignified tissues were observed in the fruit infiltrated with *Agrobacterium* suspensions harboring constructs, as described above.

5.3.3 Fruit texture and lignin content

To investigate and determine the effect of monolignol biosynthesis genes on fruit texture and lignin content, single fruits were injected with *Agrobacterium* suspension containing different constructs (Figures 39, B and C) for down- and up-regulation of individual *FaCCR*, *FaCAD*, and *FaPOD* in the fruit. Fruits injected with pBI-intron suspensions were used as control (Figure 39A).

Comparison of untreated fruits (WT) and treated fruits (pBI-intron, pBI-*FaCCRi*, pBI-*FaCADi*, pBI-*FaPODi*, pBI-*FaCCR*, pBI-*FaCAD*, or pBI-*FaPOD* fruits) showed that both firmness and lignin content were significantly increased (P <1.00E-02; Figure 41). In addition, comparison of pBI-intron control fruits and treated fruits (*FaCCR*-, *FaCAD*-, *FaPOD*-downregulated, *FaCCR*-, *FaCAD*-, or *FaPOD*-upregulated fruits) showed that firmness and lignin content were not affected significantly. Thus, firmness and lignin content were significantly increased due to infiltration with *Agrobacterium*. Hence, when individual *FaCCR*, *FaCAD*, and *FaPOD* were down-regulated and up-regulated in the fruits by agroinfiltration, up-regulation of defense genes such as *FaPOD27* affected fruit firmness and lignin to a much larger extent than the transgenes.

5.3.4 Gene expression levels

To assess the expression of phenylpropanoid biosynthesis genes in *FaCCR*-, *FaCAD*-, *FaPOD*-down-regulated, *FaCCR*-, *FaCAD*-, and *FaPOD*-up-regulated fruits, total RNA was isolated from single fruits and transcribed to cDNAs. Expression levels of *FaPAL*, *FaCHS*, *FaCCR*, *FaCAD*, and *FaPOD* genes in the treated fruits were monitored by qRT-PCR.

Expression levels of both *FaPAL* and *FaCHS* were not significantly changed in WT, pBI-*FaCCRi*, pBI-*FaCADi*, and pBI-*FaPODi* fruits, when compared to pBI-intron control fruits. However, in comparison to pBI-intron control fruits, *FaCCR* and *FaCAD* transcripts were significantly decreased (P <0.05) in pBI-*FaCCRi* and pBI-*FaCADi* fruits, respectively. They were not significantly changed in other treated fruits. Thus, the ihpRNA-*FaCCR* and -*FaCAD* construct showed sequence-specific interference with homologous *FaCCR* and *FaCAD* expression in the fruits. Additionally, *FaPOD* transcripts remained at the same level in all groups. *FaPOD* transcripts were probably not significantly affected in pBI-*FaPODi* fruits (Figure 42) due to the already low expression level of *FaPOD* in the ripe red fruit (Figure 33B).

In the case of up-regulation of monolignol genes in the fruits, expression levels of *FaPAL*, *FaCHS*, *FaCCR*, and *FaCAD* were not significantly affected in WT, pBI-*FaCCR*, pBI-*FaCAD*, and pBI-*FaPOD* fruits as compared to pBI-intron control fruits. *FaCCR* and

FaCAD transcripts were abundant in the ripe red stage of WT (Figure 33B) but did not show a significant increase in pBI-*FaCCR* and pBI-*FaCAD* fruits (Figure 43). Interestingly, *FaPOD* transcripts which are rarely expressed in the ripe red stage (Figure 33B) increased significantly (P <0.05) when *FaPOD* was overexpressed in pBI-*FaPOD* fruits. Expression level of *FaPOD* was not significantly changed in other fruits (WT, pBI-intron, pBI-*FaCCR*, and pBI-*FaCAD*; Figure 43).

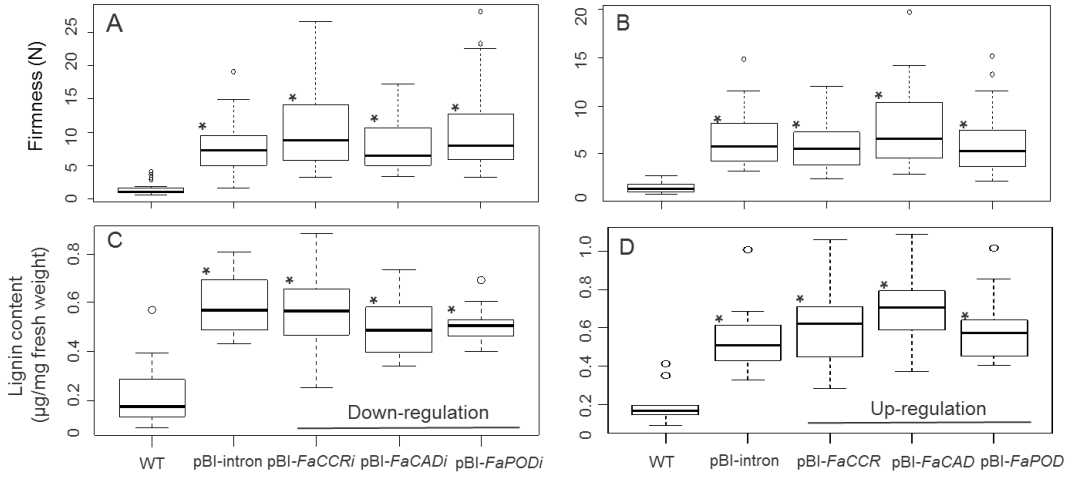

Figure 41. Fruit firmness (A, B) and lignin content (C, D) of individual *FaCCR*-, *FaCAD*-, *FaPOD*-downregulation (A, C) and -upregulation (B, D) in *F. x ananassa* cv. Elsanta.
Fruit firmness and lignin content were measured 14 days after infiltration. The box plots of firmness and lignin content show data from different groups with the following biological replicates: (A) Firmness of WT (wild type; n=26), fruits infiltrated with *Agrobacterium* suspensions containing a non-ihpRNA construct (pBI-intron; n=41) or an individual ihpRNA-mediated gene silencing construct (pBI-*FaCCRi*; n=32, pBI-*FaCADi*; n=30, pBI-*FaPODi*; n=35); (B) Firmness of WT (n=30), pBI-intron (n=41) and an individual overexpression construct (pBI-*FaCCR*; n =39, pBI-*FaCAD*; n =35, pBI-*FaPOD*; n=43); (C) Lignin content of WT (n=14), pBI-intron (n=19), pBI-*FaCCRi* (n=19), pBI-*FaCADi* (n=19), and pBI-*FaPODi* (n=19); (D) Lignin content of each group (n=10). The statistical analysis methodology used was the Wilcoxon-Mann-Whitney *U*-test for non-parametric comparison of two groups. One asterisk (*) marked in the box indicates statistically significant increased levels (P<1.00E-02) in comparison with WT and another group (Appendix E.1.1).

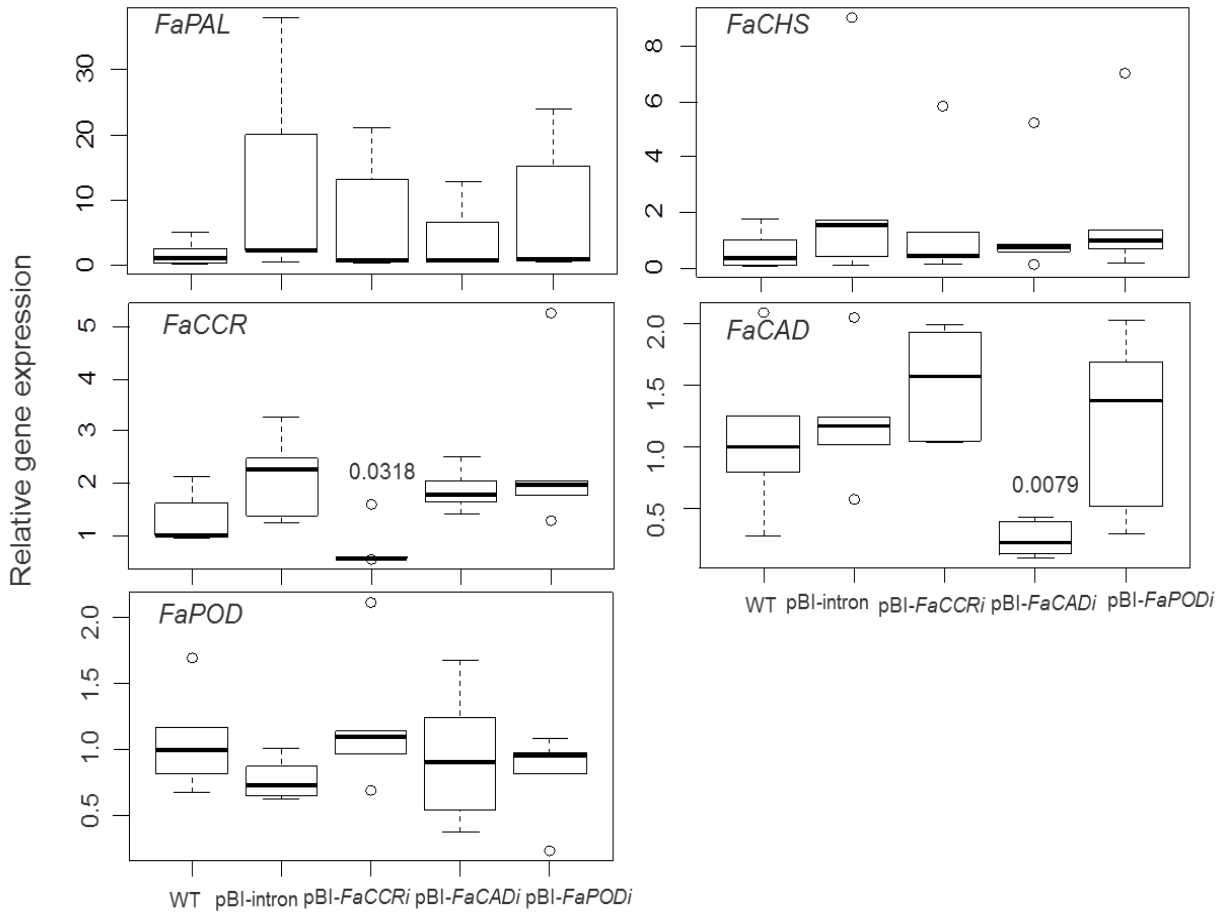

Figure 42. Relative expression profiles of down-regulated monolignol biosynthesis genes in *F. x ananassa* cv. Elsanta.

Total RNA was isolated from single WT (wild type) fruits, agroinfiltrated fruits with a non-ihpRNA construct (pBI-intron) or with individual ihpRNA-mediated gene silencing constructs (pBI-*FaCCRi*, pBI-*FaCADi*, and pBI-*FaPODi*) and transcribed to cDNAs. Expression levels of all samples were monitored by qRT-PCR with specific primers for target genes (*FaPAL*, *FaCHS*, *FaCCR*, *FaCAD*, and *FaPOD*) and the interspacer gene. The latter was used as an internal control for normalization. For each box-plot graph, one of the WT group was used as the reference (set to one) and each group contained five biological replicates. The Wilcoxon-Mann-Whitney *U*-test was used for non-parametric comparison of two groups from pBI-intron and fruits infiltrated with different constructs. Values indicate statistically decreased levels (P <0.05) and are shown in the box. (All statistical data are shown in Appendix E.2.1)

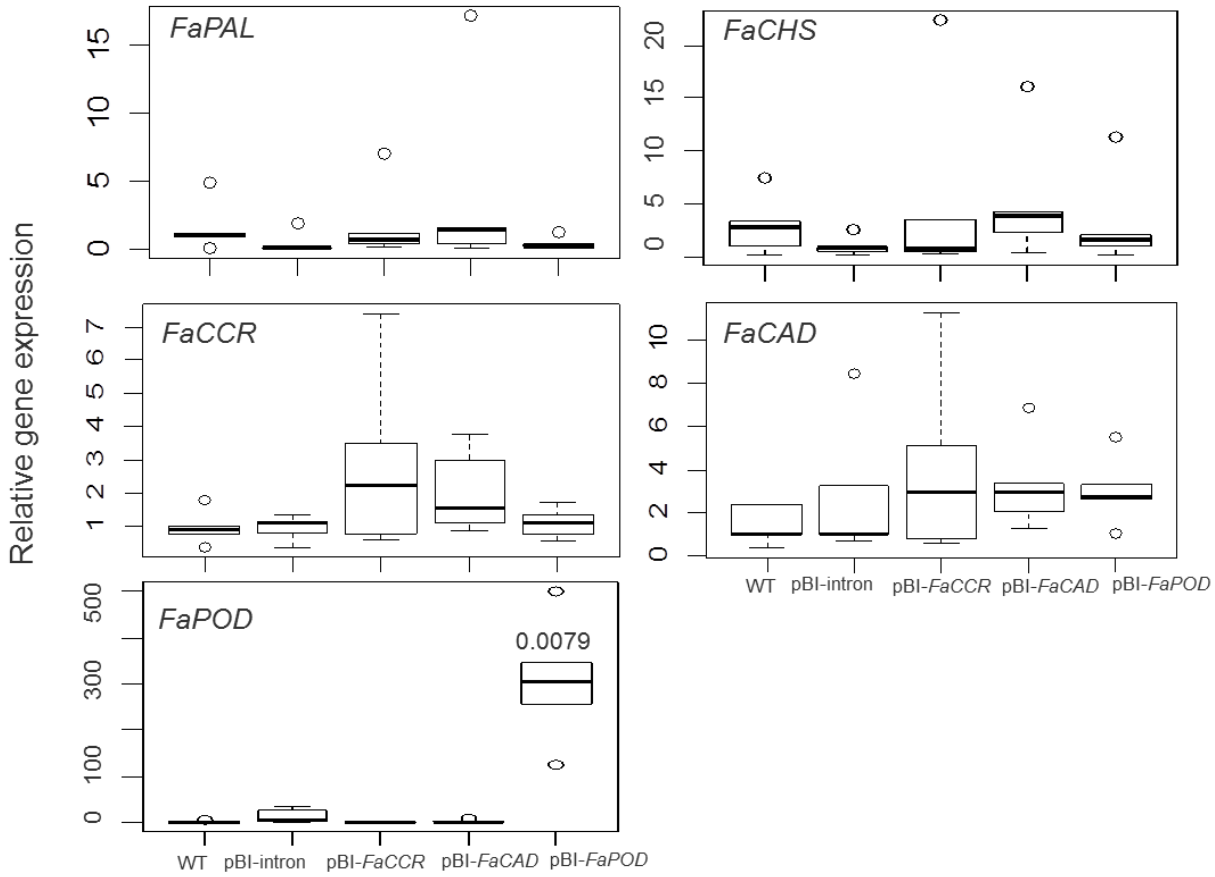

Figure 43. Relative expression profiles of up-regulated monolignol biosynthesis genes in *F. x ananassa* cv. Elsanta.

Total RNA was isolated from single WT (wild type) fruits, agroinfiltrated fruits with a non-ihpRNA construct (pBI-intron) or with individual overexpression constructs (pBI-*FaCCR*, pBI-*FaCAD*, and pBI-*FaPOD*) and transcribed to cDNAs. Expression levels of all samples were monitored by qRT-PCR with specific primers for target genes (*FaPAL*, *FaCHS*, *FaCCR*, *FaCAD*, and *FaPOD*) and the interspacer gene. The latter was used as an internal control for normalization. For each box-plot graph, one of the WT group was used as the reference (set to one) and each group contained five biological replicates. The Wilcoxon-Mann-Whitney *U*-test was used for non-parametric comparison of two groups from pBI-intron and fruits infiltrated with different constructs. Value indicates statistically increased level (P <0.05) and is shown in the box. (All statistical data are shown in Appendix E.2.2)

5.3.5 Activity assay

To assess the enzyme activity in *FaCCR*- and *FaCAD*-downregulated and upregulated fruits, crude protein was extracted from the fruits. The measurement of FaCCR and FaCAD activity was carried out using LC-UV-ESI-MS^n.

To determine FaCCR activity, coniferaldehyde formed from feruloyl-CoA was quantified by LC-UV-ESI-MS^n (Figure 44A). FaCCR activity was significantly decreased (P<0.02) in the pBI-*FaCCRi* fruits compared to WT (untreated) fruits. However, FaCCR activity also

decreased in pBI-intron control fruits as compared to WT. When *FaCCR* was up- or down-regulated in the fruits, FaCCR activity was not significantly different in the pBI-*FaCCR* and pBI-*FaCCRi* fruits as compared to pBI-intron control fruits (Figures 44, B and C).

To determine FaCAD activity, coniferyl alcohol produced from coniferaldehyde was quantified by LC-UV-ESI-MS^n (Figure 45A). When *FaCAD* was up- or down-regulated in the fruits, FaCAD activity was not reduced in the pBI-*FaCAD* fruits, but significantly decreased (P<0.02) in the pBI-*FaCADi* fruits as compared to either WT or pBI-intron control fruits (Figures 45, B and C).

FaCCR and FaCAD activity was also reduced in pBI-*FaCCR* and pBI-*FaCAD* fruits (Figures 44-45, B and C), respectively. Co-suppression of homologous genes can, at least in parts, explain this observation. As expected, FaCCR and FaCAD activity significantly decreased (P<0.02) in the pBI-*FaCCRi* and pBI-*FaCADi* fruits (Figures 44-45, B and C), respectively. We assume that dsRNA produced by pBI-*FaCCRi* and pBI-*FaCADi* can trigger PTGS to interfere with homologous *FaCCR* and *FaCAD* expression. Finally, the degradation of mRNA results in inhibition of FaCCR and FaCAD synthesis.

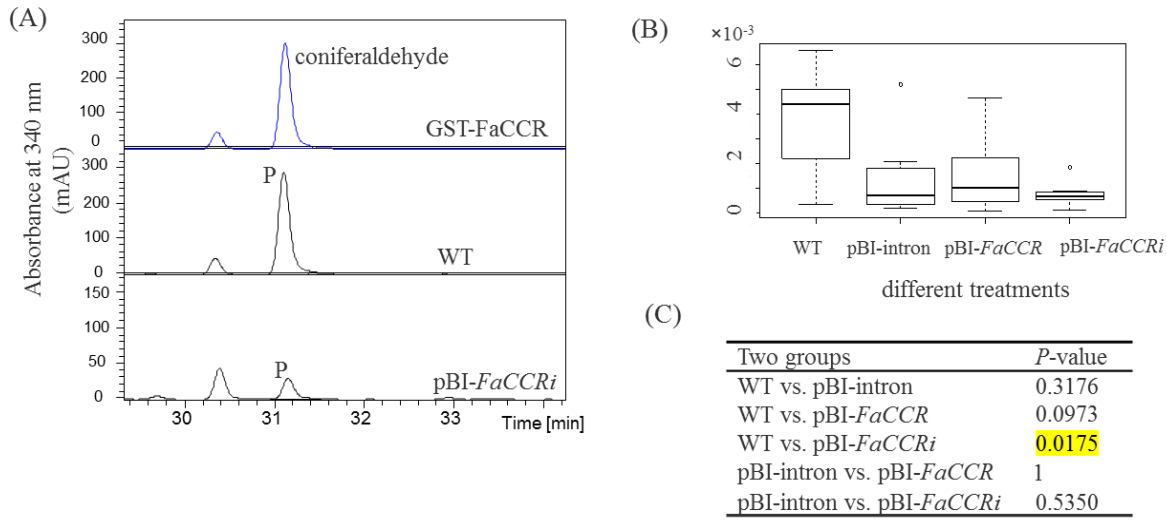

(C)

Two groups	*P*-value
WT vs. pBI-intron	0.3176
WT vs. pBI-*FaCCR*	0.0973
WT vs. pBI-*FaCCRi*	0.0175
pBI-intron vs. pBI-*FaCCR*	1
pBI-intron vs. pBI-*FaCCRi*	0.5350

Figure 44. CCR specific activity in wild-type and agroinfiltrated fruits.
Enzyme activity was measured 14 days after infiltration. (A) Coniferaldehyde (P; products) formed in the reaction was quantified at 340 nm. (B) The Box plots show data from different treatments with biological replicates (n=7). Wild type (WT), fruits infiltrated with an *Agrobacterium* suspension containing a non-ihpRNA (pBI-intron), *FaCCR*-overexpression (pBI-*FaCCR*) and *FaCCR*-ihpRNA construct (pBI-*FaCCRi*). (C) The Wilcoxon-Mann-Whitney *U*-test was used for non-parametric comparison of two groups. Values showing statistically significant decreased levels (P<0.02) are marked with a yellow background.

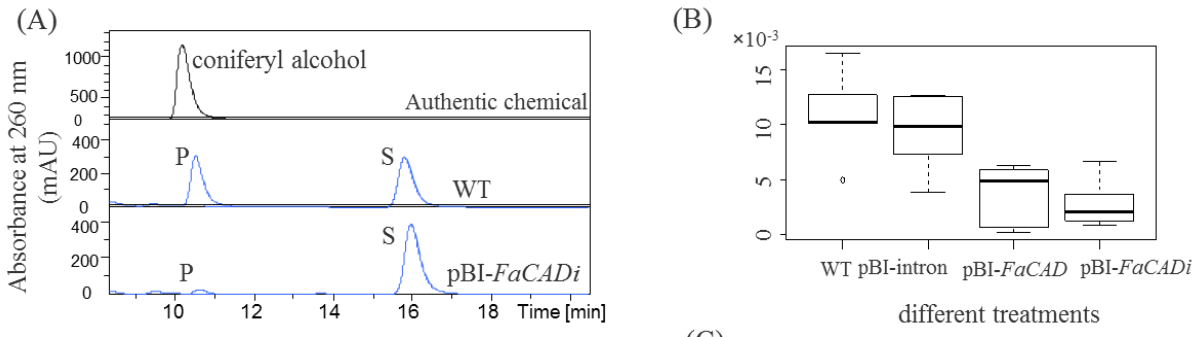

(C)

Two groups	*P*-value
WT vs. pBI-intron	0.9372
WT vs. pBI-*FaCAD*	0.0931
WT vs. pBI-*FaCADi*	0.0087
pBI-intron vs. pBI-*FaCAD*	0.0260
pBI-intron vs. pBI-*FaCADi*	0.0043

Figure 45. CAD specific activity in wild-type and agroinfiltrated fruits.
Enzyme activity was measured 14 days after infiltration. (A) Coniferyl alcohol formed in the reactions (P=coniferyl alcohol; S=coniferaldehyde) was quantified at 260 nm. (B) The Box plots show data from different treatments with biological replicates (*n*=6). Wild type (WT), fruits infiltrated with *Agrobacterium* suspensions containing a non-ihpRNA (pBI-intron), *FaCAD*-overexpression (pBI-*FaCAD*), and *FaCAD*-ihpRNA (pBI-*FaCAD*i) construct. (C) The Wilcoxon-Mann-Whitney *U*-test was used for non-parametric comparison of two groups. Values showing statistically significant decreased levels ($P<0.02$) are marked with a yellow background.

5.3.6 Metabolite levels

To study metabolite levels in the *FaCCR*-, *FaCAD*-, *FaPOD*-down-regulated, *FaCCR*-, *FaCAD*- and *FaPOD*-up-regulated fruits, lyophilized samples were extracted with methanol and analyzed by LC-UV-ESI-MS^n. Major compounds (phenolic acid derivatives, flavonols, anthocyanins, and proanthocyanidins) were quantified.

In general, levels of flavonoids (flavonols, anthocyanins, and proanthocyanidins) were not significantly changed in all treated (pBI-*FaCCRi*, pBI-*FaCADi*, pBI-*FaPODi*, pBI-*FaCCR*, pBI-*FaCAD*, and pBI-*FaPOD*) fruits compared with either WT (untreated) fruits or pBI-intron control fruits, except for pBI-*FaCCR* and pBI-*FaPOD* fruits. Levels of (epi)catechin-(epi)catechin (isomer1) and (epi)afzelechin-(epi)catechin (isomer 1) increased in pBI-*FaCCR* fruits as compared with WT (untreated) fruit. In addition to comparison with the pBI-intron control fruit, levels of kaempferol glucoside increased in both pBI-*FaCCR* and pBI-*FaPOD* fruits, as well as the level of pelargonidin-3-glucoside increased in pBI-*FaCCR* fruits. Besides, the most significant changes were observed for phenolic acid

derivatives (*p*-coumaroyl glucoside/glucose, caffeoyl glucose, and feruloyl glucose) in all treated fruits (Appendix E.3.1-3.4).

Although *p*-hydroxybenzoyl glucose and cinnamoyl glucose displayed the same level in all fruits a significantly reduced level of *p*-coumaroyl glucoside/glucose, as well as increased levels of caffeoyl glucose and feruloyl glucose (*P*<1.00E-02) were observed in all *FaCCR*-, *FaCAD*-, *FaPOD*-down-regulated (Figure 46A), and *FaCCR*- *FaCAD*-, and *FaPOD*-up-regulated fruits (Figure 46B) as compared with WT (untreated) fruits. In addition to comparison to the pBI-intron control fruits, a significantly reduced level of *p*-coumaroyl glucoside/glucose as well as an increased level of feruloyl glucose was detected in the pBI-*FaCCRi* fruits (*P*<1.00E-02), shown as plus sign in Figure 46A. These results suggest that increased levels of caffeic acid and ferulic acid are formed in all treated fruits due to agroinfiltration. These metabolites might serve as lignin precursors, which are polymerized by *FaPOD27* to form lignin in the *Agrobacterium*-infection fruits.

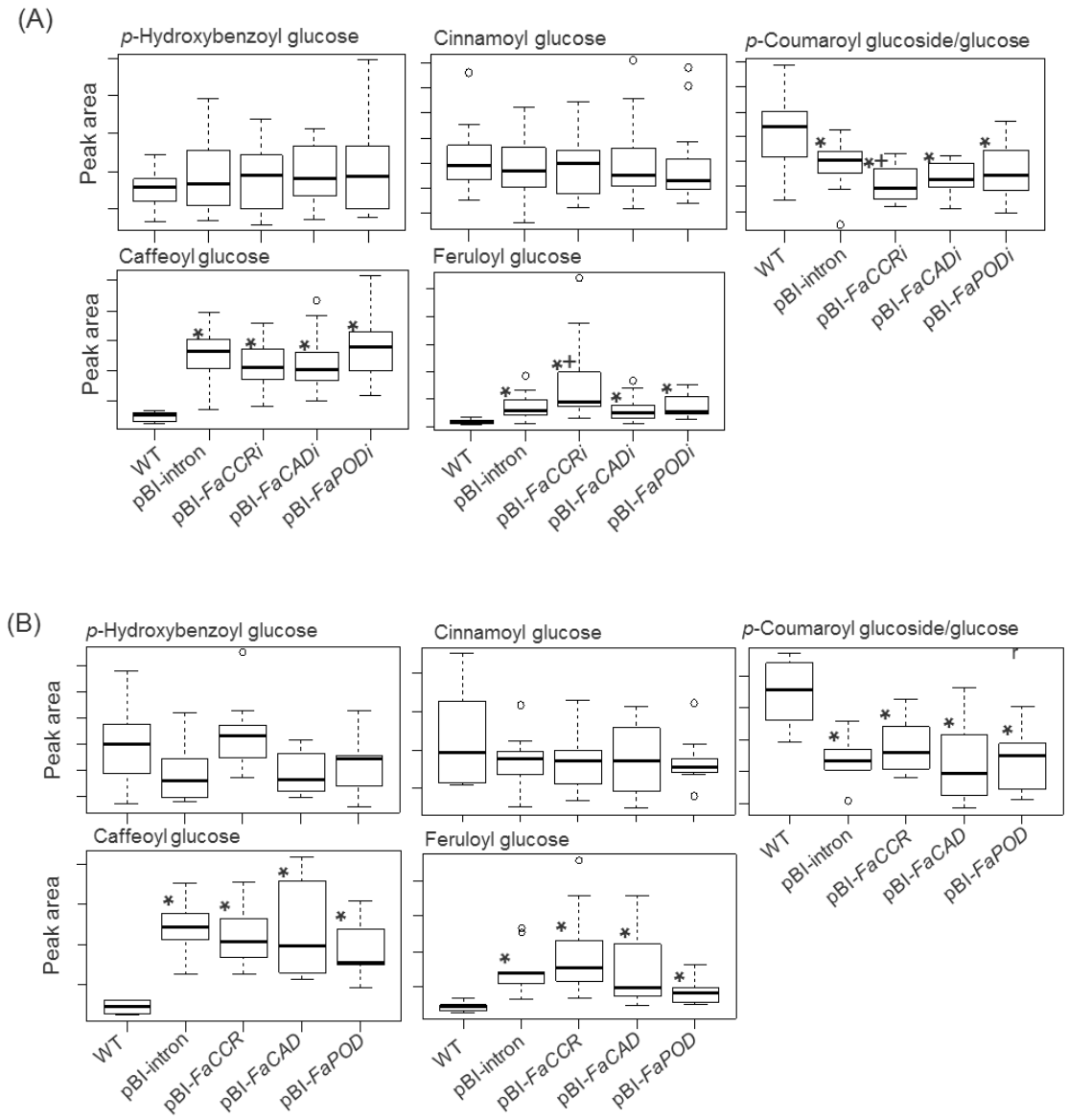

Figure 46. Metabolite levels in *FaCCR*-, *FaCAD*-, *FaPOD*-downregulated and -upregulated *F. x ananassa* cv. Elsanta fruits.

Metabolite levels were measured by LC-UV-ESI-MS^n. Each box plot shows data from different groups with the following biological replicates: (A) WT (wild type; *n*=13), fruits agroinfiltrated with a non-ihpRNA construct (pBI-intron; *n*=20), and ihpRNA-mediated gene silencing constructs (pBI-*FaCCRi*; *n*=22, pBI-*FaCADi*; *n*=23, pBI-*FaPODi*; *n*=20). (B) WT (*n*=10), pBI-intron (*n*=10) and overexpression constructs (pBI-*FaCCR*; *n*=10, pBI-*FaCAD*; *n*=10, pBI-*FaPOD*; *n*=9). Identities of the compounds were confirmed as described in methods (Table 23). Wilcoxon-Mann-Whitney *U*-test was used for non-parametric comparison of two groups. One asterisk (*) or a plus (+) in the box marks statistically significant decreased or increased levels (P<1.00E-02) in comparison with WT and another group (indicated by *) or in comparison with pBI-intron and another group (indicated by +) (Appendix E.3.1-3.4).

5.3.7 Thioacidolysis reaction and lignin composition

To determine lignin composition and estimate proportions of lignin monomers, lignin was extracted from pooled fruits of each treatment and was subjected to thioacidolysis. Thioacidolysis was performed as described by Robinson and Mansfield (2009). Etherified *p*-hydroxyphenyl (H), guaiacyl (G), syringyl (S) monomers and other lignin-derived components were detected by GC-MS under the conditions described in methods (II.2.3).

GC-MS analysis of trimethylsilylated extracts from treated fruits showed compounds with major ions at *m*/*z* 239, 266, 299, and 57 that eluted at retention times of 27.5, 29, 30.4, and 23.3 min. They correspond to H-, G-, S- monomers that were liberated by thioacidolysis and to the internal standard docosane (I.S.) (Figure 47A). The MS spectra showed the typical fragmentation pattern of the monomeric products formed from H-, G-, and S-lignin, and I.S (Figure 47B). Identity was confirmed by comparison with published data (Ralph et al., 2008; Palmer et al., 2008). Quantitative evaluation of etherified H-, G-, and S- monomers was performed on major ion chromatograms for the different treatments. Etherified H-, G-, and S- monomers were calculated based on the peak area of prominent ions related to that of the internal standards docosane for normalization.

H-, G-, and S-monomers were not detected in extracts from WT (untreated) fruits due to the low yield of lignin produced in these fruits. In contrast, H-, G-, and S-monomers were detected in all treated fruits, because higher levels of lignin were accumulated in the fruits exposed to *Agrobacterium.* Low amounts of H-monomers were detected in all treated fruits (Table 26). In comparison to the pBI-intron control treatment, *FaCAD*-silenced fruits showed a significant reduction of 58% in H-monomers. Levels of G-monomers were significantly reduced by 35%, 33%, and 32 % in the pBI-*FaCCRi*, pBI-*FaCADi*, and pBI-*FaPOD* fruits, respectively. Levels of S-monomers were significantly reduced by 22% and 13% in pBI-*FaCADi* and pBI-*FaPOD* fruits, respectively. However, amount of S-monomers was significantly elevated by 18 % in the pBI-*FaCCR* fruits. Remarkably, levels of both G- and S-monomers were significantly reduced in the pBI-*FaCADi* and pBI-*FaPOD* fruits.

In addition, *FaCCR*-down-regulated, *FaCAD*- and *FaPOD*-up-regulated fruits showed a significant increase in the S/G ratio of lignin, as compared to the pBI-intron treatment. *FaCCR*-silenced fruits had the highest increase in the S/G ratio (1.36±0.12) of lignin, as compared to all treatments (Table 26).

5.3.8 Detection of ferulic acid in treated fruits following thioacidolysis

To synthesize a ferulic acid-derived marker (Ralph et al., 2008), 4 mM of ferulic acid and 4 mM of H_2O_2 were incubated with 3960 unit of horseradish peroxidase (HRP, type VI-A,

1,280 unit/mg, Sigma). The procedure is described in methods II.3.7. After 30 min, the reaction mixture was lyophilized. The powder was dissolved in distilled dioxan and subjected to thioacidolysis (II.3.8.4.8.3). As a result, compound A1´G (ferulic acid+EtSH) and AG (ferulic acid) (Figures 48A-B) were detected by GC-MS analysis under the conditions as described in methods (II.2.3). However A1´G (ferulic acid+EtSH) and AG (ferulic acid) were not detected by GC-MS in extracts from treated fruits. A new, unknown compound was detected in pBI-*FaCCRi* fruits (Figure 48A).

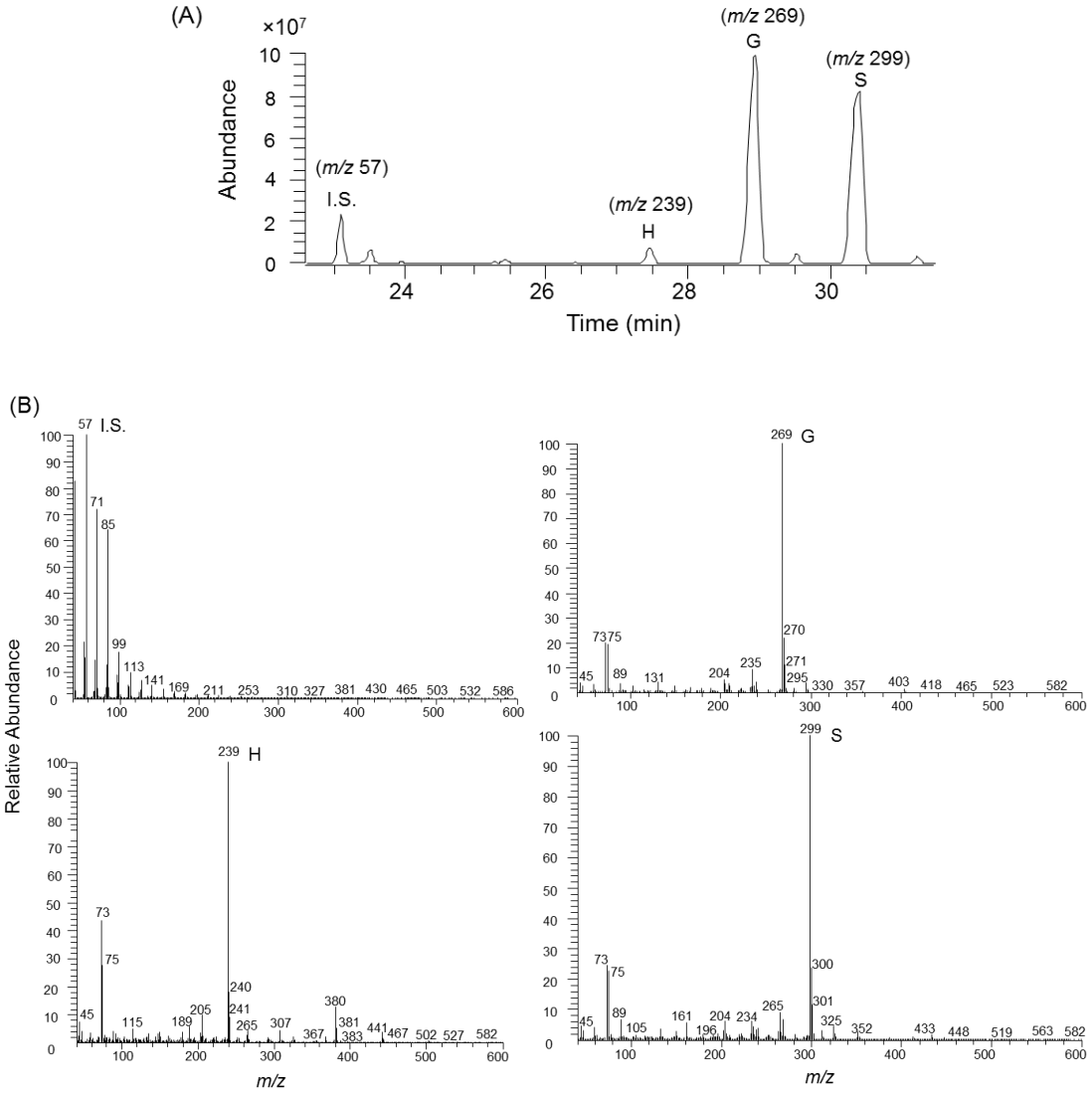

Figure 47. Trimethylsilylated thioacidolysis products from strawberry fruits infiltrated with different constructs detected by GC-MS analysis. (A) The ion chromatogram shows major monomeric products formed from H-, G-, and S-lignin, and the internal standard (I.S.). (B) Fragmentation pattern of the monomeric products and the internal standard. *m/z* = mass-to-charge ratio.

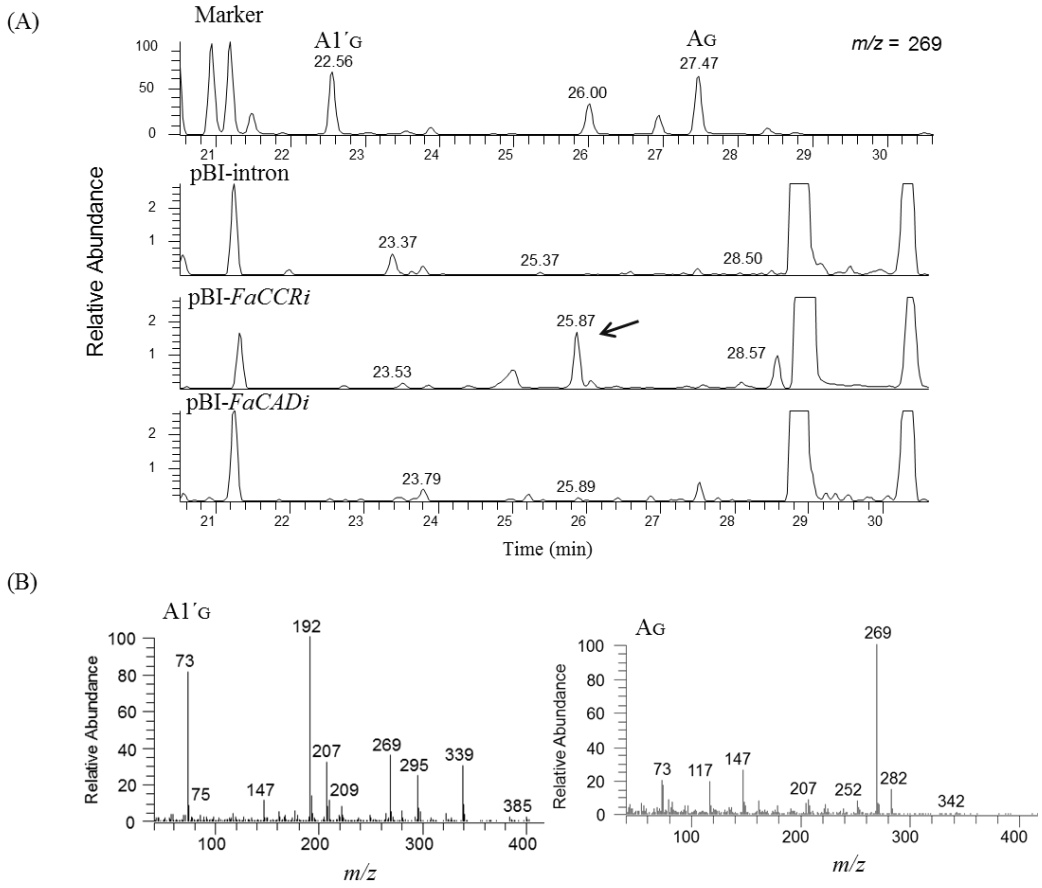

Figure 48. Thioacidolysis products formed from O-4-linked ferulic acid and differently treated strawberry fruits. (A) The ion chromatograms at *m/z* 269 show the ferulic acid markers A1´G (ferulic acid+EtSH) and AG (ferulic acid) at retention times 22.56 and 27.47 min, respectively and compounds obtained from pBI-intron, pBI-*FaCCRi*, and pBI-*FaCADi* treated fruit. (B) The identity of A1´G (ferulic acid+EtSH) and AG (ferulic acid) was confirmed by comparison of their mass spectra with published data (Ralph et al., 2008). The arrow indicates a new compound from pBI-*FaCCRi* treatment. *m/z* = mass-to-charge ratio.

Table 26. Impact of different constructs on lignin monomer composition

	Relative concentration (%, ML)			
	Proportion of thioacidolysis monomers			
	H	G	S	S/G ratio
WT	ND	ND	ND	ND
pBI-intron	0.19±0.04	3.83±0.05	3.65±0.11	0.95±0.04
pBI-*FaCCRi*	0.14±0.09	2.50±0.37*	3.38±0.21	1.36±0.12*
pBI-*FaCADi*	0.08±0.02*	2.55±0.08*	2.85±0.17*	1.12±0.10
pBI-*FaPODi*	0.13±0.02	3.93±0.01	4.09±0.27	1.04±0.07
pBI-*FaCCR*	0.17±0.03	4.02±0.22	4.29±0.03*	1.07±0.05
pBI-*FaCAD*	0.16± 0.02	3.41±0.23	4.17±0.44	1.22±0.05*
pBI-*FaPOD*	0.10±0.04	2.62±0.01*	3.19±0.03*	1.22±0.02*

For each treatment, fruits (120±20 g) were pooled to extract lignin. The lignin composition was determined as described in Figure 47. Values are the means ±SEM of duplicates of two independent analyses from the pooled lignin. ML: monomeric lignin. ND: not detected. One asterisk (*) indicates significant differences by Student *t*-test ($P<0.01$) in comparison with pBI-intron and another treatment (Appendix E.4.).

5.4 Down- and up-regulation of lignin biosynthetic genes in transgenic antisense *CHS* Calypso lines

5.4.1 Phenotype

The metabolite *p*-coumaroyl-CoA is situated at the branching point of the metabolic routes leading to either flavonoid or monolignol biosynthetic pathways. It is the common substrate for CHS, HCT, and CCR enzymes in the phenylpropanoid metabolism. Silencing of the *CHS* gene in fruits could provide more precursors (*p*-coumaroyl-CoA) for the synthesis of H-, G-, and S-lignin.

In this study, strawberry Calypso (CHS^-) fruits harboring an antisense *CHS* gene were used for infiltration by *Agrobacterium*. Calypso (CHS^-) fruits were agroinfiltrated with individual constructs (pBI-intron, pBI-*FaCCRi*, pBI-*FaCADi*, pBI-*FaPODi*, pBI-*FaCCR*, pBI-*FaCAD*, and pBI-*FaPOD*; Figures 39A-C). In addition, an *Agrobacterium* mixture was generated from *Agrobacterium* suspensions with three different constructs (Figures 39B or C) for downregulation (pBI-Si3) and upregulation (pBI-O3) of lignin biosynthetic genes in the CHS^- fruits. The preparation is described in methods (II.3.8.4).

Calypso wild type fruits (CHS^+) turned red during ripening because of the abundance of anthocyanins that accumulated during the ripe stage (Figures 49, a-b). Not surprisingly, Calypso (CHS^-) formed pink colored fruits during the ripe stage due to the silencing of the

CHS gene in the fruit leading to a lower amount of anthocyanins (Figures 49, c-d). To observe changes in textures and colors of the fruits, CHS^- fruits (Figures 49, c-d) were compared with CHS^- fruits injected with different constructs (Figures 39A-C) (Figures 49, e-h). As shown in Figure 49, fruits injected with different constructs remained white or slightly red in color and were different in appearance from the CHS^- (untreated) fruit. Comparison of the cross sections of non-infiltrated fruits (Figure 49b) with injected fruits confirmed the lack of anthocyanin accumulation in the ripe fruits (Figures 49, f and h). The results indicate that white or slightly red fruits contain the antisense *CHS* gene that leads to lower levels of anthocyanins in treated fruits. In general, textures of the fruits injected with different constructs (Figures 49 e-h) were firmer than those of non-infiltrated Calypso (CHS^-) fruits (Figures 49 c-d).

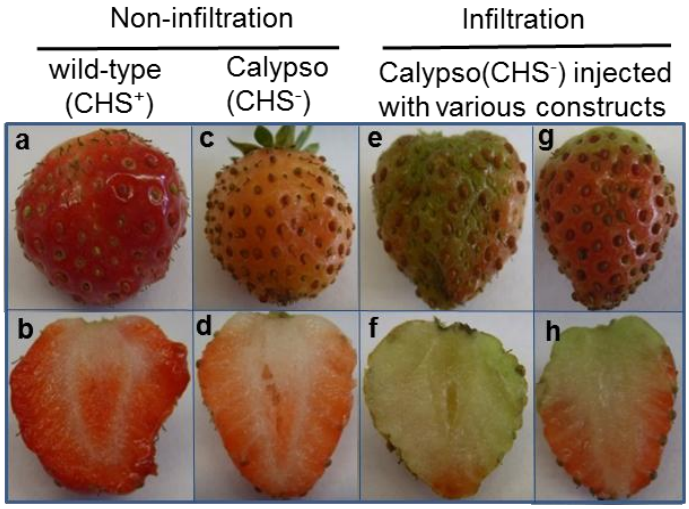

Figure 49. Comparison of non-infiltrated and infiltrated Calypso (CHS-) fruits.
All pictures were taken 14 days after infiltration. Phenotypes of non-infiltrated (a-d) and infiltrated fruits (e-h) are compared. Non-infiltrated fruits of Calypso with CHS genes (CHS^+; a, b) and Calypso with impaired CHS genes (CHS^-; c, d) are shown. Infiltrated fruits (e-h) represent Calypso fruit (CHS^-) injected with *Agrobacterium* suspensions harboring pBI-intron, *FaCCR*-, *FaCAD*-, *FaPOD*-ihpRNA, *FaCCR*-, *FaCAD*-, *FaPOD*-overexpression constructs, or combined pBI-Si3 and pBI-O3 constructs.

5.4.2 Lignin texture and lignin content

To investigate the effect of monolignol biosynthesis genes on texture and lignin content in CHS^- fruits, CHS^- fruits were agroinfiltrated with up- and downregulation constructs of lignin genes (Figures 39A-C). Comparison of CHS^- (untreated fruit) and treated CHS^- fruits (injected with pBI-intron, pBI-*FaCCRi*, pBI-*FaCADi*, pBI-*FaPODi*, pBI-Si3, pBI-*FaCCR*, pBI-*FaCAD*, pBI-*FaPOD*, and pBI-O3) displayed a significant increase in firmness (*P*

<5.00E-02) in all agroinfiltrated fruits, as shown by one asterisk in Figures 50A and B. In addition, comparison of CHS$^-$/pBI-intron control fruits and treated CHS$^-$ fruits (injected with pBI-*FaCCRi*, pBI-*FaCADi*, pBI-*FaPODi*, pBI-Si3, pBI-*FaCCR*, pBI-*FaCAD*, pBI-*FaPOD*, or pBI-O3) showed a significant increase in firmness (P<5.00E-02) in down-regulated and up-regulated fruits, as shown with a plus sign in Figures 50A and B. The increase in firmness was associated with increased lignin content in the down-regulated and up-regulated fruits (Figures 50C and D). The comparison of either CHS$^-$ (untreated fruit) or CHS$^-$/pBI-intron control fruits with other treated fruits (CHS$^-$ fruits agroinfiltrated with individual or combined down-regulation and up-regulation constructs), showed that fruit firmness and lignin content increased due to these treatments (CHS$^-$/pBI-*FaCCRi*, CHS$^-$/pBI-*FaCADi*, CHS$^-$/pBI-*FaPODi*, CHS$^-$/pBI-Si3, CHS$^-$/pBI-*FaCCR*, CHS$^-$/pBI-*FaCAD*, CHS$^-$/pBI-*FaPOD*, or CHS$^-$/pBI-O3 fruits).

5.4.3 Gene expression levels

To assess the expression of phenylpropanoid biosynthesis genes in CHS$^-$ fruits with *FaCCR*-, *FaCAD*-, *FaPOD*-down-regulated, *FaCCR*-, *FaCAD*-, *FaPOD*-up-regulated, pBI-Si3, and pBI-O3 constructs, total RNA was isolated from single fruits of each treatment and transcribed to cDNAs. Expression levels of *FaPAL*, *FaCHS*, *FaCCR*, *FaCAD*, and *FaPOD* were monitored by qRT-PCR.

When *FaCCR*, *FaCAD*, *FaPOD*, and all three genes (pBI-Si3), were down-regulated in the CHS$^-$ fruits, expression levels of both *FaPAL* and *FaCHS* were not significantly different in the treated fruits, as compared to CHS$^-$/pBI-intron control fruits, except for CHS$^-$/pBI-*FaCADi*. *FaPAL* transcripts decreased significantly in the CHS$^-$/pBI-*FaCADi* fruits. However, in comparison with CHS$^-$/pBI-intron control fruits, *FaCCR* transcript levels significantly decreased (P<0.02) in CHS$^-$/pBI-*FaCCRi* fruits, but were not significantly changed in other treated fruits. *FaCAD* transcript levels significantly decreased (P<0.02) in CHS$^-$/pBI-*FaCADi* fruits, but were not significantly changed in other treated fruits (Figure 51). *FaPOD* transcripts exhibited the same low level in all treated fruits. *FaPOD* transcripts showed already very low levels in mature fruit (Figure 33B) which probably hampers further downregulation.

When *FaCCR*, *FaCAD*, *FaPOD*, and all three genes (pBI-O3) were up-regulated in CHS$^-$ fruits, expression levels of *FaPAL*, *FaCHS*, *FaCCR*, and *FaCAD* were not significantly changed in treated fruits (CHS$^-$, CHS$^-$/pBI-*FaCCR*, CHS$^-$/pBI-*FaCAD*, CHS$^-$/pBI-*FaPOD*, and CHS$^-$/pBI-O3) as compared to CHS$^-$/pBI-intron control fruits. Interestingly, *FaPOD*

transcripts significantly increased (P<0.02) in CHS$^-$/pBI-*FaPOD* and CHS$^-$/pBI-O3 fruits. Expression levels of *FaPOD* were not significantly changed in other treated fruits (CHS$^-$/pBI-intron, CHS$^-$/pBI-*FaCCR*, and CHS$^-$/pBI-*FaCAD* fruits) (Figure 52).

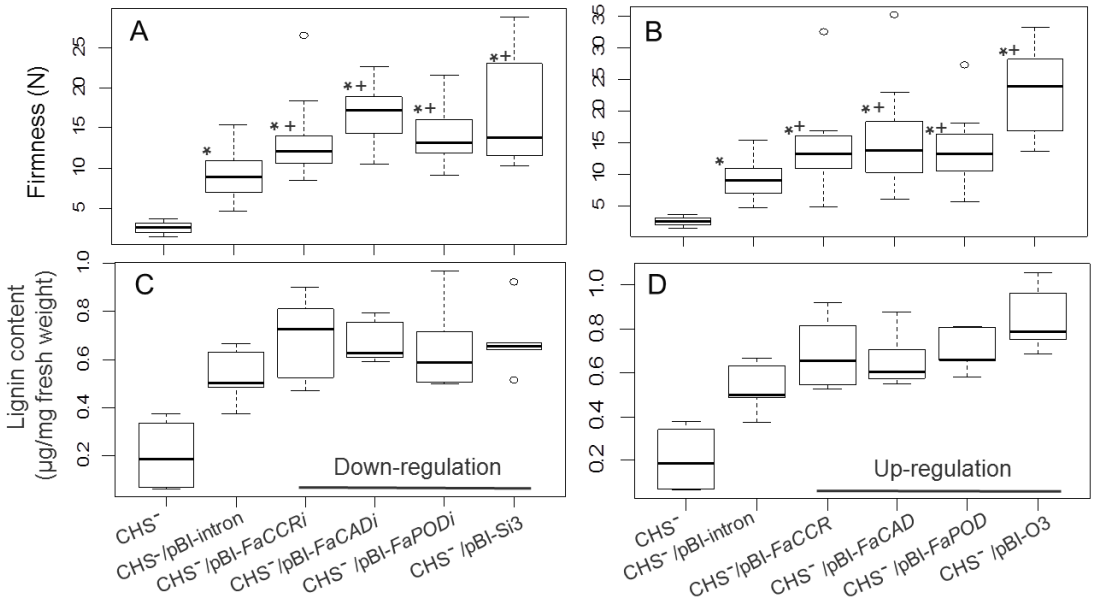

Figure 50. Fruit firmness (A, B) and lignin content (C, D) of *FaCCR*-, *FaCAD*-, *FaPOD*-downregulation and -upregulation as well as combinations in *F. x ananassa* cv. Calypso (CHS$^-$).

Fruit firmness and lignin content were measured 14 days after infiltration. Box plots of texture and lignin content include data from different groups with the following biological replicates: (A) Firmness of Calypso (CHS$^-$; n=15), Calypso (CHS$^-$) with a non-ihpRNA construct (pBI-intron; n=17), individual ihpRNA-mediated gene silencing constructs (pBI-*FaCCRi*; n =14, pBI-*FaCADi*; n=14, pBI-*FaPODi*; n=17), and combination of pBI-*FaCCRi*, pBI-*FaCADi*, and pBI-*FaPODi* (pBI-Si3; n=15). (B) Firmness of Calypso (CHS$^-$, n=15), pBI-intron (n=17), individual overexpression constructs (pBI-*FaCCR*; n=14, pBI-*FaCAD*; n=17, pBI-*FaPOD*; n=15), and combination of pBI-*FaCCR*, pBI-*FaCAD*, and pBI-*FaPOD* (pBI-O3; n=18). (C, D) Lignin content of each group (n=5). The Wilcoxon-Mann-Whitney U-test was used for non-parametric analysis of two groups. One asterisk (*) or a plus (+) in the box marks statistically significant increased levels (P<5.00E-02) in comparison with CHS$^-$ and another group (indicated by*) or in comparison with CHS$^-$/pBI-intron and another group (indicated by+) (Appendix E.1.2).

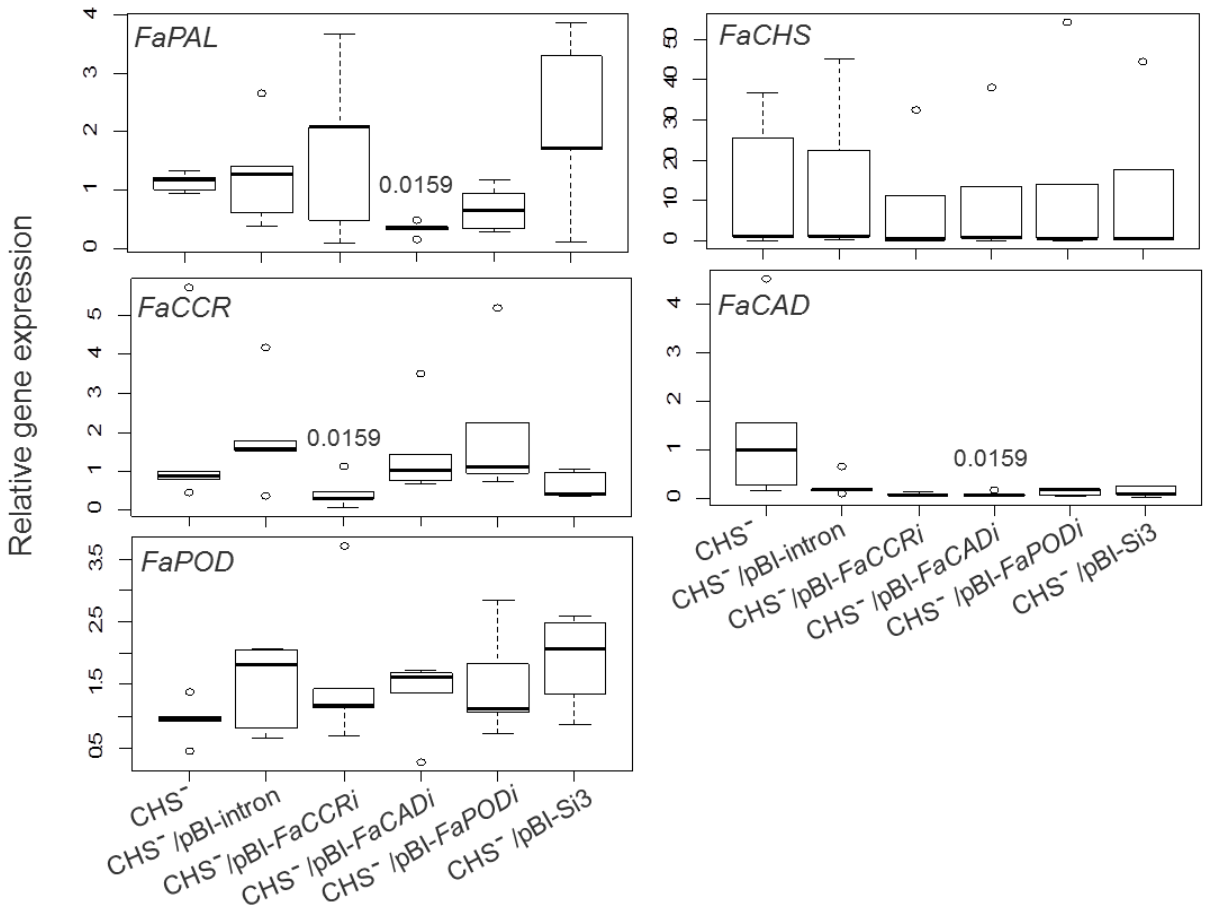

Figure 51. Relative expression profiles of individual *FaCCR*-, *FaCAD*-, *FaPOD*-downregulation, and combinations in *F. x ananassa* cv. Calypso (CHS⁻).

Total RNA was isolated from single Calypso (CHS⁻) fruits, Calypso (CHS⁻) with a non-ihpRNA construct (pBI-intron), individual ihpRNA-mediated gene silencing constructs (pBI-*FaCCRi*, pBI-*FaCADi*, and pBI-*FaPODi*), and combined pBI-*FaCCRi*, pBI-*FaCADi*, and pBI-*FaPODi* constructs (pBI-Si3). Expression levels of all samples were monitored by qRT-PCR with specific primers for target genes (*FaPAL*, *FaCHS*, *FaCCR*, *FaCAD*, and *FaPOD*) and the interspacer gene. The latter was used as an internal control for normalization. For each box-plot graph, one of the CHS⁻ groups was used as the reference (set to one) and each group had five biological replicates. The Wilcoxon-Mann-Whitney *U*-test was used for non-parametric comparison of two groups from CHS⁻/pBI-intron and another group. Values indicate statistically significant reduced levels (P <0.02) and are shown in the box. (All statistical data are shown in Appendix E.2.3)

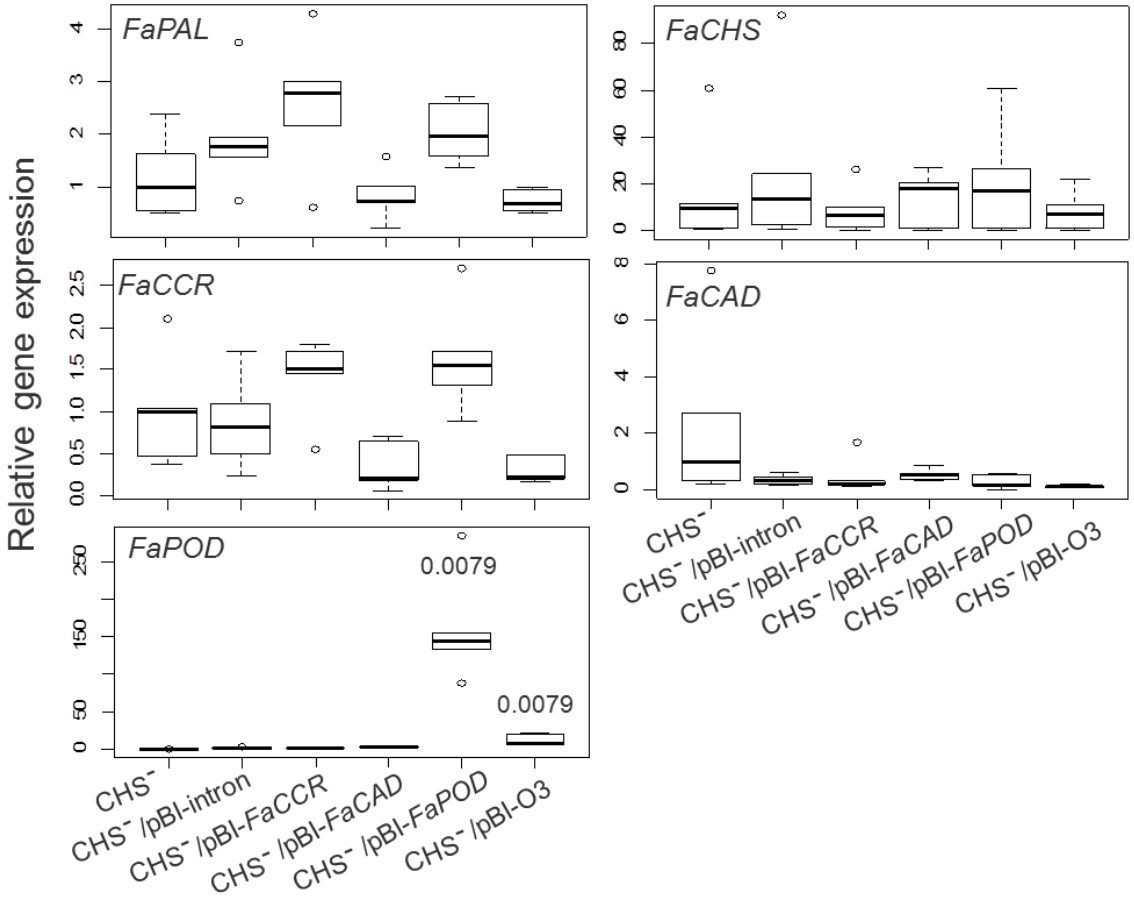

Figure 52. Relative expression profiles of individual *FaCCR*-, *FaCAD*-, *FaPOD*-upregulation, and combinations in *F. x ananassa* cv. Calypso (CHS⁻).

Total RNA was isolated from single Calypso (CHS⁻) fruits, Calypso (CHS⁻) with a non-ihpRNA construct (pBI-intron), individual overexpression constructs (pBI-*FaCCR*, pBI-*FaCAD*, and pBI-*FaPOD*), and combined pBI-*FaCCR*, pBI-*FaCAD*, and pBI-*FaPOD* constructs (pBI-O3). Expression levels of all samples were monitored by qRT-PCR with specific primers for target genes (*FaPAL*, *FaCHS*, *FaCCR*, *FaCAD*, and *FaPOD*) and the interspacer gene (IS). The latter was used as an internal control for normalization. For each box-plot graph, one of the CHS⁻ groups was used as the reference (set to one) and each group had five biological replicates. The Wilcoxon-Mann-Whitney *U*-test was used for non-parametric analysis comparison of two groups from CHS⁻/pBI-intron and another group. Values indicate statistically significant increased levels (P <0.02) and are shown in the box. (All statistical data are shown in Appendix E.2.4)

5.4.4 Metabolite levels

To study metabolite levels in *FaCCR*-, *FaCAD*-, *FaPOD*-down-regulated, *FaCCR*-, *FaCAD*-, *FaPOD*-up-regulated, pBI-Si3, and pBI-O3 fruits, lyophilized samples were extracted with methanol and analyzed by LC-UV-ESI-MS^n. In general, levels of flavonoids (flavonols, anthocyanins, and proanthocyanidins) were not significantly different in the treated fruits (CHS$^-$/pBI-*FaCCRi*, CHS$^-$/pBI-*FaCADi*, CHS$^-$/pBI-*FaPODi*, CHS$^-$/pBI-Si3, CHS$^-$/pBI-*FaCCR*, CHS$^-$/pBI-*FaCAD*, CHS$^-$/pBI-*FaPOD*, or CHS$^-$/pBI-O3) as compared with either CHS$^-$ (untreated) fruits or CHS$^-$/pBI-intron (control) fruits. Except for quercetin glucoside, kaempferol glucoside, pelargonidin-3-glucoside, pelargonidin-3-glucoside-malonate and pelargonidin-rutinoside, these compounds significantly decreased in CHS$^-$/pBI-*FaPODi*, CHS$^-$/pBI-*FaCCR*, CHS$^-$/pBI-*FaCAD*, CHS$^-$/pBI-*FaPOD*, and CHS$^-$/pBI-O3 fruits (Appendix E.5.1-5.4). However, the most significantly changed metabolites were phenolic acid derivatives. A comparison of either CHS$^-$ (untreated) or CHS$^-$/pBI-intron (control) fruits with other treated fruits showed major differences in the levels of phenolic acid derivatives (Figures 53A and B). The level of *p*-hydroxybenzoyl glucose significantly decreased (P<1.00E-02) in CHS$^-$ /pBI-*FaCAD*, CHS$^-$/pBI-*FaPOD*, and CHS$^-$/pBI-O3 fruits whereas the amounts of cinnamoyl glucose significantly decreased (P<1.00E-02) in CHS$^-$/pBI-*FaCADi*, CHS$^-$/pBI-*FaCAD*, and CHS$^-$/pBI-O3 fruits. The level of *p*-coumaroyl glucoside/glucose was not significantly affected *(*P<1.00E-02) by these treatments, except for CHS$^-$/pBI-*FaCAD*. The amount of caffeoyl glucose significantly increased (P<1.00E-02) in all treated fruits, expect for CHS$^-$/pBI-*FaCAD* whereas the level of feruloyl glucose (P<1.00E-02) significantly increased (P<1.00E-02) in CHS$^-$/pBI-*FaCCRi*, CHS$^-$/pBI-*FaCADi*, CHS$^-$/pBI-*FaPODi*, CHS$^-$/pBI-Si3, and CHS$^-$/pBI-*FaPOD* fruits.

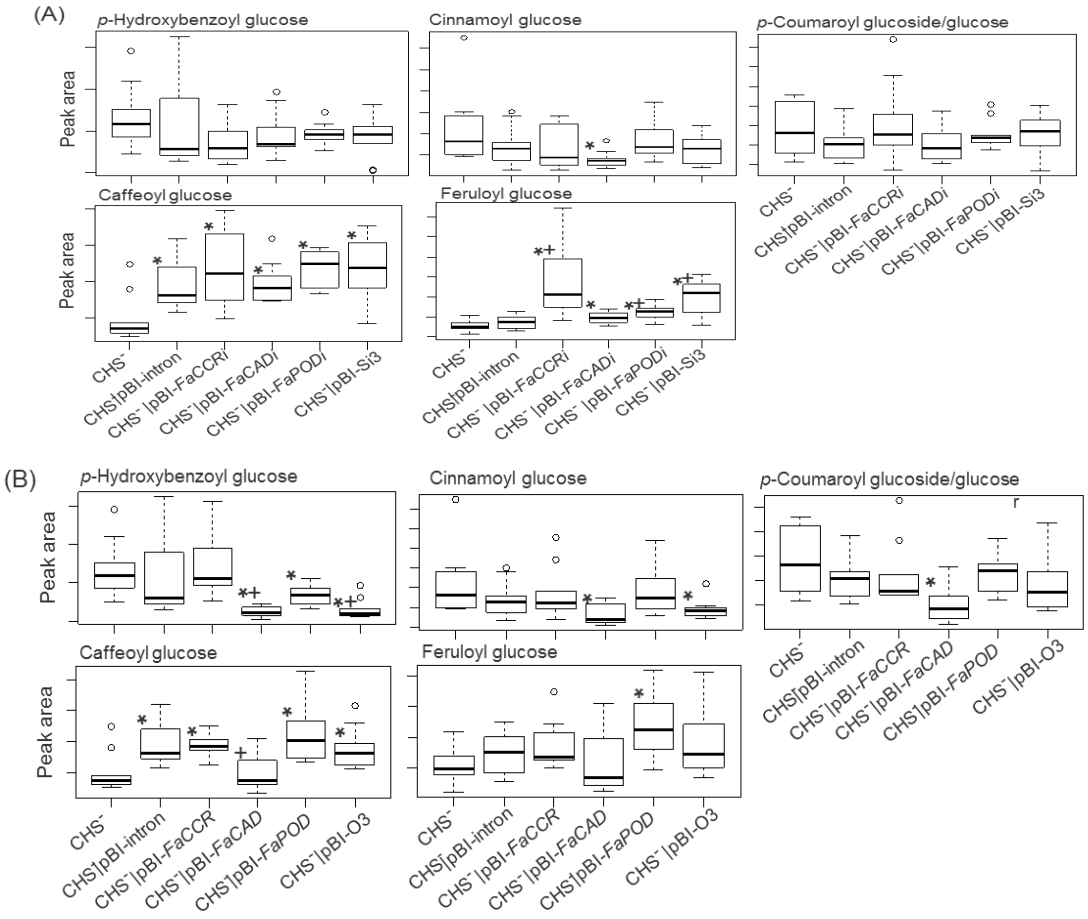

Figure 53. Metabolite levels of individual *FaCCR*-, *FaCAD*-, *FaPOD*-downregulation and-upregulation as well as combinations in *F. x ananassa* cv. Calypso (CHS$^-$).

Metabolite levels were measured by LC-UV-ESI-MS^n. Each box-plot graph shows data from different groups with biological replicates (n=5). All analyses were performed in duplicate. (A) Calypso (CHS$^-$), Calypso (CHS$^-$) with a non-ihpRNA construct (pBI-intron), individual ihpRNA-mediated gene silencing constructs (pBI-*FaCCRi*, pBI-*FaCADi*, and pBI-*FaPODi*), and combined pBI-*FaCCRi*, pBI-*FaCADi*, and pBI-*FaPODi* constructs (pBI-Si3). (B) Calypso (CHS$^-$), Calypso (CHS$^-$) with pBI-intron, individual overexpression constructs (pBI-*FaCCR*, pBI-*FaCAD*, and pBI-*FaPOD*), and combined pBI-*FaCCR*, pBI-*FaCAD*, and pBI-*FaPOD* constructs (pBI-O3). Identities of the compounds were confirmed as described in methods (Table 23). Wilcoxon-Mann-Whitney *U*-test was used for non-parametric comparison of two groups. One asterisk (*) or a plus (+) in the box marks statistically significant decreased or increased levels (P<1.00E-02) in comparison with CHS$^-$ and another group (indicated by*) or in comparison of CHS$^-$/pBI-intron and other group (indicated by+) (Appendix E.5.1-5.4).

IV. Discussion

1. Nucleotide sequences

The cultivated strawberry (*Fragaria* × *ananassa* cv. Elsanta) is an octoploid hybrid that harbors eight sets of chromosomes (2*n*=8*x*=56). As genes often exist in multiple copies, more than 8 different alleles of *FaCCR*, *FaCCAD* and *FaPOD* were found in the *Fragaria* × *ananassa* genome. Allelic differences in gene expression are a common phenomenon in plants. It was reported that among 15 genes from a hybrid maize seedling 11 genes show differential allelic expression (Guo et al., 2004). Pyrosequencing technology is a useful tool for quantification of allele-specific gene expression. For example, pyrosequencing analysis showed that a strawberry *FaPGIP* allele was expressed in leaf tissue whereas two other alleles displayed a fruit-specific expression. The distribution of allele frequency was estimated from RT-PCR products or genomic DNA samples by pyrosequencing analysis which indicated that each tissue and treatment was highly context-specific (Schaart et al., 2005). However, *FaCCR*, *FaCAD*, and *FaPOD* alleles show high identity (90.7-97.8%) at the transcript level as determined by RT-PCR and at genomic DNA level (Table 24). Almost identical regions were observed in partial genome sequences of these three genes. Only a few nucleotides were different (Appendix F). These results indicate that it is difficult to design primers for allelic differentiation of each gene by pyrosequencing analysis. Thus, the high similarity at the nucleotide level limits allelic discrimination of these three genes.

2. Amino acid sequences and biochemical characterization

2.1 FaCCR

A full-length coding sequence of *CCR* was cloned from a strawberry fruit (*F.* × *ananassa*), belonging to *CCR*s (Figure 20). Among the CCR amino acid sequences, they possess identical motifs for the NAD/NADP(H) binding site and the conserved motif (NWYCY) (Figure 21), except for AtCCR-like1-5 (*CCR*-like genes). Thus, all CCR enzymes are proposed to have similar catalyzing mechanisms for converting hydroxycinnamoyl-CoA esters to their corresponding hydroxycinnamaldehydes in the presence of NADPH.

CCRs have been demonstrated to have an important role in lignin biosynthesis (Sarni et al., 1984; Whetten et al., 1998; Tamasloukht et al., 2011). In this study, enzymatic syntheses of hydroxycinnamoyl-CoAs, the potential substrates for purified recombinant GST-CCR, were carried out with purified recombinant His-tagged 4CL from tobacco. *p*-Coumaroyl-CoA, caffeoyl-CoA, and feruloyl-CoA were synthesized by tobacco 4CL. However, the tobacco 4CL enzyme did not produce sinapoyl-CoA *in vitro*. The substrate specificity of the

recombinant His-tagged 4CL is consistent with that of tobacco Nb4CL1 (Rautengarten et al., 2010), as well as *Arabidopsis At*4CL1, *At*4CL2, and *At*4CL3 enzymes (Ehlting et al., 1999). These enzymes did not use sinapic acid as substrate *in vitro*. Unexpectedly, *Arabidopsis At*4CL5 had a good affinity for sinapic acid *in vitro* (Rautengarten et al., 2010). Some authors still question that sinapic acid is activated by 4CL to form sinapoyl-CoA in plants (Boerjan et al., 2003). It seems that plants possess various 4CL isoenzymes, which are responsible for producing different sets of hydroxycinnamoyl-CoAs *in vivo*. The hydroxycinnamoyl-CoA can be subsequently channeled into the lignin branch pathway to serve as substrates for CCRs.

Our *in vitro* results indicate that FaCCR activity is optimal at pH 6.0 in a 100 mM sodium phosphate buffer at 25℃. As reported for several species, CCR activity was observed in a broad pH range. Soybean CCR activity exhibited an optimum pH range at pH 6.0-6.2 in 100-200 mM citrate buffer at 30℃, and was stable at around pH 7.0 (Wengenmayer et al., 1976). Eucalyptus CCR activity was optimal at pH 5.3-6.5 in a potassium/sodium phosphate buffer (Goffner et al., 1994). Besides, its activity was higher in the sodium/potassium buffer, as compared to a citrate buffer with various pH values tested. Similarly, FaCCR activity was two times higher in the sodium phosphate buffer than in the citrate buffer at the same pH 6 (Figure 26A). CCRs exhibited a lower activity at pH 7.5 (Wengenmayer et al. 1976; Goffner et al. 1994; Li et al., 2005), whereas FaCCR was still active at pH 7.5 in the sodium phosphate buffer. However, FaCCR was not activity at pH 5 in the citrate buffer or at pH 9 in the Tris-HCl buffer (Figure 26A). Interestingly, enzymes belonging to a common biosynthetic pathway may have different pH requirements. Aspen CCoAOMT catalysis was optimal at pH 7.5 *in vitro* (Li et al. 1999). However, the activity of CCR at pH 7.5 was lower or negligible. Li et al. (2005) suggested that compartmentalization was probably present to accommodate independent pH environments for proper functioning of CCR and CCoAOMT. Thus, CCR catalysis in a broad pH range may play a role in regulating lignin biosynthesis.

Based on our data from kinetic analysis, the purified FaCCR protein preferred feruloyl-CoA over cinnamoyl-CoA, *p*-coumaroyl-CoA, and caffeoyl-CoA. Also, FaCCR did not have affinity to cinnamoyl-CoA. Aspen PtCCR also displayed the highest affinity with feruloyl-CoA in mixed substrates (Li et al., 2005). This was quite consistent with another angiosperm CCR protein, which can convert feruloyl-CoA with greater efficiency (Lauvergeat et al., 2001; Li et al., 2005). The poor conversion of *p*-coumaroyl-CoA by CCRs may explain the low content of H units in angiosperms (Li et al., 2005). Surprisingly, *Arabidopsis At*CCR1 has high affinity for both feruloyl-CoA and sinapoyl-CoA (Baltas et al., 2005). Indeed, there

are still many questions concerning functional redundancy in the presence of multiple *CCR in vivo*. Lignin biosynthesis is a complex genetic network, in which different routes operate to form G- and S-lignin. In angiosperms, feruloyl-CoA and sinapoyl-CoA would be converted into G and S monomers, respectively, *via* an independent or cross route (Dixon et al., 2001). Eventually, heterologous G-S lignin is formed in angiosperms.

2.2 FaCAD

The phylogenetic analysis indicated that FaCAD (*F.* × *ananassa* cv. Elsanta) belongs to group II CADs (Figure 22). The multiple sequence alignment showed that FaCAD exhibits characteristics of the zinc-containing SAD/CAD enzymes (Figure 23). As reported for different species, the PtSAD and Fxacad1 enzymes used sinapyl aldehydes as the most preferred substrate, and coniferyl aldehydes as the second preferred substrate (Li et al., 2001; Blanco-Portales et al., 2002). The FaCAD and Fxacad1 (*F.* × *ananassa* cv. Chandler) proteins share 98.1% amino acid identity. This comparison provided useful information on the biochemical properties of the FaCAD in this work.

A full-length coding sequence of *CAD* was cloned from a strawberry fruit (*F.* × *ananassa*) and was expressed in *E. coli*. Some studies have shown that overexpressed recombinant proteins accumulated in form of insoluble aggregates in *E. coli* (Waugh, 2005). Thus, the bacterial cells were cooled to 15°C before IPTG was added to reduce the accumulation of target protein in inclusion bodies (Somssich et al., 1996; Blanco-Portales et al., 2002). In this study, even though the IPTG concentration (0.1-1 mM) for the induction of bacterial cells was varied and expression was performed at 16°C for 16-18 h, enzymatic activity of FaCAD crude protein in comparison with GST control was not observed. However, purified GST-FaCAD exhibited enzymatic activity, as compared to the GST control (Figure 29A). LC-UV-ESI-MS^n did not detect a product probably because of the low amount (Figure 29B). Generally, a large protein affinity tag (GST tag, 26kDa) devours more metabolic energy during overproduction than a small tag (His tag) (Waugh, 2005). Hence, GST-FaCAD (65 kDa) (Appendix G1.A) was changed in a small tag and called His-FaCAD (43.6 kDa) (Appendix G1.B). Consequently, His-FaCAD was shown to form no products that could be detected by LC-UV-ESI-MS^n. Even though several parameters were varied for induction of either GST- and His-FaCAD (induction time and IPTG concentration), LC-UV-ESI-MS^n data showed that no products (coniferyl or sinapyl alcohol) were formed in any of the tested samples.

Similarly, the strawberry *Fxacad1* cDNA (*F.* × *ananassa* cv. Chandler) was expressed in *E.coli* and its protein was accumulated in inclusion bodies. After breaking the cells, no activity was monitored in the cell extracts of Fxacad1 by a spectrophotometer (Blanco-Portales et al., 2002). However, enzymatic activity for either purified GST-FaCAD or GST-FaCAD with $ZnCl_2$ as compared to GST was determined by spectrophotometer (Figure 29A). Thus, it seems that proteins in a crude cell extract may inhibit FaCAD activity (Appendix G1.A). Moreover, FaCAD was fused to either the GST- or His-tag for production of recombinant proteins. Large (GST) and small (His) tags have the potential to interfere with the biological activity of proteins (Waugh, 2005). Thus, FaCAD associated with affinity tags could be interfere with the structure or function of native protein.

Eukaryotic hosts, such as yeast, become a general strategy for solving solubility problems in the prokaryotes (Waugh, 2005). *Fxacad1* was expressed in *Pichia pastoris* cells and exhibited high activity with cinnamyl, coniferyl, and sinapyl aldehydes (Blanco-Portales et al., 2002). FaCAD was successfully expressed in *S. cerevisiae* and produced coniferyl alcohol (Figures 30A and B). Thus, the native protein was functionally expressed in the heterologous yeast host. Therefore pYES2-CAD, expressed in *S. cerevisiae*, would exhibit characteristics of angiosperm CAD enzymes, suggesting that it is a putative NADPH-dependent CAD.

2.3 FaPOD

Two strawberry peroxidases, FaPOD and FaPOD27, which belong to the group of plant heme peroxidase, have been analyzed in this study. FaPOD and FaPOD27, share only 31.9 % amino acid similarity at the protein level (Figure 24). As reported for several species, considerable variations in deduced amino acid sequences are present in PODs (Welinder, 1992; Welinder, 2002; Passardi et al., 2004a).

A full-length coding sequence of *FaPOD* and *FaPOD27* was cloned from a strawberry fruit (*F.* × *ananassa*), and expressed in *E. coli*. In the *E. coli* expressing system, a general problem is that prokaryotes rarely employ tRNAs for AGA and AGG arginine codons. Two AGA and AGA codons were found 28 times and eight times in the full-length coding sequence of *FaPOD* and *FaPOD27*, respectively. Genes containing these codons cannot be expressed in regular *E. coli* strains (Hushpulian et al., 2003). In order to solve the problem of rare codons in prokaryotes, the *E. coli* strain Rosetta (DE3) pLysS was used to improve protein expression. This strain of Rosetta (DE3) pLysS contained additional tRNAs, which recognized the AGA, AGG, AUA, CUA, CCC, and GGA codons (Novagen).

In this work, the supernatant of IPTG-induced bacterial cultures was collected. Several parameters were varied for induction of FaPOD (induction temperature and time, and IPTG concentration), resulting in no FaPOD protein being present in SDS-PAGE gels and no activity occurring after induction (Appendix G2.A). However, FaPOD protein (63.6 kDa) that was extracted from bacterial inclusion bodies by treatment with a high concentration of urea (solubilisation) was present in SDS-PAGE gels (Appendix G2.B). Like FaPOD, FaPOD27 formed non-soluble products in *E. coli*, but soluble protein was present in SDS-PAGE gels after solubilisation. Purified FaPOD and FaPOD27 were not observed in SDS-PAGE gels because peroxidases mostly precipitated as inclusion bodies in *E. coli*. It is a common phenomenon that peroxidases yield non-soluble products in the form of inclusion bodies in the *E. coli* expressing system (Hushpulian et al., 2003).

Nevertheless FaPOD27 was active in the *E. coli* expressing system (Figure 31). Enzymatic activity could be detected in crude protein extracts obtained from *E. coli* expressing FaPOD27. LC-UV-ESI-MS^n analysis (Figure 32) showed that dimeric products (dehydrodimer of ferulic acid) and a decarboxylation product of a dehydrodimer precursor were formed by FaPOD27, which is consistent with published data (Ward et al., 2001). These results suggested that FaPOD27 plays a role in monolignol polymerization. On the contrary, FaPOD was inactive in the *E. coli* expressing system (Figure 31) probably due to the production of large amounts of non-soluble inclusion bodies. To solve solubility problems, baculovirus-insect cells have been used as eukaryotic hosts (Waugh, 2005). Active *AtPOD33*, *AtPOD34*, and *AtPOD37* proteins have been expressed in such hosts (Carpin et al., 2001). Peroxidases can be expressed in eukaryotic cells, where the native proteins fold correctly and act as functional proteins. Whether FaPOD is a functional protein in strawberries remains to be studied. It is possible that FaPOD accepts alternative substrates to monolignols.

3. Expression levels of monolignol genes in different parts of a strawberry plant

Expression patters of four genes (*FaCCR*, *FaCAD*, *FaPOD*, and *FaPOD27*) were analyzed in different parts of the strawberry plant. Three of the four genes were highly expressed in mature fruit, whereas one of them showed high transcript levels in immature fruit (Figure 33). Expression levels of both *FaCCR* and *FaCAD* in the mature fruit were consistent with data of other strawberry cultivars (Salentijn et al., 2003). The expression patterns point to an active lignification process in the late stages of ripening. Interestingly, several motifs of the

CAD promoter region, such as transcription factor binding sites appear also in the CCR promoter region. Plant MYB proteins belong to one of the largest families of transcription factors. The coordinated developmental regulation of *EgCCR* and *EgCAD2* in *Eucalyptus gunnii* is mediated through MYB transcription factors (Rahantamalala et al., 2010). Thus, *FaCCR* and *FaCAD* are putatively coordinated by regulation during late fruit development.

The growth and development of aggregate fruits is following the steps of cell division, cell expansion, and ripening (Zhang et al., 2011). Cell growth and expansion are associated with cell extensibility, which is linked to a loosening of the cross-linking of the cell wall compounds (Passardi et al., 2005). Cell expansion is dependent on the loosening of cell wall during tomato fruit development (Andrews et al., 2000). Besides, as lignin restricts the expansion of the cell wall, lignification has to occur after cell division and expansion growth (Patzlaff et al., 2003). In this study, *FaPOD* was mainly expressed in small green to white stages that were associated with cell division or cell expansion. At the same time, *FaPOD* was not expressed in the ripening stage whereas *FaPOD27* was mainly expressed in the ripening stage of the full ripe fruit. Thus, *FaPOD27* is putatively involved in fruit lignification. The two peroxidases may putatively coordinate the balance between cell wall loosening and cross-linking during fruit development. The results suggest that *FaPOD* and *FaPOD27* genes are divergently regulated during early and late fruit development.

CCRs, CADs, and PODs are multigene families, as reported in several species (Rase et al., 2003; Lauvergeat et al., 2001; Saballos et al., 2009; Tognolli et al., 2002). The different members of CCRs, CADs, and PODs exhibit different expression patterns during plant growth and development. *TaCCR1* (*Triticum aestivum*) is mainly expressed in the stems (Ma, 2007), and *TaCCR2* (Ma and Tian, 2005) is in the roots. *TaCAD1* (*Triticum aestivum*) is also mainly expressed in the stems (Ma, 2010). Besides, different expression patterns have been observed for rice peroxidases. POXgX9 is expressed only in the roots. POX22.3 is expressed in both leaves and roots whereas POX8.1 and POX5.1 have not been detected in roots (Chittoor et al., 1997). In this work, *FaPOD* and *FaPOD27* genes show different expression patterns in strawberry plants. *FaPOD27* was mainly expressed in ripe fruits and roots, whereas *FaPOD* displayed its highest expression level in small green fruit. These data demonstrated that gene expression of lignin biosynthesis genes is divergently regulated in plant growth and development.

4. Fruits in response to wounding and *Agrobacterium* attack

Some genes are induced when plants respond to environmental stimuli including biotic and

abiotic stresses (Moura et al., 2010; Rushton and somssich, 1998). At the same time, induced genes that are involved in the phenylpropanoid and monolignol pathways are coordinately controlled (Kawaoka et al., 2000). In the present study, different responses were observed in fruits due to wounding and *Agrobacterium* treatments. Expression of *FaPOD27* was clearly induced in fruits by infection with *Agrobacterium*. *FaPOD*27 shows a low basal expression in different tissues but its transcript levels constantly increased during 10 days after agroinfiltration. Importantly, FaPOD did not show transient expression after induction. In plants, a basal level of peroxidase functions probably as housekeeping activity in either elongation or lignification (Passardi et al., 2005). However, induction of POD activity in response to pathogen attack could lead to increased lignification. This would reinforce plant cells and prevent the entry of pathogens. We assume that induced accumulation of *FaPOD*27 transcripts were required to prevent the spreading of *Agrobacterium* in infected fruits. In addition, PAL catalyzes the first step in the phenylpropaoid biosynthetic pathway and its activity affects the synthesis of a wide range of phenolic compounds, including lignin. In the study, *FaPAL* showed a transient increase at 24 h following infection by *Agrobacterium*. In barley epidermis the increase in PAL enzyme activity was associated with enhanced mRNA transcription after infection by a powdery mildew (Zierold et al., 2005). Rapid induction of *PAL* and *4CL* mRNAs was revealed in potato leaves upon *Phytophthora infestans* infection (Fritzmeier et al., 1987). PAL, COMT, 4CL, CAD and POD had increased transient activity following treatment with an elicitor derived from an ectomycorrhizal fungus (Campbell and Ellis, 1992). However, no induction of *FaCHS*, *FaCCR*, *FaCAD*, and *FaPOD* was detected in *F. x ananassa* fruits following infiltration by *Agrobacterium*. Also, wounding had no impact on transcript levels of monolignol genes in the strawberries. Elevated levels of *FaPOD27* transcripts were detected in all agroinfiltrated fruits (Figure 36) undergoing active lignin synthesis (Figure 40B, d).

It has been reported that the expression of various isoenzymes is induced by different stress signals. Rice POX8.1 and POX5.1 were induced in wounded leaves at different times. POX8.1 and POX22.3 were largely induced during resistant interactions. Unlike other isoenzymes, POXgX9 was not induced by either wounding or pathogen (Chittoor et al., 1997). As another example, *Arabidopsis AtCCR1* was not induced, but *AtCCR2* was predominantly expressed followed by *Xanthomonas campestris* (Lauvergeat et al., 2001). Different expression patterns suggest that the promoter of each gene might contain multiple *cis*-acting elements for the binding of various *trans*-acting factors (transcription factors). For example, pathogen-inducible promoters in *Arabidopsis* harbor different *cis*-acting elements

(boxes W1, W2, GCC, JERE, S, Gst1, and D) and display different expression patterns following pathogen attack or wounding treatments (Rushton et al., 2002). The presence of *cis*-acting elements and/or *trans*-acting factors could determine temporal and spatial gene expression as the plants respond to various environmental cues (Rushton and Somssich, 1998; Chittoor et al., 1997). The results indicate that different members of the lignin biosynthesis gene family are distinctly regulated in response to various stimuli.

The inducible defenses included biochemical and morphological changes, such as oxidative burst, expression of defense-related genes, and programmed cell death (van Loon et al., 2006). Inducing the expression of defense-related genes and coordinating complex interactions between defense-signaling pathways are major factors in activating a defense response by plants against pathogen attack (Rushton and Somssich, 1998). Besides, plants utilize physical and chemical barriers to hinder pathogen infection (Nicholson and Hammerschmidt, 1992). For example, the expression of peroxidase genes was induced in both the epidermis and mesophyll tissues in wheat after Bgt attack (Liu et al., 2005). In addition, monolignol units were oxidized by peroxidase to produce lignin polymer (Boerjan et al., 2003). PODs have been involved in a broad range of stress-related physiological processes, such as production of lignins, induction of lignification, and defense against pathogens (Almagro et al., 2009). In this work, *Agrobacterium*-infected fruits, concomitant with inducing *FaPOD27* expression, clearly showed an increase in firmness and lignin content, as well as induction of lignification (Figure 40B, d). Likewise, CAD and POD activities increased in LYQ fruit, concomitant with the increase in lignin content (Cai et al., 2006). Moreover, the overexpression of TRX1 in transgenic tomato plants was linked to an increase in lignin content (Mansouri et al., 1999).

The abundance of *FaCCR* and *FaCAD* transcripts in the mature fruit may produce sufficient monolignol supplies that are oxidized by FaPOD27 to form lignin in *Agrobacterium*-infected fruit. These results indicated that increased expression levels of *FaPOD27* provoke the enhanced production of lignin in *Agrobacterium*-infected fruits. Thus, *FaPOD27* is presumably involved in the lignin synthesis associated with the defense response.

5. Individual down- and up-regulation of monolignol genes in fruits (*F.* × *ananassa* cv. Elsanta)

Fruit firmness and lignin content

To demonstrate the direct role of monolignol genes in regulating lignin content in plants, monolignol genes were transiently down-regulated by RNAi and overexpressed in strawberry fruits. Enhanced fruit firmness in agroinfiltrated fruits was associated with increased lignin production in treated fruits, as compared to wild-type (untreated) fruits (Figure 41). This comparative result demonstrated a clear correlation between fruit firmness and lignin content. It has been demonstrated that lignification and lignin formation is induced by pathogen infection (Dixon, 2001; Reimers and Leach, 1991). These reactions are common in a plant's defense against penetration by pathogens. In this work, lignin staining showed that lignin accumulated in treated fruits exposed to *Agrobacterium* (Figure 40B, d). The important role of monolignol biosynthetic genes in the formation of CWA (cell wall apposition) in wheat against pathogen penetration has been demonstrated (Bhuiyan et al., 2009). Induced lignin formation is essential for resistance to pathogen penetration. Thus, it is possible that deposition of lignin in agroinfiltrated fruits led to reinforced cell walls, resulting in enhanced firmness in treated fruits.

Phenotype

Phenotypes can change upon silencing and overexpression of gene products in plants. When monolignol genes are introduced into plants, transgenic plants show normal or abnormal phenotypes, depending on the impact of lignin content. For example, an abnormal phenotype was exhibited when total lignin content decreased in CCR-down-regulated plants (Piquemal et al., 1998). On the contrary, the *Zmccr1*$^{-}$ mutant exhibited normal growth with little effect on lignin content (Tamasloukht et al., 2011). Down-regulation of CAD in plants did not significantly affect total lignin and plants exhibited a normal phenotype (Ralph et al., 1998). It was assumed that lignification was sufficiently plastic to enable CAD-down-regulated plants to form lignin from hydroxycinnamylaldehydes (Humphreys and Chapple, 2002). However, reduction in the level of CCR transcripts led to insufficient lignin formation to support normal development, resulting in abnormal phenotypes (Piquemal et al., 1998). In addition, overexpression of POD in tobacco was associated with an elevated level of lignin content, and transgenic plants exhibited slower growth (Whetten et al., 1998). In this study, the lignin content of agroinfiltrated fruits expressing down- and up-regulation constructs of monolignol genes was the same as in the pBI-intron control fruits but significantly higher than the lignin level in untreated fruits (Figure 41). At the same time, all fruits exhibited normal growth and development (Figures 40A, b and d).

Metabolite

LC-UV-ESI-MS^n analyses indicated that the level of *p*-coumaroyl glucoside/glucose decreased in all treated fruits, whereas the levels of caffeoyl glucose and feruloyl glucose increased (Figure 54). It has already been reported that some glucosylated derivatives of phenylpropanoids accumulated in CCR-down-regulated plants and *FaCHS*-silenced strawberry fruits (Tu et al., 2010; van der Rest et al., 2006; Dauwe et al., 2007; Hoffmann et al., 2006; Lunkenbein et al., 2006b). Moreover, hydroxycinnamic acids accumulate exclusively in strawberries as conjugates but levels of the glucose ester may reflect the levels of their corresponding acid precursors (Määttä-Riihinen et al., 2004). Therefore, the levels of caffeoyl glucose and feruloyl glucose probably correspond to the levels of caffeic and ferulic acid in strawberry fruits, respectively (Figure 54). Caffeic acid is the precursor of ferulic acid, coniferyl alcohol, and sinapyl alcohol, leading to the formation of G and S lignin. The methylation of caffeic acid to ferulic acid is catalyzed by caffeic acid-O-methyltransferase (COMT) (Boerjan et al., 2003). An increased level of ferulic acid in plants, exposed to bacterial infection, suggested the existence of a defense response to prevent bacterial infection in these plants (Parrott et al, 2002).

In particular, the level of coumaric acid decreased in CCR-down-regulated lines of perennial ryegrass, whereas levels of caffeoylquinic acid, caffeoyl shikimic acid, ferulic acid, and sinapic acid increased in these transgenic plants (Tu et al., 2010). The result is consistent with the data that showed decreased levels of *p*-coumaroyl glucoside/glucose in *FaCCR*-silenced fruits (Figure 46A), suggesting that coumaric acid is converted to caffeic acid to fuel the lignin pathway. It has been reported that low levels of *CCR* divert *p*-coumaroyl-CoA esters into the synthesis of flavonoids, resulting in the accumulation of flavonol conjugates in CCR-deficient plants (Tu et al., 2010; van der Rest et al., 2006). In this study, *FaCCR*-silenced fruits with a lack of functional CCR accumulated less *p*-coumaroyl-CoA esters. However, the levels of flavonol conjugates were not affected.

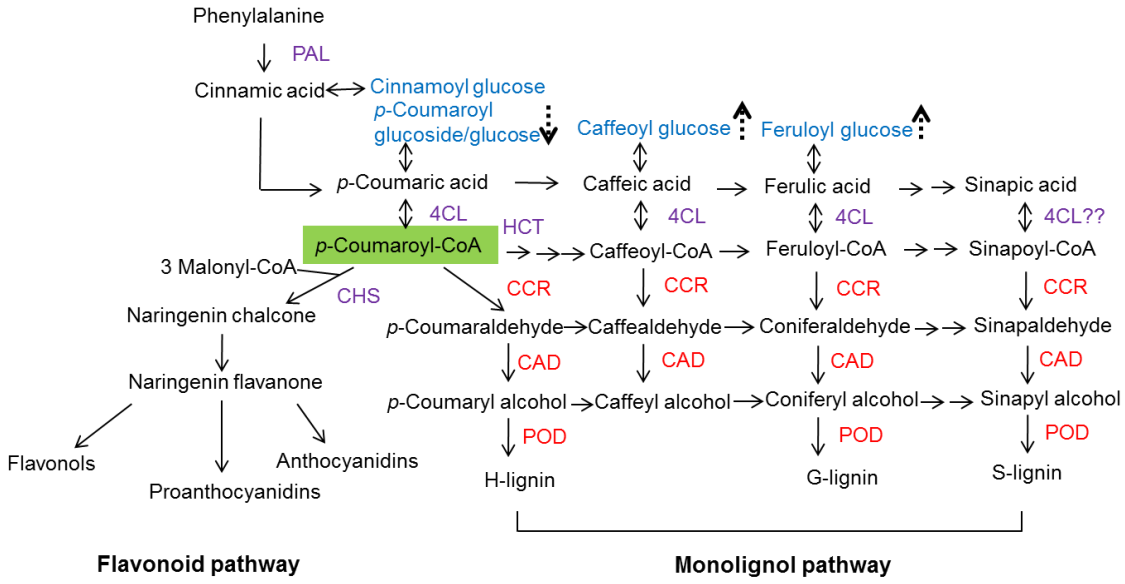

Figure 54. Flavonoid and monolignol biosynthetic pathways in the fruit following infiltration by *Agrobacterium*.
Enzymes and their abbreviations are as follows: PAL, phenylalanine ammonia lyase; 4CL, 4-coumaroyl-CoA ligase; CHS, chalcone synthase; HCT, hydroxycinnamoyl transferase; CCR, cinnamoyl-CoA reductase; CAD, cinnamyl alcohol dehydrogenase; POD, peroxidase. Arrow with dashed lines indicate compounds that are up- ( ) or down-regulated ( ) when fruits were agroinfiltrated with pBI-intron (control constructs), down- and up-regulation constructs of individual genes (*FaCCR*, *FaCAD*, or *FaPOD*). The green shade indicating *p*-coumaroyl-CoA is the common precursor for both the flavonoid and monolignol pathway. Red *CCR*, *CAD*, and *POD* indicate down- and up-regulated genes.

Increase in lignin content

Lignin content and composition play an important role in evaluating the results of genetic biotechnologies. Reduced flux from coumaroyl-CoA, caffeoyl-CoA, and feruloyl-CoA to H, G, and S units, respectively, leads to enhanced accumulation of coumaric acid, cinnamic acid, and ferulic acid (Tu et al., 2010). It has been demonstrated that ferulic acid is incorporated in the lignin polymer in CCR-deficient plant species (Ralph et al., 2008; Vanholme et al., 2010). Upon *Botrytis allii* attack, soluble and cell-wall bound conjugates of ferulic acid (feruloyl tyramine and feruloyl-3´-methoxytyramine) accumulated in onion epidermis to reinforce the cell wall by cross-linking (McLusky et al., 1999). In contrast, in CAD-deficient plant species, it has been demonstrated that cinnamyl aldehyde is incorporated into the lignin polymer (Lapierre et al., 1999; Whetten et al., 1998; Dauwe et al., 2007). In recent years, valuable markers for the incorporation of ferulic acid and hydroxycinnamyl aldehyde into lignin

polymers have been established (Ralph et al., 2008; Palmer et al., 2008). In this work, agroinfiltrated fruits, expressing RNAi-mediated gene silencing and overexpression constructs of monolignol genes, caused changes in the levels of hydroxycinnamate derivatives. However, the ferulic acid was not detected in the treated fruits after thioacidolysis by GC-MS. Ferulic acid linked in lignin may yield too low amounts after thioacidolysis. Similarly, ferulic acid was also not detected in the *Zmccr1*$^{-}$ mutant due to the low amount of ferulic acid which is released by thioacidolysis (Tamasloukht et al., 2011). Remarkably, a novel compound was detected in *FaCCR*-silenced fruits but remained unknown (Figure 48A). Besides, incorporation of hydroxycinnamyl aldehyde into lignin has not been observed in pBI-*FaCADi* after thioacidolysis. Low levels of monomers derived from aldehydes were obtained by thioacidolysis in studies performed by Stewart et al. (1997). NMR studies showed β-O-4 coupled hydroxycinnamyl aldehyde structures in lignin of CAD-down-regulated tobacco (Ralph et al., 2001).

Caffeic acid and ferulic acid are major precursors in lignin biosynthesis (Boerjan et al., 2003; Ralph et al., 2008). Independent of the construct used for agroinfiltration, all treated fruits accumulated glucose esters derivatives of these phenylpropanoic acids. Elevated levels of these precursors indicate an increased flux towards lignin as they may be incorporated into lignin and may lead to enhanced lignin content in treated fruits. CCR- or CAD-down-regulation in angiosperms led to increased incorporation of ferulic acid and hydroxycinnamaldehydes into the lignin polymer (Ralph et al., 2008; Vanholme et al., 2010; Lapierre et al., 1999). The incorporation of hydroxycinnamaldehydes and ferulic acid into the lignin polymers of *FaCAD*- or *FaCCR*-silenced fruits could not be observed but cannot be excluded due to the low amount of lignin produced by strawberry fruits and the low incorporation rate detected by others. In addition, the lignin content of *FaPOD*-silenced fruits is the same as that of the pBI-intron control fruits. Overall, the similar increase in lignin content in all treated fruits is mainly attributed to the pathogen response of the fruit, namely the induction of *FaPOD27* which probably overrules other effects that may be related with the silencing and overexpression of monolignol genes.

Modification of proportions of monolignols

Gene expression of *FaCCR* and *FaCAD*, and their related enzymatic activities could be efficiently suppressed by RNAi in pBI-*FaCCRi* and pBI-*FaCADi* strawberries. It has been reported that CCR-deficient plants such as tobacco, *Arabidopsis*, and maize had decreased flux from feruloyl-CoA to G and S units (Chabannes et al., 2001; Ralph et al., 2008;

Tamasloukht et al., 2011). In CCR- and CAD-down-regulated tobacco, the reduced enzyme activities also affected the proportion of monolignols in the lignin polymer (Chabannes et al., 2001). The increase in the S/G ratio of lignin in *FaCCR*-silenced fruits was consistent with CCR-deficient maize (Tamasloukht et al., 2011). Besides, GC-MS results showed that G units significantly decreased in *FaCCR*-silenced fruits, as well as G and S units significantly decreased in *FaCAD*-silenced fruits, as compared to pBI-intron control fruits (Table 26). In an *in vitro* study, GST-CCR was highly specific to feruloyl-CoA. This result was reflected in *FaCCR*-silenced fruits, which showed a decreased flux from feruloyl-CoA to G units. The recombinant FxaCAD1 (*F.* × *ananassa* cv. Chandler) enzyme was highly specific for coniferyl and sinapyl aldehydes *in vitro* (Blanco-Portales et al., 2002). This result may be reflected in *FaCAD*-silenced fruits, which displayed decreased fluxes from coniferyl and sinapyl aldehydes to G and S units. Moreover, the lignin monomeric composition of WT (untreated) fruits could not be determined by GC-MS because the lignin content was too low in the untreated fruits as also demonstrated by phloroglucinol staining (Figure 40B, c). *FaPOD* transcripts were not significantly affected in pBI-*FaPODi* fruits (Figure 42) and monomeric composition of lignin was not changed as compared with lignin from pBI-intron fruits (Table 26).

Expression levels of *FaCCR* and *FaCAD* genes were not significantly affected in pBI-*FaCCR* and pBI-*FaCAD* fruits, respectively (Figure 43). When compared with pBI-intron control fruits, pBI-*FaCCR* fruits exhibited no effect on G units because similar FaCCR activity was measured in pBI-*FaCCR* and pBI-intron control fruits (Figure 44). However, pBI-*FaCAD* fruits exhibited a slight decrease in G units due to a slightly decreased level of FaCAD activity that was measured in *FaCAD* fruits (Figure 45). In addition, enhanced *FaPOD* transcripts may not have a direct effect on total lignin content, but levels of G and S units decreased significantly in pBI-*FaPOD* fruits (Table 26). Hence, FaPOD is proposed as regulator of lignin composition. Possible explanations are that FaPOD catalyzes a reaction that limits monolignol supply for lignin formation or inhibits the activity of other POD isoenzymes to modulate overall POD activity, and regulate the proportion of G and S units in lignin. The results show that FaPOD activity is related with lignin composition.

Angiosperm lignin is mainly composed of G and S units, and few H units (Boerjan et al., 2003; Whetten et al., 1998; Tu et al., 2010). A reduction in H units was observed in the early lignification stage when *CCR* was down-regulated in maize (Tamasloukht et al., 2011). We observed that the amounts of H units significantly decreased in *FaCAD*-silenced fruits (Table 26).

Altogether, variations in the S to G unit ratios of lignin may be attributed to the fact that different monolignol genes were introduced or silenced in the fruits whereas the constant lignin content in all treated fruits may be attributed to elevated transcript levels of *FaPOD27*. *FaPOD27* is putatively responsible for the incorporation of hydroxycinnamates into lignin.

6. Down- and up-regulation of monolignol genes in CHS$^-$ fruits

In CHS$^-$ fruits the increase in firmness upon agroinfiltration of different constructs was also associated with an increase in lignin content. A comparison revealed that fruits agroinfiltrated with silencing and overexpression constructs produced firmer fruits than CHS$^-$/pBI-intron control fruits (Figure 50). In contrast, firmness and lignin content of Elsanta fruits expressing constructs to down- and up-regulated monolignol genes were the same as in the pBI-intron control fruits. We assume that the silencing of the *CHS* gene in CHS$^-$ fruits provides additional precursors (*p*-coumaroyl-CoA) available for monolignol biosynthesis, resulting in increased lignin content in CHS$^-$ fruits. Another possible explanation is the relation between flavonoid content and auxin transport. It was shown that the accumulation of flavonoids in HCT$^-$ plants led to the inhibition of auxin transport and reduction of plant growth (Besseau et al., 2007). Remarkably, auxin transport can be restored in HCT$^-$/CHS$^-$ plants due to lower levels of flavonoids in the plants. Restoration of auxin transport also led to increased yields of lignin. In accordance with this model, CHS$^-$ fruits contained lower levels of flavonoids, as compared to Calypso fruits (Appendix E.5.5.), resulting in higher lignin content in CHS$^-$ fruit (Figure 50). It has been shown that auxin affected growth of strawberry fruits and early fruit development and acted to delay ripening (Given et al., 1988) whereas fruit ripening is associated with rapid softening (Zhang et al., 2010). Thus, we assume that increased auxin transport in CHS$^-$ fruits expressing different constructs (Figure 39) corresponding to *FaCCR*, *FaCAD*, and *FaPOD* led to delayed ripening, which impacts on fruit firmness.

In addition, the expression of phenylpropanoid biosynthesis genes in *FaCCR*-, *FaCAD*-, *FaPOD*-down-regulated, *FaCCR*-, *FaCAD*-, and *FaPOD*-up-regulated fruits (Figures 51-52) is quite consistent with the results for Elsanta fruits (Figures 42-43). In particular, *FaPAL* and *FaCAD* transcripts simultaneously decreased in CHS$^-$/pBI-*FaCADi* fruits. *FaPOD* transcripts significantly increased in CHS$^-$/pBI-O3 fruits, but *FaPAL*, *FaCCR*, and *FaCAD* transcripts decreased in the CHS$^-$/pBI-O3 fruits. In contrast, one of two differential *PAL* genes was up-regulated in *CCR*-, *CAD*- , and combined CCR-/CAD-down-regulated tobacco plants. Besides, transcript profiling exhibited differential gene expression patterns in the three transgenic lines, including induction of transcription factor genes (Dauwe et al., 2007).

Therefore, CHS$^-$ fruits expressing different individual and combined gene constructs (pBI-Si3 and pBI-O3) might alter the transcript levels of other unknown phenylpropanoid biosynthesis genes, suggesting regulation of the flux through primary and secondary metabolism in response to changes in the monolignol biosynthesis.

Hydroxycinnamic acids are intermediates, which are produced and converted to their corresponding aldehydes and alcohols by combined action of PAL, 4CL, CCR, and CAD in the general phenylpropanoid pathway (Boerjan et al., 2003; Weng and Chapple, 2010). Low levels of *FaPAL* transcripts in CHS$^-$/pBI-*FaCADi* and CHS$^-$/pBI-*FaCAD* fruits, as well as CHS$^-$/pBI-*FaPOD* fruits, were reflected at the metabolite levels, because these fruits accumulated lower levels of cinnamoyl-glucose-ester (Figure 53). In addition, low levels of *FaPAL* and *FaCCR* transcripts in CHS$^-$/pBI-*FaCAD* and CHS$^-$/pBI-O3 fruits affected the accumulation of *p*-hydroxybenzoyl glucose and cinnamoyl glucose. However, *FaPAL* transcripts were not changed in CHS$^-$/pBI-*FaPOD* fruit, but *p*-hydroxybenzoyl glucose significantly decreased (Figure 53B). It is suggested that a complement of enzymes exists that may be responsible for monolignol synthesis in plants without invoking hydroxycinnamic acids, other than cinnamate and *p*-coumarate as intermediates (Humphreys and Chapple, 2002). In the CHS$^-$ fruit background, the treated fruits showed the existence of a complex regulatory network within the phenylpropanoid metabolism.

V. Conclusion

Significant induction of *FaPOD27* expression was observed in fruits exposed to *Agrobacterium* harboring different constructs. The high *FaPOD27* expression levels were associated with increased fruit firmness, as well as the formation of lignin. Expression of *FaCCR* and *FaCAD* was successfully down-regulated through RNAi whereas *FaPOD* was overexpressed during fruit ripening. The results significantly improve our understanding of the genetic control of lignin biosynthesis in strawberry fruits. *FaPOD27* should be considered as a key gene for improving the firmness of strawberry fruit.

References

Aaby, K., Skrede, G., Wrolstad, R.E. (2005) Phenolic composition and antioxidant activities in flesh and achenes of strawberries (*Fragaria* × *ananassa*). J. Agric. Food Chem. **53**: 4032-4040.

Abbott, D., Wang, M.B., Waterhouse, P. (2000) A single copy of a virus-derived transgene encoding hairpin RNA gives immunity to barley yellow dwarf virus. Mol. Plant Pathol. **1**: 347-356.

Almagro, L., Gómez Ros, L.V., Belchi-Navarro, S., Bru, R., Ros Barceló, A., Pedreño, M.A. (2009) Class III peroxidases in plant defence reactions. J. Exp. Bot. **60**:377-390.

Almeida, J.R.M., D'Amico, E., Preuss, A., Carbone, F., de Vos, C.H.R., Deiml, B., Mourgues, F., Perrotta, G., Fischer, T.C., Bovy, A.G., Martens, S., Rosati, C. (2007) Characterization of major enzymes and genes involved in flavonoid and proanthocyanidin biosynthesis during fruit development in strawberry (*Fragaria* × *ananassa*). Arch. Biochem. Biophys. **465**:61-71.

Andrews, J., Malone, M., Thompson, D.S., Ho, L.C., Burton, K.S. (2000) Peroxidase isozyme patterns in the skin of maturing tomato fruit. Plant Cell Environ. **23**: 415-422.

Baltas, M., Lapeyre, C., Bedos-Belval, F., Maturano, M., Saint-Aguet, P., Roussel, L., Duran, H., Grima-Pettenati, J. (2005) Kinetic and inhibition studies of cinnamoyl-CoA reductase 1 from *Arabidopsis thaliana*. Plant Physiol. Biochem. **43**: 746-753.

Bennett, M. D. (2004) Perspectives on polyploidy in plants: ancient and neo. Biol. J. Linn. Soc. **82**:411-423.

Bernstein, E., Caudy, A.A., Hammond, S.M., Hannon, G.J. (2001) Role for a bidentate ribonuclease in the initiation step of RNA interference. Nature **409**: 363-366.

Besseau, S., Hoffmann, L., Geoffroy, P., Lapierre, C., Pollet, B., Legrand, M. (2007) Flavonoid accumulation in *Arabidopsis* repressed in lignin synthesis affects Auxin transport and plant Growth. Plant Cell **19**:148-162.

Beuerle, T. Pichersky, E. (2002) Enzymatic synthesis and purification of aromatic coenzyme A esters. Anal. Biochem. **302**:305-312.

Bhuiyan, N.H., Selvaraj, G., Wei, Y., King, J. (2009) Gene expression profiling and silencing reveal that monolignol biosynthesis plays a critical role in penetration defence in wheat against powdery mildew invasion. J. Exp. Bot. **60**:509-521.

Blanco-Portales, R., Medina-Escobar, N., López-Ráez, J.A., González-Reyes, J.A., Villalba, J.M., Moyano, E., Caballero, J.L., Muñoz-Blanco, J. (2002) Cloning, expression and immunolocalization pattern of a cinnamyl alcohol dehydrogenase gene from strawberry (*Fragaria* × *ananassa* cv. Chandler). J. Exp. Bot. **53**: 1723-1734.

Blee, K.A., Choi, J.W., O'Connell, A.P., Schung, W., Lewis, N.G., Bolwell, G.P. (2003) A lignin specific peroxidase in tobacco whose antisense suppression leads to vascular tissue modification. Phytochemistry **64**: 163-176.

Boerjan, W., Ralph, J., Baucher, M. (2003) Lignin biosynthesis. Annu. Rev. Plant Biol. **54**:519-546.

Bonello, P., Blodgett, J.T. (2003) *Pinus nigra- Sphaeropsis sapinea* as a model pathosystem to investigate local and systemic effects of fungal infection of pines. Physiol. Mol. Plant Pathol. **63**: 249-261.

Bourne, M. (2002) Food Texture and Viscosity: Concept and Measurement. Geneva, New York, London, Academic Press.

Bradford, M.M. (1976) A rapid and sensitive method for the quantification of microgram quantities of protein utilizing the principle of protein-dye binding. Anal. Biochem.**72**:248-254.

Brill, E.M., Abrahams, S., Hayes, C.M., Jenkins, C.L.D., Watson, J.M. (1999) Molecular characterization and expression of a wound-inducible cDNA encoding a novel cinnamyl-alcohol dehydrogenase enzyme in lucerne. Plant Mol. Biol. **41**:279-291.

Bunsiri, A., Ketsa, S., Paull, R. E. (2003) Phenolic metabolism and lignin synthesis in damaged pericarp of mangosteen fruit after impact. Postharvest Biol. Technol. **29**:61-71.

Cai, C., Xu, C.J., Li, X., Ferguson, I.B., Chen, K.S. (2006) Accumulation of lignin in relation to change in activities of lignification enzymes in loquat fruit flesh after harvest. Postharvest Biol. Technol. **40**:163-169.

Campbell, M.M., Ellis, B.E. (1992) Fungal elicitor-mediated responses in pine cell cultures. I. Induction of phenylpropanoid metabolism. Planta **186**: 409-417.

Carpin, S., Crevecoeur, M., de Meyer, M., Simon, P., Greppin, H., Penel, C. (2001) Identification of a Ca^{2+}-pectate binding site on an apoplastic peroxidase. Plant Cell **13**:511-520.

Chabannes, M., Barakate, A., Lapierre, C., Marita, J.M., Ralph, J., Pean, M., Danoun, S., Halpin, C., Grima-Pettenati, J., Boudet, A.M. (2001) Strong decrease in lignin content without significant alteration of plant development is induced by simultaneous down-regulation of cinnamoyl-CoA reductase (CCR) and cinnamyl alcohol dehydrogenase (CAD) in tobacco plants. Plant J. **28**:257-270.

Chapple, C.C.S., Vogt, T., Ellis, B.E., Somerville, C.R. (1992) An Arabidopsis mutant defective in the general phenylpropanoid pathway. Plant Cell **4**: 1413-1424.

Chapple, C., Carpita, N. (1998) Plant cell walls as targets for biotechnology. Curr. Opin. Plant Biol. **1**:179-l 85.

Chittoor, M., Leach, J.E., White, F.F. (1997) Differential induction of a peroxidase gene family during infection of rice by *Xanthomonas oryzae* pv. *oryzae*. Mol. Plant Microbe Interact. **10**: 861-871.

Clifford, M. N. (1974) Specificity of acidic phloroglucinol reagents. J. Chromatogr. **94**:321-324.

Cohn, J., Sessa, G., Martin, G. B. (2001) Innate immunity in plants. Curr. Opin. Immunol. **13**:55-62.

Cosio, C., Dunand, C. (2009) Specific functions of individual class III peroxidase genes. J. Exp. Bot. **60**:391-408.

Darrow, G. (1966) The Strawberry: History, Breeding and Physiology. Holt Rinehart & Winston, New York.

Dauwe, R., Morreel, K., Goeminne, G., Gielen, B., Rohde, A., Van Beeumen, J., Ralph, J., Boudet, A.M., Kopka, J., Rochange, S.F., Halpin, C., Messens, E., Boerjan, W. (2007) Molecular phenotyping of lignin-modified tobacco reveals associated changes in cell-wall metabolism, primary metabolism, stress metabolism and photorespiration. Plant J. **52**:263-285.

Delessert, C., Wilson, I., Van Der Straeten, D., Dennis, E., Dolferus, R. (2004) Spatial and temporal analysis of the local response to wounding. Plant Mol. Biol. **55**: 165-181.

Dixon, R.A. (2001) Natural products and disease resistance. Nature **411**: 843-847.

Dixon, R.A, Chen, F., Guo, D., Parvathi, K. (2001) The biosynthesis of monolignols: a "metabolic grid", or independent pathways to guaiacyl and syringyl units? Phytochemistry **57**:1069-1084.

Dixon, R. A., Reddy, M.S.S. (2003) Biosynthesis of monolignols. Genomic and reverse genetic approaches. Phytochemistry Reviews **2**:289-306.

Ehlting, J., Büttner, D., Wang, Q., Douglas, C.J., Somssich, I.E., Kombrink, E. (1999) Three 4-coumarate: coenzyme A ligases in *Arabidopsis thaliana* represent two evolutionarily divergent classes in angiosperms. Plant J. **19**:9-20.

Ehlting, J., Mattheus, N., Aeschliman, D.S., Li, E., Hamberger, B., Cullis, I.F., Zhuang, J., Kaneda, M., Mansfield, S.D., Samuels, L., Ritland, K., Ellis, B.E., Bohlmann, J., Douglas, C.J. (2005) Global transcript profiling of primary stems from *Arabidopsis thaliana* identifies candidate genes for missing links in lignin biosynthesis and transcriptional regulators of fiber differentiation. Plant J. **42**:618-640.

El Mansouri, I., Mercado, J.A., Santiago-Dó menech, N., Pliego-Alfaro, F., Valpuestra, V., Quesada, M.A. (1999) Biochemical and phenotypical characterization of transgenic tomato plants overexpression a basic peroxidase. Physiol. Plant. **106**:355-362.

Escamilla-Trevino, L.L., Shen, H., Uppalapati, S.R., Ray, T., Tang, Y., Hernandez, T., Yin, Y., Xu, Y., Dixon, R.A. (2010) Switchgrass (*Panicum virgatum*) possesses a divergent family of cinnamoyl CoA reductases with distinct biochemical properties. New Phytol. **185**: 143-155.

Evtuguin, D.V., Neto, C.P., Silva, A.M.S., Domingues, P.M., Amado, F.M.L., Robert, D., Faix, O. (2001) Comprehensive study on the chemical structure of dioxane lignin from plantation Eucalyptus globulus wood. J. Agric. Food Chem. **49**:4252-4261.

Feuillet, C., Lauvergeat, V., Deswarte, C., Pilate, G., Boudet, A., Grima-Pettenati, J. (1995) Tissue- and cell-specific expression of a cinnamyl-alcohol dehydrogenase promoter in transgenic poplar plants. Plant Mol. Biol. **27**:651-667.

Fossen, T., Rayyan, S., Andersen, O.M. (2004) Dimeric anthocyanins from strawberry (*Fragaria* × *ananassa*) consisting of pelargonidin 3-glucoside covalently linked to four flavan-3-ols. Phytochemistry **65**:1421-1428.

Franke, R., Hemm, M.R., Denault, J.W., Ruegger, M.O., Humphreys, J.M., Chapple, C. (2002) Changes in secondary metabolism and deposition of an unusual lignin in the *ref8* mutant of *Arabidopsis*. Plant J. **30**:47-59.

Gabaldón, C., López-Serrano, M., Pedreño, M.A., Ros Barceló, A. (2005) Cloning and molecular characterization of the basic peroxidase isoenzyme from *Zinnia elegans*, an enzyme involved in lignin biosynthesis. Plant Physiol. **139**:1138-1154.

Galliano, H., Cabane, M., Eckerskorn, C., Lottspeich, F., Sandermann, H., Ernst, D. (1993) Molecular cloning, sequence analysis and elicitor-/ozone-induced accumulation of cinnamyl alcohol dehydrogenase from Norway spruce (*Picea abies*). Plant Mol. Biol. **23**: 145-156.

Given, N.K., Venis, M.A., Grierson, D. (1988) Hormonal regulation of ripening in the strawberry, a non-climacteric fruit. Planta **174**:402-406.

Goffner, D., Campbell, M.M., Campargue, C., Clastre, M., Borderies, G., Boudet, A., Boudet, A.M. (1994) Purification and characterization of cinnamoyl-CoA:NADP oxidoreductase in *Eucalyptus gunnii* Plant Physiol.**106**: 625-632.

Grima-Pettenati, J., Feuillet, C., Goffner, D., Borderies, G., Boudet, A.M. (1993) Molecular cloning and expression of a Eucalyptus gunnii cDNA clone encoding cinnamyl alcohol dehydrogenase. Plant Mol. Biol. **21**:1085-1095.

Gu, L., Kelm, M.A., Hammerstone, J.F., Beecher, G., Holden, J., Haytowitz, D., Prior, R.L. (2003) Screening of food containing proanthocyanidins and their structural characterization using LC-MS/MS and thiolytic degradation. J. Agric. Food Chem. **51**:7513-7521.

Guo, M., Rupe, M.A., Zinselmeier, C., Habben, J., Bowen, B.A., Smith, O.S. (2004) Allelic variation of gene expression in maize hybrids. Plant Cell **16**:1707-1716.

Halpin, C., Knight, M.E., Foxon, G.A., Campbell, M.M., Boudet, A.M., Boon, J.J., Chabbert, B., Tollier, M.-T., Schuch, W. (1994) Manipulation of lignin quality by downregulation of cinnamyl alcohol dehydrogenase. Plant J. **6**:339-350.

Hancock, J.F. (1999) Strawberries. New York: CABI Publishing.

Hannon, G.J. (2002) RNA interference. Nature **418**:244-251.

Hart, A. (2001) Mann-Whitney test is not just a test of medians: differences in spread can be important. Br. Med. J. **323**:391-393.

Hawkins, S., Boudet, A. (2003) 'Defence lignin' and hydroxycinnamyl alcohol dehydrogenase activities in wounded Eucalyptus gunnii. Eur. J. For. Pathol. **33**: 91-104.

Hayashi, T. (2006) The science and lore of the plant cell wall. Brown Walker Press. Boca Ration, Florida USA. pp 285-293.

Hoffmann, L., Besseau, S., Geoffroy, P., Ritzenthaler, C., Meyer, D., Lapierre, C., Pollet, B., Legrand, M. (2004) Silencing of hydroxycinnamoyl-coenzyme A shikimate/quinate hydroxycinnamoyltransferase affects phenylpropanoid biosynthesis. Plant Cell **16**:1446-1465.

Hoffmann, T. (2001) Signaltransduktion von Abscisinsäure in *Arabidopsis thaliana*: Transiente Expression in Protoplasten als Modellsystem. Dissertation, Technischen Universität München.

Hoffmann, T., Kalinowski, G., Schwab, W. (2006) RNAi-induced silencing of gene expression in strawberry fruit (*Fragaria* × *ananassa)* by agroinfiltration. A rapid assay for gene function analysis. Plant J. **48**: 818-826.

Humphreys, J.M., Chapple, C. (2002) Rewriting the lignin roadmap. Curr. Opin. Plant Biol. **5**: 224-229.

Hushpulian, D.M., Savitski, P.A., Rojkova, A.M., Chubar, T.A., Fechina,V.A., Sakharov, I.Yu., Lagrimini, L.M., Tishkov, V.I., Gazaryan, I.G. (2003) Expression and refolding of tobacco anionic peroxidase from *E. coli* inclusion bodies. Biochemistry (Moscow) **68**: 1189-1194.

Jiménez-Bermúdez, S., Redondo-Nevado, J., Muñoz-Blanco, J., Caballero, J.L., López-Aranda, J.M., Valpuesta, V., Pliego-Alfaro, F., Quesada, M.A., Mercado, J.A. (2002) Manipulation of strawberry fruit softening by antisense expression of a pectate lyase gene. Plant Physiol. **128**: 751-759.

Kawaoka, A., Kaothien, P., Yoshida, K., Endo, S., Yamada, K., Ebinuma, H. (2000) Functional analysis of tobacco LIM protein Ntlim1 involved in lignin biosynthesis. Plant J. **22**: 289-301.

Kawasaki, T., Koita, H., Nakatsubo, T., Hasegawa, K., Wakabayashi, K., Takahashi, H., Umemura, K., Umezawa, T., Shimamoto, K. (2006) Cinnamoyl-CoA reductase, a key enzyme in lignin biosynthesis, is an effector of small GTPase Rac in defense signaling in rice. Proc. Natl. Acad. Sci. USA. **103**:230-235.

Kim, S.J., Kim, K.W., Cho, M.H., Franceschi, V.R., Davin, L.B., Lewis, N.G. (2007) Expression of cinnamyl alcohol dehydrogenases and their putative homologues during Arabidopsis thaliana growth and development: Lessons for database annotations? Phytochemistry **68**: 1957-1974.

Kim, S.J., Kim, M.R., Bedgar, D.L., Moinuddin, S.G., Cardenas, C.L., Davin, L.B., Kang, C., Lewis, N.G. (2004) Functional reclassification of the putative cinnamyl alcohol dehydrogenase multigene family in *Arabidopsis*. Proc. Natl. Acad. Sci. USA. **101**: 1455-1460.

Kim, Y.H., Kim, C.Y., Son, W.K., Park, D.S., Kwon, S.Y., Lee, H.S., Bang, J.W., Kwak, S.S. (2008) Overexpression of sweetpotato swpa4 peroxidase results in increased hydrogen peroxide production and enhances stress tolerance in tobacco. Planta **227**: 867-881.

Kim, Y.J., Kim, D.G., Lee, S.H., Lee, I. (2006) Wound-induced expression of the ferulate 5-hydroxylase gene in *Camptotheca acuminata*. Biochim. Biophys. Acta **1760**: 182-190.

Knee, M., Sargent, J.A., Osborne, D.J. (1977) Cell wall metabolism in developing strawberry fruit. J. Exp. Bot. **28**: 377-396.

Koutaniemi, S., Warinowski, T., Kärkönen, A., Alatalo, E., Fossdal, C.G., Saranpää, P., Laakso, T., Fagerstedt, K.V., Simola, L.K., Paulin, L., Rudd, S., Teeri, T.H. (2007) Expression profiling of the lignin biosynthetic pathway in Norway spruce using EST sequencing and real-time RT-PCR. Plant Mol. Biol. **65**:311-328.

Kusumoto, D. (2005) Concentrations of lignin and wall-bound ferulic acid after wounding in the phloem of *Chamaecyparis obtusa*. Trees-Struct. Funct. **19**: 451-456.

Lacombe, E., Hawkins, S., Van Doorsselaere, J., Piquemal, J., Goffner, D., Poeydomenge, O., Boudet, A.M., Grima-Pettenati, J. (1997) Cinnamoyl CoA reductase, the first committed enzyme of the lignin branch biosynthetic pathway: cloning, expression and phylogenetic relationships. Plant J. **11**:429-441.

Lagrimini, L.M., Bradford, S., Rothstein, S. (1990) Peroxidase induced wilting in transgenic tobacco plants. Plant Cell **2**:7-18.

Lagrimini, L.M., Joly, R.J., Dunlap, J.R., Liu, T.T. (1997) The consequence of peroxidase overexpression in transgenic plants on root growth and development. Plant Mol. Biol. **33**:887-895.

Lapierre, C., Pollet, B., Petit-Conil, M., Toval, G., Romero, J., Pilate, G., Leple, J.C., Boerjan, W., Ferret, V., De Nadai, V., Jouanin, L. (1999) Structural alterations of lignins in transgenic poplars with depressed cinnamyl alcohol dehydrogenase or caffeic acid *O*-methyltransferase activity have an opposite impact on the efficiency of industrial kraft pulping. Plant Physiol. **119**:153-163.

Lauvergeat, V., Lacomme, C., Lacombe, E., Lasserre, E., Roby, D., Grima-Pettenati, J. (2001) Two cinnamoyl-CoA reductase (CCR) genes from *Arabidopsis thaliana* are ifferentially expressed during development and in response to infection with pathogenic bacteria. Phytochemistry **57**: 1187-1195.

Lazo, G.R., Pascal, A.S., Ludwig, R.A. (1991) A DNA transformation-competent *Arabidopsis* genomic library in *Agrobacterium*. Biotechnology **9**: 963-967.

Lefever, G., Vieuille, M., Delage, N., D'Harlingue, A., de Monteclerc, J., Bompeix, G. (2004) Characterization of cell wall enzyme activities, pectin composition, and technological criteria of strawberry cultivars (*Fragaria* × *ananassa* Duch). J. food Sci. **69**:221-226.

Li, L., Cheng, X.F., Leshkevich, J., Umezawa, T., Harding, S.A., Chiang, V.L. (2001) The last step of syringyl monolignol biosynthesis in angiosperms is regulated by a novel gene encoding sinapyl alcohol dehydrogenase. Plant Cell **13**: 1567-1585.

Li, L., Cheng, X., Lu, S., Nakatsubo, T., Umezawa, T., Chiang, V.L. (2005) Clarification of cinnamoyl co-enzyme A reductase catalysis in monolignol biosynthesis of Aspen. Plant Cell Physiol. **46**:1073-1082.

Li, L., Osakabe, Y., Joshi, C.P., Chiang, V.L. (1999) Secondary xylem-specific expression of caffeoyl-coenzyme A 3-O-methyltransferase plays an important role in the methylation pathway associated with lignin biosynthesis in loblolly pine. Plant Mol. Biol. **40**: 555-565.

Li, X., Chapple, C. (2010) Understanding lignifications: Challenges beyond monolignol biosynthesis. Plant Physiol. **154**:449-452.

Li, Y., Kajita, S., Kawai, S., Katayama, Y., Morohoshi, N. (2003) Down-regulation of an anionic peroxidase in transgenic aspen and its effect on lignin characteristics. J. Plant Res. **116**: 175-182.

Liao, Z., Chen, M., Guo, L., Gong, Y., Tang, F., Sun, X., Tang, K. (2004) Rapid isolation of high-quality total RNA from *Taxus* and *Ginkgo*. Prep. Biochem. Biotech. **34**: 209-214.

Liu, G., Sheng, X., Greenshields, D.L., Ogieglo, A., Kaminskyj, S., Selvaraj, G., Wei, Y. (2005) Profiling of wheat class III peroxidase genes derived from powdery mildew-attacked epidermis reveals distinct sequence-associated expression patterns. Mol. Plant Microbe Interact. **18**: 730-741.

Livak, K.J., Schmittgen, T.D. (2001) Analysis of relative gene expression data using real-time quantitative PCR and the $2^{-\Delta\Delta CT}$ method. Methods **25**: 402-408.

Lodhi, M.A., Ye, G.N., Weeden, N.F., Reisch, B.I. (1994) A simple and efficient method for DNA extraction from grapevine cultivars *Vitis* species. Plant Mol. Bio. Rep. **12**: 6-13.

Lunkenbein, S., Bellido, M., Aharoni, A., Salentijn, E.M.J., Kaldenhoff, R., Coiner, H.A., Muñoz-Blanco, J., Schwab, W. (2006a) Cinnamate metabolism in ripening fruit. Characterization of a UDP-glucose: cinnamate glucosyltransferase from strawberry. Plant Physiol. **140**:1047-1058.

Lunkenbein, S., Coiner, H.A., Ric de Vos, C.H., Schaart, J.G., Boone, M.J., Krens, F.A., Schwab, W., Salentijn, E.M.J. (2006b) Molecular characterization of a stable antisense chalcone synthase phenotype in strawberry (*Fragaria* × *ananassa*). J. Agric. Food Chem. **54**:2145-2153.

Lüderitz, T., Schatz, G., Grisebach, H. (1982) Enzymic synthesis of lignin precursors. Purification and properties of 2-coumarate: CoA ligase from cambial sap of spruce (*Picea abies* L.). Eur. J. Biochem. **123**: 583-586.

Määttä-Riihinen, K.R, Kamal-Eldin, A., Törrönen, A.R. (2004) Identification and quantification of phenolic compounds in berries of Fragaria and Rubus species (family Rosaceae). J. Agric. Food Chem. **52**: 6178-6187.

Ma, Q.H. (2007) Characterization of a cinnamoyl-CoA reductase that is associated with stem development in wheat. J. Exp. Bot. **58**:2011-2021.

Ma, Q.H. (2010) Functional analysis of a cinnamyl alcohol dehydrogenase involved in lignin biosynthesis in wheat. J. Exp. Bot. **61**: 2735-2744.

Ma, Q.H., Tian, B. (2005) Biochemical characterization of a cinnamoyl-CoA reductase from wheat. Biol. Chem. **386**: 553-560.

Ma, Y., Sun, H., Zhao, G., Dai, H., Gao, X., Li, H., Zhang, Z. (2008) Isolation and characterization of genomic retrotransposon sequences from octoploid strawberry (*Fragaria* × *ananassa* Duch.). Plant Cell Rep. **27**: 499-507.

Manning, K. (1998) Genes for fruit quality in strawberry. CAB International, Wallingford, UK, pp 51-61, ISBN 0-85199-281-1.

Mansouri, I.E., Mercado, J.A., Santiago-Doménech, N., Pliego-Alfaro, F., Valpuesta, V., Quesada, M.A. (1999) Biochemical and phenotypical characterization of transgenic tomato plants overexpression a basic peroxidase. Physiol. Plant **106**: 355-362.

Marjamaa, K., Kukkola, E.M., Fagerstedt, K.V. (2009) The role of xylem class III peroxidases in lignifications. J. Exp. Bot. **60**:367-376.

Martinez, A.T., Speranza, M., Ruiz-Duenas, F.J., Ferreira, P., Camarero, S., Guillen, F., Martinez, M.J., Gutierrez, A., del Rio, J.C. (2005) Biodegradation of lignocellulosics: microbial, chemical, and enzymatic aspects of the fungal attack of lignin. Int. Microbiol. **8**: 195-204.

McLusky, S.R., Bennett, M.H., Beale, M.H., Lewis, M.J., Gaskin, P., Mansfield, J.W. (1999) Cell wall alterations and localized accumulation of feruloyl-3'-methaxytyramine in onion epidermis at sites of attempted penetration by *Botrytis allii* are associated with actin polarization, peroxidases activity and suppression of flavonoid biosynthesis. Plant J. **17**: 523-534.

Medina-Escobar, N., Cárdenas, J., Moyano, E., Caballero, J.L., Muñoz-Blanco, J. (1997) Cloning, molecular characterization and expression pattern of a strawberry ripening-specific cDNA with sequence homology to pectate lyase from higher plants. Plant Mol. Biol. **34**: 867-877.

Meyer, K., Shirley, A.M., Cusumano, J.C., Bell-Lelong, D.A., Chapple, C. (1998) Lignin monomer composition is determined by the expression of a cytochrome P450-dependent monooxygenase in *Arabidopsis*. Proc. Natl. Acad. Sci. USA. **95**: 6619-6623.

Moerschbacher, B.M., Noll, U., Gorrichon, L., Reisener, H-J. (1990) Specific inhibition of lignification breaks hypersensitive resistance of wheat to stem rust. Plant Physiol. **93**: 465-470.

Moura, J.C.M.S., Bonine, C.A.V., Viana, J.O.F., Dornelas, M.C., Mazzafera, P. (2010) Abiotic and biotic stresses and changes in the lignin content and composition in plants. J. Integr. Plant Biol. **52**: 360-376.

Napoli, C., Lemieux, C., Jorgensen, R. (1990) Introduction of a chimeric chalcone synthase gene into petunia results in reversible co-suppression of homologous genes *in trans*. Plant Cell **2**:279-289.

Nicholson, R.L., Hammerschmidt, R. (1992) Phenolic compounds and their role in disease resistance. Annu. Rev. Phytopathol. **30**:369-389.

Nogata, Y., Ohta, H., Voragen, A.G.J. (1993) Polygalacturonase in strawberry fruit. Phytochemistry **34**:617-620.

O'Malley, D.M., Porter, S., Sederoff, R.R. (1992) Purification, characterization, and cloning of cinnamyl alcohol dehydrogenase in loblolly pine (*Pinus taeda* L). Plant Physiol. **98**:1364-1371.

Palmer, N.A., Sattler, S.E., Saathoff, A.J., Funnell, D., Pedersen, J.F., Sarath, G. (2008) Genetic background impacts soluble and cell wall-bound aromatics in brown midrib mutants of sorghum. Planta **229**:115-127.

Parrott, D.L., Anderson, A.J., Carman, J.G. (2002) *Agrobacterium* induces plant cell death in wheat (*Triticum aestivum* L.). Physiol. Mol. Plant Pathol. **60**: 59-69.

Passardi, F., Cosio, C., Penel, C., Dunand, C. (2005) Peroxidases have more functions than a Swiss army knife. Plant Cell Rep. **24**: 255-265.

Passardi, F., Longet, D., Penel, C., Dunand, C. (2004a) The class III peroxidase multigenic family in rice and its evolution in land plants. Phytochemistry **65**: 1879-1893.

Passardi, F., Penel, C., Dunand, C. (2004b) Performing the paradoxical: how plant peroxidases modify the cell wall. Trends Plant Sci. **9**: 534-540.

Passardi, F., Tognolli, M., de Meyer, M., Penel, C., Dunand, C. (2006) Two cell wall associated peroxidases from Arabidopsis influence root elongation. Planta **223**:965-974.

Patzlaff, A., McInnis, S., Courtenay, A., Surman, C., Newman, L.J., Smith, C., Bevan, M.W., Mansfield, S., Whetten, R.W., Sederoff, R.R., Campbell, M.M. (2003) Characterisation of a pine MYB that regulates lignification. Plant J. **36**:743-754.

Pedreira, J., Herrera, M.T., Zarra, I., Revilla, G. (2011) The overexpression of *AtPOD37*, an apoplastic peroxidase, reduces growth in *Arabidopsis*. Physiol. Plant. **141**:177-187.

Pereira, D.M., Valentão, P., Pereira, J.A., Andrade, P.B. (2009) Phenolics: From Chemistry to Biology. Molecules **14**:2202-2211.

Perkins-Veazie, P. (1995) Growth and ripening of strawberry fruit. Horticultural Reviews **17**:267-297.

Petersen, M., Strack, D., Matern, U. (1999) Biosynthesis of Phenylpropanoids and Related Compounds. (Sheffield, UK: Sheffield Academic Press).

Pichon, M., Courbou, I., Beckert, M., Boudet, A.M., Grima-Pettenati, J. (1998) Cloning and characterization of two maize cDNAs encoding cinnamoyl-CoA reductase (CCR) and differential expression of the corresponding genes. Plant Mol. Biol. **38**:671-676.

Piquemal, J., Lapierre, C., Myton, K., O'Connell, A., Schuch, W., Grima-Pettenati, J., Boudet, A.M. (1998) Down-regulation of cinnamoyl-CoA reductase induces significant changes of lignin profiles in transgenic tobacco plants. Plant J. **13**: 71-83.

Potter, D., Eriksson, T., Evans, R.C., Oh, S., Smedmark, J.E.E., Morgan, D.R., Kerr, M., Robertson, K.R., Arsenault, M., Dickinson, T.A., Campbell C.S. (2007) Phylogeny and classification of Rosaceae. Plant Syst. Evol. **266**: 5-43.

Potter, D., Luby, J.J., Harrison, R.E. (2000) Phylogenetic relationships among species of Fragaria (Rosaceae) inferred from non-coding nuclear and chloroplast DNA sequences. Syst. Bot. **25**: 337-348.

Raab, T., López-Ráez, J.A., Klein, D., Caballero, J.L., Moyano, E., Schwab, W., Muñoz-Blanco, J. (2006) FaQR, required for the biosynthesis of the strawberry flavor compound 4-hydroxy-2,5-dimethyl-3(2H)-furanone, encodes an enone oxidoreductase. Plant Cell **18**: 1023-1037.

Raes, J., Rohde, A., Christensen, J.H., Van de Peer, Y., Boerjan, W. (2003) Genome-wide characterization of the lignification toolbox in *Arabidopsis*. Plant Physiol. **133**: 1051-1071.

Rahantamalala, A., Rech, P., Martinez, Y., Chaubet-Gigot, N., Grima-Pettenati, J., Pacquit, V. (2010) Coordinated transcriptional regulation of two key genes in the lignin branch pathway-*CAD* and *CCR*-is mediated through MYB- binding sites. BMC Plant Biol. **10**:130-142.

Ralph, J., Hatfield, R.D., Piquemal, J., Yahiaoui, N., Pean, M., Lapierre, C., Boudet, A.M. (1998) NMR characterization of altered lignins extracted from tobacco plants down-regulated for lignification enzymes cinnamyl alcohol dehydrogenase and cinnamoyl-CoA reductase. Proc. Natl. Acad. Sci. USA. **95**: 12803-12808.

Ralph, J., Kim, H., Lu, F., Grabber, J.H., Leple, J.C., Berrio-Sierra, J., Derikvand, M.M., Jouanin, L., Boerjan, W., Lapierre, C. (2008) Identification of the structure and origin of a thioacidolysis marker compound for ferulic acid incorporation into angiosperm lignins (and an indicator for cinnamoyl CoA reductase deficiency). Plant J. **53**: 368-379.

Ralph, J., Lapierre, C., Marita, J.M., Kim, H., Lu, F., Hatfield, R.D., Ralph, S., Chapple, C., Franke, R., Hemm, M.R., Van Doorsselaere, J., Sederoff, R.R., O'Malley, D.M., Scott, J.T., MacKay, J.J., Yahiaoui, N., Boudet, A., Pean, M., Pilate, G., Jouanin, L., Boerjan, W. (2001) Elucidation of new structures in lignins of CAD- and COMT-deficient plants by NMR. Phytochemistry **57**:993-1003.

Rautengarten, C., Baidoo, E., Keasling, J.D., Scheller, H.V. (2010) A simple method for enzymatic synthesis of unlabeled and radiolabeled hydroxycinnamate-CoA. Bioenerg. Res. **3**:115-122.

Reimers, P.J., Leach, J.E. (1991) Race-specific resistance to *Xanthomonas oryzae* pv. *oryzae* conferred by bacterial blight resistance gene Xa-10 in rice (*Oryza sativa*) involves accumulation of a lignin-like substance in host tissues. Physiol. Mol. Plant Pathol. **38**:39-55.

Robinson, A.R, Mansfield, S.D. (2009) Rapid analysis of poplar lignin monomer composition by a streamlined thioacidolysis procedure and near-infrared reflectance-based prediction modeling. Plant J. **58**:706-714.

Ronald, H.A.P. (2002) RNA silencing: the genome's immune system. Sci. **296**:1263-1265.

Rosli, H.G., Civello, P.M., Martínez, G.A. (2004) Changes in cell wall composition of three *Fragaria* × *ananassa* cultivars with different softening rate during ripening. Plant Physiol. Biochem. **42**:823-831.

Ruiz-Dueñas, F.J., Camarero, S., Perez-Boada, M., Martinez, M.J., Martinez, A.T. (2001) A new versatile peroxidase from Pleurotus. Biochem. Soc. Trans. **29**: 116-122.

Rushton, P.J., Reinstädler, A., Lipka, V., Lippok, B., Somssich, I.E. (2002). Synthetic plant promoters containing defined regulatory elements provide novel insights into pathogen- and wound-induced signaling. Plant Cell **14**:749-762.

Rushton, P.J, Somssich, I.E. (1998) Transcriptional control of plant genes responsive to pathogens. Curr. Opin. Plant Biol. **1**:311-315.

Saballos, A., Ejeta, G., Sanchez, E., Kang, C., Vermerris, W. (2009) A genomewide analysis of the cinnamyl alcohol dehydrogenase family in Sorghum [*Sorghum bicolor* (L.) Moench] identifies *SbCAD2* as the *Brown midrib6* gene. Genetics **181**: 783-795.

Salentijn, E.M.J., Aharoni, A., Schaart, J.G., Boone, M.J., Krens, F.A. (2003) Differential gene expression analysis of strawberry cultivars that differ in fruit-firmness. Physiol. Plant. **118**: 571-578.

Santos-Buelga, C., Scalbert, A. (2000) Proanthocyanidins and tanninlike compounds: nature, occurrence, dietary intake, and effects on nutrition and health. J. Sci. Food Agric. **80**: 1094-1117.

Sarni, F., Grand, C., Boudet, A.M. (1984) Purification and properties of cinnamoyl-CoA reductase and cinnamyl alcohol dehydrogenase from poplar stems (*Populus* × *eurarnericana*). Eur. J. Biochem. **139**: 259-265.

Sato, Y., Demura, T., Yamawaki, K., Inoue, Y., Sato, S., Sugiyama, M., Kukuda, H. (2006) Isolation and characterization of a novel peroxidase gene ZPO-C whose expression and function are closely associated with lignification during tracheary element differentiation. Plant Cell Physiol. **47**: 493-503.

Schaart, J.G., Mehli, L., Schouten, H.J. (2005) Quantification of allele-specific expression of a gene encoding strawberry polygalacturonase-inhibiting protein (PGIP) using Pyrosequencing^{TM}. Plant J. **41**: 493-500.

Schwab, W., Hoffmann, T., Kalinowski, G., Preuß, A. (2011) Functional genomics in strawberry fruit through RNAi-mediated silencing. Genes, Genomes, Genomics **5**:91-101.

Shulaev, V., Sargent, D.J., Crowhurst, R.N., Mockler, T.C., Folkerts, O., Delcher, A.L., Jaiswal., P., Mockaitis, K., Liston, A., Mane, S.P., Burns, P., Davis, T.M., Slovin, J.P., Bassil, N., Hellens, R.P., Evans, C., Harkins, T., Kodira, C., Desany, B., Crasta, O.R., Jensen, R.V., Allan, A.C., Michael, T.P., Setubal, J.C., Celton, J.M., Rees, D.J.G., Williams, K.P., Holt, S.H., Ruiz Rojas, J.J., Chatterjee, M., Liu, B., Silva, H., Meisel, L., Adato, A., Filichkin, S.A., Troggio, M., Viola, R., Lynn Ashman, T., Wang, H., Dharmawardhana, P., Elser, J., Raja, R., Priest, H.D., Bryant, D.W., Fox, S.E., Givan, S.A., Wilhelm, L.J., Naithani, S., Christoffels, A., Salama, D.Y., Carter, J., Lopez Girona, E., Zdepski, A., Wang, W., Kerstetter, R.A., Schwab, W., Korban, S.S., Davik, J., Monfort, A., Denoyes-Rothan, B., Arus, P., Mittler, R., Flinn, B., Aharoni, A., Bennetzen, J.L., Salzberg, S.L., Dickerman, A.W., Velasco, R., Borodovsky, M., Veilleux, R.E., Folta, K.M. (2011) The genome of woodland strawberry (*Fragaria vesca*). Nature Genet. **43**:109-118.

Singh, K.K., Reddy, B.S. (2006) Post-harvest physico-mechanical properties of orange peel and fruit. J. food Eng. **73**: 112-120.

Smith, N.A., Singh, S.P., Wang, M.-B., Stoutjesdijk, P., Green, A., Waterhouse, P.M., (2000) Total silencing by intron-silencing by intron-spliced hairpin RNAs. Nature **407**:319-320.

Soltani, B.M., Ehlting, J., Hamberger, B., Douglas, C.J. (2006) Multiple cis-regulatory elements regulate distinct and complex patterns of developmental and wound-induced expression of *Arabidopsis thaliana* 4CL gene family members. Planta **224**: 1226-1238.

Somssich, I.E., Wernert, P., Kiedrowski, S., Hahlbrock, K. (1996) *Arabidopsis thaliana* defense-related protein ELI3 is an aromatic alcohol: $NADP^+$ oxidoreductase. Proc. Natl. Acad. Sci. USA. **93**: 14199-14203.

Stewart, D., Yahiaoui, N., McDougall, G.J., Myton, K., Marque, C., Boudet, A.M., Haigh, J. (1997) Fourier-transform infrared and Raman spectroscopic evidence for the incorporation of cinnamaldehydes into the lignin of transgenic tobacco (*Nicotiana tabacum* L.) plants with reduced expression of cinnamyl alcohol dehydrogenase. Planta **201**: 311-318.

Stöckigt, J., Zenk, M.H. (1975) Chemical syntheses and properties of hydroxycinnamoyl-coenzyme A derivatives. Z. Naturforsch. **30**: 352-358.

Tamasloukht, B., Wong Quai Lam, M.S., Martinez, Y., Tozo, K., Barbier, O., Jourda, C., Jauneau, A., Borderies, G., Balzergue, S., Renou, J.P., Huguet, S., Martinant, J.P., Tatout, C., Lapierre, C., Barrière, Y., Goffner, D., Pichon, M. (2011) Characterization of a cinnamoyl-CoA reductase 1 (CCR1) mutant in maize: effects on lignification, fibre development, and global gene expression. J. Exp. Bot. **62**:3837-3848.

Teixeira, F.K., Menezes-Benavente, L., Margis, R., Margis-Pinheiro, M. (2004) Analysis of the molecular evolutionary history of the ascorbate peroxidase gene family: inferences from the rice genome. J.Mol. Evol. **59**: 761-770.

Tognolli, M., Penel, C., Greppin, H., Simon, P. (2002) Analysis and expression of the class III peroxidase large gene family in *Arabidopsis thaliana*. Gene **288**: 129-138.

Tokunaga, N., Kaneta, T., Sato, S., Sato, Y. (2009) Analysis of expression profiles of three peroxidase genes associated with lignification in *Arabidopsis thaliana*. Physiol. Plantarum. **136**: 237-249.

Tu, Y., Rochfort, S., Liu, Z., Ran, Y., Griffith, M., Badenhorst, P., Louie, G.V., Bowman, M.E., Smith, K.F., Noel, J.P., Mouradov, A., Spangenberg, G. (2010) Functional analyses of caffeic acid O-Methyltransferase and Cinnamoyl-CoA-reductase genes from perennial ryegrass (*Lolium perenne*). Plant Cell **22**:3357-3373.

Vance, V., Vaucheret, H. (2001) RNA silencing in plants-defense and counterdefense. Sci. **292**:2277-2280.

van der Rest, B., Danoun, S., Boudet, A.M., Rochange, S.F. (2006) Down-regulation of cinnamoyl-CoA reductase in tomato (*Solanum lycopersicum* L.) induces dramatic changes in soluble phenolic pools. J. Exp. Bot. **57**:1399-1411.

Vanholme, R., Demedts, B., Morreel, K., Ralph, J., Boerjan, W. (2010) Lignin biosynthesis and structure. Plant Physiol. **153**:895-905.

van Loon, L.C., Rep, M., Pieterse, C.M. (2006) Significance of inducible defense-related proteins in infected plants. Annu. Rev. Phytopathol. **44**:135-162.

Vaucheret, H., Béclin, C., Fagard, M. (2001) Post-transcriptional gene silencing in plants. J. Cell Sci. **114**:3083-3091.

Vitali, A., Botta, B., Delle Monache, G., Zappitelli, S., Ricciardi, P., Melino, S., Petruzelli, R., Giardina, B. (1998) Purification and partial characterization of a peroxidase from plant cell cultures of *Cassia didymobotrya* and biotransformation studies. Biochem. J. **331**:513-519.

Vogt, T. (2010) Phenylpropanoid biosynthesis. Mol. Plant **3**:2-20.

Walter, M.H., Schaf, J., Hess, D., Geibel, M., Treutter, D., Feucht, W. (1994) Gene activation in lignin biosynthesis: pattern of promoter activity of a tobacco cinnamyl-alcohol dehydrogenase gene. Acta Hortic. **381**:162-168.

Ward, G., Hadar, Y., Bilkis, I., Konstantinovsky, L., Dosoretz, C.G. (2001) Initial steps of ferulic acid polymerization by lignin peroxidase. J. Biol. Chem. **276**:18734-18741.

Waterhouse, P.M., Wang, M.-B., Finnegan, E.J. (2001a) Role of short RNAs in gene silencing. Trends Plant Sci. **6**: 297-301.

Waterhouse, P.M., Wang, M.-B., Lough, T. (2001b) Gene silencing as an adaptive defence against viruses. Nature **411**:834-842.

Waugh, D.S. (2005) Making the most of affinity tags. Trends Biotechnol. **23**:316-320.

Welinder, K.G. (1992) Superfamily of plant, fungal and bacterial peroxidases. Curr. Opin. Struct. Biol. **2:** 388-393.

Welinder, K.G., Justesen, A.F., Kjaersgård, I.V., Jensen, R.B., Rasmussen, S.K., Jespersen, H.M., Duroux, L. (2002) Structural diversity and transcription of class III peroxidases from *Arabidopsis thaliana*. Eur. J. Biochem. **269**: 6063-6081.

Wengenmayer, H., Ebel, J., Grisebach, H. (1976) Enzymic synthesis of lignin precursors: purification and properties of a cinnamoyl-CoA: NADPH reductase from cell suspension cultures of soybean (Glycine max). Eur. J. Biochem. **65**: 529-536.

Weng, J.-K., Chapple, C. (2010) The origin and evolution of lignin biosynthesis. New Phytol. **187**: 273-285.

Wesley, S.V., Helliwell, C.A., Smith, N.A., Wang, M., Rouse, D.T., Liu, Q., Gooding, P.S., Singn, S.P., Abbott, S., Stoutjesdijk, P.A., Robinson, S.P., Gleave, A.P., Green, A.G., Waterhouse, P.M. (2001) Construct design for efficient, effective and high-throughput gene silencing in plants. Plant **27**:581-590.

Whetten, R.W., MacKay, J.J., Sederoff, R.R. (1998) Recent advances in understanding lignin biosynthesis. Annu. Rev. Plant Physiol. Plant Mol. Biol. **49**:585-609.

Yokoyama, R., Nishitani, K. (2006) Identification and characterization of *Arabidopsis thaliana* genes involved in xylem secondary cell walls. J. Plant Res.**119**: 189-194.

Zhang, J., Wang, X., Yu, O., Tang, J., Gu, X., Wan, X., Fang, C. (2011) Metabolic profiling of strawberry (*Fragaria* × *ananassa* Duch.) during fruit development and maturation. J. Exp. Bot. **62**:1103-1118.

Zhang, S.H., Yang, Q., Ma, R.C. (2007) Erwinia carotovora ssp. Carotovora infection induced "defense lignin" accumulation and lignin biosynthetic gene expression in chinese cabbage (*Brassica rapa* L. ssp. pekinensis). J. Integr. Plant Biol. **49**: 993-1002.

Zierold, U., Scholz, U., Schweizer, P. (2005) Transcriptome analysis of *mlo*-mediated resistance in the epidermis of barley. Mol. Plant Pathol. **6**: 139-151.

VII. Appendix

A. Degenerate primers designed

A.1. CCR

The degenerate CCR-FD primer, based on the translation of deduced amino acids (GenBank database) to their corresponding nucleotides, was designed as follows:

Name	Sequences (5' to 3')	Accession numbers
CCR-FD:	**atg cct gYY gat VHY WSM tcW**	**(in this study)**
CCR	atg cct gtt gat gct tca tca	(*Populus trichocarpa*, AJ224986)
CCR_AJ	atg cct gtt gat gct tca tca	(*Populus balsamifera*, AJ295838)
CCR_AY	atg cct gct gat cac agc tct	(*F. ananassa* CCR-1 allele, AY285922)
CCR1	atg cct gtc gat att tca tca	(*P. trichocarpa*, XM_002332042)
CCR2	atg cct gtc gat act tca tca	(*P. trichocarpa*, XM_002332044)
CCR3	atg cct gtc gat act tca tca	(*P. trichocarpa*, XM_002332047)
CCR4	atg cct gtc gat act tca tca	(*P. trichocarpa*, XM_002332048)
CCR5	atg cct gtc gat act tca tca	(*P. trichocarpa*, XM_002299223)
CCR6	atg cct gtc gat act tca tca	(*P. trichocarpa*, XM_002299224)
CCR7	atg cct gtt gat gct tca tca	(*P. trichocarpa*, XM_002303809)

(A double underline indicates H= A/T/C; M=A/C; S=G/C; V=G/A/C; W= A/T; Y=T/C)

The degenerate CCR-RD primer, based on the translation of deduced amino acids (GenBank database) to their corresponding nucleotides, was designed as follows:

Name	Sequences (5' to 3')	Accession numbers
CCR-RD	**TTATTGRATYTTSAHRGASTC**	**(in this study)**
CCR	TTATTGAATTTTCAAAGACTC	(*P. trichocarpa*, AJ224986)
CCR_AJ	TTATTGAATTTTCAAAGACTC	(*Populus balsamifera*, AJ295838)
CCR_AY	TTATTGGATCTTGATGGACTC	(*F. ananassa* CCR-1 allele, AY285922)
CCR2	TTATTGAATTTTCACAGAGTC	(*P. trichocarpa*, XM_002332044)
CCR7	TTATTGAATTTTCAAAGACTC	(*P. trichocarpa*, XM_002303809)

(A double underline indicates H= A/T/C; R= G/A; S=G/C; Y=T/C)

A.2. CAD

The degenerate CAD-FD and CAD-RD primer, based on the translation of deduced amino acids (GenBank databases) to their corresponding nucleotides, were designed as follows:

Name	Sequences (5’ to 3’)	Accession numbers
CAD-FD	**ATGKCTATCGAGCAAGAACAC**	**(in this study)**
CAD_U	ATGGCTATCGAGCAAGAACAC	(*F. ananassa,* U63534)
CAD_A	ATGTCTATCGAGCAAGAACAC	(*F. ananassa,* AF320110)
CAD-RD	**TTAAGASCTARCCTTCAGTGT**	**(in this study)**
CAD_U	TTAAGACCTAACCTTCAGTGT	(*F. ananassa,* U63534)
CAD_A	TTAAGAGCTAGCCTTCAGTGT	(*F. ananassa,* AF320110)

(A double underline indicates K= G/T; R= G/A; S=G/C)

B. The main coding sequence used for constructs

B.1. The full-length coding sequence of *FaCCR* (accession number JX290510)

atgcctgttgataactgctcttcactttccggccatggccaaactgtgtgtgtcaccggagccggaggcttcttcgcttcttggttggtga
agctcctgctggagagaggctataatgtgagaggaaccgtcagaaacccagaggacccaaagaatgctcatctgagggagctgga
aggagccaaagagaggctgagcttgcggaaagccgatcttctggatttcgagagcctgaaagaagccattaacggctgtgatggcg
ttttccacactgcatcgcctgtaactgatgatccggaacaaatggtggaaccggcagtgaatggaacaaagaatgtgatcgttgccgc
tgctgaagccaaggttaaacgcgtcgtcttcacgtcttcaatcggtgccgtctacatggacccagcccgaggtcccgatgtcgttgtcg
acgagtcttgttggagtgacctcgagttttgcaagaacaccaagaactggtactgctacggcaaagctgtggcggagcaagcagcgt
gggaagaggccaaagagagaggagtggacttggtggtggtgaacccagttctggtgcttggaccactgctccaaccaaccatcaa
cgccagcatcatccacattctcaagtacttgactggctcggccaagacttatgccaattctgttcaggcctatgtgcatgtcaaggatgt
ggcattagcacacatactggtgtacgaaactccctcggcatctggccgttatctctgcgccgagagcgtccttcaccgtggagatgtg
gtcgaaatcctcgccaagttcttccctgaataccccatacccagcaagttgaaagacgatgggaaacccagagcaataccctacaag
ttttcaaaccagaagctacaagacttgggtttggagttcacttctgtgaaacagagcctatatgacactgtcaagagcttgcaggagaa
gggtcaccttaaggttcctacaaagcaagaagaagactccttcaaaatccaataa

B.2. The full-length coding sequence of *FaCAD* (accession number JX290511)

atgtctatcgagcaagaacaccccaagaaggcatctggatgggctgcaagagattcatctggtgttctctctcccttcaatttctacaga
agggaaaccggagagaaagacgtgacgttcaaagtgttgtactgtgggatttgccattcggaccttcacatggtcaagaatgaatgg
ggcttctctacctattctctggttccagggcatgagattgttggtgaagttacggaagtagggagcaaagtacaaaaatttaaagttgga
gacagagtcggtgttggatgcattgtgggatcttgccgatcttgtgaaaattgtaccgaccaccttgagaactactgccccaaacagat
actcacttacggtgccaagtactacgacggaagcaccacctatggcggttactctgacattatggtggccgatgaacacttcatagtac
gcatcccagacaacttgcctcttgatggtgctgcgccgctcctatgtgccgggattacaacctacagccccctgagatatttcggactt
gacaagcccggcatgcatgtaggtgtggtcggcctaggcggtttaggccacgtcgccgtgaagtttgccaaggctatgggagtgaa
ggttacagtgatcagtacgtcccctaagaaagaggaggaagctcttaaacacctaggagctgactcgtttttggttagccgcgaccaa
gatcaaatgcaggctgccattggtaccatggatgggatcattgacacagtttctgcacaacatcctctcctgcctttgattggtttgttgaa
ctctcatggagagcttgttatggttggtgcaccagagaagcctcttgaactgccagtttttcctttactcatgggaagaaagatggtagct
ggtagcggcattgggggtatgaaggagacacaagagatgatagattttgcagccaagcacaacattacagcagacatcgaagtcat
accaatcgactacttgaacactgctatggagcgtctagtcaaagcagatgtcagataccgttttgtcatcgacattggaaacacactga
aggctagctcttaa

B.3. The full-length coding sequence of FaPOD (accession number JX290512)

atgggttccagagctctcttcttcttctttgccttgctatctctctcagcagtgctttgctttgctgagagcaatgaagaagaccctggtctt
gttatgaacttctatagtgactcatgtcctcaggctgaggagatcgtcagagagcaggtcaagcttctctacaagcgccacaagaaca
ctgctttctcttggctcaggaacatcttccatgactgtgctgtccagtcatgtgatgcttcactacttttggactcaacaaggaggtctttgt
ctgagaaggaaatggacagaagctttgggatgagaaacttcaggtacattgaggagatcaaagaagcattagagagggagtgccct
ggagttgtttcttgctcagatattcttgtcttgtcagccagagaaggagttgttaggctaggaggtccattcatccctcttaaaactggaag
gagagatggtagaaggagcagagctgagatccttgaggagtaccttcctgaccacaatgagagcatgtcaactgttcttgagaaattc
tctgccatgggcattgacacccctggagttgttgcccttcttggagctcacagtgttggaagaacacactgtgtgaagctggtgcaccg
tttgtacccagaagtagacccagctctgaacccagaccatgtccctcacatgcttaagaagtgccctgatgccatccctgaccccaag
gcagtccagtacgtgaggaatgaccgtggtacccccatgatcttcgacaacaactactacaggaacatcttggacaacaagggtttg
atgatggtggaccaccagcttgccacagacaagaggaccaagccctatgtcaagaagatggccaaaagccaggactatttcttcaa
ggagttcacaagagccttcaccattctctccgagaacaaccctcttaccggagacaagggagagatcaggcaacagtgcaatgtgg
ccaacaagctccactag

B.4. The full-length coding sequence of FaPOD27 (accession number JX290513)

atggctgctacttcaaagctcatcttcctcctgatccaagggatcgttctgctttctgttcttgactgtgcaaatgcacagggactgaaagt
agggttctatgcgaagtcgtgcccggaagctgaggccatagtgaagaaggttatcgctcaaaccttgtcggtagcaccttcacttggt
ggtcctttgctgagaatgcatttccatgattgctttgtcaggggttgcgacggttcagtgctactgaattcttcatcaaaccaagccgaga
aggatgcaattccaaacctaagtcttcgagggtatggagtcattgacagagtcaagtctgctttggagaaagcatgccctggagtggtt
tcatgttctgacatcttagccgttgtagctagagatgtcgtcgtcgcggacatgggagtacattgggatgttgaaactggacgaagaga
tggtaatgtatcaaacatgatagatgccttgcgaaatctcccagcacctagttcaaacatctcttcattaaaatcaagctttgcatcaaag
ggtctaagcgctaaagatcttgtagtactatcagggagtcacaccatcgggacatctcactgctcttccttcaccaaccgtctttataact
tcaccggaaagaacgtaaacgataccgatcccaccttggatagcaactacattgcaaagttgaagatgaaatgcaagcccaacgac
caaactactctcgttgagatggatcctgggagtttcaagacatttgacggttcttactatactcttgtggccaagagaaggggtctctttc
agtcagatgcagctcttcttgatgacagtgaaaccaaagcttacgtgacaagccatgccgtaccaaagggagaagctagtttcttgaa
ggattttggtgtttcaatggtgaacatgggaaggatcggagttctcacggggaatgcaggagagatcaggaaagtgtgcagcaagat
caattag

C. The partial coding sequence was used for ihpRNA constructs

C.1. The backbone:

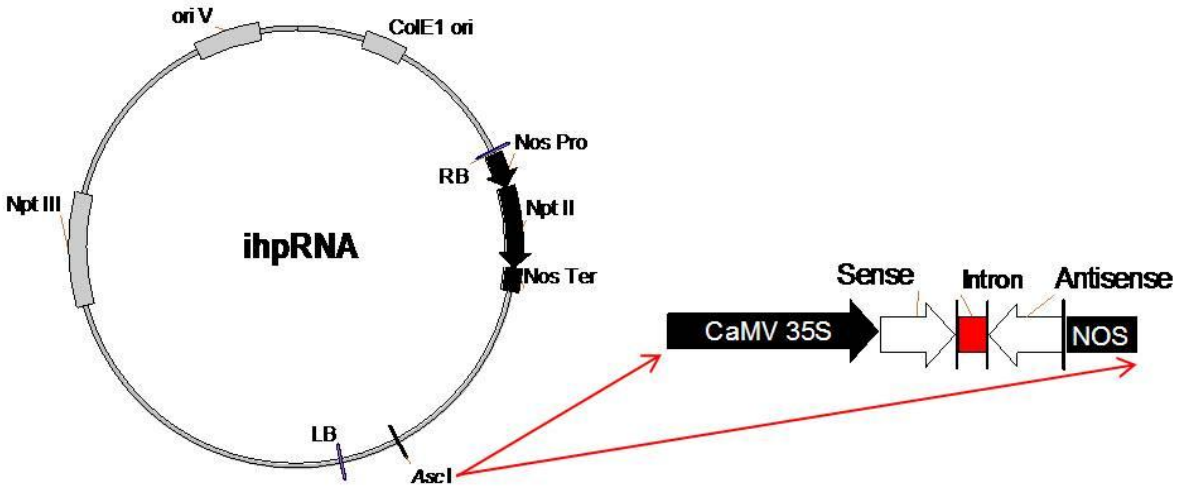

C.2. The following coding sequence (300 bp) was used in sense and antisense orientations:

C.2.1. *FaCCR*:

gtcgtcttcacgtcttcaatcggtgccgtctacatggacccagcccgaggtcccgatgtcgttgtcgacgagtcttgttggagtgacctc
gagttttgcaagaacaccaagaactggtactgctacagcaaagctgtggcggagcaagcagcgtgggaagaggccaaagagaga
ggagtggacttggtggtggtgaacccagttctggtgcttggaccactgctccaaccaaccatcaacgccagcatcatccacattctca
agtacttgactggctcggccaagacttatgccaattct

C.2.2. *FaCAD*:

ttctacagaagggaaaccggagagaaagacgtgacgttcaaagtgttgtactgtgggatttgccattcggaccttcacatggtcaaga
atgaatggggcttctctacctattctctggttccagggcatgagattgttggtgaagttacggaagtagggagcaaagtacaaaaattta
aagttggagacagagtcggtgttggatgcattgtgggatcttgccgatcttgtgaaaattgtaccgaccaccttgagaactactgcccc
aaacagatactcacttacggtgccaagtactac

C.2.3. *FaPOD*:

ctctacaagcgccacaagaacactgctttctcctggctcaggaacatcttccatgactgtgctgtccagtcatgtgatgcttcactactttt
ggactcaacaaggaggtctttgtctgagaaagaaatggacagaagctttgggatgagaaacttcaggtacattgaggagatcaagga
agcattagagagggagtgccctggagttgtttcttgctcagatattcttgtcctgtcagccagagaaggagttgttaggctaggaggtc
cattcatccctcttaaaactggaaggagagat

C.2.4. *FaPOD27*:

atggctgctacttcaaagctcatcttcctcctgatccaagggatcgttctgctttctgttcttgactgtgcaaatgcacagggactgaaagt
agggttctatgcgaagtcgtgcccggaagctgaggccatagtgaagaaggttatcgctcaaaccttgtcggtagcaccttcacttggt
ggtcctttgctgagaatgcatttccatgattgctttgtcaggggttgcgacggttcagtgctactgaattcttcatcaaaccaagccgaga
aggatgcaattccaaacctaagtcttcga

D. Standard curves

- BSA

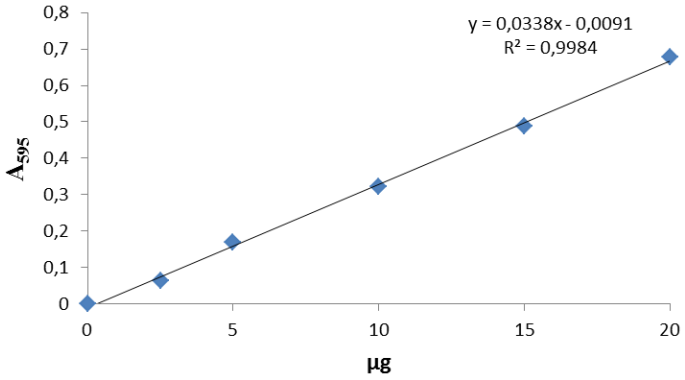

- coniferaldehyde

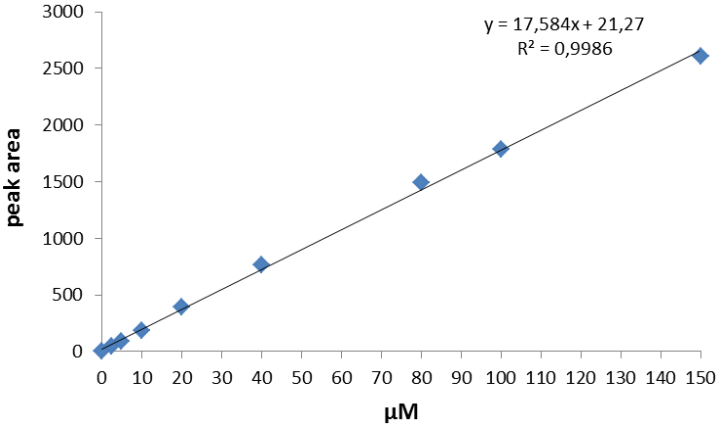

- coniferyl alcohol

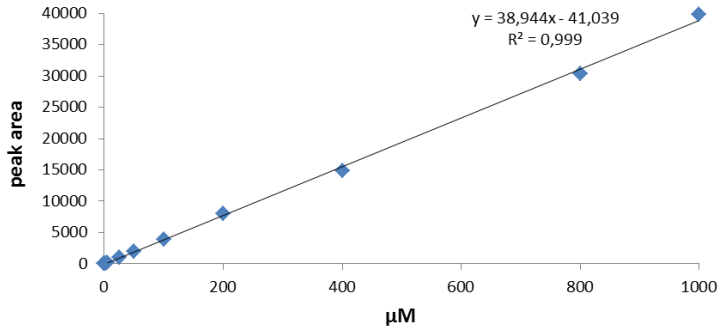

E. Statistical analysis

E.1. Firmness and lignin content

E.1.1. pBI-intron vs. down- and up-regulation of individual *FaCCR*, *FaCAD*, and *FaPOD* in Elsanta

A. Fruit firmness (down-regulation)

Two groups	*P*-value
WT vs. pBI-intron	5.2E-16*
WT vs. pBI-*FaCCRi*	2.4E-15*
WT vs. pBI-*FaCADi*	1.9E-14*
WT vs. pBI-*FaPODi*	2.2E-16*
pBI-intron vs. pBI-*FaCCRi*	1.2E-01
pBI-intron vs. pBI-*FaCADi*	9.9E-01
pBI-intron vs. pBI-*FaPODi*	1.4E-01

B. Fruit firmness (up-regulation)

Two groups	*P*-value
WT vs. pBI-intron	2.2E-16*
WT vs. pBI-*FaCCR*	2.2E-16*
WT vs. pBI-*FaCAD*	2.2E-16*
WT vs. pBI-*FaPOD*	2.2E-16*
pBI-intron vs. pBI-*FaCCR*	1.3E-01
pBI-intron vs. pBI-*FaCAD*	6.6E-01
pBI-intron vs. pBI-*FaPOD*	2.0E-01

C. Lignin content (down-regulation)

Two groups	*P*-value
WT vs. pBI-intron	2.4E-07*
WT vs. pBI-*FaCCRi*	2.9E-06*
WT vs. pBI-*FaCADi*	5.1E-06*
WT vs. pBI-*FaPODi*	2.2E-06*
pBI-intron vs. pBI-*FaCCRi*	4.9E-01
pBI-intron vs. pBI-*FaCADi*	1.4E-02
pBI-intron vs. pBI-*FaPODi*	1.7E-02

D. Lignin content (down-regulation)

Two groups	*P*-value
WT vs. pBI-intron	4.3E-05*
WT vs. pBI-*FaCCR*	4.3E-05*
WT vs. pBI-*FaCAD*	2.2E-05*
WT vs. pBI-*FaPOD*	2.2E-05*
pBI-intron vs. pBI-*FaCCR*	2.8E-01
pBI-intron vs. pBI-*FaCAD*	3.6E-02
pBI-intron vs. pBI-*FaPOD*	3.9E-01

One asterisk (*) indicates significantly increased levels (*P* <1.00E-02).

E.1.2. CHS$^-$/pBI-intron vs. down- and up-regulation of individual *FaCCR*, *FaCAD*, and *FaPOD* in Calypso (CHS$^-$)

A. Fruit firmness (down-regulation)

treatments	*P*-value
CHS$^-$ vs. pBI-intron	3.5E-09*
CHS$^-$ vs. pBI-*FaCCRi*	2.6E-08*
CHS$^-$ vs. pBI-*FaCADi*	4.6E-06*
CHS$^-$ vs. pBI-*FaPODi*	3.5E-09*
CHS$^-$ vs. pBI-Si3	1.3E-08*
pBI-intron vs. pBI-*FaCCRi*	1.5E-02*
pBI-intron vs. pBI-*FaCADi*	9.1E-06*
pBI-intron vs. pBI-*FaPODi*	3.5E-04*
pBI-intron vs. pBI-Si3	1.7E-04*

B. Fruit firmness (up-regulation)

treatments	*P*-value
CHS$^-$ vs. pBI-intron	3.5E-09*
CHS$^-$ vs. pBI-*FaCCR*	2.6E-08*
CHS$^-$ vs. pBI-*FaCAD*	3.5E-09*
CHS$^-$ vs. pBI-*FaPOD*	1.3E-08*
CHS$^-$ vs. pBI-O3	1.9E-09*
pBI-intron vs. pBI-*FaCCR*	3.6E-02*
pBI-intron vs. pBI-*FaCAD*	7.6E-03*
pBI-intron vs. pBI-*FaPOD*	6.1E-03*
pBI-intron vs. pBI-O3	1.3E-08*

One asterisk (*) indicates significantly increased levels (*P* <5.00E-02).

E.2. RNA levels

E.2.1. pBI-intron vs. down-regulation of individual *FaCCR*, *FaCAD*, and *FaPOD* in Elsanta

	P-value				
Two groups	*FaPAL*	*FaCHS*	*FaCCR*	*FaCAD*	*FaPOD*
WT vs. pBI-intron	0.3095	0.4206	0.0952	0.8413	0.2222
pBI-intron vs. pBI-*FaCCRi*	0.5476	0.6905	0.0318*	0.5476	0.0952
pBI-intron vs. pBI-*FaCADi*	0.5476	0.8413	1	0.0079*	0.8413
pBI-intron vs. pBI-*FaPODi*	0.6905	0.8413	1	1	0.5476

One asterisk (*) indicates significantly decreased levels (P <0.05).

E.2.2. pBI-intron vs. up-regulation of individual *FaCCR*, *FaCAD*, and *FaPOD* in Elsanta

	P-value				
Two groups	*FaPAL*	*FaCHS*	*FaCCR*	*FaCAD*	*FaPOD*
WT vs. pBI-intron	0.3095	0.1508	0.8413	0.5476	0.1508
pBI-intron vs. pBI-*FaCCR*	0.0952	0.6905	0.4206	1	0.1508
pBI-intron vs. pBI-*FaCAD*	0.3095	0.1508	0.1508	0.4206	0.3095
pBI-intron vs. pBI-*FaPOD*	0.1508	0.3095	0.6905	0.4206	0.0079*

One asterisk (*) indicates significantly increased levels (P <0.05).

E.2.3. CHS$^-$/pBI-intron vs. down-regulation of individual *FaCCR*, *FaCAD*, and *FaPOD* in Calypso (CHS$^-$)

	P-value				
Two groups	*FaPAL*	*FaCHS*	*FaCCR*	*FaCAD*	*FaPOD*
CHS$^-$ vs. CHS$^-$/pBI-intron	0.8413	1	0.5476	0.1508	0.4206
CHS$^-$/pBI-intron vs. CHS$^-$/pBI-*FaCCRi*	0.8413	0.4206	0.0159*	0.0318	1
CHS$^-$/pBI-intron vs. CHS$^-$/pBI-*FaCADi*	0.0159*	0.5476	0.4206	0.0159*	0.4206
CHS$^-$/pBI-intron vs. CHS$^-$/pBI-*FaPODi*	0.2222	0.6905	1	0.4206	1
CHS$^-$/pBI-intron vs. CHS$^-$/pBI-Si3	0.3095	0.5476	0.1508	0.5476	0.3095

One asterisk (*) indicates significantly decreased levels (P <0.02).

E.2.4. CHS$^-$/pBI-intron vs. up-regulation of individual *FaCCR*, *FaCAD*, and *FaPOD* in Calypso (CHS$^-$)

	P-value				
Two groups	*FaPAL*	*FaCHS*	*FaCCR*	*FaCAD*	*FaPOD*
CHS$^-$ vs. CHS$^-$/pBI-intron	1	0.6905	0.3095	0.3095	0.4206
CHS$^-$/pBI-intron vs. CHS$^-$/pBI-*FaCCR*	0.2222	0.5476	0.4206	0.5476	0.8413
CHS$^-$/pBI-intron vs. CHS$^-$/pBI-*FaCAD*	0.0952	0.8413	0.0556	0.2222	0.0952
CHS$^-$/pBI-intron vs. CHS$^-$/pBI-*FaPOD*	0.1508	1	0.6905	0.5476	0.0079*
CHS$^-$/pBI-intron vs. CHS$^-$/pBI-O3	0.0318	0.4206	0.0318	0.0318	0.0079*

One asterisk (*) indicates significantly increased levels (P <0.02).

E.3. Metabolite levels

E.3.1. WT vs. down-regulation of individual *FaCCR*, *FaCAD*, and *FaPOD* in Elsanta

Phenolic acid derivatives	WT vs. pBI-intron	WT vs. pBI-*FaCCRi*	WT vs. pBI-*FaCADi*	WT vs. pBI-*FaPODi*
p -Hydroxybenzoyl glucose	3,92E-01	5,78E-01	2,67E-01	3,72E-01
Cinnamoyl glucose	4,34E-01	5,33E-01	4,35E-01	1,69E-01
p -Coumaroyl glucoside/glucose	4,86E-03*	5,85E-06*	4,75E-05*	1,62E-03*
Caffeoyl glucose	3,49E-09*	1,36E-09*	8,66E-10*	3,49E-09*
Feruloyl glucose	2,38E-06*	2,71E-09*	9,38E-06*	4,19E-08*
Flavonols				
Kaempferol glucoside	4,35E-02	9,13E-02	9,33E-02	5,49E-01
Quercetin glucoside	3,16E-01	6,25E-01	2,02E-01	1,58E-01
Catechin	8,42E-01	9,60E-01	6,26E-01	6,24E-01
Anthocyanins				
Pelargonidin 3-glucoside	1,69E-01	2,04E-01	1,96E-02	7,58E-01
Pelargonidin 3-glucoside-malonate	1,10E-01	2,16E-01	8,69E-02	9,86E-01
Pelargonidin 3-rutinoside	4,13E-01	2,87E-01	6,03E-01	5,49E-01
Proanthocyanidins				
(Epi)catechin-(epi)catechin (isomer 1)	8,13E-01	2,87E-01	9,48E-01	4,34E-01
(Epi)catechin-(epi)catechin (isomer 2)	1,28E-01	9,60E-01	2,81E-01	8,70E-01
(Epi)afzelechin-(epi)catechin (isomer 1)	8,13E-01	8,01E-01	5,80E-01	8,70E-01
(Epi)afzelechin-(epi)catechin (isomer 2)	5,73E-01	7,75E-01	3,79E-01	5,98E-01

One asterisk (*) indicates significantly decreased or increased levels (P <1.00E-02).

E. 3.2. pBI-intron vs. down-regulation of individual *FaCCR*, *FaCAD*, and *FaPOD* in Elsanta

Phenolic acid derivatives	WT vs. pBI-intron	pBI-intron vs. pBI-*FaCCRi*	pBI-intron vs. pBI-*FaCADi*	pBI-intron vs. pBI-*FaPODi*
p -Hydroxybenzoyl glucose	3,92E-01	6,63E-01	8,19E-01	9,04E-01
Cinnamoyl glucose	4,34E-01	8,91E-01	9,71E-01	6,40E-01
p -Coumaroyl glucoside/glucose	4,86E-03*	4,97E-04*	1,15E-02	1,83E-01
Caffeoyl glucose	3,49E-09*	9,94E-02	5,22E-02	7,18E-01
Feruloyl glucose	2,38E-06*	3,51E-03*	3,40E-01	7,99E-01
Flavonols				
Kaempferol glucoside	4,35E-02	8,32E-01	8,76E-01	2,01E-01
Quercetin glucoside	3,16E-01	1,56E-01	9,71E-01	2,01E-01
Catechin	8,42E-01	7,37E-01	9,71E-01	4,45E-01
Anthocyanins				
Pelargonidin 3-glucoside	1,69E-01	9,11E-01	7,74E-02	4,29E-01
Pelargonidin 3-glucoside-malonate	1,10E-01	8,91E-01	5,07E-01	1,83E-01
Pelargonidin 3-rutinoside	4,13E-01	8,13E-01	7,09E-01	1,14E-01
Proanthocyanidins				
(Epi)catechin-(epi)catechin (isomer 1)	8,13E-01	1,72E-01	7,45E-01	1,27E-01
(Epi)catechin-(epi)catechin (isomer 2)	1,28E-01	2,15E-02	5,87E-01	1,95E-02
(Epi)afzelechin-(epi)catechin (isomer 1)	8,13E-01	9,31E-01	8,57E-01	5,47E-01
(Epi)afzelechin-(epi)catechin (isomer 2)	5,73E-01	9,31E-01	6,91E-01	9,68E-01

One asterisk (*) indicates significantly decreased or increased levels (P <1.00E-02).

E.3.3. WT vs. up-regulation of individual *FaCCR*, *FaCAD*, and *FaPOD* in Elsanta

Phenolic acid derivatives	WT vs. pBI-intron	WT vs. pBI-*FaCCR*	WT vs. pBI-*FaCAD*	WT vs. pBI-*FaPOD*
p -Hydroxybenzoyl glucose	1,90E-01	5,29E-01	1,66E-01	4,97E-01
Cinnamoyl glucose	4,81E-01	3,93E-01	3,15E-01	6,61E-01
p -Coumaroyl glucoside/glucose	4,33E-05*	7,25E-04*	1,51E-03*	4,11E-04*
Caffeoyl glucose	1,08E-05*	1,08E-05*	1,08E-05*	2,17E-05*
Feruloyl glucose	2,17E-05*	2,17E-05*	1,30E-04*	9,74E-04*
Flavonols				
Kaempferol glucoside	6,31E-01	1,85E-02	8,92E-02	4,35E-02
Quercetin glucoside	4,81E-01	5,24E-02	1,23E-01	1,82E-01
Catechin	7,96E-01	2,18E-01	2,80E-01	4,97E-01
Anthocyanins				
Pelargonidin 3-glucoside	9,71E-01	1,47E-02	2,18E-01	1,33E-01
Pelargonidin 3-glucoside-malonate	9,12E-01	5,24E-02	4,81E-01	4,00E-01
Pelargonidin 3-rutinoside	9,12E-01	7,53E-02	1,90E-01	4,00E-01
Proanthocyanidins				
(Epi)catechin-(epi)catechin (isomer 1)	3,15E-01	5,20E-03*	4,33E-02	3,50E-02
(Epi)catechin-(epi)catechin (isomer 2)	2,48E-01	1,90E-01	4,81E-01	3,56E-01
(Epi)afzelechin-(epi)catechin (isomer 1)	6,84E-01	8,93E-03*	1,85E-02	4,35E-02
(Epi)afzelechin-(epi)catechin (isomer 2)	1,66E-01	1,90E-01	7,53E-02	1,56E-01

One asterisk (*) indicates significantly decreased or increased levels (*P* <1.00E-02).

E. 3.4. pBI-intron vs. up-regulation of individual *FaCCR*, *FaCAD*, and *FaPOD* in Elsanta

Phenolic acid derivatives	WT vs. pBI-intron	pBI-intron vs. pBI-*FaCCR*	pBI-intron vs. pBI-*FaCAD*	pBI-intron vs. pBI-*FaPOD*
p -Hydroxybenzoyl glucose	1,90E-01	1,85E-02	7,39E-01	4,00E-01
Cinnamoyl glucose	4,81E-01	9,12E-01	1,00E+00	9,05E-01
p -Coumaroyl glucoside/glucose	4,33E-05*	5,79E-01	5,29E-01	9,05E-01
Caffeoyl glucose	1,08E-05*	5,29E-01	5,29E-01	9,47E-02
Feruloyl glucose	2,17E-05*	3,93E-01	2,80E-01	1,72E-02
Flavonols				
Kaempferol glucoside	6,31E-01	6,84E-03*	6,30E-02	7,62E-03*
Quercetin glucoside	4,81E-01	2,80E-01	5,79E-01	7,80E-01
Catechin	7,96E-01	2,80E-01	1,23E-01	2,78E-01
Anthocyanins				
Pelargonidin 3-glucoside	9,71E-01	2,17E-05*	5,24E-02	2,79E-02
Pelargonidin 3-glucoside-malonate	9,12E-01	1,47E-02	2,48E-01	1,33E-01
Pelargonidin 3-rutinoside	9,12E-01	1,90E-01	1,90E-01	3,56E-01
Proanthocyanidins				
(Epi)catechin-(epi)catechin (isomer 1)	3,15E-01	1,66E-01	3,53E-01	4,00E-01
(Epi)catechin-(epi)catechin (isomer 2)	2,48E-01	4,33E-02	1,05E-01	1,13E-01
(Epi)afzelechin-(epi)catechin (isomer 1)	6,84E-01	3,55E-02	3,55E-02	7,89E-02
(Epi)afzelechin-(epi)catechin (isomer 2)	1,66E-01	2,48E-01	7,53E-02	2,78E-01

One asterisk (*) indicates significantly decreased or increased levels (*P* <1.00E-02).

E.4. lignin composition

P-values	H	G	S	S:G
pBI-*FaCCRi*	3,6E-01	2,1E-03*	2,6E-01	2,2E-03*
pBI-*FaCADi*	4,4E-03*	3,5E-05*	6,2E-04*	2,1E-02
pBI-*FaPODi*	3,4E-02	3,8E-01	3,1E-02	4,6E-02
pBI-*FaCCR*	5,1E-01	2,0E-01	1,2E-03*	5,9E-02
pBI-*FaCAD*	2,5E-01	2,8E-02	9,0E-02	8,4E-05*
pBI-*FaPOD*	1,5E-02	6,4E-04*	8,0E-03*	1,1E-04*

One asterisk (*) indicates significant difference levels (*P* <1.00E-02).

E.5. Metabolite levels in CHS⁻ fruits

E. 5.1. CHS⁻ vs. down-regulation of individual *FaCCR*, *FaCAD*, and *FaPOD* in Calypso (CHS⁻)

Phenolic acid derivatives	CHS- vs. CHS-/pBI-intron	CHS- vs. CHS-/pBI-*FaCCRi*	CHS- vs. CHS-/pBI-*FaCADi*	CHS- vs. CHS-/pBI-*FaPODi*	CHS- vs. CHS-/pBI-Si3
p -Hydroxybenzoyl glucose	2,18E-01	5,24E-02	7,53E-02	1,66E-01	1,66E-01
Cinnamoyl glucose	2,48E-01	4,33E-02	7,25E-04*	4,81E-01	1,43E-01
p -Coumaroyl glucoside/glucose	2,18E-01	9,12E-01	2,18E-01	6,84E-01	5,79E-01
Caffeoyl glucose	6,84E-03*	1,05E-03*	3,89E-03*	3,25E-04*	7,25E-04*
Feruloyl glucose	1,43E-01	2,17E-05*	8,93E-03*	2,06E-04*	3,25E-04*
Flavonols					
Kaempferol glucoside	6,84E-01	7,53E-02	4,81E-01	1,90E-01	5,79E-01
Quercetin glucoside	1,43E-01	1,23E-01	1,15E-02	2,48E-01	3,15E-01
Catechin	7,96E-01	7,39E-01	5,79E-01	4,36E-01	9,71E-01
Anthocyanins					
Pelargonidin 3-glucoside	6,31E-01	7,96E-01	1,90E-01	3,15E-01	3,93E-01
Pelargonidin 3-glucoside-malonate	7,39E-01	3,53E-01	1,23E-01	4,81E-01	1,00E+00
Pelargonidin 3-rutinoside	7,96E-01	9,71E-01	9,12E-01	5,24E-02	4,36E-01
Proanthocyanidins					
(Epi)catechin-(epi)catechin (isomer 1)	6,31E-01	8,53E-01	9,12E-01	2,18E-01	7,39E-01
(Epi)catechin-(epi)catechin (isomer 2)	7,96E-01	1,00E+00	9,71E-01	7,53E-02	6,31E-01
(Epi)afzelechin-(epi)catechin (isomer 1)	4,36E-01	7,39E-01	5,29E-01	9,71E-01	3,93E-01
(Epi)afzelechin-(epi)catechin (isomer 2)	7,96E-01	4,81E-01	3,15E-01	8,53E-01	2,48E-01

E. 5.2. CHS⁻/pBI-intron vs. down-regulation of individual *FaCCR*, *FaCAD*, and *FaPOD* in Calypso (CHS⁻)

p -Hydroxybenzoyl glucose	3,93E-01	7,39E-01	5,29E-01	9,12E-01
Cinnamoyl glucose	7,39E-01	1,90E-01	4,81E-01	9,12E-01
p -Coumaroyl glucoside/glucose	2,48E-01	7,39E-01	1,66E-01	3,53E-01
Caffeoyl glucose	3,93E-01	5,29E-01	6,30E-02	2,18E-01
Feruloyl glucose	1,30E-04*	3,53E-01	8,93E-03*	3,89E-03*
Flavonols				
Kaempferol glucoside	5,24E-02	2,48E-01	1,43E-01	4,81E-01
Quercetin glucoside	6,84E-01	1,66E-01	1,00E+00	5,79E-01
Catechin	8,53E-01	9,12E-01	1,90E-01	7,96E-01
Anthocyanins				
Pelargonidin 3-glucoside	6,31E-01	8,92E-02	2,18E-01	2,18E-01
Pelargonidin 3-glucoside-malonate	9,12E-01	6,30E-02	2,80E-01	6,31E-01
Pelargonidin 3-rutinoside	7,39E-01	1,00E+00	8,93E-03*	2,80E-01
Proanthocyanidins				
(Epi)catechin-(epi)catechin (isomer 1)	9,12E-01	8,53E-01	2,18E-01	4,81E-01
(Epi)catechin-(epi)catechin (isomer 2)	9,12E-01	9,71E-01	2,88E-02	4,36E-01
(Epi)afzelechin-(epi)catechin (isomer 1)	7,96E-01	8,53E-01	5,79E-01	7,96E-01
(Epi)afzelechin-(epi)catechin (isomer 2)	7,39E-01	7,39E-01	4,81E-01	3,93E-01

One asterisk (*) indicates significantly decreased or increased levels (P <1.00E-02).

E. 5.3. CHS$^-$ vs. up-regulation of individual *FaCCR*, *FaCAD*, and *FaPOD* in Calypso (CHS$^-$)

p -Hydroxybenzoyl glucose	2,18E-01	9,12E-01	1,08E-05*	8,93E-03*	1,30E-04*
Cinnamoyl glucose	2,48E-01	3,53E-01	2,09E-03*	6,31E-01	2,88E-03*
p -Coumaroyl glucoside/glucose	2,18E-01	3,15E-01	3,89E-03*	4,81E-01	8,92E-02
Caffeoyl glucose	6,84E-03*	3,89E-03*	1,00E+00	2,09E-03*	5,20E-03*
Feruloyl glucose	1,43E-01	3,55E-02	9,12E-01	1,51E-03*	7,53E-02
Flavonols					
Kaempferol glucoside	6,84E-01	6,31E-01	8,92E-02	1,23E-01	1,51E-03*
Quercetin glucoside	1,43E-01	3,53E-01	1,05E-03*	4,81E-01	1,85E-02
Catechin	7,96E-01	7,39E-01	1,90E-01	7,96E-01	7,53E-02
Anthocyanins					
Pelargonidin 3-glucoside	6,31E-01	7,96E-01	7,58E-05*	7,53E-02	4,87E-04*
Pelargonidin 3-glucoside-malonate	7,39E-01	3,93E-01	4,33E-05*	8,92E-02	3,25E-04*
Pelargonidin 3-rutinoside	7,96E-01	5,79E-01	3,53E-01	5,79E-01	4,81E-01
Proanthocyanidins					
(Epi)catechin-(epi)catechin (isomer 1)	6,31E-01	3,93E-01	3,15E-01	7,39E-01	9,12E-01
(Epi)catechin-(epi)catechin (isomer 2)	7,96E-01	5,79E-01	1,90E-01	4,81E-01	3,93E-01
(Epi)afzelechin-(epi)catechin (isomer 1)	4,36E-01	7,39E-01	7,39E-01	9,12E-01	5,29E-01
(Epi)afzelechin-(epi)catechin (isomer 2)	7,96E-01	7,96E-01	3,93E-01	7,39E-01	2,48E-01

One asterisk (*) indicates significantly decreased or increased levels (P <1.00E-02).

E. 5.4. CHS$^-$/pBI-intron vs. up-regulation of individual *FaCCR*, *FaCAD*, and *FaPOD* in Calypso (CHS$^-$)

Phenolic acid derivatives	CHS-/pBI-intron vs. CHS-/pBI-*FaCCR*	CHS-/pBI-intron vs. CHS-/pBI-*FaCAD*	CHS-/pBI-intron vs. CHS-/pBI-*FaPOD*	CHS-/pBI-intron vs. CHS-/pBI-O3
p -Hydroxybenzoyl glucose	1,66E-01	2,10E-04*	7,39E-01	2,88E-03*
Cinnamoyl glucose	5,79E-01	3,55E-02	3,93E-01	3,15E-01
p -Coumaroyl glucoside/glucose	9,12E-01	1,15E-02	4,81E-01	3,93E-01
Caffeoyl glucose	5,29E-01	8,93E-03*	4,36E-01	1,00E+00
Feruloyl glucose	7,96E-01	1,90E-01	6,30E-02	6,84E-01
Flavonols				
Kaempferol glucoside	4,36E-01	8,92E-02	7,53E-02	8,93E-03*
Quercetin glucoside	7,96E-01	8,93E-03*	4,81E-01	2,80E-01
Catechin	6,31E-01	2,48E-01	4,81E-01	3,55E-02
Anthocyanins				
Pelargonidin 3-glucoside	6,31E-01	2,06E-04*	7,53E-02	4,87E-04*
Pelargonidin 3-glucoside-malonate	7,96E-01	2,17E-05*	3,55E-02*	7,58E-05*
Pelargonidin 3-rutinoside	6,31E-01	4,81E-01	5,79E-01	3,93E-01
Proanthocyanidins				
(Epi)catechin-(epi)catechin (isomer 1)	2,80E-01	3,15E-01	6,31E-01	1,00E+00
(Epi)catechin-(epi)catechin (isomer 2)	3,15E-01	2,48E-01	2,18E-01	4,36E-01
(Epi)afzelechin-(epi)catechin (isomer 1)	3,93E-01	9,71E-01	3,93E-01	9,71E-01
(Epi)afzelechin-(epi)catechin (isomer 2)	6,31E-01	8,53E-01	7,96E-01	3,53E-01

One asterisk (*) indicates significantly decreased or increased levels (*P* <1.00E-02).

E.5.5. Calypso (WT) vs. Calypso (CHS$^-$)

Phenolic acid derivatives	WT vs. CHS-	pBI-intron vs. CHS-/pBI-intron
Flavonols		
Kaempferol glucoside	3,13E-01	7,54E-04*
Quercetin glucoside	2,84E-01	3,84E-03*
Catechin	6,93E-01	8,46E-01
Anthocyanins		
Pelargonidin 3-glucoside	2,10E-05*	3,24E-04*
Pelargonidin 3-glucoside-malonate	1,70E-04*	4,52E-03*
Pelargonidin 3-rutinoside	7,84E-01	4,22E-01
Proanthocyanidins		
(Epi)catechin-(epi)catechin (isomer 1)	6,93E-01	2,67E-01
(Epi)catechin-(epi)catechin (isomer 2)	6,48E-01	3,50E-01
(Epi)afzelechin-(epi)catechin (isomer 1)	9,27E-01	6,73E-02
(Epi)afzelechin-(epi)catechin (isomer 2)	8,32E-01	6,19E-01

One asterisk (*) indicates significantly increased levels (*P* <1.00E-02).

F. Partial genome sequences

F.1. Partial *gCCR* sequences containing one intron

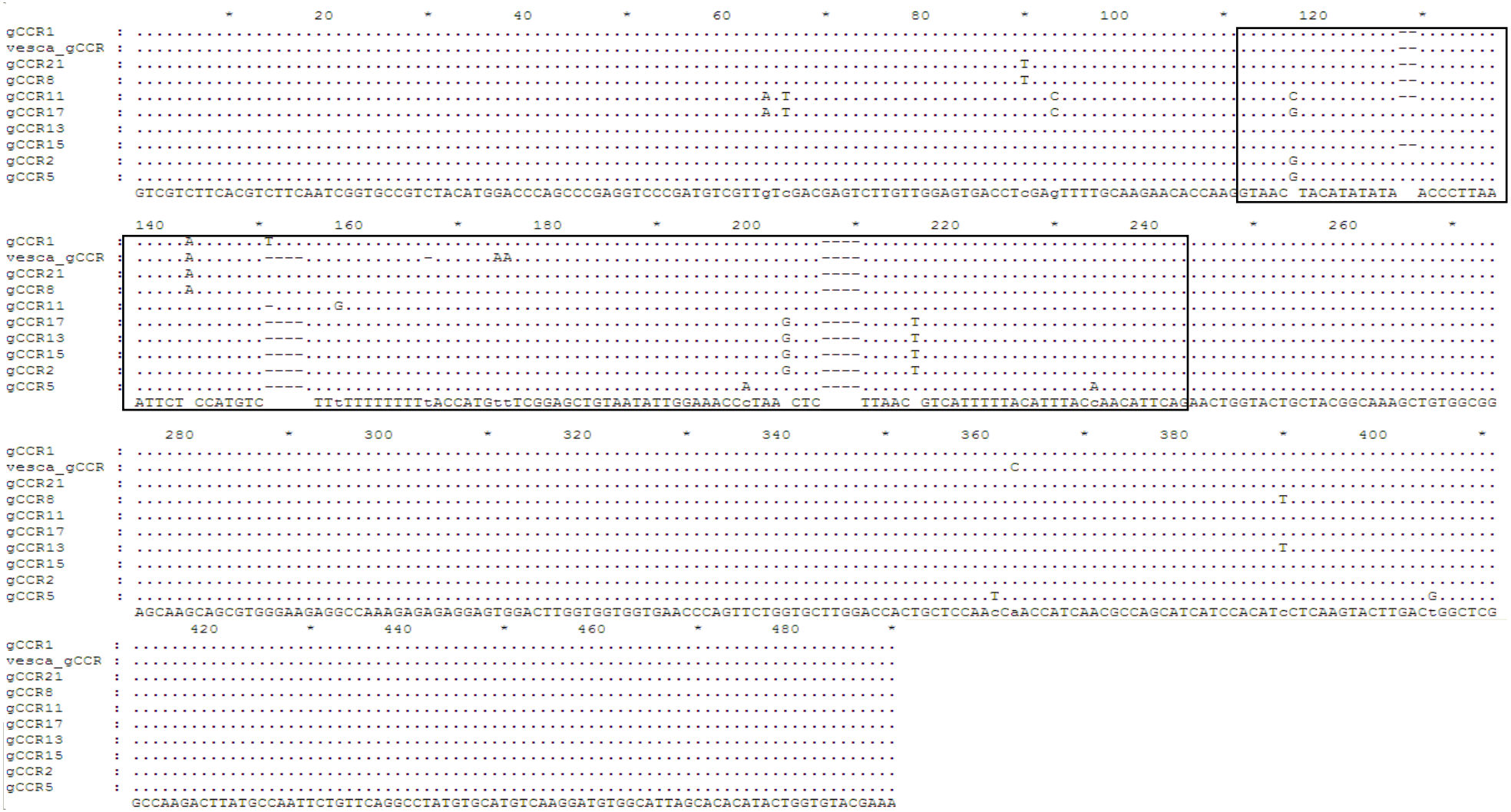

F.2. Partial *gCAD* sequences containing one intron

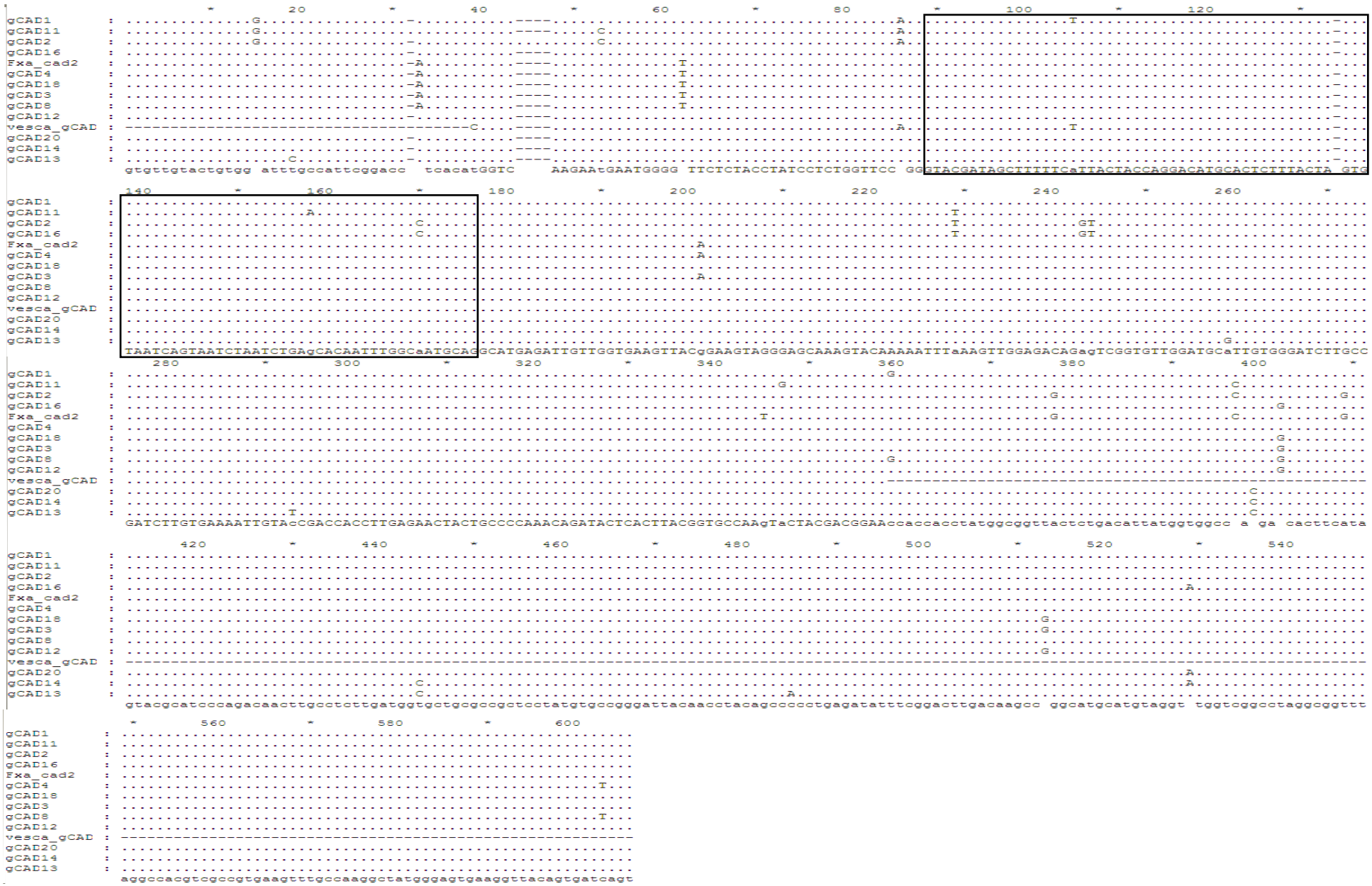

F.3. Partial *gPOD* sequences containing one intron

G. SDS-PAGE

G1. Expression of FaCAD protein in *E. coli* strain BL21(DE3)pLysS.

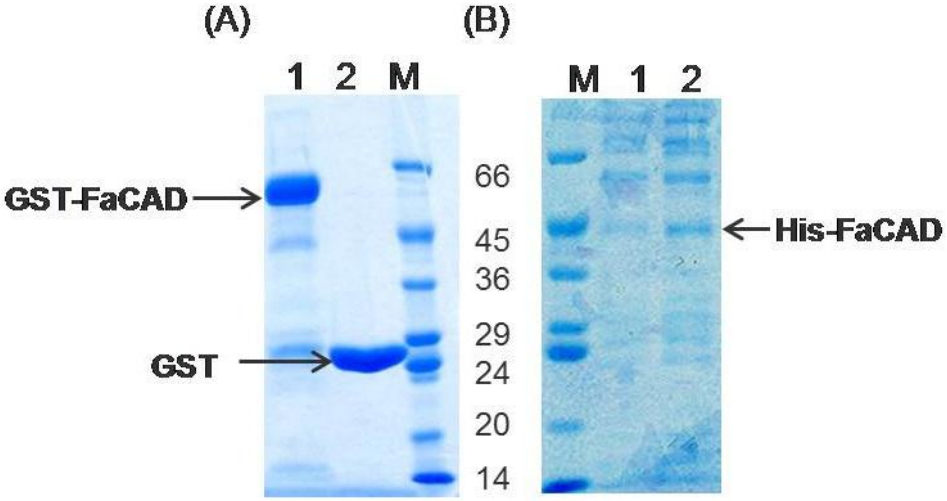

Lane (M) molecular mass markers; (A) purified recombinant GST-FaCAD (10 µg protein, lane 1) and GST (10 µg protein, lane 2) after induction of protein with 0.2 mM IPTG at 16℃; (B) purified recombinant His-FaCAD (10 µg protein, lane 1-2), after induction of protein with 0.5 mM IPTG at 37℃ (B, lane 1) or 16℃ (B, lane 2).

G2. SDS-PAGE of FaPOD crude protein

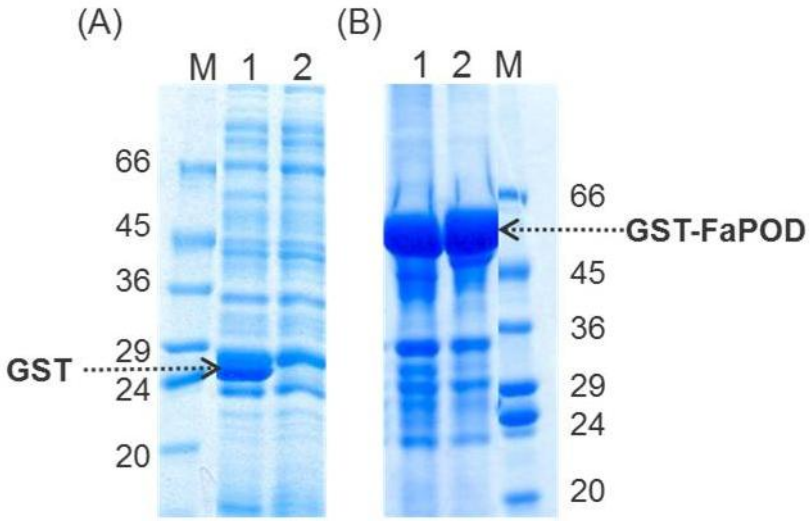

Lane (M) molecular mass markers; (A) total protein extract from *E. coli* strain Rosetta (DE3) pLysS harboring the empty vector (pGEX-4X-1), and FaPOD (30 µg protein, lane 1-2), after induction of protein with 0.5 mM IPTG at 16℃; (B) soluble crude protein GST-FaPOD (20 µg protein, lane 1-2) from solubilized pellets containing 50 mM Tris-HCl buffer (pH8.5) with 6M Urea and 1mM DTT (Hushpulian et al., 2003).